A Critical Assessment of Two Phase Flow Characterization of Soil

by

Rosanna Tse

Bachelor of Science in Civil and Environmental Engineering
University of California, Berkeley 1994

Submitted to the Department of Civil and Environmental Engineering
in Partial Fulfillment of the Requirements for the Degree of

Master of Science in Civil and Environmental Engineering

at the

Massachusetts Institute of Technology

June 1997

Author _____
Department of Civil and Environmental Engineering
June 1997

Certified By _____
Lynn Gelhar
Professor, Civil and Environmental Engineering
Thesis Supervisor

Accepted By _____
Joseph M. Sussman
Chairman, Departmental Committee on Graduate Studies

A Critical Assessment of Two Phase Flow Characterization of Soils

by

Rosanna Tse

Submitted to the Department of Civil and Environmental Engineering on May 27,1997 in Partial Fulfillment of the Requirements for the Degree of Master of Science in Civil and Environmental Engineering

Abstract

Difficulties associated with the direct measurement of unsaturated hydraulic conductivity have prompted the development of empirical models that predict unsaturated conductivity using transformations of the more easily measured moisture retention and saturated hydraulic conductivity data. This thesis evaluates the predictive ability of three such models: the Brooks & Corey model, the Campbell model, and the van Genuchten model. Seven soil types totaling 71 soil samples are analyzed.

Predictive models use measured saturated hydraulic conductivity and parameters generated from the moisture retention curve to predict the unsaturated hydraulic conductivity. A nonlinear least-squares optimization procedure is applied to the moisture retention data to generate the best fit parameters. Results from the analysis indicate that these models do not accurately predict the unsaturated conductivity. The models do not characterize the natural variability found in aquifers. A correlation is observed between the error in prediction and the mean grain size; deviations between the measured and predicted conductivity increase as the texture of the material becomes coarser.

Saturated conductivity is used as the match point for the predicted models. Researchers have suggested that a measured unsaturated conductivity point near the region of interest will result in a better prediction. An implicit assumption within this theory is that the slope of the predicted conductivity curve reflects the actual slope. Analysis concludes that predicted slope does not represent the actual slope.

The use of Leverett scaling is common in modeling applications. Capillary pressure curves are scaled by the spatially variable saturated hydraulic conductivity in order to obtain a single curve representative of any point within the aquifer. Results indicate that Leverett scaling does reflect the general trends in capillarity seen at each of the sites, but does not represent the variability seen among individual samples at a site.

Thesis Supervisor: Lynn Gelhar
Title: Professor

Acknowledgments

First and foremost, I would like to thank the Parsons Foundation and MIT for funding my research. Without their support, this thesis would never have been possible.

Many individuals have contributed to this thesis. Raziuddin Khaleel of the Westinghouse Hanford Company, John Nimmo of the U. S. Geological Survey, Peter Wierenga of the University of Arizona, Dan Stephens of Daniel B. Stephens & Associates, Inc., and Don Polmann of Florida's West Coast Regional Water Supply Authority generously supplied the data used in our analysis. Richard Hills of New Mexico State University, Paul Hsieh of the U. S. Geological Survey, and Linda Abriola of the University of Michigan provided invaluable advice.

To Dr. Lynn Gelhar, thank you for your patience and your willingness to share with me your immense understanding of groundwater hydrology. Your insight and depth of knowledge never ceases to amaze me.

To Bruce Jacobs, thank you for all the research advice and support. It was a pleasure being your teaching assistant.

My stay at MIT is filled with fond memories. Thanks to all my friends in the Parsons Lab who have made MIT a pleasant place to be. Special thanks goes to Julie, Nicole, Karen F, Karen P, Ken, Guiling, Sanjay, Rob, and Dave. A super duper thanks goes to Julie who edited my thesis.

Pat Dixon and Cynthia Stewart have been a tremendous help to me. I would never have survived MIT without their assistance.

Living at Ashdown has been one of the best decisions I have ever made. My thanks goes to all my friends at Ashdown, especially my fellow 4th floor residents, who have kept me sane. Special thanks goes to my roommate, Cathy, who has been with me all the way. Your support and encouragement has meant a lot to me. Thanks also goes to Rebecca, Kathy, Victor, Richard, Kate, Mary, Winnie, Susan, and Inn.

Last, but definitely not least, my thanks goes to my family. Your love, support, and encouragement has kept me going. Thank you mom, dad, grandma, Sus, Jess, Ed, Elaine, Frances, Glenn, Ricky, Mitchell, Uncle Bill, Dan, Derek, and Carmen.

Table of Contents

List of Figures

List of Tables

Chapter 1

Introduction

1.1 Introduction

Numerical modeling is increasingly used to characterize the complex nature of flow and transport in the subsurface environment. Its use in the characterization of two phase fluid flow through the unsaturated zone of an aquifer is of particular interest. An accurate understanding of the flow properties in the unsaturated zone is critical in estimating contaminant transport, determining soil infiltration, and calculating recharge to the aquifer. At present, our capacity to create complex subsurface models far exceeds our ability to characterize the physical system it describes. The accuracy of these models rely heavily on the quality of the measured data provided. Basic soil properties significantly influence the outcome of these models.

The unsaturated hydraulic conductivity plays an integral role in determining the flow characteristics of the unsaturated zone. However, the direct measurement of this hydraulic property is often difficult. Typical problems associated with the measurement of the unsaturated conductivity include high costs, tedious and time consuming measurement techniques, the hysteretical nature of the soil properties, logistical difficulties, the immense

amount of data required to accurately represent the extensive variability of the soil, and the selection of a measurement technique that can measure conductivity values that span several orders of magnitude.

These difficulties in the direct measurement of unsaturated conductivity have prompted the development of empirical models that predict unsaturated conductivity. The empirical models calculate the relative unsaturated hydraulic conductivity from more easily measured moisture retention and saturated hydraulic conductivity data. Figure 1.1 displays a typical moisture retention curve. The predictive models fall under three general categories: tension dependent models, saturation dependent models, and pore connectivity models.

Tension dependent models rely on existing measured unsaturated conductivity values to extrapolate the rest of the conductivity curve. Saturation dependent models predict the unsaturated conductivity curves based solely on the saturation value, but these models do not produce unique curves for different soils. Pore connectivity models predict the unsaturated conductivity from the measured saturated hydraulic conductivity and moisture retention data. A specific conductivity curve is generated for each individual soil type. The goal of this thesis is to assess the performance of four predictive unsaturated conductivity models derived from the pore connectivity theory.

1.2 Background

The pore connectivity models relate unsaturated conductivity to moisture retention through statistical analysis of the pore size distribution. Purcell (1949) and Childs and Collis-George (1950) are recognized as the instigators of the pore connectivity theory. Deviation

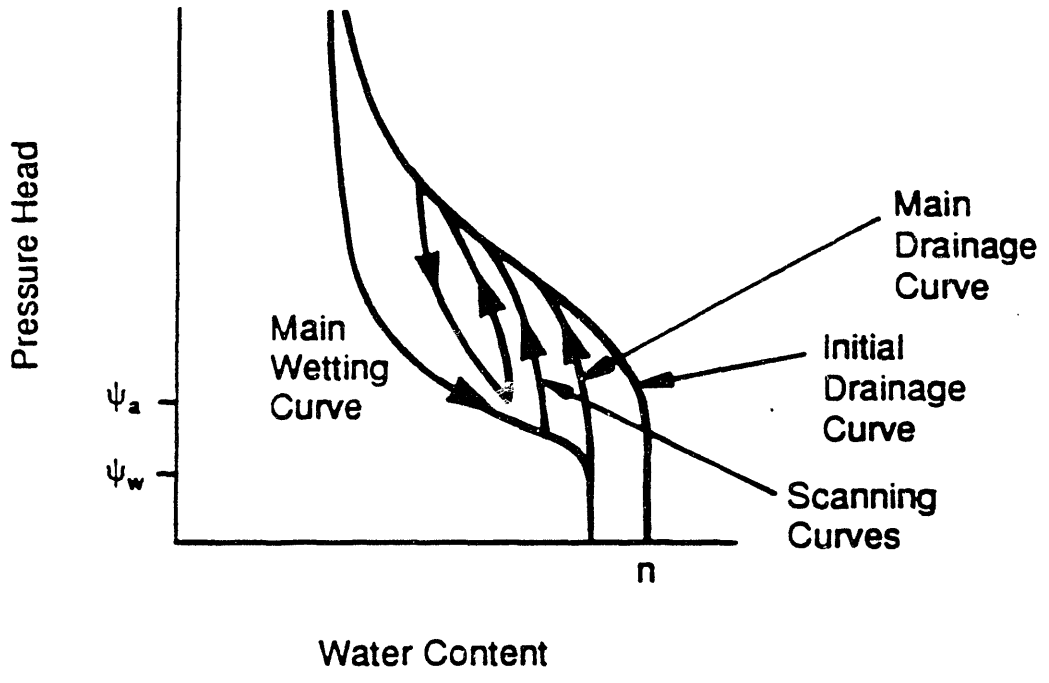

Figure 1.1: Typical Moisture Retention Curve (From Stephens, 1996).

among the various models is attributed to differences in the interpretation of pore geometry and the estimate of its contributions to total permeability.

Models based on Purcell's theory view the pores as a bundle of straight capillaries having a specific radii distribution function. Using Purcell's theory, Gates and Lietz (1950) derive a relationship between the unsaturated conductivity, the capillary tension, and the moisture content for the wetting phase. Fatt and Dykstra (1951) and Burdine (1953) modify Purcell to account for tortuosity in the flow path. Burdine also derives a relationship between conductivity and moisture content for the nonwetting phase.

The Childs and Collis-George (CCG) theory models the flow through the porous medium as flow through varying pore sizes that are randomly connected at a rejoined interface. Wyllie and Gardner (1958) derive a relationship between conductivity and moisture retention by simplifying the CCG theory. They assume that the pores are actually parallel capillary tubes traversing randomly joined thin layers of soil. Mualem applies his own adjustments to the CCG theory and comes up with a different relationship.

Four closed form analytical unsaturated conductivity models evolve from these established pore connectivity relationships. These models predict unsaturated conductivity using the measured saturated conductivity and parameters estimated from the moisture retention data. Brooks & Corey (1964) characterize the moisture retention curve as a power law and apply the Burdine relationship to generate a closed form equation for the unsaturated conductivity. Campbell (1974) also models the moisture retention curve as a power law, but applies the Childs and Collis-George relationship. van Genuchten (1980) represents the moisture retention curve with a mathematical S-shape function and applies both the Burdine and Mualem relationships to generate two different predictive unsaturated conductivity equations. Russo (1988) assumes that unsaturated conductivity follows the Gardner exponential model, a tension dependent model, and backtracks an expression for the moisture retention curve using the Mualem theory.

1.3 Relevant Literature

There have been many comparisons of these predictive models with measured data. Stephens and Rehfeldt (1985) evaluate the performance of the van Genuchten model in predicting the unsaturated conductivity for a fine sand. Measured values of moisture content and unsaturated conductivity gravitate towards the wet range. The authors conclude that the van Genuchten approach sufficiently predicts the conductivity for this fine sand within the measured moisture content regime, but specifically state that predictions may not be accurate for the dry regions. A few measurements of conductivity and moisture retention must be made in the dry range before an absolute conclusion can be reached regarding the overall performance of the van Genuchten model.

Stephens and Rehfeldt also conduct a series of tests to assess the sensitivity of the conductivity predictions to the moisture content parameters θ_r, the residual moisture content, and θ_s, the saturated moisture content. Results indicate that the model is highly sensitive to the value of θ_r. Predicted conductivities may differ by more than one order of magnitude depending on the choice of θ_r. The value of θ_s also influences the predicted conductivity, but the associated error is not as large as that for θ_r.

Russo (1988) compares the Brooks & Corey, van Genuchten, and Russo model with two soils, a hypothetical sandy loam and a silt loam. The van Genuchten model provides the best fit to the measured data. Russo acknowledges that model evaluations based on just two soils is not sufficient. In order to accurately evaluate which model works best, model comparisons based on many different soil types must be performed.

Keuper and Frind (1991) scale a series of moisture of retention curves for Borden sands using a modified Leverett scaling relationship. The Leverett concept takes the various moisture retention curves and scales them into a single curve for all the sand

samples. Keuper et al. use this scaled curve in their numerical analysis to represent the moisture retention in the aquifer at any single point. A Brooks & Corey curve is fitted through the scaled data. The parameters from the Brooks & Corey moisture retention expression are then used to generate an unsaturated conductivity curve. A conductivity curve is estimated for both the wetting and nonwetting phase from the corresponding Brooks & Corey unsaturated conductivity expression. Numerical simulations modeling contaminant migration are then carried out in a spatially correlated, random conductivity field to illustrate the influence of the fluid properties.

Yates et al. (1992) analyzes the van Genuchten model on 36 soil samples taken from 23 different soils. The soil types range from clay to sands. A majority of the soil types are fine soils. The analysis compares the measured and predicted conductivity using the standard van Genuchten predictive method based on a match point at saturated conductivity, the van Genuchten method with a match point at some selected unsaturated conductivity value, the van Genuchten method with an extra variable constant, l, and two simultaneous fits with measured unsaturated conductivity data. The authors find that the predictive approach is the least accurate of all the methods and that it introduces a systematic bias into the unsaturated conductivity estimates. The best fit is obtained by one of the simultaneous fits. The use of a different match point did not significantly improve the calculated unsaturated conductivity values. Although the predictive method performed the worst, Yates et al. stress that this does not invalidate the method. The soils studied in this analysis do not represent the entire range of soil types. Additional soil types must be tested before a definitive conclusion can be made.

With the exceptions of Stephens et al. and Keuper et al., all analyses of the predictive models focus primarily on fine textured materials, such as clays and silts, at a relatively high moisture content (> 10%). Khaleel et al. specifically looks at the performance of the van Genuchten/Mualem relationship at low moisture contents for the

Hanford sands. The highly heterogeneous Hanford sands contrast nicely with the homogeneous sands previously studied. Khaleel et al. conclude that the van Genuchten predictive method shows noticeable deviation from the measured values, especially at low moisture contents. The use of a different conductivity match point from the unsaturated conductivity region results in an improvement.

1.4 Thesis Objectives

The specific objectives of this study are the following:

- To evaluate the performance of the Brooks & Corey, Campbell, Russo, and van Genuchten models in predicting the unsaturated conductivity of aquifer-like materials at low moisture contents.
- To assess the influence of changing the match point for these models.
- To investigate the concept of Leverett scaling.

1.5 Thesis Outline

This thesis is organized into six chapters. Chapter 2 summarizes the various types of unsaturated conductivity models and presents a detailed description of the four models used in our analysis. Chapter 3 concentrates on the curve fitting methodology. In Chapter 4, the data selection process is discussed and a brief description of each data set is presented. Chapter 5 analyzes the curve fitting results. Chapter 6 presents the conclusions and suggestions for future research.

Chapter 2

Unsaturated Hydraulic Conductivity Models

This chapter summarizes the various types of models used to calculate unsaturated hydraulic conductivity. This review follows the format presented by Mualem (1986). Section 1 discusses the variables and definitions commonly found in unsaturated conductivity equations. Sections 2, 3, and 4 present the different categories of conductivity models, namely tension dependent models, saturation dependent models, and pore connectivity models. Section 5 discusses coupled moisture retention/unsaturated conductivity models that predict unsaturated conductivity using only measured saturated hydraulic conductivity and moisture retention data.

2.1 Relevant Notation and Definitions

Unsaturated conductivity models attempt to predict conductivity values through measured soil properties and characteristics, such as moisture content or capillary tension. Table 2.1

lists standard variables and definitions that appear ubiquitously in the unsaturated conductivity literature.

2.2 Tension Dependent Models

When supplied with an incomplete set of unsaturated conductivity data, capillary tension models provide a relatively straightforward and simplistic way to estimate the unknown unsaturated conductivity values. Capillary tension models rely on existing measured conductivities to systematically extrapolate the rest of the conductivity curve for any known tension.

Application of the models serves multiple purposes. Use of these models can minimize the number of measurements required for adequate representation of actual field conditions. They also provide closed form analytical equations used to solve unsaturated flow problems. In addition to saving time and improving accuracy, a closed form solution simplifies the computational procedure used in numerical simulations.

One of the earliest and most widely used unsaturated hydraulic conductivity models is formulated by Gardner (1957):

$$K_r(\psi) = \exp(-\alpha\psi) \tag{2.1}$$

where

α = an empirical soil parameter

Gardner derives this analytical equation relating unsaturated hydraulic conductivity to capillary tension as a plausible solution to Richard's Equation (1931) for a steady state flow scenario. Gardner (1958) determined acceptable values of α for various soil types. These

Standard Variables

θ actual water content

θ_r residual water content

θ_S saturated water content

ψ capillary pressure

K unsaturated hydraulic conductivity

K_S saturated hydraulic conductivity

K_r relative hydraulic conductivity

S saturation

S_e effective saturation

Standard Definitions

$$K_r = \frac{K}{K_s}$$

$$S_e = \frac{(\theta - \theta_r)}{(\theta_s - \theta_r)}$$

Table 2.1: Common Variables and Definitions Found in Unsaturated Conductivity Literature.

general values may be used to obtain a rough estimate of the hydraulic conductivity when no data are available.

This exponential model is frequently employed by many soil scientists because of its simple form. Recent research involving the stochastic analyses of steady and transient unsaturated flow in heterogeneous media (Yeh et al., 1985; Mantoglou and Gelhar, 1987) have adopted the Gardner exponential model to represent the local unsaturated hydraulic conductivity.

Although simplistic in nature, the Gardner exponential model does have certain limitations. The model does not hold well over a wide range of values. Hence, the equation is valid only for a limited range of values of capillary tension.

Brooks and Corey (1964) suggest an alternate analytical form relating the conductivity to capillary tension :

$$K_r = \left(\frac{\psi}{\psi_{cr}} \right)^{-n} \qquad \text{for} \qquad \psi \leq \psi_{cr}$$

$$K = K_s \qquad \text{for} \qquad \psi \geq \psi_{cr}$$

where

ψ_{cr} = an empirically determined critical capillary tension value

n = a soil determined empirical parameter

This power law model is extremely popular in the petroleum industry.

Obvious shortcomings of the Brooks and Corey model include its high degree of non-linearity and its inherent discontinuity near the critical capillary tension point. This poses a distinct problem for numerical models that simulate fluid flow in the unsaturated zone and makes it very difficult to deal with analytically. The discontinuity in the slope can prevent rapid convergence in the model simulations.

Other exponential (Rijtema, 1965) and power law (Wind, 1955) models have also been proposed. The parameters for these formulas differ slightly from Gardner and Brooks and Corey. These formulas have not found the same degree of wide acceptance and usage as the two models previously discussed. Tension based models also take on other mathematical forms. For example, King (1964) proposes a model using the hyperbolic cosine function.

2.3 Saturation Dependent Models

Models in this category stem from the assumption that flow through the unsaturated porous media resembles laminar flow through a capillary tube. By assuming this capillary tube concept, the saturation based models are able to represent the microscopic flow through the porous media by macroscopically measured flow parameters, such as hydraulic conductivity and average velocity. Equations, such as the Hagen-Poiseuille, that link the microscopic level to the macroscopic level form the theoretical basis behind these models. Saturation dependent models are convenient, but they do not produce unique conductivity curves for different soil textures.

Averjanov (1950) views unsaturated flow as flow in parallel, uniform, cylindrical capillary tubes. The wetting fluid forms a homogeneous film along the cylinder wall, whereas the nonwetting fluid occupies the central portion of the tube. Based on these limiting conditions, the following relationship between unsaturated conductivity and saturation is derived:

$$K_r = S_e^{3.5}$$

Yuster (1951) essentially solves the same equations as Averjanov, but imposes slightly different flow conditions. Yuster assumes that the nonwetting fluid in the center of the tube flows under the same gradient as the wetting fluid. The solution is also in a power law form, but the exponent varies:

$$K_r = S_e^{2.0}$$

Kozeny (1927) develops a model for saturated hydraulic conductivity assuming flow through spherical porous media:

$$K_s = \left(\frac{g}{C\upsilon A_s^2} \right) \theta_s^3 \tag{2.2}$$

where

g = gravity acceleration

υ = kinematic viscosity

A_S = solid surface area

C = flow configuration constant

Irmay (1954) generalizes Equation 2.2 to represent flow through unsaturated porous media. Since the actual values of A_S and C are impossible to accurately determine, Irmay suggests that K_S act as a substitute for A_S and C. This yields:

$$K_r = S_e^3$$

Brooks and Corey (1964) observe that Averjanov's relationship seems to agree over a larger variety of soils than Irmay. From the above equations, one can obviously see that slightly different interpretations in the flow conditions leads to significant differences in

the equation exponents. This indicates that K values may be influenced by the flow conditions.

Mualem (1978) makes an interesting modification to the macroscopic concept by choosing a slightly different approach. Once again, a general power relationship is assumed:

$$K_r = S_e^n$$

where

n = a soil parameter

Mualem attempts to determine the value of n by matching the equation to experimental data for 50 different soils. No single optimal value for n is found. Instead the analysis indicates that a large range of possible values for n exists. Values for n span a lower limit of 2.5 to a fairly high value of 24.5 for fine textured soils. Instead of fixing the exponent n as a constant, Mualem defines it as a soil water characteristic parameter.

Statistical analysis of the retention data obtained from the 50 soils exhibit a correlation between the soil parameter, n, and the energy associated with the wilting point, w:

$$w = \int_{\theta_r}^{\theta_s} \gamma_w \psi d\theta$$

where

w = the energy required to drain a unit bulk volume from saturation to the wilting point at ψ = -15000 cm

γ_w = the specific weight

Using available moisture retention data, Mualem plots n versus w and derives an empirical linear relationship between these parameters:

$$n = 3.0 + 0.015\, w$$

Mualem tests this model and finds good agreement between the measured and predicted conductivity values.

2.4 Pore Connectivity Models

Pore connectivity based models relate unsaturated hydraulic conductivity to moisture retention and saturated conductivity measurements through statistical analysis of the pore size distribution. The purpose of these models is to predict the conductivity curve from measured moisture retention and saturated conductivity data. No actual measurements of unsaturated conductivity are necessary.

Models in this category regard the porous medium as a set of randomly distributed, interconnected pores. The moisture retention curve is viewed as the pore radii distribution function. Flow in the porous media is controlled by the statistical probability of the random pores connecting. Models primarily differ in their interpretation of the pore geometry and the estimate of its contribution to total permeability. Models either regard the pores as a bundle of capillaries or as random connections located at a rejoined cross section.

2.4.1 Capillary Tube Models

Purcell (1949) models the pores in soil as a bundle of parallel, straight capillary tubes. Gates and Lietz (1950) apply the Purcell theory and establish the following relationship between conductivity, capillary tension, and moisture content:

$$K_r(\theta) = \frac{\int_0^{\theta} \frac{d\theta}{\psi^2}}{\int_0^{\theta_{sat}} \frac{d\theta}{\psi^2}}$$

Fatt and Dykstra (1951) modify the above equation by accounting for tortuosity in the flow path:

$$K_r(\theta) = \frac{\int_0^{\theta} \frac{d\theta}{\psi^{2+b}}}{\int_0^{\theta_{sat}} \frac{d\theta}{\psi^{2+b}}}$$

The tortuosity factor, b, varies for different soil types.

Burdine (1953) also modifies Gates and Lietz, but use a different tortuosity relationship. The tortuosity correction factor selected is the square of the effective saturation.

$$K_r(\theta) = S_e^2 \frac{\int_0^{\theta} \frac{d\theta}{\psi^2}}{\int_0^{\theta_{sat}} \frac{d\theta}{\psi^2}} \tag{2.3}$$

Burdine applies the same capillary model to derive a complimentary relationship for the nonwetting fluid, K_{rnw},

$$K_{rnw}(\theta) = (1 - S_e)^2 \frac{\int_0^{\theta} \frac{d\theta}{\psi^2}}{\int_0^{\theta_{sat}} \frac{d\theta}{\psi^2}} \tag{2.4}$$

Experimental results show good agreement between measured and predicted values using the Burdine relationships.

2.4.2 Rejoined Cross Section Models

Childs and Collis-George (1950) model flow through a porous medium as flow through varying pore sizes that are randomly connected at a rejoined interface. The flow is controlled by the smaller of the two connecting pores in the sequence. Only pores in direct

sequence contribute to the overall conductivity. Only a single connection exists between the pores. Various other investigators (Millington and Quirk, 1961; Jackson et al., 1965; and so forth) have tested this theory and have modified it.

Wyllie and Gardner (1958) simplify this theory by assuming that the porous medium is made up of randomly joined thin layers traversed by parallel capillary tubes. The flow is controlled by the interface between the layers.

Mualem (1976) applies the Childs and Collis-George theory and arrives at the following relationship:

$$K_r(\theta) = S_e^n \left[\frac{\int_0^{\theta} \frac{d\theta}{\psi}}{\int_0^{\theta_{sat}} \frac{d\theta}{\psi}} \right]^2 \qquad (2.5)$$

Mualem tests this relationship on 45 soils and concludes that the optimal value for n is 0.5.

2.5 Coupled Moisture Retention and Unsaturated Conductivity Models

This section reviews four coupled moisture retention/unsaturated conductivity models. These models propose a mathematical equation for the moisture retention curve, apply the equation to a pore connectivity model, and then provide a closed form analytical solution relating the unsaturated conductivity to moisture retention and saturated conductivity. The advantage of these models is that they can predict the unsaturated conductivity from more easily measured moisture retention and saturated conductivity values. This thesis will focus on how well the Brooks & Corey, Campbell, and van Genuchten models can predict unsaturated conductivity. The Russo model is also analyzed, but the data available for this model are limited.

2.5.1 Brooks & Corey

Brooks & Corey (1964) characterize the moisture retention curve as a power law relationship:

$$S_e = \left(\frac{\psi_b}{\psi}\right)^{\lambda} \qquad \text{for} \qquad \psi \geq \psi_b \tag{2.6}$$

where

λ = pore size distribution index

ψ_b = capillary tension at the bubbling pressure

The bubbling pressure is related to the maximum pore size forming a continuous network of flow channels within the porous medium. Brooks & Corey (1964) substitute their moisture retention equation into Equations 2.3 and 2.4, resulting in an explicit equation relating the moisture retention and saturated conductivity to the unsaturated conductivity. Solutions for both the wetting and nonwetting phase are derived. The wetting phase relationships are:

$$K_r = (S_e)^{\frac{2+3\lambda}{\lambda}} \tag{2.7}$$

for $\psi \geq \psi_b$

$$K_r = \left(\frac{\psi_b}{\psi}\right)^{2+3\lambda} \tag{2.8}$$

The nonwetting relationships are:

$$K_{rnw} = (1 - S_e)^2 \left(1 - S_e^{\frac{2+\lambda}{\lambda}}\right) \tag{2.9}$$

for $\psi \geq \psi_b$

$$K_{rnw} = \left[1 - \left(\frac{\psi_b}{\psi}\right)^{\lambda}\right]^2 \left[1 - \left(\frac{\psi_b}{\psi}\right)^{2+\lambda}\right] \tag{2.10}$$

2.5.2 Campbell

Campbell (1974) represents the moisture retention curve by

$$\psi = \psi_e \left(\frac{\theta}{\theta_s} \right)^{-b} \tag{2.11}$$

where

ψ_e = the air entry water potential

b = an empirically determined constant

The Campbell equation differs from Brooks & Corey. First, Campbell assumes that there is no residual moisture content. Second, the Campbell equation is valid for values of tension below the bubbling pressure.

Campbell applies the Childs and Collis-George model and derives a conductivity retention relationship for the wetting phase only.

$$K_r = \left(\frac{\theta}{\theta_s} \right)^{2b+3} \tag{2.12}$$

$$K_r = \left(\frac{\psi_e}{\psi} \right)^{2+\frac{2}{b}} \tag{2.13}$$

Near saturation, Equation 2.11 faces a sharp discontinuity. This break in the retention curve is a result of the gradual entry of air near the saturation region. Clapp and Hornberger (1978) suggest a modification to the moisture retention equation to account for this discontinuity. At the inflection point (S_i , ψ_i) of the moisture retention curve near saturation, Equation 2.11 is replaced by a parabolic expression

$$\psi = -m(S-n)(S-1) \qquad \text{for} \qquad S_i \le S \le 1 \tag{2.14}$$

where

$$S = \left(\frac{\theta}{\theta_s}\right)$$

$$m = \frac{\psi_i}{(1-S_i)^2} - \frac{\psi_i b}{S_i(1-S_i)}$$

$$n = 2S_i - \left(\frac{\psi_i b}{mS_i}\right) - 1$$

Equation 2.14 passes through the point (S_i , ψ_i) and (1,0) and the derivative, $d\psi/dS$, of both Equations 2.11 and 2.14 are equal at the inflection point.

2.5.3 Russo/Gardner

Russo (1988) assumes that the relationship between conductivity and capillary pressure follows the Gardner exponential model (Equation 2.1). An accompanying equation for the moisture retention curve is derived by selecting Gardner's conductivity relationship as a closed form solution to Mualem's model (Equation 2.5) and backing out a relationship between saturation and capillary tension.

$$S_e = \left(e^{-0.5\alpha\psi}(1+0.5\alpha\psi)\right)^{\frac{2}{(m+2)}} \qquad (2.15)$$

where

α = the Gardner empirical parameter

m = $2n$ (n is an empirical parameter in Mualem's model)

2.5.4 van Genuchten

van Genuchten (1980) represents the moisture retention curve with

$$S_e = \left[\frac{1}{1+(\alpha\psi)^n}\right]^m \qquad (2.16)$$

where

α, n, m = empirical parameters

van Genuchten substitutes this equation into Mualem's model (Equation 2.5) and solves. A closed form analytical solution is obtained when the constraint m = 1 - 1/*n* is imposed. Solutions for the wetting phase are derived:

$$K_r = S_e^{\frac{1}{2}}\left[1-\left(1-S_e^{\frac{1}{m}}\right)^m\right]^2 \qquad (2.17)$$

when $m = 1-\frac{1}{n}$

$$K_r = \frac{\left\{1-(\alpha\psi)^{n-1}\left[1+(\alpha\psi)^n\right]^{-m}\right\}^2}{\left[1+(\alpha\psi)^n\right]^{\frac{m}{2}}} \qquad (2.18)$$

Parker et al. (1987) derive the nonwetting solution:

$$K_{rnw} = (1-S_e)^{\frac{1}{2}}\left[\left(1-S_e^{\frac{1}{m}}\right)^m\right]^2 \qquad (2.19)$$

van Genuchten also derives relationships between the conductivity and the moisture retention using Burdine's theory (Equation 2.4).

$$K_r = (S_e)^2\left[1-\left(1-S_e^{\frac{1}{m}}\right)^m\right] \qquad (2.20)$$

when $m = 1-\frac{2}{n}$

$$K_r = \frac{1-(\alpha\psi)^{n-2}\left[1+(\alpha\psi)^n\right]^{-m}}{\left[1+(\alpha\psi)^n\right]^{2m}} \qquad (2.21)$$

Demond and Roberts (1993) derive the nonwetting counterpart

$$K_{rnw} = (1 - S_e)^2 \left[\left(1 - S_e^{\frac{1}{m}} \right)^m \right] \qquad (2.22)$$

At high tension, where $(\alpha\psi)^n >> 1$, the van Genuchten/Burdine combination becomes the Brooks & Corey model. Since we are already evaluating the Brooks & Corey model, our analysis of the van Genuchten model will focus only on the van Genuchten/Mualem predictive equations.

Chapter 3

Curve Fitting Methodology

This chapter describes the curve fitting technique applied to generate the moisture retention parameters used in predicting the unsaturated hydraulic conductivity. The first section discusses the use of a nonlinear optimization procedure, its key parameters, and the initial values used for the parameters. The second section presents the model calibration process. The third section details the procedure used to select valid data points for the Brooks & Corey model.

3.1 Curve Fitting Technique

The data analysis/graphics application program KaleidaGraph™ provided the analytical means to evaluate the moisture retention data and produce the optimal values for the fitting parameters. The general curve fit function in KaleidaGraph™ allows the user to define a general form equation and its determining parameters. The program then applies a nonlinear least-squares optimization procedure to the data values and generates the optimal parameter values for the user defined equation. The nonlinear least-squares optimization is

performed using the Levenberg-Marquardt algorithm. This program presents a powerful and effective technique for performing data analysis.

3.1.1 Nonlinear Optimization Function

As mentioned in Chapter 2, our assessment of two phase flow characterization of soils will focus on four coupled moisture retention/unsaturated hydraulic conductivity models. We are interested in how well these models can predict unsaturated hydraulic conductivity using only moisture retention data. The models are the Brooks & Corey/Burdine model, the Campbell model, the Russo/Gardner model, and the van Genuchten/Mualem model (with $m = 1 - 1/n$).

The analysis focuses on the low moisture content region of the moisture retention curve. We are primarily interested in the ability of these predictive models to accurately assess the unsaturated hydraulic conductivity of the vadose zone in an aquifer. Typical moisture contents found in the vadose zone are in the low moisture regime of the moisture retention curve. This regime is characterized by low unsaturated hydraulic conductivity.

Selecting the form of the defining equation in our general curve fit will affect the optimization process. If we define the moisture retention equation in terms of $\theta(\psi)$ and optimize on a linear scale, we lose resolution of the moisture retention curve at low moisture contents (Figure 3.1). The residual moisture content for sand and other coarse soils is typically just a few percent of the saturated water content. By using a linear scale to optimize θ, the low moisture content values might simply be relegated as error. This will result in an inaccurate value for the residual water content. Stephens et al. (1985) show that the value of the residual moisture content has a significant influence on the shape of the predicted hydraulic conductivity curve near the low conductivity region (Figure 3.2). Thus, this form of the moisture retention equation does not meet our needs.

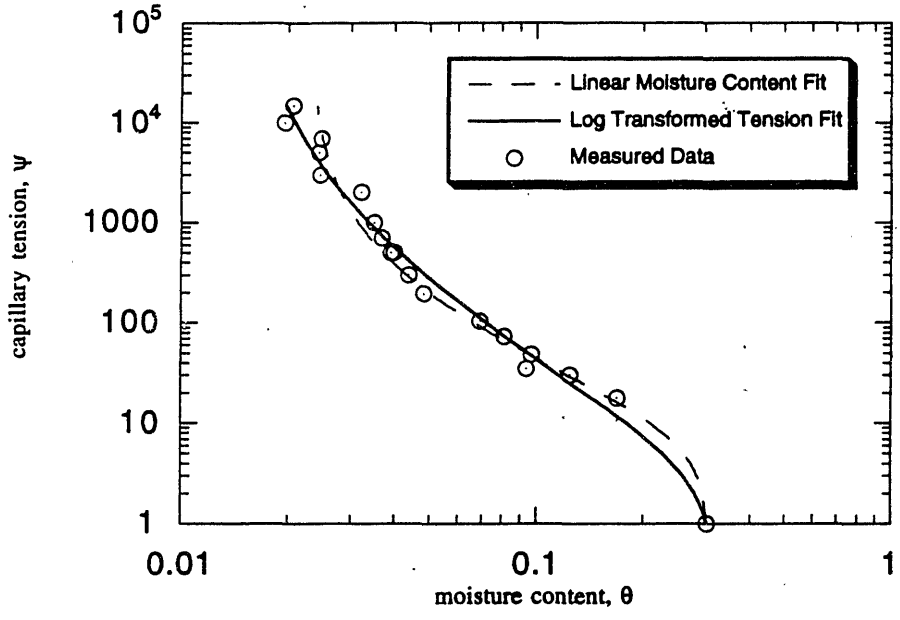

Figure 3.1: Comparison of Moisture Retention Fits Obtained with $\theta(\psi)$ and $\log\psi(\theta)$.

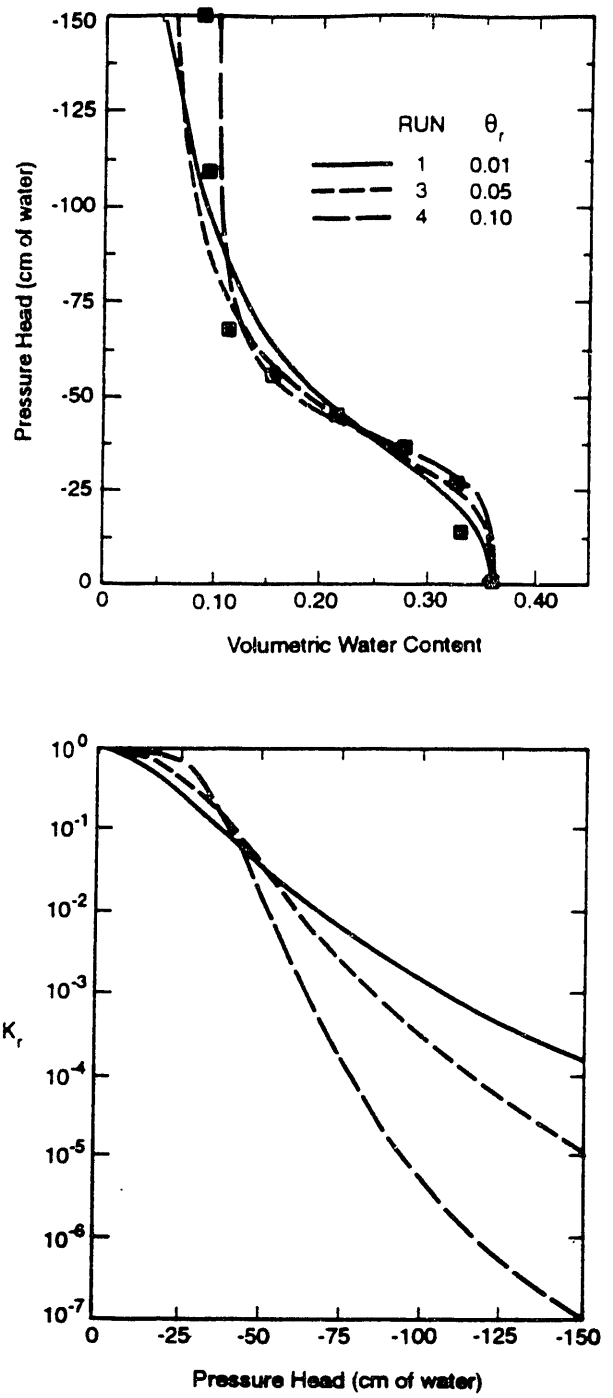

Figure 3.2: Sensitivity of Calculated Hydraulic Conductivity to Residual Moisture Content in Uniform Sand. (From Stephens et al., 1985)

Defining the moisture retention equation in terms of $\psi(\theta)$ enables the optimization process to emphasize the high tension/low moisture content region. This meets our primary objective of highlighting the low moisture content region. However, in doing so, it tends to neglect the fit near the low tension/high moisture content region. On a linear scale, the measured tension data span up to four orders of magnitude. This wide range of values makes it difficult to accurately optimize the retention curve at low tension values.

Selection of a logarithmically transformed scale for $\psi(\theta)$ allows us to emphasize the low moisture content range, yet still provide a reasonable fit in the high moisture content region (Figure 3.1). By implementing the log transformed scale, tension values are reduced to the same order of magnitude. The curve fit procedure minimizes the relative error between data points on a log scale as oppose to minimizing the absolute error on a linear scale. The error values will be more uniform over the entire range of tension and will provide a more accurate representation of the data.

The following form of the moisture retention equation for each model is used in the optimization procedure:

Brooks & Corey

$$\log \psi = \log \psi_b - \left(\frac{1}{\lambda}\right)\log\left(\frac{\theta - \theta_r}{\theta_s - \theta_r}\right) \qquad \text{for} \quad \psi \geq \psi_b \qquad (3.1)$$

Campbell

$$\log \psi = \log \psi_e - b\log\left(\frac{\theta}{\theta_s}\right) \qquad (3.2)$$

Russo

$$\log\theta = \log\left[\theta_r + (\theta_s - \theta_r)\left(e^{-0.5\alpha\psi}(1+0.5\alpha\psi)\right)^{\frac{2}{m+2}}\right] \tag{3.3}$$

van Genuchten

$$\log\psi = \frac{\left(\left(\frac{\theta-\theta_r}{\theta_s-\theta_r}\right)^{\frac{-1}{m}} - 1\right)^{\frac{1}{n}}}{\alpha} \tag{3.4}$$

The KaleidaGraph™ general curve fit employs a nonlinear least-squares optimization procedure to minimize an objective function. For the Brooks & Corey, Campbell, and van Genuchten models, the objective function, O(b), has the general form:

$$O(b) = \sum_{i=1}^{N}\left\{w_i\left[\log\psi_i - \hat{\log}\,\psi_i(b)\right]\right\}^2 \tag{3.5}$$

where

N	=	the number of moisture retention data in the sample
w_i	=	weighting coefficients for a single data value
$\log\psi_i$	=	the log of the measured tension value
$\hat{\log}\,\psi_i(b)$	=	the log of the calculated tension value
b	=	the model parameter vector

The Russo/Gardner model objective function has the form:

$$O(b) = \sum_{i=1}^{N}\left\{w_i\left[\log\theta_i - \hat{\log}\,\theta_i(b)\right]\right\}^2 \tag{3.6}$$

where

N	=	the number of moisture retention data in the sample
w_i	=	weighting coefficients for a single data value
$\log \theta_i$	=	the log of the measured content value
$\hat{\log} \theta_i(b)$	=	the log of the calculated water content value
b	=	the model parameter vector

The weighting coefficient is used to place more or less weight on a single data value based on a priori information regarding the reliability of the data point. In all of our analyses, the weighting coefficient was set to unity.

The model parameter vector, b, contains the unknown coefficients in our general equation. In the nonlinear least-squares optimization process, the parameters are adjusted until a local minimum value of squared error is found. A more detailed discussion of the model parameters is presented in a later section.

All algorithms and equations used in the calculation of the general curve fit can be found in the book *Numerical Recipes in C* by William H. Press, Brian P. Flannery, Saul A. Teukolsky, William T. Vetterling, Cambridge University Press (KaleidaGraph™ reference guide).

3.1.2 Optimization Output

Once the curve fit optimization is finished, KaleidaGraph™ generates a fitted curve through the data points and displays an output box that contains the optimized equation parameters (Figure 3.3). In addition to the parameter values and its associated error, the box also shows the initial estimates for the parameters, the sum of the squared errors, χ^2, and the value of either R or R^2. The sum of the squared error is calculated using the general form:

KaleidaGraph Parameters		
y = vg(0.01, 1.5,.01,.32)		
	Value	Error
θ_r	0.014573	0.0017608
n	1.4781	0.046843
a	0.32462	0.13338
θ_s	0.31993	0.013818
Chisq	0.35178	NA
R	0.99175	NA

Figure 3.3: Typical Optimized Parameter Output Box Displayed by KaleidaGraph™ for a General Curve Fit.

$$\chi^2 = \sum_i^N \left(\frac{y_i - f(x_i)}{\sigma_i} \right)^2$$

where

y_i = the measured value

$f(x_i)$ = the calculated value

σ_i = the weight

In our analysis, the value of the weight is set at unity.

3.1.3 Model Parameters

The model parameters for the moisture retention curve varies from model to model. Table 3.1 lists the parameters allowed for each model.

Model	Parameters
Brooks & Corey	θ_r, λ, Ψ_b
Campbell	Ψ_e, b
Russo	θ_r, θ_s, m, α
van Genuchten	θ_r, θ_s, n, m, α

Table 3.1: Summary of Parameters Allowed for Each Model.
(Note: The parameters m and α are not the same between the Russo and van Genuchten models)

In the van Genuchten analysis, the restricted case where $m = 1 - 1/n$ is selected because it provides a simple, closed form analytical expression for the unsaturated hydraulic conductivity. Hence, m is no longer a parameter in our optimization process for the van Genuchten model.

In some instances, the parameter θ_S in the Russo and van Genuchten models is set equal to the measured soil porosity. Selecting a fixed value of θ_S is desirable when there is insufficient data on the moisture retention curve to define a reasonable value. In the situation where we have a well defined moisture retention curve, choosing θ_S as an optimized parameter for the van Genuchten model will result in a more accurate definition of the sharp downturn in the moisture retention curve near the saturation region. In general, KaleidaGraph™ was allowed to determine the optimal value of θ_S whenever possible. Figure 3.4 illustrates the noticeable difference in the moisture retention fit acquired for the Hanford soil sample 0-072 with different θ_S constraints.

Modifications to the parameter are necessary for ill defined moisture retention curves. For some data sets, the values of θ_r or θ_S had to be defined. The optimized values for these data sets did not provide reasonable values for these parameters. Negative values of θ_r and values of θ_S greater than unity are obtained in these cases. The following chapter indicates the data sets that require modifications to the parameters.

3.1.4 Initial Parameter Estimates

The nonlinear optimization process requires the user to specify initial estimates of the parameter values. These initial guesses are used to generate the optimal parameter values. It is crucial that reasonable expected values of the parameters are specified. Initial values are chosen from suggested values found in recent literature (Khaleel et. al, 1995 and Russo, 1988). The initial values vary from soil to soil. Different initial values for θ_r and α are chosen depending on its textural classification. Compared to finer soils such as the silts, sands generally have smaller initial guesses. For the soils where the moisture retention curves were ill defined near the residual water content, values of θ_r close to its

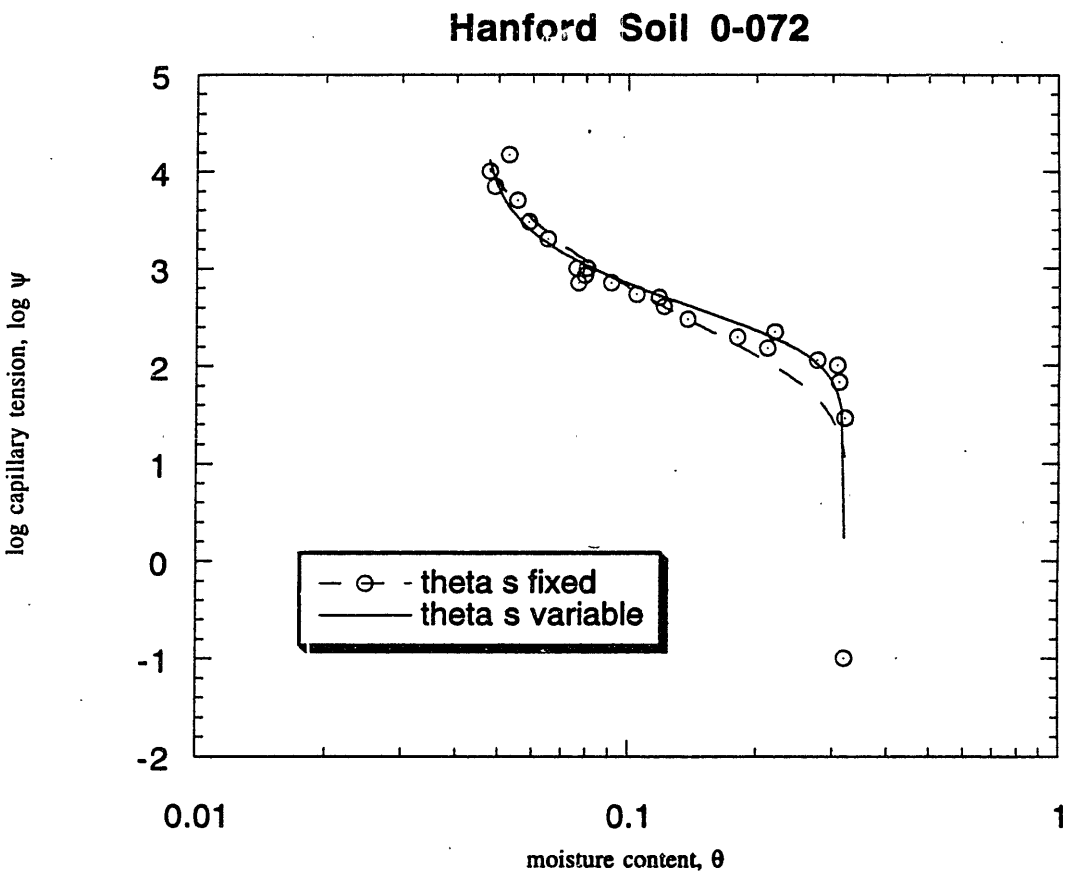

Figure 3.4: Comparison of the Moisture Retention Fit Obtained Using Different Constraints on θ_S.

Models	Initial Parameter Estimates
Brooks & Corey	θ_r (sand) = 0.01
	θ_r (silt) = 0.1
	λ = 0.1
	ψ_b = 1
Campbell	ψ_e = 1
	b = 0.1
Russo	θ_r = 0.01
	θ_s = porosity
	m = 1
	α = 1
van Genuchten	θ_r (sand) = 0.01
	θ_r (silt) = 0.1
	θ_s = porosity
	n = 1.5
	α (sand) = 0.001
	α (silt) = 0.01

Table 3.2: Initial Parameter Estimates

last measured moisture content value are selected. Table 3.2 lists the initial values generally used for each model.

3.1.5 Sensitivity of Initial Parameter Estimates

To test the sensitivity of the optimization process to the initial parameter estimates, the fitting procedure is performed on the same sample for different initial values (Figure 3.5). For well defined moisture retention curves, the difference is negligible. For ill defined moisture retention curves, the resulting values for θ_r or θ_s are arguably much more sensitive to the initial specified values. In these cases, the initial value for θ_r is either visually estimated from the moisture retention graph or fixed at a value deemed reasonable for a similar soil texture. An initial guess for θ_s near porosity is usually sufficient to produce a reasonable value for θ_s. In a few cases, the parameter θ_s had to be fixed.

3.2 Model Calibration

Khaleel et al. (1995) uses the computer program RETC (Leij et al., 1991) to evaluate the performance of the van Genuchten model for the Hanford soils. RETC is a nonlinear, least squares curve fitting procedure that optimizes specified model parameters for nonlinear equations with multiple parameters. Our analysis uses the program KaleidaGraph™ in place of RETC.

Russo (1988) derives the Russo/Gardner model and fits it to two distinct soils, one hypothetical and one actual. The following sections illustrate the differences between our curve fitting procedure and those employed by Khaleel and Russo.

Hanford 2-1636
van Genuchten Curve Fit

y = vg(.018,1.7080,.1385,.30)		
	Value	Error
θ_r	0.014573	0.0017608
n	1.4781	0.046843
α	0.32462	0.13338
θ_s	0.31993	0.013817
Chisq	0.35178	NA
R	0.99175	NA

y = vg(0.01, 1.5,.01,.32)		
	Value	Error
θ_r	0.014573	0.0017608
n	1.4781	0.046843
α	0.32462	0.13338
θ_s	0.31993	0.013818
Chisq	0.35178	NA
R	0.99175	NA

Figure 3.5: Comparison of Estimated Parameter Values for Hanford Sample 2-1636 Using Different Initial Parameter Values.

3.2.1 RETC

RETC is a versatile computer program capable of finding the optimal parameters for the van Genuchten and Brook & Corey models under varying parameter constraints. The program allows the model parameters to be determined by using only moisture retention data or both measured moisture retention data and unsaturated conductivity data. RETC optimizes an alternate form of the van Genuchten equation:

$$\theta = \theta_r + \frac{(\theta_s - \theta_r)}{\left[1 + (\alpha\psi)^n\right]^m}$$

with the objective function

$$O(b) = \sum_{i=1}^{N}\left\{w_i\left[\theta_i - \hat{\theta}_i(b)\right]\right\}^2 + \sum_{i=N+1}^{M}\left\{W_1 W_2 w_i\left[Y_i - \hat{Y}_i(b)\right]\right\}^2$$

where

θ_i	=	the measured moisture content
$\hat{\theta}_i$	=	the calculated moisture content
Y_i	=	the measured unsaturated hydraulic conductivities
$\hat{Y}_i$	=	the calculated unsaturated hydraulic conductivities
b	=	the parameter vector
N	=	the number of moisture retention data
M	=	total number of measured data (retention and conductivity)
W_1, W_2	=	weighing factor between retention and conductivity data
w_i	=	weighing factor for a single data point

The RETC objective function optimizes $\theta(\psi)$, whereas the defined KaleidaGraph™ objective function (Equation 3.5) optimizes log $\psi(\theta)$. Use of different objective functions results in slightly different calculated parameter values. Figure 3.6 shows the optimized

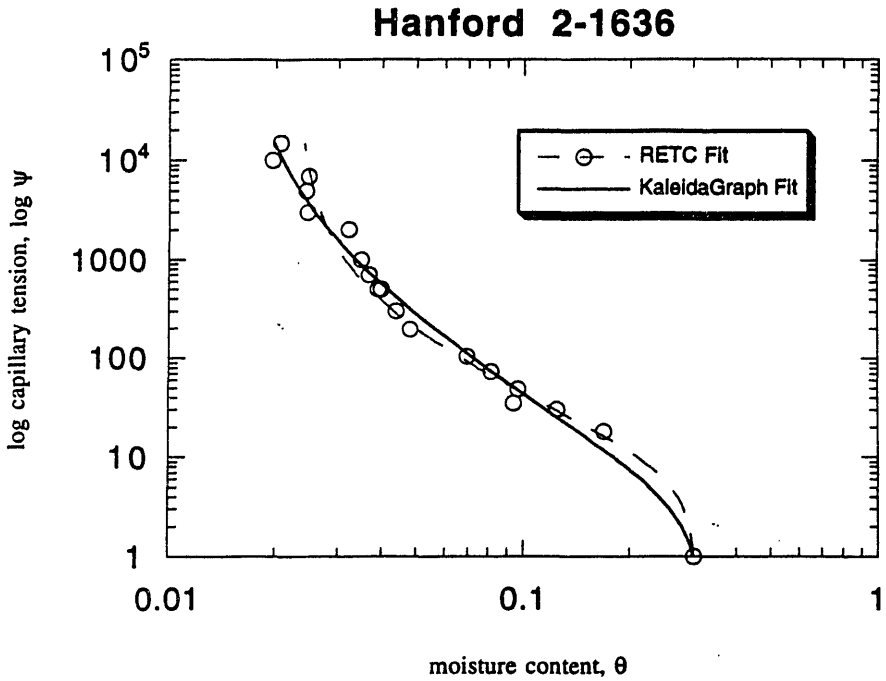

KaleidaGraph Parameters		
	Value	Error
θ_r	0.014573	0.0017608
n	1.4781	0.046843
α	0.32462	0.13338
θ_s	0.31993	0.013818
Chisq	0.35178	NA
R	0.99175	NA

RETC Parameters		
	Value	Error
θ_r	0.022871	0.0030328
n	1.7077	0.073383
α	0.13854	0.022656
θ_s	0.30735	0.0067038
Chisq	0.0005718	NA
R^2	0.99339	NA

Figure 3.6: Comparison of KaleidaGraph™ and RETC Generated Curve Fits for Hanford Sample 2-1636 Using Different Objective Functions.

parameters generated by the two varying functions for the Hanford sample 2-1636. Parameter values for the RETC curve fit are taken from Khaleel et al. (1995).

The van Genuchten parameters generated by the two methods differ slightly. The parameters vary because the emphasis of the governing equations differ. The KaleidaGraph™ analysis focuses on the low moisture content region by optimizing with respect to log ψ. RETC optimizes θ, thus concentrating on the high moisture content region. The difference in regional emphasis is apparent in Figure 3.6.

To compare the optimization ability of KaleidaGraph™ against RETC, the RETC objective function is entered into KaleidaGraph™ and a fitted curve is generated for Hanford sample 2-1636. Results from this test present a form of model calibration. If KaleidaGraph™ is comparable to RETC, the generated parameter values should be the same. RETC parameter values are taken from Khaleel et al. (1995). As seen in Table 3.3, the optimized parameter values are essentially the same.

3.2.2 Russo/Gardner

To calibrate the Russo model, data for the Parker silt loam soil is read off the graph in Russo (1988). An optimization is then performed on the measured data using Equations 3.3 and 3.6. The purpose of this analysis is to replicate Russo's parameter values for this soil. Table 3.4 compares the KaleidaGraph™ generated results versus the Russo values found in the literature. As seen in Figure 3.7, the fitted curve does not accurately represent the measured data. Significantly different parameter values are generated in our optimization process. Results vary because Russo uses additional data to constrain the parameter search. Russo's objective function is :

$$O(b) = \sum_{i=1}^{N} \left\{ w_i \left[Q(t_j) - \hat{Q}(t_j, b) \right] \right\}^2 + \left\{ v \left[\theta(h_{15}) - \hat{\theta}(h_{15}, b) \right] \right\}^2$$

Parameter	KaleidaGraph™	RETC
θ_r	0.022871	0.023
n	1.7077	1.7080
α	0.13854	0.1385
θ_s	0.30735	0.3073

Table 3.3: Comparison of KaleidaGraph™ and RETC Generated Parameter Values Using the Same Objective Function.

Parameter	KaleidaGraph™	Russo
θ_r	0.16136	0.186
α (m^{-1})	2.128	4.995
m	571.88	0.021

Table 3.4: Comparison of KaleidaGraph™ and Russo Parameter Values

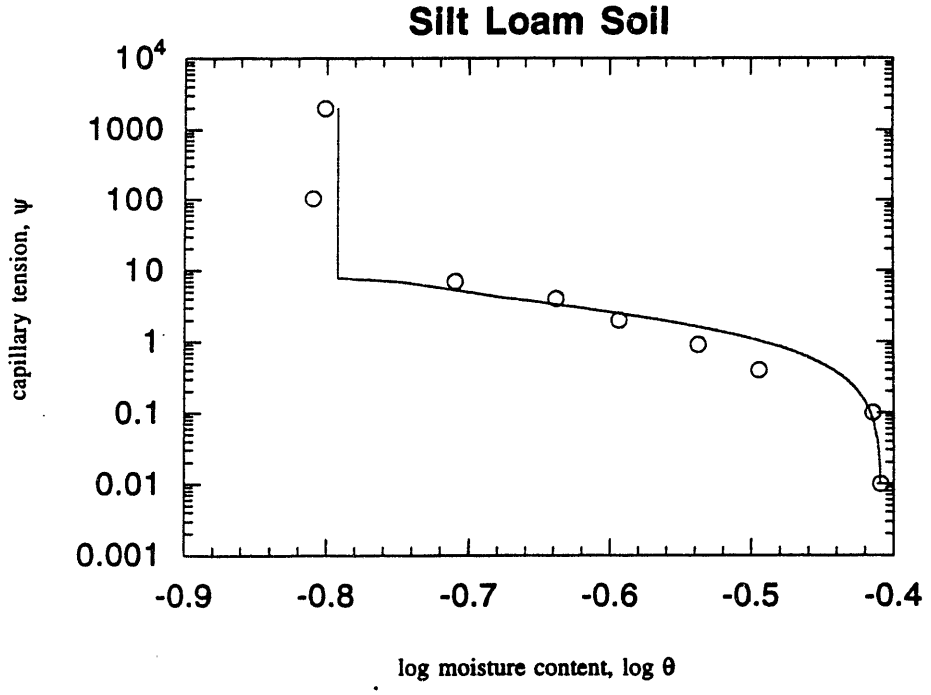

Russo Parameters		
	Value	Error
θ_r	0.16136	0.010189
α	212.8	0.10933
m	571.88	113.66
Chisq	0.0091334	NA
R^2	0.95035	NA

Figure 3.7: KaleidaGraph™ Generated Curve Fit for Parker Silt Loam Using the Russo Model.

where

$Q(t_j)$ = the set of cumulative outflow measurements at specified times t_j

$\hat{Q}(t_j, b)$ = the numerically calculated value of the outflow corresponding to the trial vector of parameter values, b

$\theta(h_{15})$ = the measured moisture content at h = -15,000 cm H_2O

$\hat{\theta}(h_{15}, b)$ = the predicted moisture content at h = -15,000 cm H_2O

w_j = weighing factor

v = weighing factor

The parameter values from KaleidaGraph™ might have reproduced Russo's values if extra constraints had been added.

3.3 Data Validation Procedure for the Brooks & Corey Model

The Brooks & Corey moisture retention relationship was discovered by plotting log S_e as a function of log ψ. The resulting graph of the log transformed variables is a straight line with the negative slope, λ. The Brooks & Corey theory holds only for values of tension, ψ, greater than or equal to the tension at the bubbling pressure, ψ_b. In order to obtain a proper fit to the model, points near saturation that are below the bubbling pressure tension are not included in the curve fitting procedure.

Since the bubbling pressure tension and the residual water content are parameters in the optimization process, a graph of log S_e versus log ψ is not possible. A method used to select the relevant data points is devised. The curve fit will only select these validated data

points in determining the slope and bubbling pressure tension value. An assumption is made that θ_r is relatively small compared to the measured values of θ. A graph of log θ versus log ψ is generated to represent the graph of the log S_e versus log ψ. In accordance with the original Brooks & Corey method, a straight line is drawn through the data points. Any data point near saturation that deviates from the general linear trend is excluded from the curve fit. This procedure is used on the Hanford and INEL soils.

Chapter 4

Data Description

A total of 71 soil samples, supplied from seven data sets, is analyzed. The first section in this chapter details the criteria used to select the data sets. The second section briefly describes each data source, mentions the techniques used for data measurement, and discusses any modifications made to the curve fitting parameters.

The computer disk accompanying this thesis contains the measured values of moisture retention and unsaturated conductivity used in the analysis. All files are saved as Macintosh tab delineated text files. Each soil type has an individual file. The soil sample number is located in the first column of the file.

4.1 Data Selection Process

The primary purpose of the analysis is to assess the ability of these predictive models to accurately characterize the unsaturated conductivity in aquifer like materials. Typical aquifer materials consist of sandy, coarse soils. The relatively dry vadose zone located just above the saturated aquifer usually resides in the low moisture content region. Hence, data

sets emphasizing these properties are selected. The data consists primarily of measured moisture retention and unsaturated conductivity values obtained from sands and sandy loam material. The Hanford data set measures capillary tension up to extremely high values, thus giving a detailed picture of the low moisture content region.

A secondary purpose of the data selection process is to choose data sets that indicate some measure of consistency to the fitting process. Data sets that contain multiple samples from the same aquifer provide the repetition needed to search for consistent trends. All data samples in a single data set are measured by the same techniques and by the same individuals. Thus, differences between the soil samples cannot be attributed to differences in the measurement techniques. This gives us a good indication of the soil variability in aquifer soils. Soil samples from the same aquifer also represent a collection of similar soils of varying pore size distributions and saturated conductivity values.

4.2 Data Sources

This section provides a concise summary of the site description, the experimental procedures used to measure the data values, and the changes made to the curve fitting parameters. For more detailed information regarding the site characterization and measurement process for each site, the reader is advised to refer to the referenced papers. A thorough summary of current laboratory and in-situ field measurement techniques for moisture retention and hydraulic conductivity can be found in Hillel (1980) and Stephens (1996).

4.2.1 Cape Cod Data Set

Soil samples from this set are taken from a glacial aquifer located on Cape Cod, Massachusetts. The Cape Cod unconfined aquifer is a large sand and gravel outwash plain

that was deposited during the retreat of the continental ice sheets from southern New England about 12,000 years ago (LeBlanc et al., 1991). This aquifer is the primary source of freshwater for the inhabitants of Cape Cod and all its visitors. At present, the site is contaminated by several pollutant plumes which threaten the underlying aquifer. Extensive tests have been conducted on Cape Cod by the U. S. Geological Survey in an effort to characterize the site.

The upper region of the aquifer is characterized as medium to coarse sand with some gravel. Six data samples are provided by Mace (1994). The moisture retention data focuses on the high moisture content range. Values of θ range from 0.095 to 0.23. Insufficient data is supplied to accurately define the entire moisture retention curve. The sharp curves near the saturated water content and the residual water content could not be described. Hence, the model parameters θ_r and θ_s had to be fixed for all the models. The value of θ_s is set at the measured porosity and the value of θ_r is estimated at 0.01. This value of θ_r is consistent with the average values of θ_r calculated from the Hanford sands.

4.2.2 Hanford Data Set

The Hanford site is situated in the arid Columbia Basin located in the southeastern region of Washington state. It resides on the US. Department of Energy's Hanford site, approximately 35 km northwest of Richland, Washington. The surface soils were deposited during a series of catastrophic glacial floods, occurring as recent as 13,000 years ago (Khaleel et al., 1995). These glacial deposits principally consist of sands and gravels of miscellaneous sizes. Extensive tests have been performed at the Hanford site to measure moisture retention and unsaturated hydraulic conductivity at very low saturation values. Capillary tension values up to 15,000 cm are measured.

Sample	Coarse Sand (0.2 - 2 mm), %	Fine Sand (0.02 - 0.2 mm), %	Silt (0.002 - 0.02 mm), %	Clay (<0.002 mm), %	Median Grain Size (d_{50}), mm	SSHC Bulk Density (g/cm^3)	Centrifuge Bulk Density (g/cm^3)
1-1417	24	68	7	1	0.095	1.67	1.79
1-1419	90	10	0	0	0.55	1.64	1.63
2-1636	85	15	0	0	0.48	1.61	1.62
2-1637	80	20	0	0	0.33	1.60	1.65
2-1638	81	19	0	0	0.60	1.72	1.82
2-1639	93	7	0	0	0.70	1.60	1.64
2-2225	80	20	0	0	0.33	1.61	1.60
2-2226	95	5	0	0	1.00	1.68	1.67
2-2227	94	6	0	0	0.72	1.67	1.63
2-2228	98	2	0	0	0.90	1.62	1.62
2-2229	95	5	0	0	0.68	1.62	1.59
2-2230	34	52	11	3	0.10	1.71	1.74
2-2232	92	8	0	0	0.68	1.71	1.71
2-2233	92	8	0	0	0.68	1.64	1.64
2-2234	86	14	0	0	0.88	1.75	1.82
0-072	27	54	10	9	0.08	1.75	1.67
0-079	0	73	22	5	0.03	1.61	1.68
0-080	8	79	8	5	0.05	1.60	1.50
0-083	38	47	8	7	0.10	1.68	1.55
0-099	58	30	7	5	0.30	1.70	1.79
0-107	80	13	5	2	0.32	1.57	1.54
0-113	74	22	1	3	0.30	1.63	1.62

Table 4.1: Particle Size Distribution and Bulk Density for the Hanford Samples.

Data for twenty two repacked soil samples were provided by Raziuddin Khaleel of the Westinghouse Hanford Company. Table 4.1 lists the particle size distribution, the mean grain size, and the bulk density for each sample. Moisture retention data collected for the drainage cycle span such a wide range of values that two measurement techniques are required. Both the pressure cell method and the pressure plate extraction method are used. The first method measures capillary tension values up 1000 cm. The second method measures up to 15,000 cm. Saturated hydraulic conductivity is measured using a constant head permeameter. The unsaturated hydraulic conductivity is measured in the laboratory using two methods: the steady state head control method and the ultracentrifuge method.

The detailed moisture retention data provided supply a complete description of the moisture retention curves. No parameters are fixed and KaleidaGraph™ is able to optimize all the model parameters.

4.2.3 Idaho National Engineering Laboratory (INEL) Data Set

The Idaho National Engineering Laboratory (INEL) is located on the semi-arid eastern Snake River Plain in southeastern Idaho. The lab was established in 1949 as a facility to build, operate, and test nuclear reactors. In the southwest corner of INEL is the Radioactive Waste Management Complex (RWMC) which acts as a storage area for chemical, low level radioactive and transuranic radioactive wastes. The waste is stored in 55 gallon drums and buried in trenches excavated from the surface sediments.

The eastern Snake River Plain is a structural basin underlain by basaltic rock. The overlying surface sediments consist predominately of flood plain and wind blown deposits. In addition to INEL, the eastern Snake River Plain also houses one of the world's largest aquifers, the Snake River Plain aquifer. The water table is located 180 m beneath the surface soil in the underlying basaltic rock formation. In its natural state, the surface sediments consist of highly structured, aggregated soil. The undisturbed soil is

characterized as a distinctly layered, extremely variable soil containing macropores and a large degree of aggregated material.

Multiple tests were conducted to ascertain the physical and hydraulic characteristics of the surface sediments. A simulated waste trench was constructed to represent the RWMC trench used for radioactive waste storage. Tests were then performed on soil samples from the simulated waste trench and on soil samples from a nearby undisturbed area.

Moisture retention and unsaturated conductivity data are measured at four depths. Each depth contains four samples, two measurements from the disturbed soil (soil from the simulated trench) and two measurements from the undisturbed soil. The soils samples are labeled in the following format: u(a) 30 cm. This format translates into undisturbed soil sample *a* taken at the depth of 30 cm. A total of 16 soil samples at 4 measured depths is available. The moisture retention and conductivity data is provided by John Nimmo of the US. Geological Survey. Additional information regarding physical properties can be found in Shakofsky (1995).

The INEL soil is generally classified as a either a sandy silt or a clayey silt. The moisture retention data is determined using a modified pressure cell method. Saturated hydraulic conductivity is measured using the falling head method. Unsaturated hydraulic conductivity data is generated using the one-step outflow method.

The INEL moisture retention data emphasizes data in the high moisture content regime. Each moisture retention data set has only one low tension measurement near the 0.01 cm region. By including this point in our curve fitting analysis, we are in essence fixing the θ_S parameter at that measured water content. As seen in Figure 4.1(a), ill fitting moisture retention curves are obtained with the van Genuchten model.

One of the primary goals of this analysis is to allow the best fit possible for the moisture retention data using the selected models. In addition, the dominant area of interest

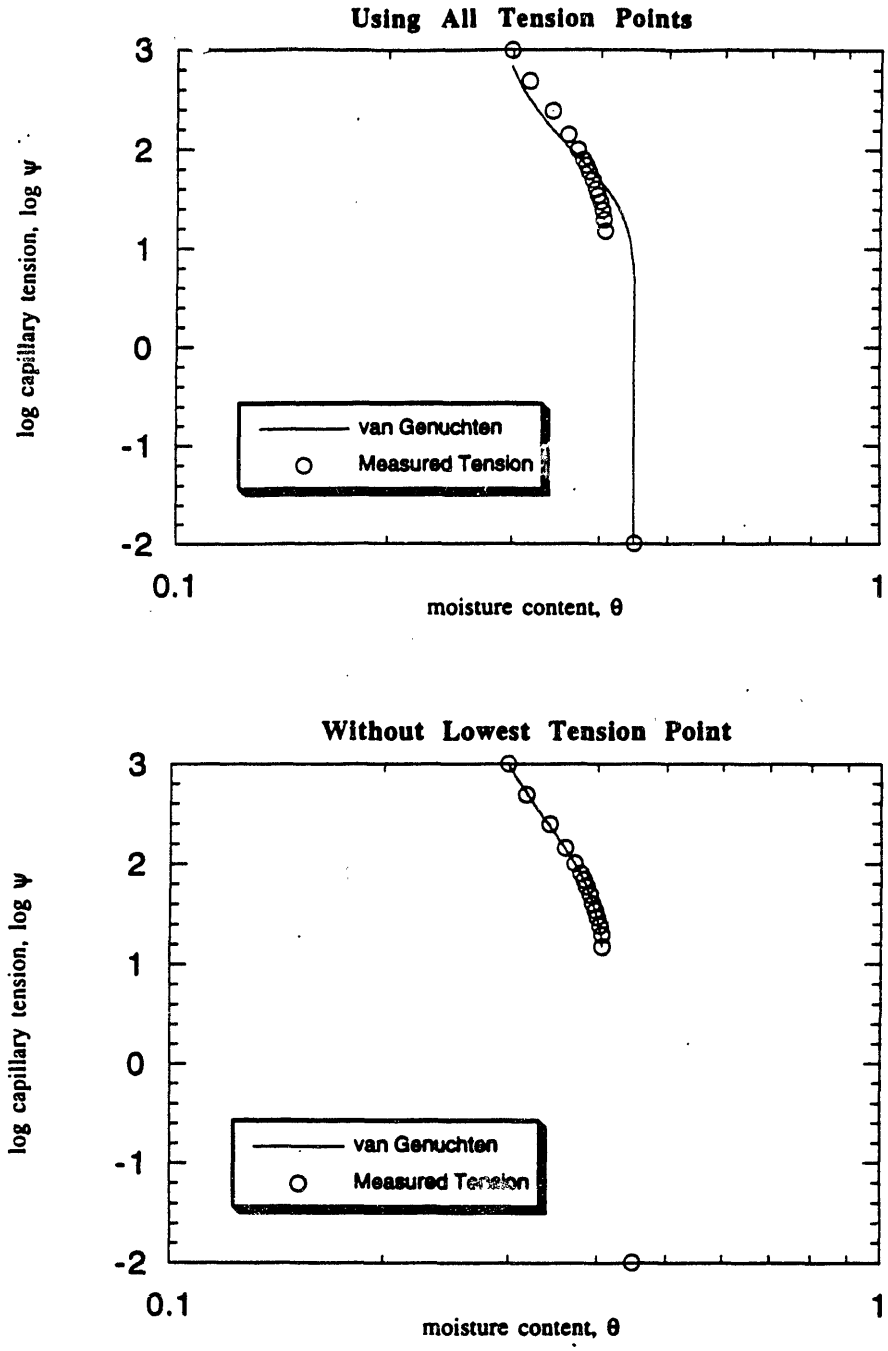

Figure 4.1: (a) Fitted Moisture Retention Curve for INEL Data Using All Tension Points (b) Fitted Moisture Retention Curve for INEL Data Without the Lowest Tension Point.

is at the low moisture content region where the unsaturated soil resides. Thus, the low tension point near the saturated water content is neglected in the optimization process of the van Genuchten model. Figure 4.1(b) illustrates the improved fit obtained by deleting this point. Once again, θ_S is an optimized parameter. A much better curve fit develops.

Two of the soils samples, namely u(b) 30 cm and u(b) 80 cm, produce negative values of θ_r. For these two cases, a value for θ_r is determined by looking at the moisture retention curve and estimating the value of θ_r at which the curve near the residual moisture content becomes vertical. The values chosen are close to the last measured value of the moisture retention. The resulting van Genuchten fits are acceptable (Figure 4.2).

In 3 soil samples, select moisture retention data points seemed to deviate from the general shape of the moisture retention curve (Figure 4.3). These points are regarded as measurement uncertainty and are discarded in the curve fitting process.

4.2.4 Las Cruces Data Set

The Las Cruces trench site is a 26.4 m long by 4.8 m wide by 6.0 m deep trench located on the New Mexico State University college ranch. It is approximately 40 km northeast of Las Cruces, New Mexico. The purpose behind constructing this experimental site was to provide undisturbed soil samples for soil property characterization. Multiple tests on the physical and hydraulic properties of the soil were performed. Analysis of the particle size distribution indicate that the soils are mainly sands, sandy loams, loamy sands, and sandy clay loams (Wierenga et al, 1991).

Of the many samples taken from the excavated trench, unsaturated hydraulic conductivity measurements are performed on 5 samples. The conductivity data for these samples are read off conductivity versus tension graphs provided by Peter Wierenga of the University of Arizona. Moisture retention and saturated conductivity values are obtained from the Las Cruces Trench Site Database located on the internet. The address is

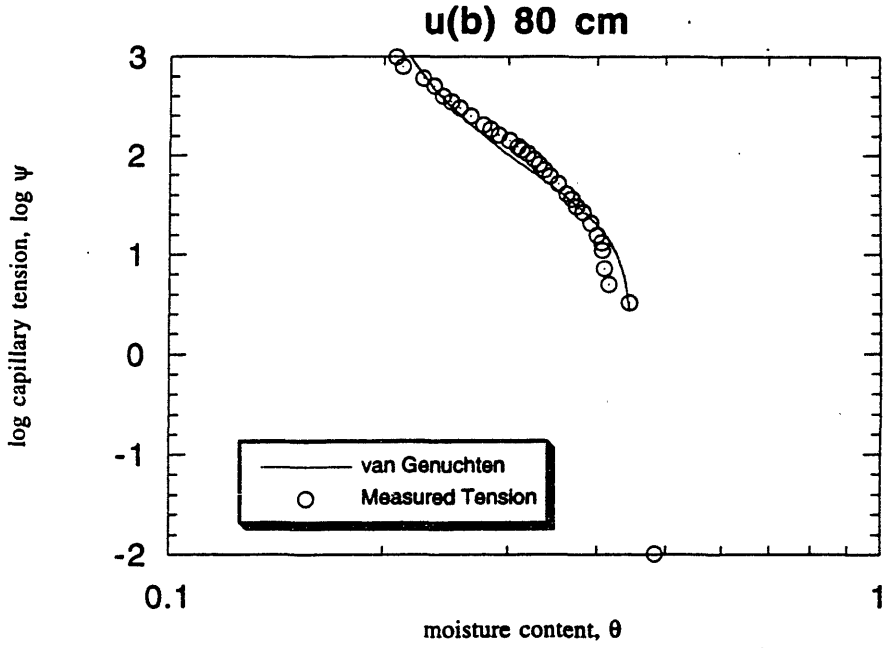

y = vg(.18,1.5,.01,.49)		
	Value	Error
n	1.5199	0.033581
α	0.042876	0.0058183
θ_s	0.44631	0.0021862
Chisq	0.71343	NA
R^2	0.94519	NA

Figure 4.2: van Genuchten Fitted Moisture Retention Curve for INEL Sample u(b) 80 cm.

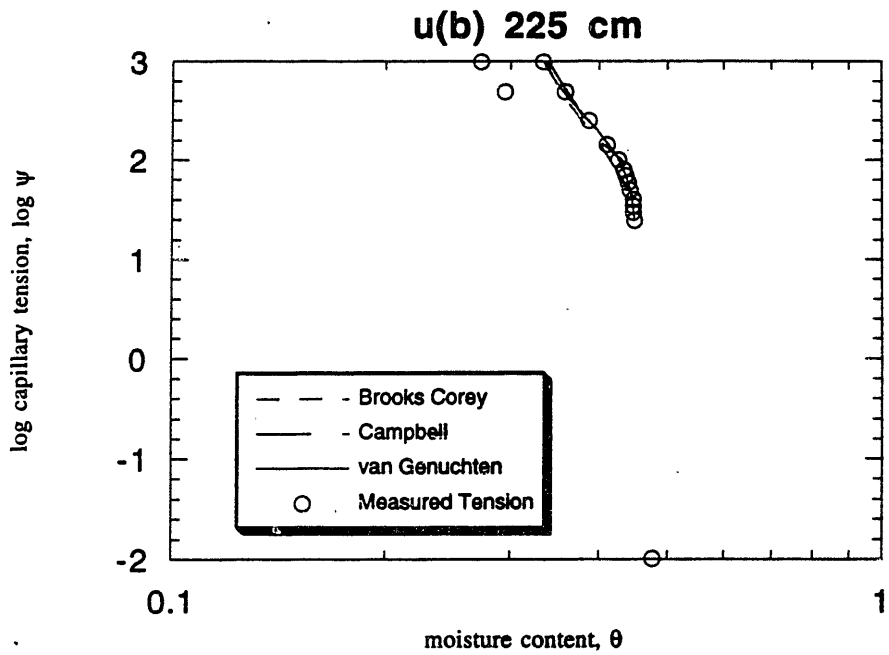

y = bc(.30044,.1,1,.45122)		
	Value	Error
λ	0.55632	0.045027
Ψ_h	76.218	8.6571
Chisq	0.022848	NA
R^2	0.97449	NA

y = camp(1,.1,.45122)		
	Value	Error
Ψ_e	37.44	3.6554
b	11.51	0.81923
Chisq	0.15002	NA
R^2	0.94722	NA

y = vg(0.27,1.5,.01,.48)		
	Value	Error
θ_r	0.30044	0.0088312
n	1.7724	0.096068
α	0.0068872	0.00025951
θ_s	0.45122	0.0006644
Chisq	0.0058463	NA
R^2	0.99794	NA

Figure 4.3: INEL Moisture Retention Curve Showing Deviation From General Shape.

ftp://meftp.nmsu.edu/pub/soils/. Additional moisture retention tests are also performed on the 5 soil samples. The values of these additional points are on moisture retention graphs supplied by Wierenga.

The unsaturated conductivity values are calculated by establishing a steady flow in the 3-inch cores and measuring the gradient at 1 cm from the inlet and 1 cm from the outlet with pressure transducers. Laboratory saturated hydraulic conductivity values are determined by a modified version of the outflow method. Moisture retention data is measured using a pressure cell method.

The moisture retention data from the soil samples contain the water content at zero tension. This point is excluded from the optimization process because the use of a logarithmically transformed scale did not permit a zero tension point. The data point immediately following the zero tension point is substantially lower in moisture content. Poor resolution of the moisture retention curve near saturation results. The optimization process for the van Genuchten method is not able to define a reasonable θ_S value. Hence, θ_S for each soil sample is fixed at the water content measured at zero tension.

4.2.5 Maddock Data Set

In situ unsaturated hydraulic conductivity experiments were conducted at the Oakes sub-branch of the Carrington Irrigation Station during 1972 and 1973. The station is situated 8 km south of Oakes, North Dakota. The soil found in this region is referred to as Maddock sandy loam.

Unsaturated hydraulic conductivity was measured in the field using the instantaneous profile method. Moisture retention was measured in the lab using a pressure cell method. Particle size distribution, bulk density, moisture retention data, and unsaturated conductivity data can all be obtained from Carvallo et al. (1976). Moisture retention and unsaturated conductivity values are tabulated for 14 soil samples. The

Maddock data does not contain measurements of saturated hydraulic conductivity. The problem encountered with the Las Cruces moisture retention data for the van Genuchten analysis is also present in the Maddock data. Once again, the value of θ_S is set equal to the moisture content at zero tension.

4.2.6 Plainfield Data Set

The 5 data sets for Plainfield sand are taken from Mualem's soil catalog. The soil catalog numbers are 4101, 4102, 4103, 4104, and 4105. Moisture retention curves are generated using only the data obtained from the drainage process. The moisture retention data is measured using a porous plate setup. Unsaturated conductivity versus tension is measured by establishing steady flow in a soil column. No model parameters are fixed.

4.2.7 Sevilleta Data Set

The Sevilleta National Wildlife Refuge is located approximately 32 km north of Socorro, New Mexico. It occupies an old flood plain area of the Rio Salado, a tributary of the Rio Grande. Soils in this area typically consist of relatively uniform, unconsolidated, fine fluvial sand (Stephens et al., 1985).

The moisture retention and hydraulic conductivity data points for 3 soil samples are obtained from graphs found in Knowlton (1984). The moisture retention values are measured using the hanging column method. Unsaturated hydraulic conductivity data is measured using the in situ instantaneous profile method. Saturated hydraulic conductivity versus depth is measured using a shelby tube permeameter. Values of saturated conductivity are chosen by selecting the measured conductivity value closest to each of the 3 sample depths. The moisture retention data is sufficiently detailed, so none of the model parameters are fixed.

Chapter 5

Analysis of Curve Fitting Results

This chapter discusses the results of the curve fit optimizations. Section one presents a mathematical analysis of the relationship of the slope of the unsaturated hydraulic conductivity curves predicted by the Brooks & Corey, van Genuchten, and Campbell methods. Section 2 scrutinizes the accuracy of the predictive models. Section 3 looks at the influence of selecting a different match point for the conductivity models. Section 4 focuses on the concept of Leverett scaling.

5.1 Unsaturated Hydraulic Conductivity Slope Analysis

The Brooks & Corey and Campbell equations for the moisture retention curve are in the basic form of a power law. At high tension values, where $(\alpha\psi)^n >> 1$, the van Genuchten moisture retention equation also takes on the form of a power law. By equating the

parameters from the moisture retention equation of the three models, an analysis on the predicted slopes of the corresponding conductivity equations is performed.

5.1.1 Comparison Between the Brooks & Corey and van Genuchten Models

At high tension, the van Genuchten moisture retention equation is approximated by the following power law :

$$S_e \approx (\alpha\psi)^{-mn} \qquad \text{when} \quad (\alpha\psi)^n >> 1$$

By equating the above approximation to Brooks & Corey (Equation 2.6), the following relationships result:

$$\alpha = \left(\frac{1}{\psi_b}\right)$$

$$\lambda = mn$$

Assuming that λ = mn, the relationship between the conductivity slopes on a log transformed scale is evaluated by making a simple parameter analysis of the power exponents. By performing a general binomial expansion,

$$\left(1 - S^a\right)^b \approx 1 - bS^a \qquad \text{for} \quad S << 1$$

the van Genuchten conductivity relationship with constraint m = 1 - 1/n (Equation 2.17) converts to a power law form similar to the Brooks & Corey conductivity equation (Equation 2.7).

$$K_r \cong S_e^{\frac{1}{2}}\left[1 - \left(1 - mS_e^{\frac{1}{m}}\right)\right]^2$$

$$\cong S_e^{\frac{1}{2}}\left(mS_e^{\frac{1}{m}}\right)^2 \qquad \text{for } S_e << 1$$

$$\cong mS_e^{\frac{1}{2}+\frac{2}{m}}$$

Equating the power exponents between the two models results in:

$$\frac{2}{\lambda}+3=\frac{2}{m}+\frac{1}{2} \tag{5.1}$$

Substituting $\lambda = mn$ into Equation 5.1, we get

$$m=\frac{4}{5}\left(1-\frac{1}{n}\right)$$

This contradicts our initial assumption that m = 1 - 1/n and shows that the Brooks & Corey and the van Genuchten models are entirely different predictive models. In fact, this analysis concludes that the Brooks & Corey conductivity slope is steeper than the van Genuchten slope (Table 5.1).

5.1.2 Comparison Between the Brooks & Corey and Campbell Method

Comparison of Campbell (Equation 2.11) with Brooks & Corey (Equation 2.6) gives

$$\lambda=\frac{1}{b}$$

Setting the power exponent of the Campbell conductivity equation (Equation 2.12) equal to the power exponent of the Brooks & Corey conductivity equation (Equation 2.7), the following equality is observed:

$$b=\frac{1}{\lambda}$$

Brooks & Corey and Campbell have the same slope, but the basic assumptions for each model differ. First, Campbell assumes that there is no residual moisture content. Second, there is no specific range of tension for which the Campbell equation is invalid. The

m	λ	Brooks & Corey Slope[1]	van Genuchten Slope[2]
0.33	0.5	7	6.5
0.5	1.0	5	4.5
0.67	2.0	4	3.5
0.75	3.0	3.67	3.17
0.9	9.0	3.22	2.72

Note: (1) Brooks & Corey Slope = $S_{bc} = \frac{2}{m} + 1$

(2) van Genuchten Slope = $S_{vg} = \frac{2}{m} + \frac{1}{2} = S_{bc} - \frac{1}{2}$

Table 5.1: Comparison of Calculated Slopes Between the Brooks & Corey and van Genuchten Models.

Brooks & Corey model is valid only when $\psi \geq \psi_b$ and assumes that there is a residual moisture content.

5.2 Results of the Predictive Models

This section discusses how the predictive method performs for each soil type. Analysis of the predictive fit for the unsaturated hydraulic conductivity is limited to data from Cape Cod, Hanford, INEL, Las Cruces, Plainfield, and Sevilleta. The Maddock data does not contain saturated hydraulic conductivity values, thus prediction of the unsaturated hydraulic conductivity curve is not possible.

Brooks & Corey and van Genuchten curve fits are generated for all the data sets. Predictions using Campbell's method are tested on Cape Cod, INEL, Las Cruces, and Sevilleta. The Russo model is only fitted to two samples in the Cape Cod data set.

A summary of the overall performance of the models can be found at the end of this section. The KaleidaGraph™ generated curve fits for the moisture retention and conductivity data can be found in the appendix.

5.2.1 Criteria for Fit Acceptability

The criteria for judging the success of the fit depends on the intended use for the predicted unsaturated conductivity curves. The simple case of water movement through a vertical profile illustrates this dichotomy in performance acceptance. The slope, $dK/d\theta$, of a conductivity curve is typically fairly steep. Data from the conductivity curve can be used in two ways.

If we assume that the flux through the vertical profile is known, we can use the unsaturated conductivity curve to predict the moisture content. Since the conductivity curve

is steep, a large error in the conductivity prediction does not result in a sizable error in the moisture content. In fact, the difference between the calculated and the actual moisture content may be minimal. A relatively large deviation between the measured and predicted conductivity curve will still be judged acceptable for this application.

The judgment criteria changes drastically if the opposite scenario is chosen. Assuming that the moisture content is known, we can use the conductivity curve to predict the unsaturated conductivity value. A small deviation between the measured and predicted conductivity curve will result in a substantial error in unsaturated conductivity value. Error in the conductivity can vary by orders of magnitude. This application for the conductivity curve has a much lower tolerance for error. A predictive fit judged acceptable for the first case may be judge entirely unacceptable for this case.

This application dependent aspect of the performance criteria dictates the acceptable amount of error between the predicted and actual values. The performance of the predictive models will vary from application to application. In our analysis, a predictive fit was deemed acceptable if the predictive curve varied from the measured data by less than an order of magnitude.

5.2.2 Cape Cod

The moisture retention data for the Cape Cod soil is ill defined near the low saturation region. During the optimization process, this results in a negative value for θ_r, a theoretically impossible situation. To remedy this problem, θ_r is removed as an optimization parameter for the curve fit procedure and is introduced as a fixed value. Current literature (Khaleel, 1995) suggests that a value of θ_r in the range of 0 to 0.03 is fairly typical for a coarse sand. Hence, the value of 0.01 is selected for the Cape Cod sands.

For the Brooks & Corey, Campbell, and van Genuchten methods, the fitted moisture retention curve provides excellent agreement with the measured data. For each soil core, the curve goes through practically every measured data point. Only one data point in core 14a noticeably departs from the curve. The Russo model also generates a good moisture retention fit for cores 12a and 17a.

Although the fitted moisture retention curves are essentially perfect, the predicted unsaturated conductivity curves deviate from the measured values. All three methods tend to underestimate the conductivity values for this coarse sand. Predictions using the Brooks & Corey and Campbell method fall within one order of magnitude for all the samples. In fact, the Brooks & Corey and Campbell predictions are essentially the same. The van Genuchten conductivity values vary up to 1.2 orders of magnitude. Four out of 5 van Genuchten predictions fall within one order of magnitude. All three models seem to predict the unsaturated conductivity reasonably well.

Although the Russo moisture retention fits are acceptable, the predicted unsaturated conductivity curve are absolutely unacceptable. Values of conductivity are underestimated by 20 to 40 orders of magnitude (Figure 5.1). Given the results of these predictions, the Russo model is no longer used for further analysis.

5.2.3 Hanford

Fits of the moisture retention curves to the measured data also fare well for the Hanford soils. Both the Brooks & Corey and van Genuchten models follow the general trend of the moisture retention data. The sharp turn in the moisture retention data near the saturation point is relatively well defined by the van Genuchten model. A few of the curve fits underestimate the rapid downturn, but in general, the van Genuchten curves accurately represent the region.

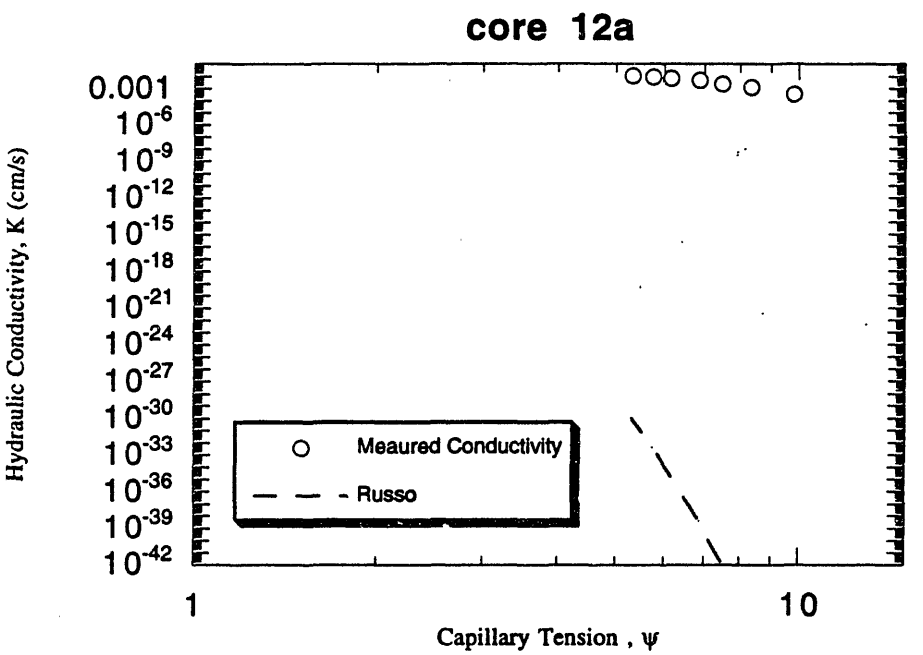

Figure 5.1: Russo Predicted Conductivity Curve for Cape Cod Core 12a.

The quality of the predicted unsaturated conductivity curves fluctuate significantly for the Hanford sands. The fits for both methods range from acceptable to woefully inadequate. The unsaturated conductivity data for the Hanford soil is measured by two different techniques, the steady state head control method and the ultracentrifuge method. Measured conductivity values between the two methods deviate drastically within certain samples. Differences in experimental data can be as high as two orders of magnitude (Figure 5.2). Data from the centrifuge samples also register moisture content values that are higher than the measured porosity (Figure 5.2). Compared with the steady state head control values, the ultracentrifuge measurements tends to underestimate the conductivity values.

Several reasons may contribute to this variation in measured values. Information on the physical properties of the soil samples indicate that the measured bulk densities for several samples differ between the two experiments. Khaleel et al. (1995) evaluate the effects of density variations on the centrifuge samples and conclude that the deviations cannot be attributed solely to differences in the density. Another plausible explanation lies in the possible compaction of the soil samples during the centrifuge process. The effects stemming from compaction have not been investigated. Experiments testing this theory need to be performed. Given the unexplained variations in the centrifuge data and the proven reliability of the steady state head control method, data from the centrifuge measurements is not considered when comparing the measured and predicted conductivities.

The success of the predictions also relies on the quality of the measured data. In a few samples, the measured unsaturated conductivity data are scattered and do not follow a consistent pattern (Figure 5.3). In other cases, the measured value of K_s is ill defined (Figure 5.4). Uncertainty in measurement will contribute to the deviation between the predicted and measured values of conductivity.

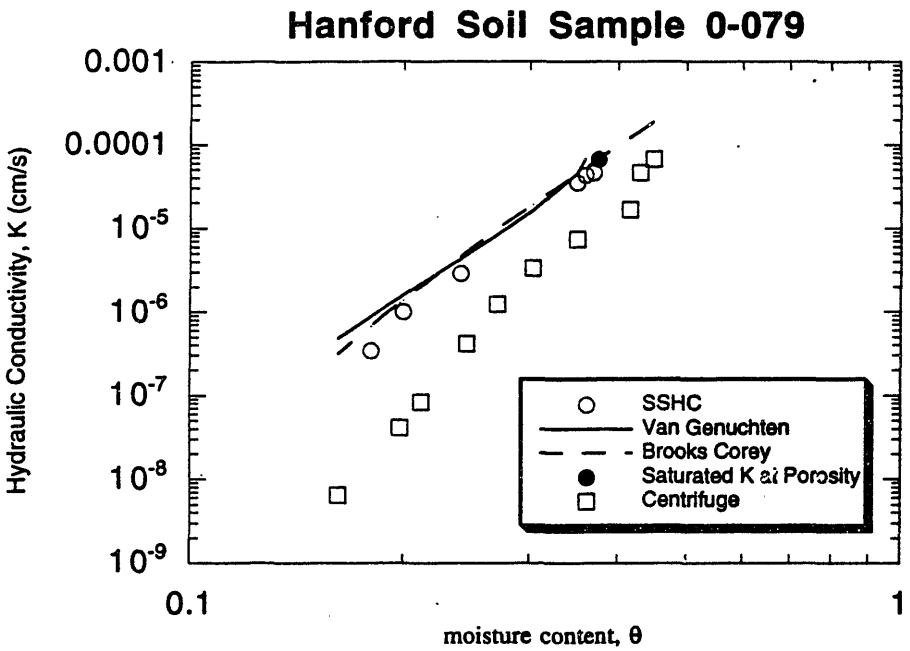

Figure 5.2: Hanford Soil Sample 0-079. This sample shows (a) the difference between SSHC and Ultracentrifuge measured data, (b) measured moisture contents greater than porosity for the ultracentrifuge measurements, and (c) an example of a good prediction.

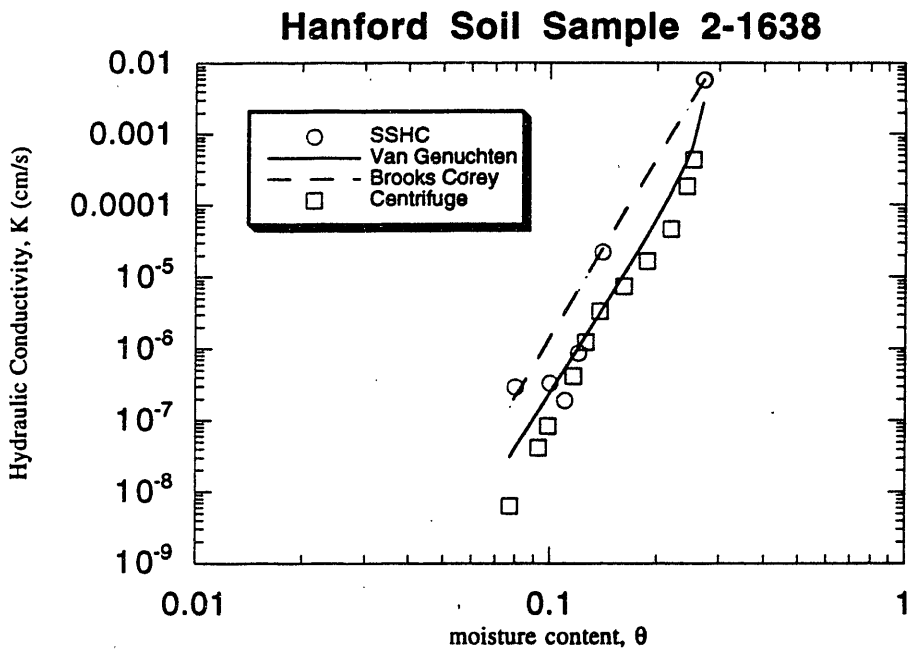

Figure 5.3: An Example of Scattered Conductivity Data for the Hanford Soils.

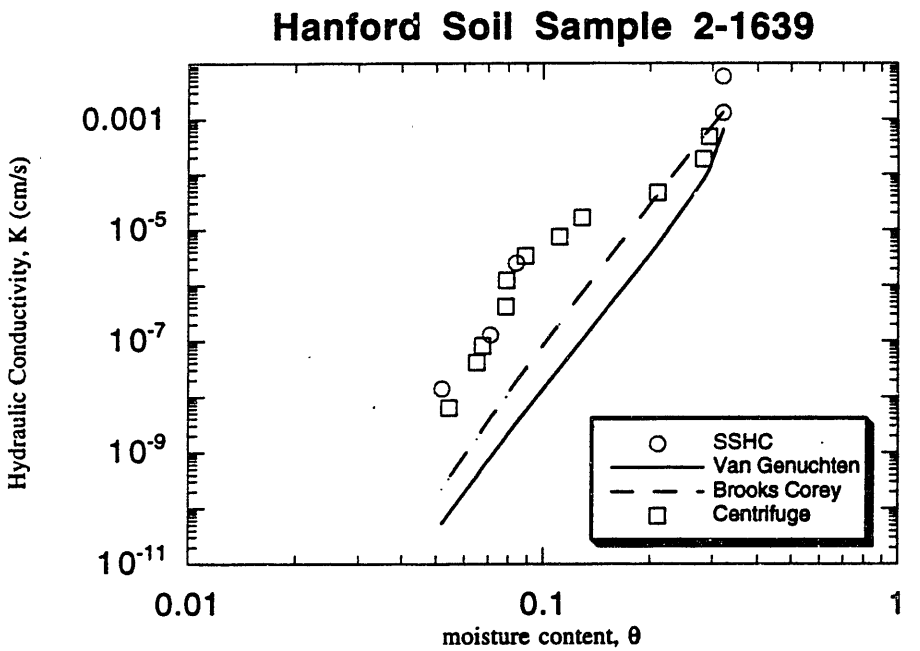

Figure 5.4: Hanford Sample 2-1639. This sample shows (a) an example of conductivity data in which K_S is ill defined and (b) an example of an unacceptable fit.

The predictive curves generated by the Brooks & Corey and van Genuchten methods are very similar. As shown in the previous mathematical analysis, the slope of the Brooks & Corey predictions tends to be steeper than the van Genuchten (Figure 5.5). Good predictions associated with Brooks & Corey model usually implied acceptable predictions by the van Genuchten model. Figures 5.2 and 5.4 illustrate the wide range of predictions obtained. Figure 5.2 displays an example of an acceptable prediction. Figure 5.4 shows an entirely unacceptable prediction.

The majority of the Brooks & Corey predictions are within 2 orders of magnitude. Only one sample falls outside this range. The van Genuchten predictions, minus the same sample, fall within 2.5 orders of magnitude. Quite a few of the Hanford samples for both methods fall within the acceptable order of magnitude.

A general trend visualized from the conductivity curves is a strong tendency in both methods of supplying better predictions for the fine sand samples. The conductivity curve for coarse sand samples are consistently underestimated by both methods. As the mean grain size increases, the deviation between the measured and predicted values also increases. The Brooks & Corey and van Genuchten methods seem more suitable for predicting the fine sands samples than the coarse sand samples.

5.2.4 Idaho National Engineering Laboratory (INEL)

As discussed previously in section 4.2.3, the INEL moisture retention data is altered to allow a favorable fit to the van Genuchten model. Brooks & Corey, Campbell, and van Genuchten curve fits are generated for this soil. The fitted moisture retention curves for van Genuchten correspond well with the measured data. The fits associated with Brooks & Corey and Campbell do not agree as well as van Genuchten with the actual measured data.

The unsaturated conductivity graphs contain a measured conductivity point that falls beyond the predicted curves. We can attribute this outlying point to our curve fitting

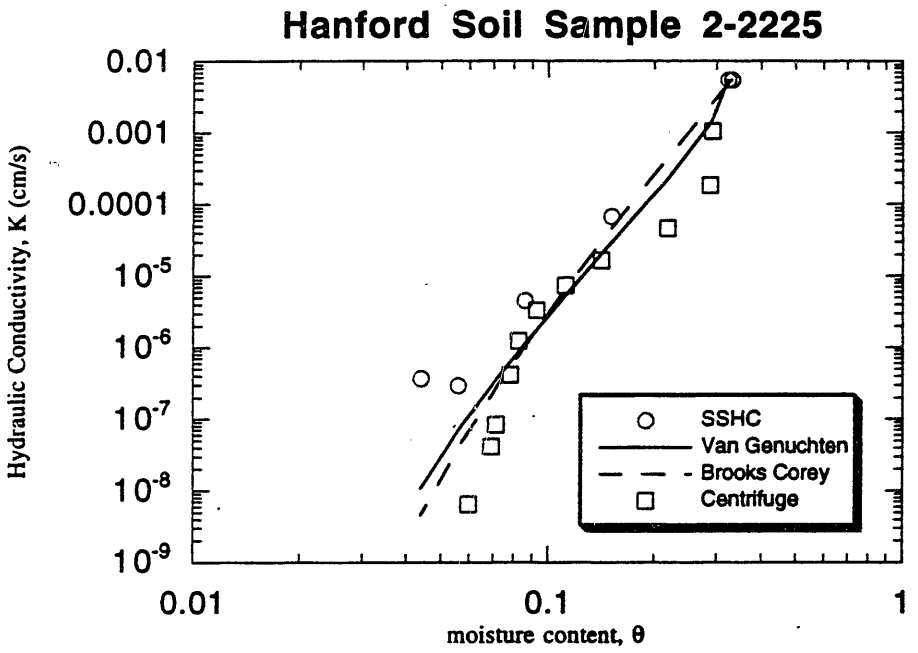

Figure 5.5: The Brooks & Corey Predicted Slope Compared to the van Genuchten Predicted Slope.

procedure. In selecting the data points used to generate the van Genuchten curve, we neglect the low tension point near saturation. By doing so, we are allowing the curve fitting program to determine the optimal value for the saturated moisture content. The optimized saturation moisture content is usually less than the measured value.

This van Genuchten determined value is then selected as the saturated moisture content for both the Brooks & Corey and Campbell methods. The measured value of saturated hydraulic conductivity is assigned to this water content. The predictive curves for unsaturated conductivity are then generated for the samples. Any measured conductivity value with a moisture content greater than the van Genuchten determined value appears as a outlying point. We neglect these points in our analysis.

The predicted unsaturated conductivity curves significantly deviate from the measured values. All three models tend to overpredict the unsaturated hydraulic conductivity. A majority of the predicted van Genuchten conductivities differ from the measured data by 1 to 2 orders of magnitude. The Brooks & Corey and Campbell models display even higher departures from the measured values, falling between 1 to 2.5 orders of magnitude. For the Campbell model, significant deviations between the measured and predicted conductivity values occur near the low moisture content region. As the moisture content decreased, deviations from the measured data increased. Predictive fits from all three methods are unacceptable for the INEL silts.

5.2.5 Las Cruces

Once again, the measured and fitted moisture retention data agreed well with the Brooks & Corey and van Genuchten models. A less favorable fit is associated with the Campbell method. The Campbell curve fits agree well with the measured data for samples 4-25, 5-34, and 7-21, but do not match well with samples 3-34 and 8-49.

For all three models, acceptable conductivity predictions are obtained for 3 of the 5 soil cores. The remaining two samples deviate between 1 to 1.5 orders of magnitude for Brooks & Corey and between 1.5 and 2 orders of magnitude for Campbell and van Genuchten. Predicted conductivites for the Brooks & Corey method deviate much less than Campbell and van Genuchten.

5.2.6 Maddock

Moisture retention curves are fitted to the data for Brooks & Corey, Campbell, and van Genuchten models. The fitted curves for Brooks & Corey and van Genuchten match the measured data well. The Campbell fit produces a linear line that does not represent the nonlinear data. Unsaturated conductivity curves are not generated because the saturated conductivity is not measured. Results from the moisture retention fit are used in the match point analysis (Section 5.3).

5.2.7 Plainfield

After analyzing the Plainfield sand, it was discovered that the sand samples are not representative of the actual Plainfield sand. Each of the 5 samples have been specifically sieved to obtain a particular range of grain sizes. These uniform, narrowly distributed soil samples do not provide moisture retention curves that are indicative of their natural environment. Thus, the soil samples for Plainfield sand are invalidated from our curve fit analysis.

5.2.8 Sevilleta

The Brooks & Corey, Campbell, and van Genuchten fitted moisture retention curves matched the measured data quite well. Excellent agreement is also found between the predicted and measured values of unsaturated hydraulic conductivity for the Brooks &

Corey and van Genuchten models. The Campbell model shows excellent agreement between the measured and predicted conductivity at the high water content regime, but starts to break down at the low moisture content range. Deviations in the Campbell predictions are as high as 1.5 orders of magnitude at the lowest moisture content.

5.2.9 Summary

Comparison between the different soil types illustrates a few consistent trends found within the curve fitting analysis. These trends are defined by textural, rather than structural, characteristics. A definite correlation exists between the predictive accuracy of the Brooks & Corey, Campbell, and van Genuchten models and the mean soil grain size. From the Cape Cod analysis, the Russo/Gardner model appears to be an inadequate model for predicting conductivity using just moisture retention data. Additional constraints need to be specified in the Russo model.

There is a direct relationship between the measured and predicted conductivity deviation and the mean grain size. Using the saturated hydraulic conductivity as an indicator of the grain size, graphs of the mean error versus K_S are plotted (Figures 5.6 - 5.8). The mean error is defined as:

$$mean\ error = \frac{\sum_{i=1}^{N}(\delta_i)}{N}$$

where

δ_i = log $K_{predicted}$ - log $K_{measured}$

N = the number of measured K data points

The deviation pattern is evident from the graphs. As the saturated conductivity increases, the mean error accordingly increases.

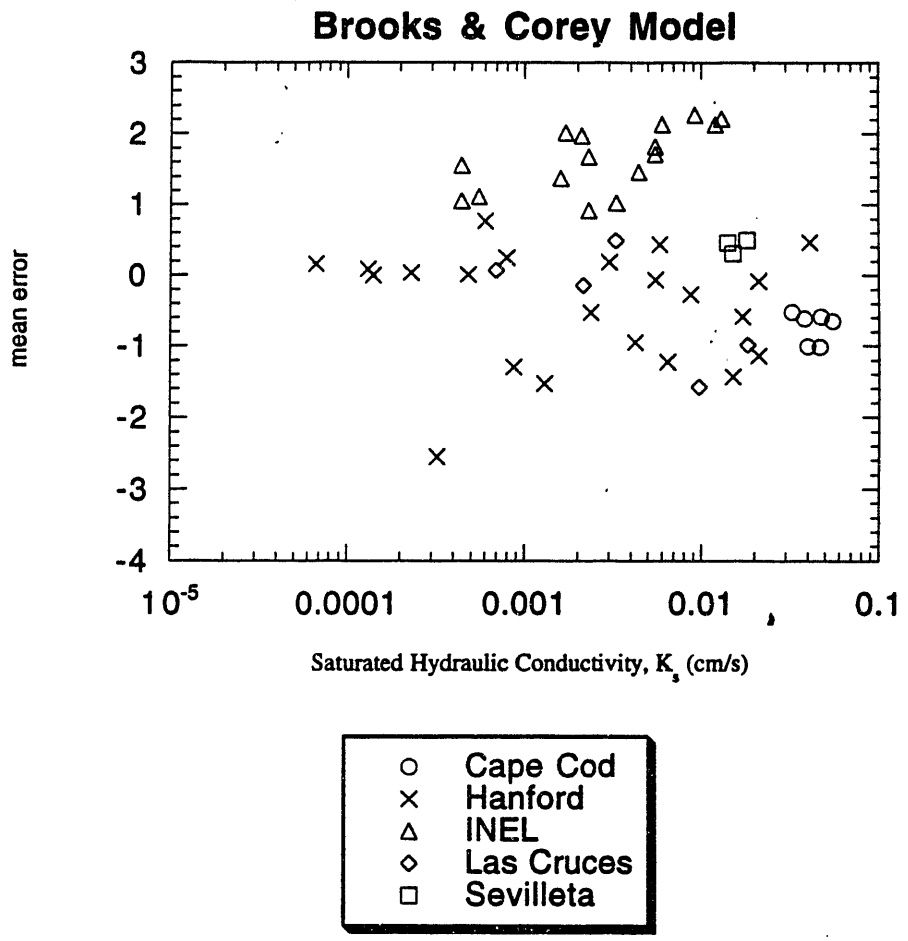

Figure 5.6: Mean Error Versus K_S for the Brooks & Corey Model.

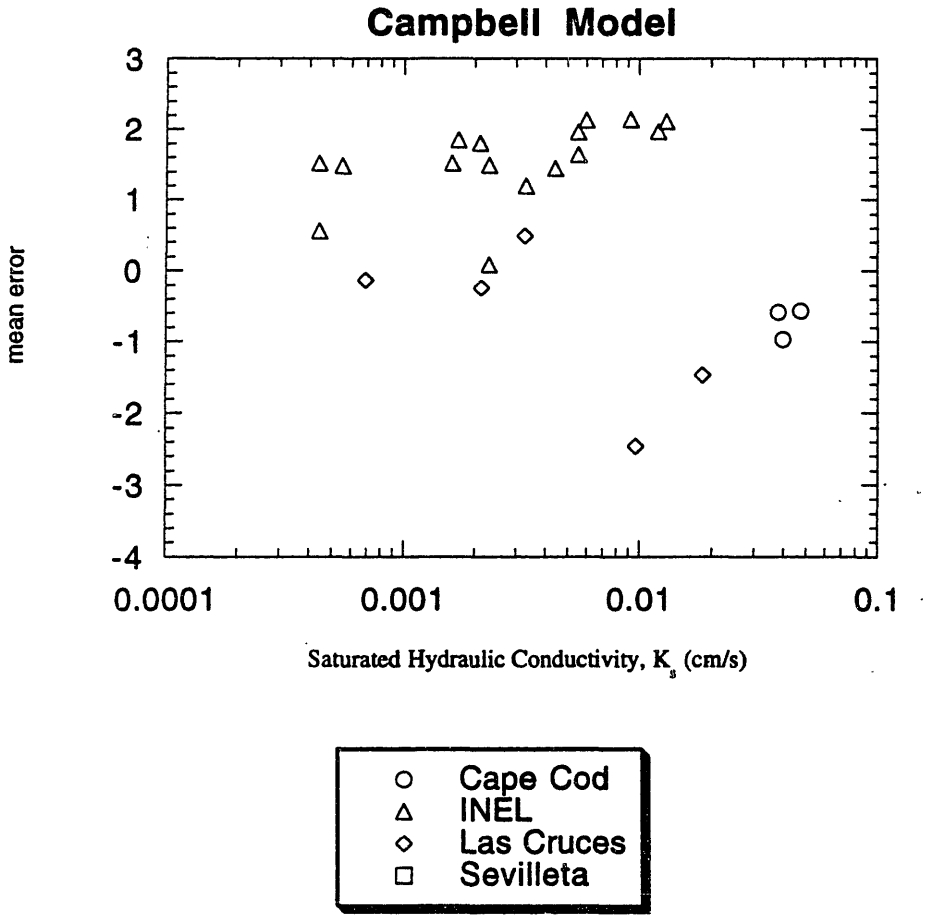

Figure 5.7: Mean Error Versus K_S for the Campbell Model.

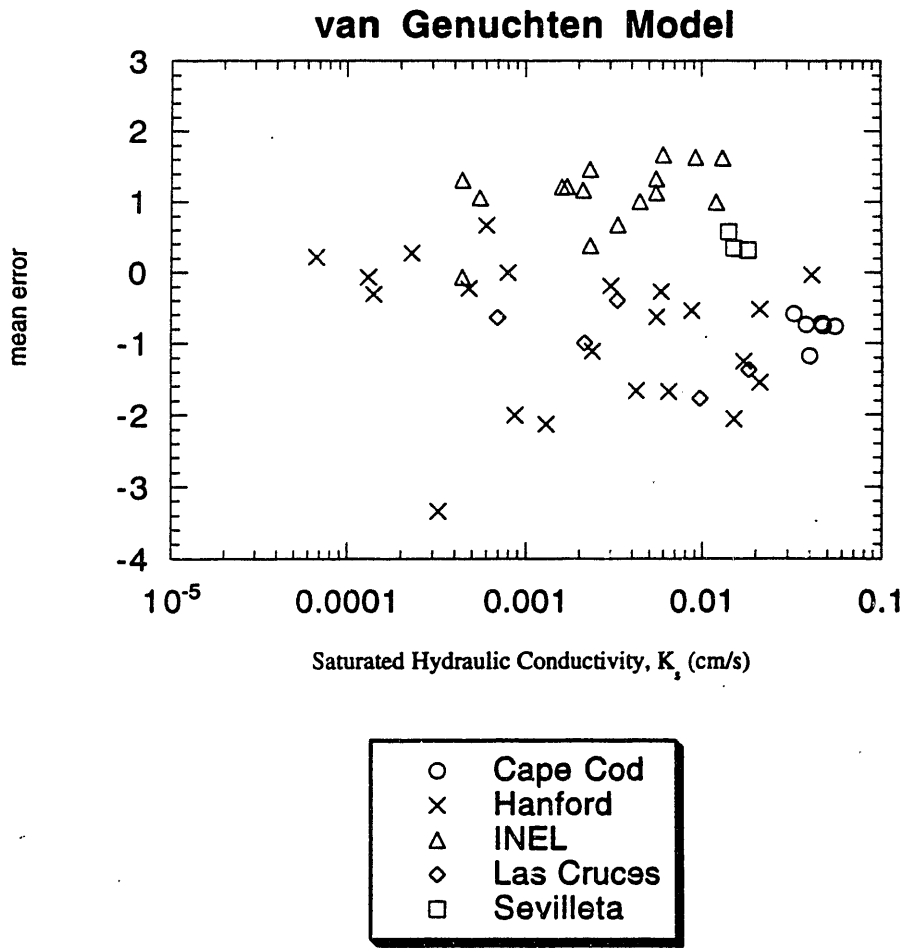

Figure 5.8: Mean Error Versus K_S for the van Genuchten Model.

The saturated hydraulic conductivity does not seem to be a reliable indicator for grain size. The range of saturated conductivity values for the INEL silts is almost just a wide as the range for the Hanford sands. The inherent differences between the two soil textures is not adequately represented. A different parameter needs to be selected to portray the varying grain sizes.

The parameters ψ_b, ψ_e, and α are chosen to represent the grain sizes for the Brooks & Corey, Campbell, and van Genuchten models respectively. These three parameters are a measure of the largest pore size that exists within the soil. The values of ψ_b, ψ_e, and $1/\alpha$ indicate the length of the capillary rise above the water table. As the grain size increases, the length of the capillary rise decreases. To characterize the trend of increasing error with increasing grain size, graphs of mean error versus the inverse of ψ_b and ψ_e are plotted. Figures (5.9 - 5.11) show the plots of mean error vs $1/\psi_b$, mean error versus $1/\psi_e$, and mean error versus α. The systematic departure of the coarser material is more dramatically characterized by these three parameters than by K_s. A general bias of underestimating the coarser sands is evident.

The INEL silts significantly deviate from the apparent trend. All three models consistently overpredict the conductivity values. If the trend is correct, the models should have predicted the conductivity values reasonably well. An explanation for this deviation lies in the nature of the soil. The INEL silts are a highly structured, aggregated soil. Large blocks of silt aggregate together and act like larger grains. The aggregated nature of the soil influences the measured saturated conductivity and the measured moisture retention data.

The aggregation may produce soil pores in the INEL silt which are larger than expected in an unstructured silty material. This leads to higher measured saturated conductivities. The unusually high range of K_s for this silt reflects the aggregated nature of the soil. Hence, it is of no surprise that the predictive models overestimate the unsaturated conductivity.

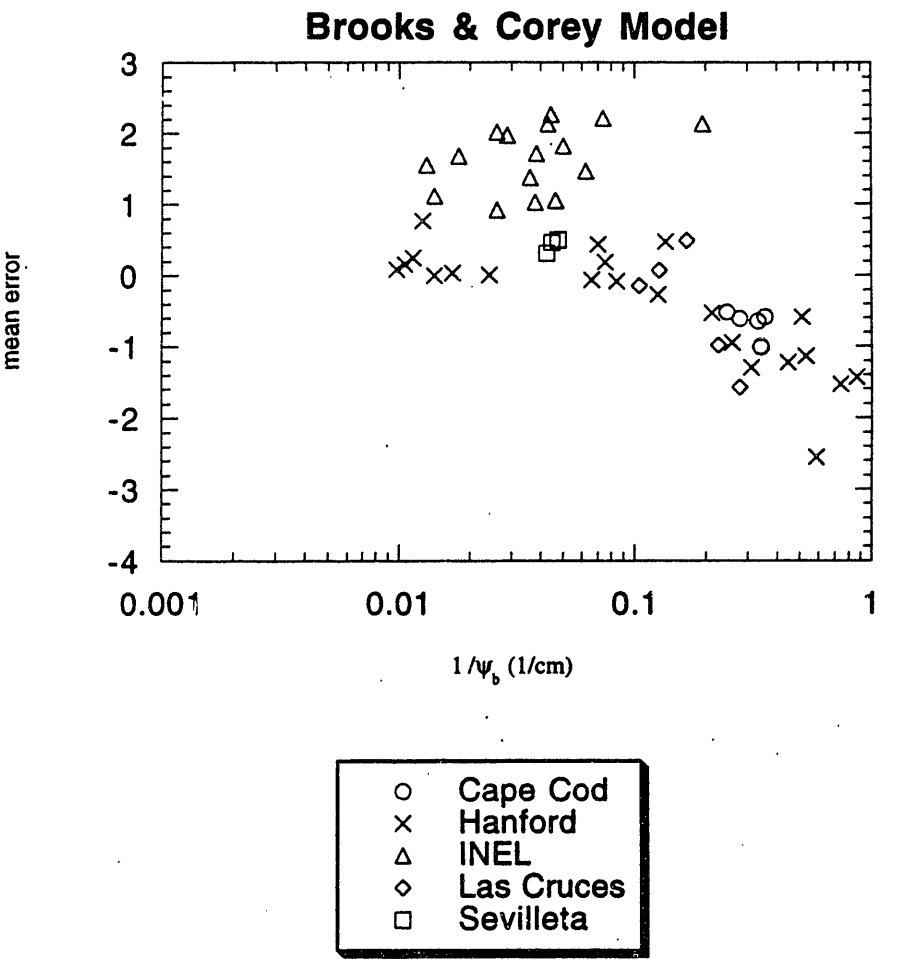

Figure 5.9: Mean Error Versus $1/\psi_b$ for the Brooks & Corey Model.

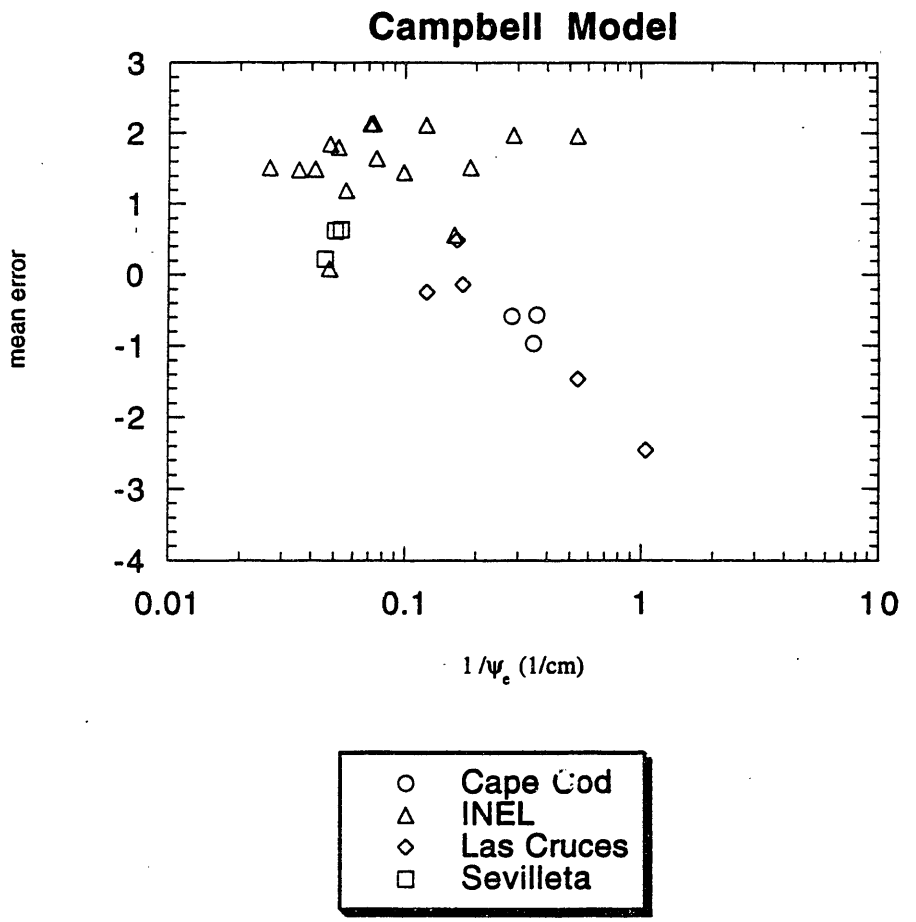

Figure 5.10: Mean Error Versus $1/\psi_e$ for the Campbell Model.

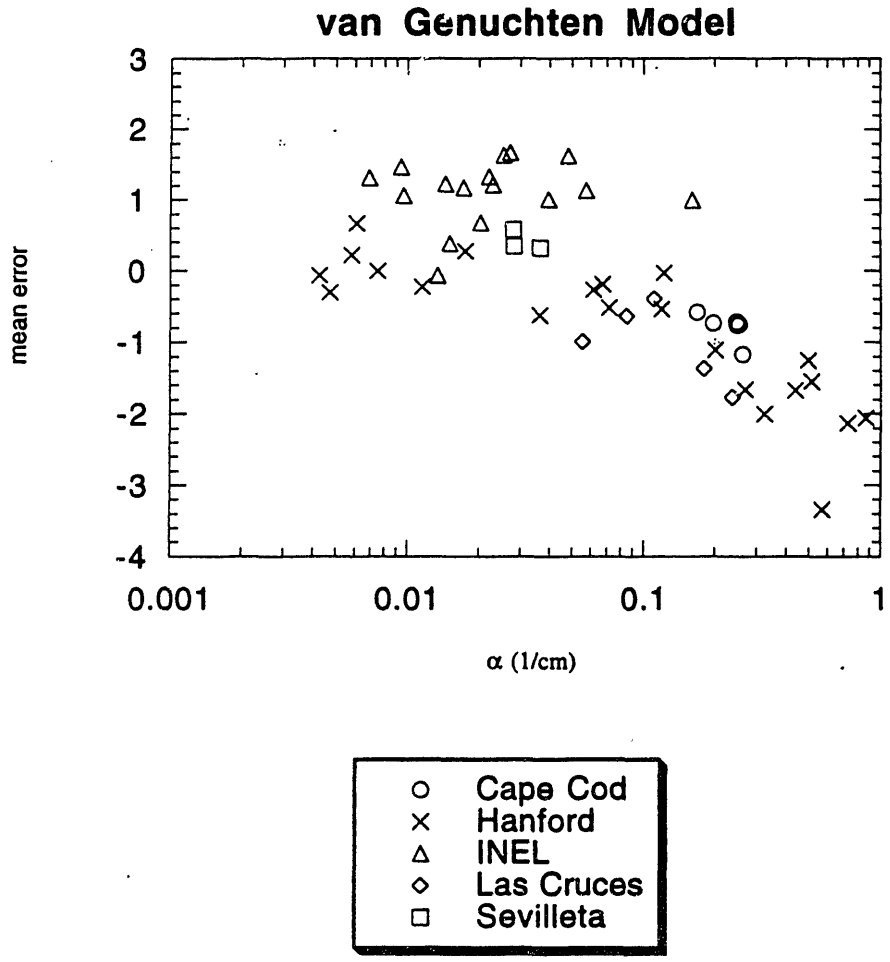

Figure 5.11: Mean Error Versusα for the van Genuchten Model.

Figures 5.12 - 5.14 show the plots of root mean square error versus $1/\psi_b$, $1/\psi_e$, and α respectively. The root mean square error (rms) is calculated by:

$$rms = \sqrt{\frac{\sum_{i=1}^{N}(\delta_i)^2}{N}}$$

Neglecting the INEL data, the Brooks & Corey model generally has a lower rms error than van Genuchten. The Brooks & Corey model is slightly better in predicting the conductivity.

Although the Campbell model also has comparable errors, it is not a good predictor of conductivity at the low moisture content region. The model predicts fairly well at high moisture contents, but breaks down in the low moisture region. The largest deviations are located in the low conductivity regime. Since this is the range of interest, the Campbell model does not meet the acceptance criteria.

5.3 Match Point Selection

The Brooks & Corey, Campbell, and van Genuchten models all use K_s as the match point to predict the unsaturated hydraulic conductivity. Recent studies by van Genuchten and Nielsen (1985) and others recommend that a different match point be used. Use of K_s as a match point does not make sense for our analysis. Our area of interest on the moisture retention curve is at the low moisture content region. A match point at K_s is a poor indicator of the behavior of the unsaturated hydraulic conductivity at the low moisture regime. A more suitable match point appears to be an unsaturated conductivity value near the region of interest.

Moisture retention values near the saturation point are typically difficult to determine because of the steep slope. As the curve approaches the saturation point, rapid changes

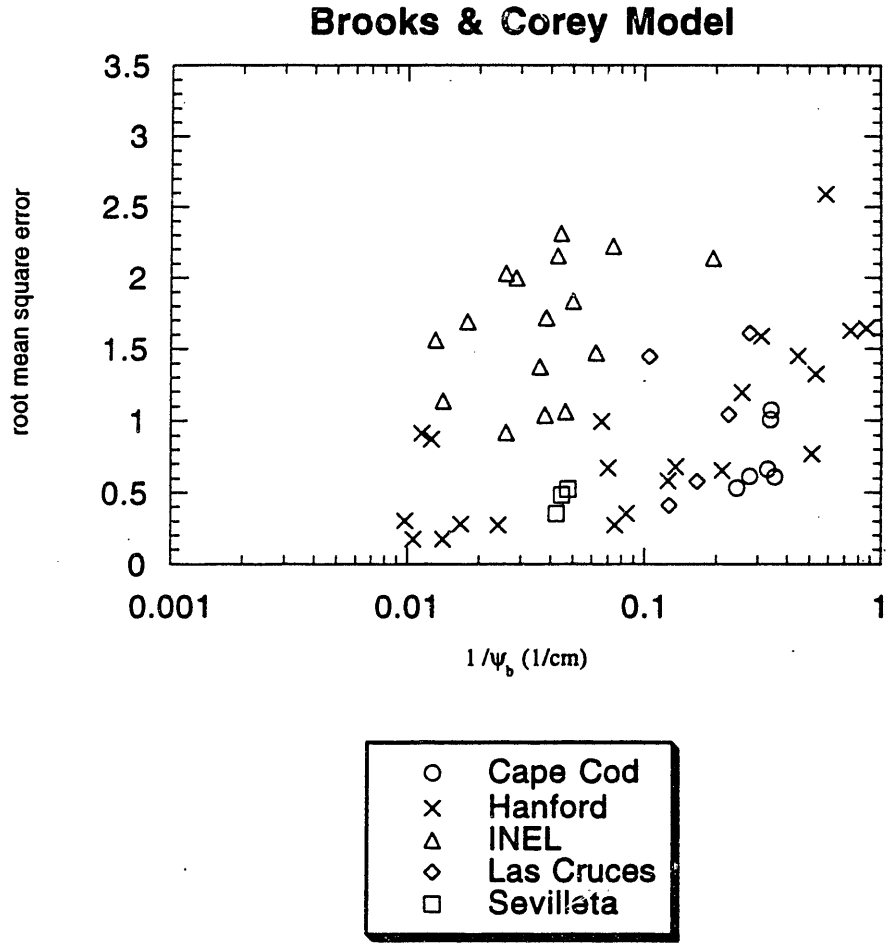

Figure 5.12: Root Mean Square Error Versus $1/\psi_b$ for the Brooks & Corey Model.

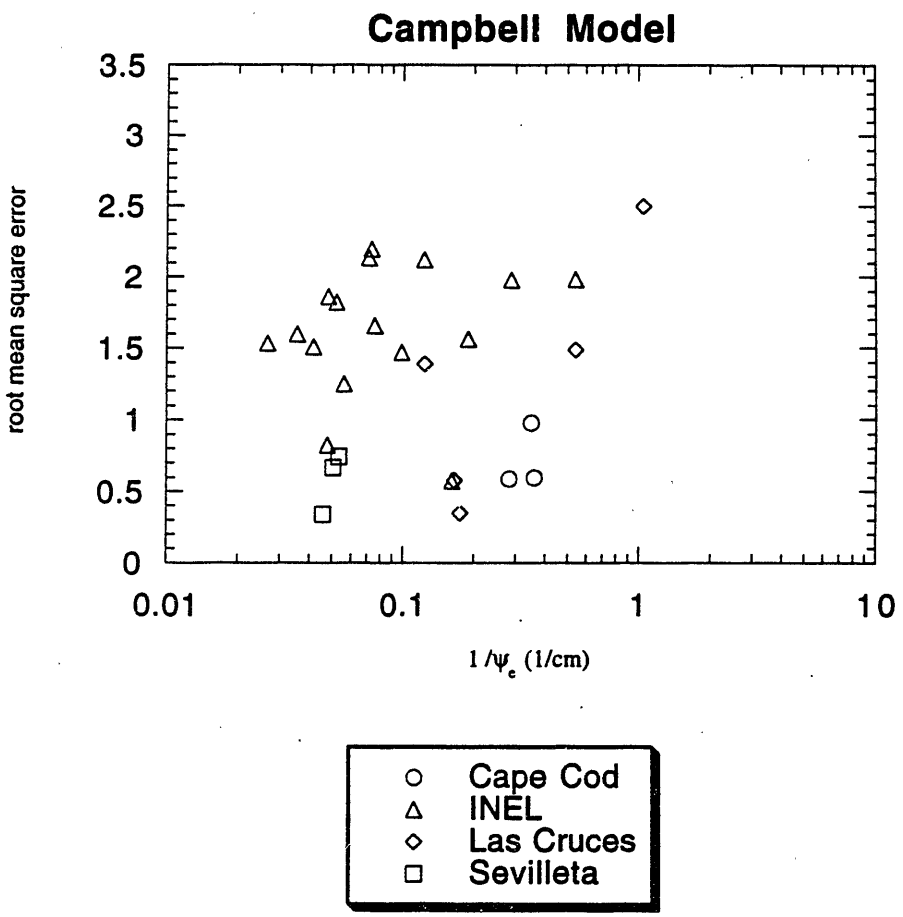

Figure 5.13: Root Mean Square Error Versus $1/\psi_e$ for the Campbell Model.

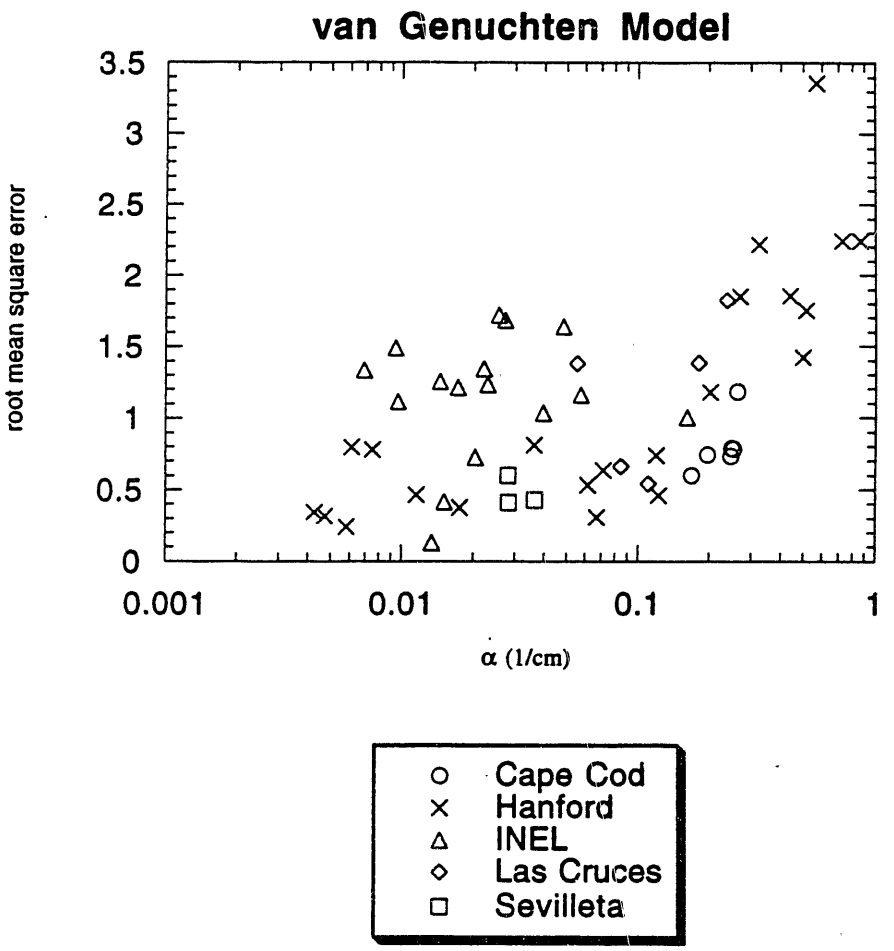

Figure 5.14: Root Mean Square Error Versus α for the van Genuchten Model.

occur and the curve takes on the form of a vertical line. Small errors in measurement of the moisture content in this region can result in large errors in the predicted unsaturated hydraulic conductivity (Figure 5.15). The value of K_s is primarily determined by the structural properties of the soil. Soil structural properties are characterized as highly variable in the natural environment. Given the extreme variability of K_s, accurate measurement of its value is difficult to achieve. Uncertainty in the measured value of K_s is substantial.

Luckner et al. (1989) derives a form of the van Genuchten equation that allows an arbitrary match point. Using the Luckner modified method, Yates et al. (1992) and Khaleel et al. (1995) both show that selecting a different match point near saturation does reduce the error between the measured and predicted values of unsaturated hydraulic conductivity, but each reached a different conclusion regarding the success of the procedure. Yates et al. concluded that the new scaling point does not significantly improve the conductivity predictions. Khaleel et al. reaches the opposite conclusion.

A crucial assumption implied by this match point theory is that the models accurately predict the slope of the unsaturated conductivity curve. If the theory is correct, the predicted conductivity curve is actually parallel to the measured curve. Obtaining the true curve can be done by simply selecting a different match point. The original match point, K_s, selected by the models is not a sensible choice.

A statistical approach is developed to measure the validity of this theory. Assuming that the actual slope is predicted by the model, the relative difference, δ, of the log predicted conductivity and log measured conductivity for each data point should be exactly the same. For each soil sample, a graph of either δ versus $\log\theta$ or δ versus $\log\psi$ is plotted. A linear regression is then performed on the data. If the predicted curve is just an offset of the true curve, the regression slope, $d(\delta)/d(\log\theta)$, should be zero. Figures 5.16 - 5.18 show the calculated regression slopes for each soil sample. Results clearly indicate

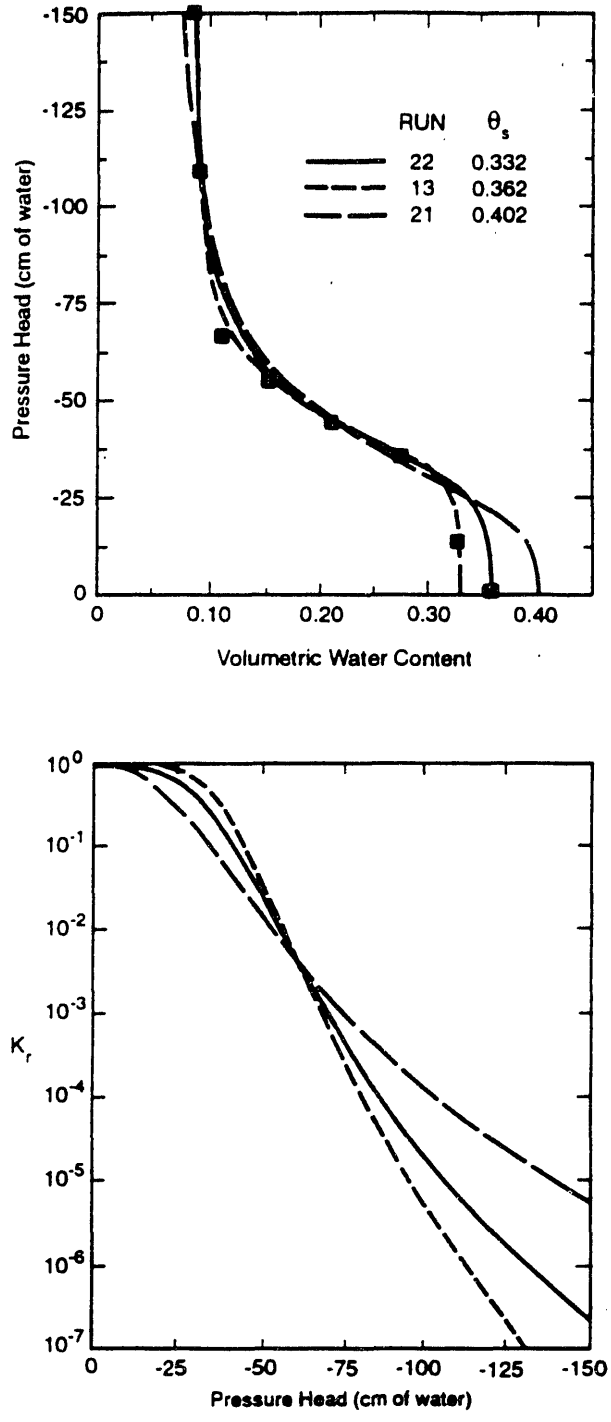

Figure 5.15: Sensitivity of Calculated Hydraulic Conductivity to Saturated Moisture Content for Uniform Sand (From Stephens, 1985).

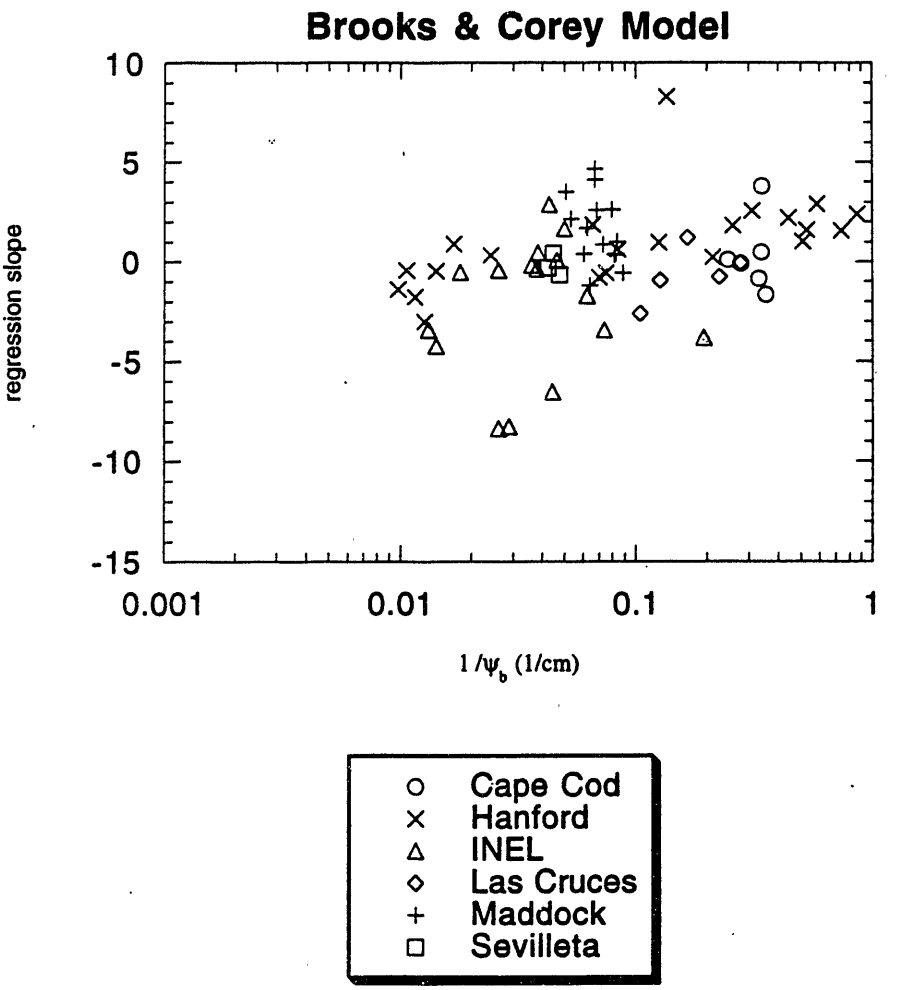

Figure 5.16: Regression Slope Versus $1/\psi_b$ for the Brooks & Corey Model.

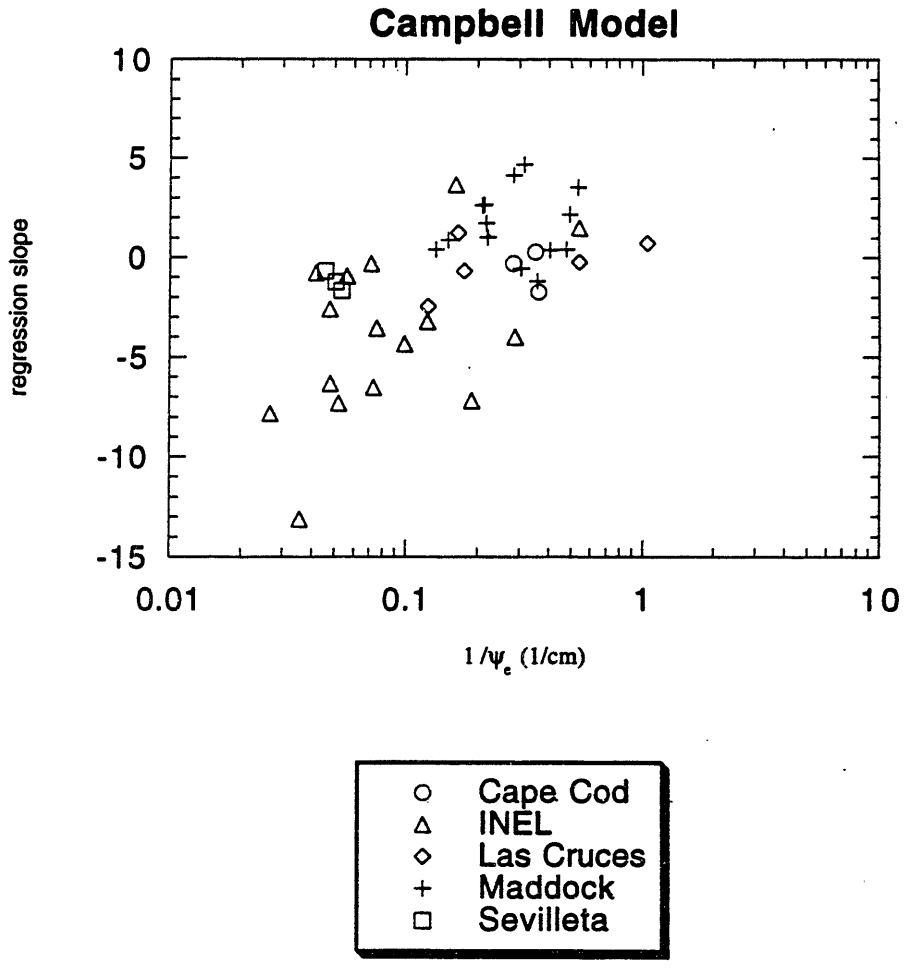

Figure 5.17: Regression Slope Versus $1/\psi_e$ for the Campbell Model.

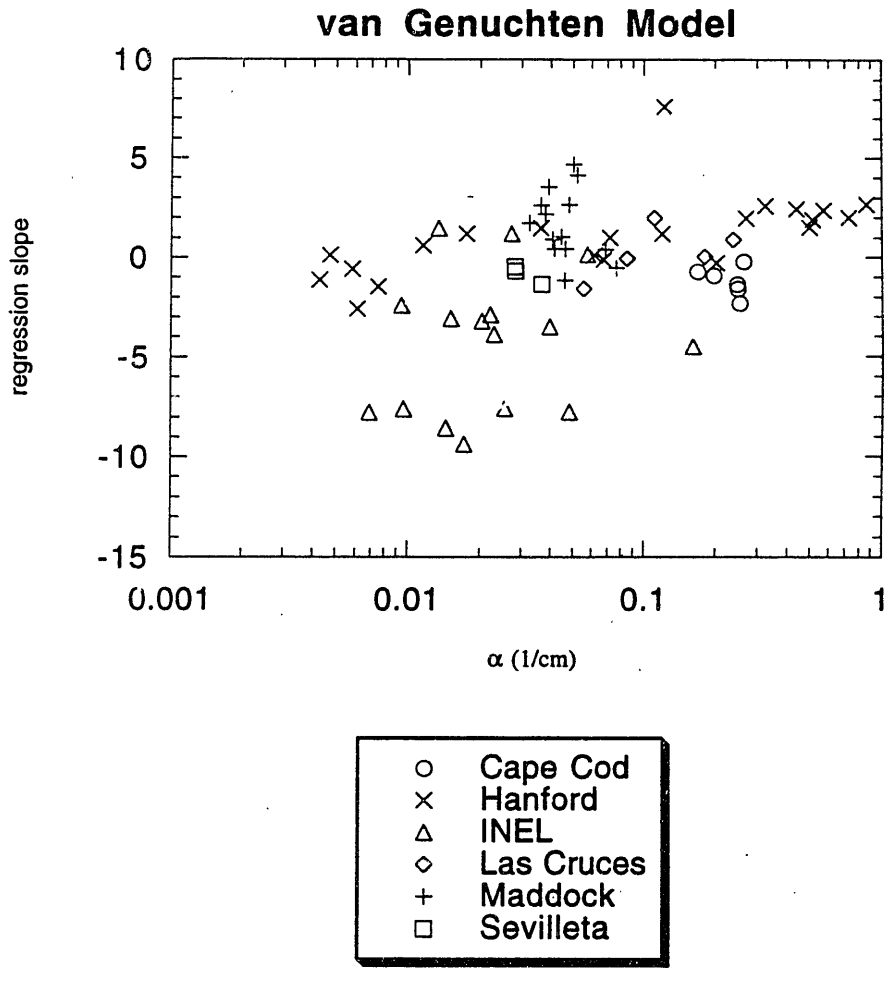

Figure 5.18: Regression Slope Versus α for the van Genuchten Model.

that the selection of a different match point is not sufficient. The regression slopes fluctuate tremendously and do not hover around zero.

A trend is identified from the Hanford soil, the largest data set. Slopes are negative at low α values and positive at high α values. At the high α end, the predicted conductivity values are underestimated. A positive slope indicates that the predicted slope is steeper than the actual slope. At the low α end, the conductivity values that are overestimated correspond with a negative slope. This tells us that the predicted conductivity curve is not steep enough.

Almost all the slopes for the INEL soil reside in the negative region. As mentioned in the previous section, the INEL conductivities are overpredicted. Once again, the slope of the predicted conductivity curve is not steep enough for the finer grained materials. Underpredicted conductivity curves tend to have a positive slope, while overpredicted conductivity curves have negative slopes. This implies that the largest deviation between the measured and predicted conductivity values occur at the low moisture content region.

The value of the regression slope relates to the error in the exponent of the predictive conductivity equations. Assuming that both the measured and predicted conductivity curves are defined by simple power laws, we get:

$$K_{\text{measured}} = C_m \theta^N \tag{5.2}$$

$$K_{\text{predicted}} = C_p \theta^{N+S} \tag{5.3}$$

where

C_m, C_p = constants

N = the actual conductivity slope

$N + S$ = the predicted conductivity slope

Dividing Equation 5.2 into 5.3 and performing a logarithmic transformation results in:

$$\frac{K_{\text{predicted}}}{K_{\text{measured}}} = \left(\frac{C_p}{C_m}\right)\theta^S \tag{5.4}$$

$$\log\left(\frac{K_{\text{predicted}}}{K_{\text{measured}}}\right) = S\log(\theta) + \log\left(\frac{C_p}{C_m}\right) \tag{5.5}$$

The regression slope is defined as:

$$\text{regression slope} = \frac{d\delta}{d(\log\theta)}$$

where

δ = $\log K_{\text{predicted}}$ - $\log K_{\text{measured}}$.

Taking the derivative of equation 5.5 gives

$$\frac{d\left(\log\frac{K_{\text{predicted}}}{K_{\text{measured}}}\right)}{d(\log\theta)} = S = \frac{d(\delta)}{d(\log\theta)}.$$

Hence, the regression slope is equal to the error in the exponents. It is interesting to note that the error between a single measured and predicted conductivity value is influenced by two different factors: the error between the conductivity curve slopes, S, and the value of the moisture content, θ, of interest (Equation 5.4). As you move further away from the match point, the error steadily increases. The deviation between a single measured and predicted value has absolutely no dependence on the actual slope, N.

Regression slope values range between -15 to 10. These are significant errors. Selecting a match point at coordinates (θ_1 , K_1), Equation 5.4 becomes

$$\frac{K_{\text{predicted}}}{K_{\text{measured}}} = \left(\frac{\theta}{\theta_1}\right)^S.$$

Assuming a match point moisture content of 0.3 and a regression slope of 3, the error between the predicted and measured conductivity at $\theta = 0.05$ is

$$\frac{K_{predicted}}{K_{measured}} = \left(\frac{0.05}{0.3}\right)^3 = \left(\frac{1}{6}\right)^3.$$

The predicted conductivity will underestimate the measured value by a factor of 216, well over two order of magnitudes. This shows why the saturated conductivity value is not considered to be a good match point.

5.4 Leverett Scaling

Pore space within soils may be visualized as a series of capillary tubes or circular rods. Given this idealized assumption, a single relationship between the capillary pressure and saturation can be derived for similar soil types. This simplified concept suggests that the moisture retention curves of different soils can literally be reduced to a common curve by selecting an appropriate scaling factor. Based on fluid and medium properties, the scaling factor normalizes the relationship between the capillary pressure and saturation for each soil type.

Leverett (1941) employs dimensional analysis to derive a semi-empirical equation which establishes this constant relationship between tension and saturation. This equation is known as the J-Leverett function:

$$J = J(S_e) = \left(\frac{P_c}{\sigma}\right)\sqrt{\frac{k}{\phi}} \tag{5.6}$$

where

P_C = the capillary pressure

σ = the surface tension

k = the permeability of the medium

ϕ = the porosity

A consistent system of units must be used in defining the J function.

The theory behind the J-Leverett function is that there is some dimensionless relationship that exists between capillary pressure and saturation. The van Genuchten moisture retention equation specifically relates the capillary pressure to the saturation. If we non-dimensionalize the van Genuchten equation by using a scaling factor, the resulting expression can be regarded as a J-Leverett function. The key parameters in van Genuchten that influence the general shape of the moisture retention curve are α and n. Figure 5.19 shows the relationship between α and n for the various data sets. A slight trend is observed with the Hanford soils, as α increases n decreases. The value of n is affected by the soil grain size.

Figure 5.20 (a) displays the influence of n on the moisture retention curve expressed in the dimensionless form $\alpha\psi$ versus S_e; and clearly shows that n has a strong influence on the curves in this form. In keeping with the Leverett concept, an approximate single non-dimensional form of the van Genuchten relationship can be obtained by scaling the moisture retention curve. The van Genuchten equivalent of the J-Leverett function is obtained by scaling the value of $\alpha\psi$ by its value at some selected effective saturation value, $1/N$:

$$J(S_e) = \frac{\alpha\psi}{(\alpha\psi)_{\frac{1}{N}}} = \left(\frac{\left[S_e^{\frac{-1}{m}} - 1 \right]}{\left[N^{\frac{1}{m}} - 1 \right]} \right)^{\frac{1}{n}} \tag{5.7}$$

where

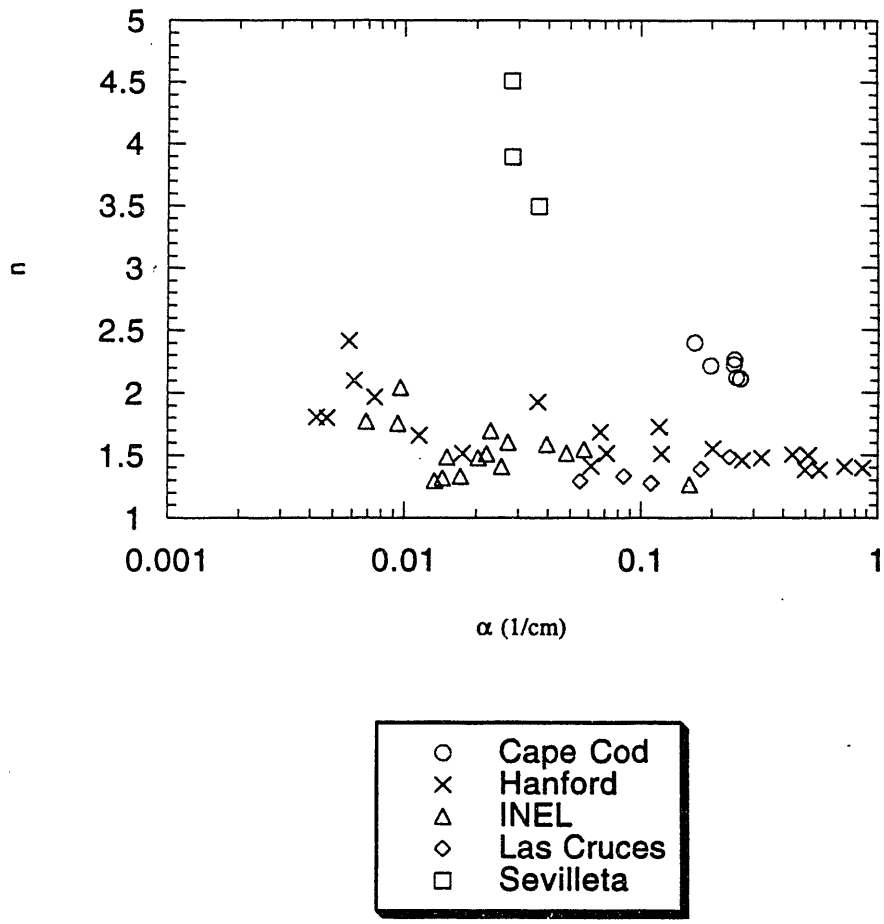

Figure 5.19: Graph of n Versus α for the van Genuchten Model.

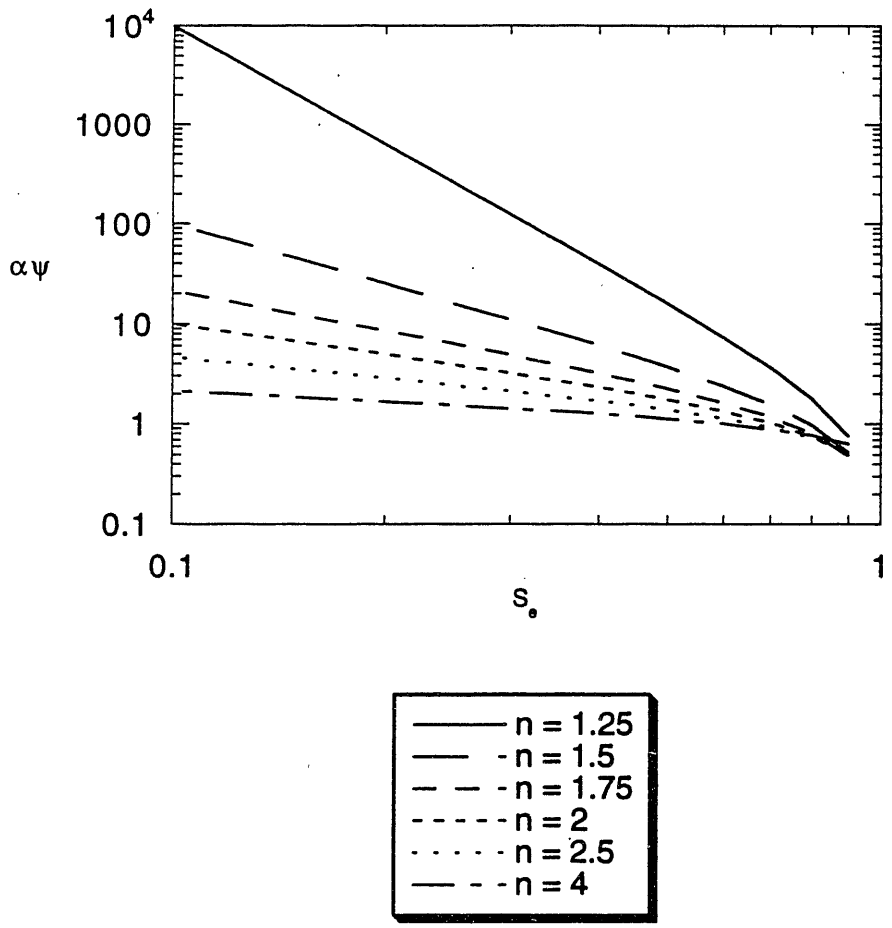

Figure 5.20 (a): Graph Showing the Influence of the van Genuchten parameter *n* on the Moisture Retention Curve.

N = the inverse of the matching effective saturation value

$(\alpha\psi)_{\frac{1}{N}}$ = the value of $\alpha\psi$ at an effective saturation of $1/N$

Figure 5.20 (b) shows the scaled moisture retention curves at a matching effective saturation point of 1/3. The scaled moisture retention curves do not scale onto a single curve. Moisture retention curves with varying values of n do not have the same shape. The slopes between the moisture retention curves are different. The use of a scaling factor does not alter the slope of the original curve. The scaling factor just scales the curves to intersect at a common point, the selected effective saturation value. If the moisture retention curves are to collapse onto a common curve, modification to the original slope of the moisture retention curve must occur. Therefore, we can conclude that Leverett scaling is not valid over a wide range of n values.

Although the scaled retention curves still do not fall onto the same curve, Leverett scaling appears to have some merit over a narrow range of n. With the exception of Sevilleta, each individual soil used in our analysis falls within a fairly narrow range of n. The value of n for the majority of the Hanford soil is between 1.4 to 1.9. Hence an analysis of Leverett-like scaling on these soils may be performed.

By substituting the relationship

$$K_s = \frac{kg}{\upsilon}$$

where

K_S = the saturated conductivity

g = gravity constant

ρ = the fluid density

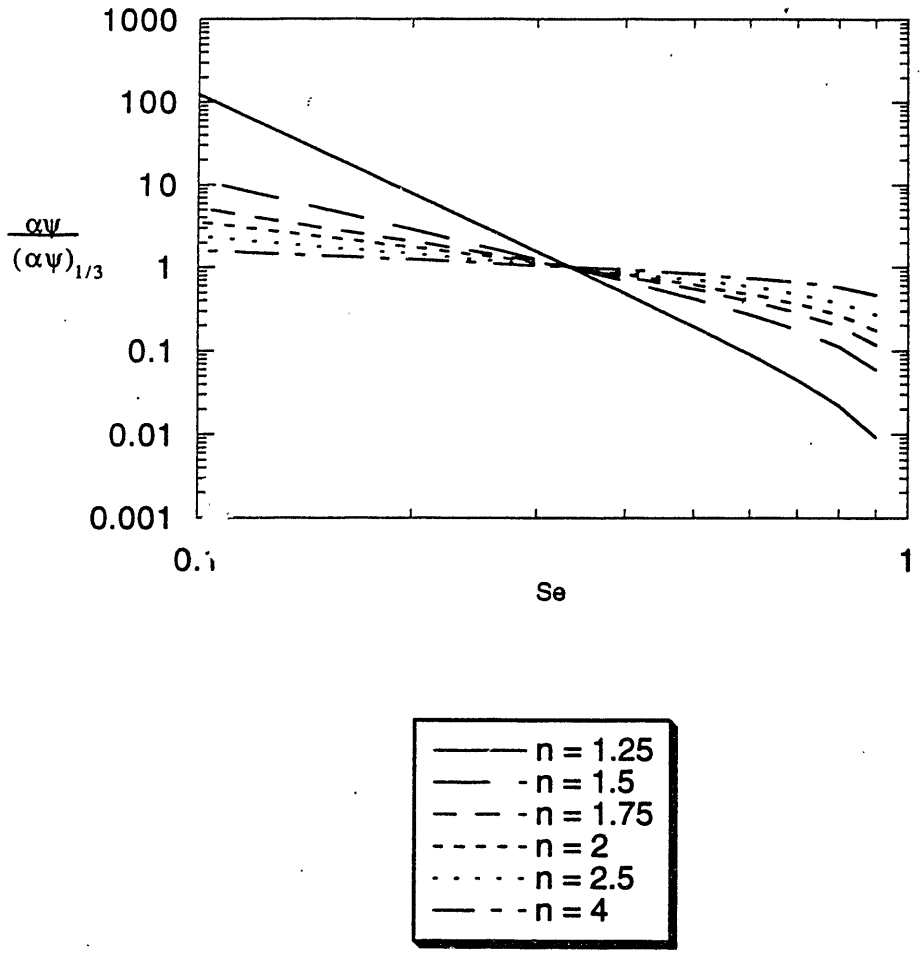

Figure 5.20 (b): Scaled Moisture Retention Curves for Various Values of n at an Effective Saturation Match Point of 1/3 .

ν = kinematic viscosity

and Equation 5.7 into 5.6, the following equality is observed:

$$\alpha = C\sqrt{\frac{K_s}{\phi}}$$

where

C = a constant

We have assumed that the surface tension is constant. If Leverett-like scaling holds over a narrow range of n , graphing a versus $\frac{K_s}{\phi}$ for each soil type on a log transformed scale should show a linear slope of 0.5. As seen in Figure 5.21, the calculated slopes for all the soil types, except Sevilleta, are quite close to 0.5. Although most of the slopes exhibit a Leverett-like trend, the data points do not all fall onto the fitted straight line. The data points are quite scattered around the linear line. For Cape Cod, INEL, and Las Cruces the deviation from the line is fairly small. The Hanford data displays the largest amount of scatter. Though the data points exhibit a large amount of uncertainty, a general trend is observed from the Hanford soil. We see a corresponding increase in α as $\frac{K_s}{\phi}$ increases.

Evidently Leverett scaling does represent the general trend in capillary pressure characteristics of the soils investigated here, but certainly does not capture much of the variability seen among individual samples. The indication is that Leverett scaling will not capture the natural variability of capillarity encountered in field soils.

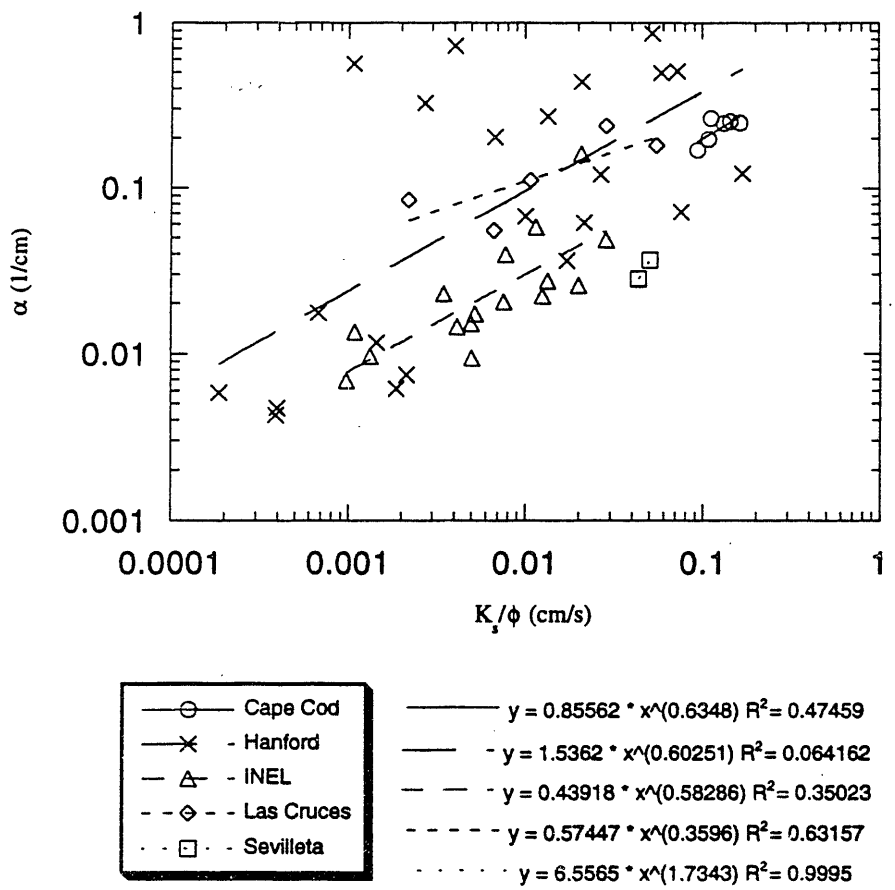

Figure 5.21: Graph of α Versus $\frac{K_s}{\phi}$.

Chapter 6

Conclusions

6.1 Summary

The purpose of this thesis is to critically assess the reliability of unsaturated hydraulic conductivity models that predict conductivity using only moisture retention data and saturated hydraulic conductivity. Specifically, the focus is on the predictive ability of the Brooks & Corey, Campbell, and van Genuchten models in estimating conductivity values for aquifer like materials. Soil samples from 6 distinct sites are analyzed. The soil textures range from coarse sands to fine silts.

Soil in the unsaturated zone of the aquifer resides in the low moisture regime of the moisture retention curve. Accurate prediction of the unsaturated conductivity is crucial when modeling contaminant transport through the vadose zone or recharge to the aquifer. The relevant range of conductivity values associated with the unsaturated zone is typically orders of magnitude smaller than the saturated conductivity. Thus, the analysis concentrates on the low moisture content region that is characterized by low unsaturated conductivity values.

Results from the analysis indicate that the predictive methods generally do not work in predicting the unsaturated hydraulic conductivity. There is no supporting evidence that shows that these models accurately characterize the natural variability in the aquifer. Although the analysis concludes that the models are inadequate, there are a few interesting trends represented in the data.

- A direct correlation exists between the predictive error and the mean grain size. Deviations between the measured and predicted conductivity increase as the texture of the material becomes coarser. The models predict conductivities for the fine to medium sands fairly well, but consistently underpredict the coarse sands.
- The Brooks & Corey model is slightly better at predicting sands than the van Genuchten model.
- The Campbell model predicts well in the high moisture content range, but breaks down at low moisture contents.

Recent questions have been raised by researchers regarding the selection of the saturated conductivity as the match point for these models. If the area of interest on the conductivity curve is in the low moisture content region, then using the saturated conductivity as a match point for the predictions may not be adequate. Investigators suggest selecting an unsaturated conductivity value near the region of interest as a plausible match point. An inherent assumption in this theory is that the slope of the predicted conductivity curve reflects the actual slope. A statistical analysis is performed to evaluate this theory. The conclusions are:

- The slope of the predicted conductivity curve does not represent the actual slope.
- Predicted slopes of the coarse sands are steeper than the actual slopes

- Predicted slopes of the fine sands are not steep enough.
- The total error between a single measured and predicted conductivity value is determined by the difference between the predicted and measured slope and the value of the moisture content of interest. As you move further away from the match point, the error between the values increase.

In numerical modeling of heterogeneous soils, the capillary pressure curves are often scaled by the spatially variable saturated hydraulic conductivity such that a single curve represents any point within the aquifer. The concept of Leverett scaling has been used to represent spatially variable moisture retention and relative permeability characteristics (Keuper, 1991). Conclusions on our analysis of J-Leverett function are:

- The soils from each site do show a general trend of the van Genuchten parameter α increasing as the square root of the ratio of saturated conductivity and porosity, as implied by Leverett scaling.

- The natural variability in capillarity among individual soil samples from a site is not captured by Leverett scaling.

6.2 Future Research

Several aspects of the work in this study can be continued. First, hysteresis of the moisture retention curve is not addressed in this analysis. The emphasis of the study is on the drainage cycle. Research on the predictive ability of the models using the wetting cycle values may prove interesting. Second, the Brooks & Corey and van Genuchten models both contain predictive equations for the nonwetting phase. Data sets (Demond, 1988 and

TerraTek, 1994) of the measured unsaturated conductivity of the nonwetting phase do exist. Finally, the concept of Leverett-like scaling does warrant some additional research. The soils at each site do reflect the general trends in capillarity implied by Leverett scaling, but Leverett scaling does not represent the variability seen among individual samples at a site. Perhaps a modified form of the J-Leverett function is the solution.

References

Averjanov, S. F., About permeability of subsurface soils in case of incomplete saturation, *English Collection*, 7, 19-21, 1950.

Bear, J., *Dynamics of Fluids in Porous Media*, 764 pp., American Elsevier, New York, 1972.

Bear, J., *Hydraulics of Groundwater*, 567 pp., McGraw-Hill, New York, 1979.

Brooks, R. H. and A. T. Corey, Hydraulic properties of porous media, *Hydrol. Pap. 3*, 27 pp., Colo. State Univ., Fort Collins, 1964.

Burdine, N. T., Relative permeability calculations from pore size distribution data, *Trans. Am. Inst. Min. Metall. Eng.*, 198, 71-78, 1953.

Campbell, G. S., A simple method for determining unsaturated conductivity from moisture retention data, *Soil Science*, 117(6), 311-314, 1974.

Campbell, G. S., *Soil Physics With BASIC*, 150 pp., Elsevier, New York, 1985.

Carvallo, H. O., D. K. Cassel, J. Hammond, and A. Bauer, Spatial variability of in situ unsaturated hydraulic conductivity of Maddock sandy loam, *Soil Sci.*, 121(1), 1-8, 1976.

Childs, E. C., and N. Collis-George, The permeability of porous materials, *Proc. R. Soc. London, Ser. A*, 201, 392-405, 1950.

Clapp, R. B., and G. M. Hornberger, Empirical equations for some soil hydraulic properties, *Water Resour. Res.*, 14(4), 601-604, 1978.

Demond, A. H., Capillarity in two-phase liquid flow of organic contaminants in groundwater, Ph.D. thesis, 211 pp., Stanford Univ., Stanford, Calif., 1988.

Demond, A. H., and P. V. Roberts, An examination of relative permeability relations for two-phase flow in porous media, *Water Resour. Bull.*, 23(4), 617-628, 1987.

Demond, A. H., and P. V. Roberts, Effect of interfacial forces on two-phase capillary pressure relationships, *Water Resour. Res.*, 27(3), 423-437, 1991.

Demond, A. H., and P. V. Roberts, Estimation of two-phase relative permeability relationships for organic liquid contaminants, *Water Resour. Res.*, 29(4), 1081-1090, 1993.

Fatt, I., and H. Dykstra, Relative permeability studies, *Trans. Am. Inst. Min, Metall. Pet. Eng.*, 192, 249-255, 1951.

Fetter, C. W., *Contaminant Hydrogeology*, 458 pp., Macmillan Publishing, New York, 1993.

Gardner, W. R., Some steady-state solutions of the unsaturated moisture flow equation with application to evaporation from a water table, *Soil Sci.*, 85, 228-232, 1958.

Gates, J. I., and W. T. Lietz, Relative permeabilities of California cores by the capillary-pressure method, drilling and production practice, *Am. Pet. Inst.*, Q, 285-298, 1950.

Hillel, D., *Fundamentals of Soil Physics*, 413 pp., Academic Press, 1980.

Irmay, S., On the hydraulic conductivity of unsaturated soils, *Trans. Am. Geophys. Union*, 35, 463-467, 1954.

Jackson, R. D., Reginato, R. J., and C. H. M. van Bavel, Comparison of measured and calculated hydraulic conductivities of unsaturated soils, *Water Resour. Res.*, 1, 375-380, 1965.

Jury, W. A., W. R. Gardner, and W. H. Gardner, *Soil Physics, 5th ed.*, 328 pp., John Wiley & Sons, New York, 1991.

Keuper, B. H., and E. O. Frind, Two-phase flow in heterogeneous porous media, 1, model development, *Water Resour. Res.*, 27(6), 1049-1057, 1991.

Keuper, B. H., and E. O. Frind, Two-phase flow in heterogeneous porous media, 2, model application, *Water Resour. Res.*, 27(6), 1059-1070, 1991.

Khaleel, R., Personal communication with Dr. Lynn Gelhar containing Hanford moisture retention and unsaturated conductivity data, 1996.

Khaleel, R., J. F. Relyea, and J. L. Conca, Evaluation of van Genuchten-Mualem relationships to estimate unsaturated hydraulic conductivity at low water contents, *Water Resour. Res.*, 31(11), 2659-2668, 1995.

King, L. G., Imbibition of fluids by porous solids, Ph.D. thesis, Colorado State Univ., Ft. Collins, Colorado, 1964.

Knowlton, R. G., A field study and numerical simulation of natural ground-water recharge, M. S. thesis, 135 pp., New Mexico Institute of Mining and Technology, Socorro, New Mexico, 1984.

Knowlton, R. G., A field study and numerical simulation of natural ground-water recharge, appendices, M. S. thesis, New Mexico Institute of Mining and Technology, Socorro, New Mexico, 1984.

Kool, J. B., and J. C. Parker, Development and evaluation of closed-form expressions for hysteretic soil hydraulic properties, *Water Resour. Res.*, 23(1), 105-114, 1987.

Laliberte, G. E., A. T. Corey, and R. H. Brooks, Properties of unsaturated porous media, *Hydrol. Pap. 17*, 40 pp., Colo. State Univ., Fort Collins, 1966.

Leij, F. J., M. T. van Genuchten, S. R. Yates, W. B. Russel, and F. Kaveh, RETC: A computer program for describing and analyzing soil water retention and hydraulic conductivity data, M. T. van Genuchten et al. (ed.) Proc. Int. Worksh. indirect methods for estimation the hydraulic properties of unsaturated soils, Univ. of Calif., Riverside, Riverside, Calif., 1989.

Lenhard, R. J., J. C. Parker, and S. Mishra, On the correspondence between Brooks-Corey and van Genuchten models, *Journal of Irrigation and Drainage Engineering*, 115(4), 1989.

Lenhard, R. J., and J. C. Parker, A model for hysteretic constitutive relations governing multiphase flow, 2, Permeability-saturation relations, *Water Resour. Res.*, 23(12), 2197-2206, 1987.

Luckner, L., M. T. van Genuchten, and D. R. Nielsen, A consistent set of parametric models for the two-phase flow of immiscible fluids in the subsurface, *Water Resour. Res.*, 25(10), 2187-2193, 1989.

Mace, R. A., Steady-state flow and non-reactive transport in unsaturated sand and gravel cores, M. S. thesis, University of Waterloo, Waterloo, Ontario, Canada, 1994.

Mantoglou, A., and L. W. Gelhar, Stochastic modeling of large-scale transient unsaturated flow systems, *Water Resour. Res.*, 23(1), 37-46, 1987.

Millington, R. J., and J. P. Quirk, Permeability of porous solids, *Faraday Soc. Trans.*, 57, 1200-1206, 1961.

Milly, P. C. D, Estimation of Brooks-Corey parameters from water retention data, *Water Resour. Res.*, 23(6), 1085-1089, 1987.

Mualem, Y., A new model for predicting the hydraulic conductivity of unsaturated porous media, *Water Resour. Res.*, 12(3), 513-522, 1976.

Mualem, Y., A catalogue of the hydraulic properties of unsaturated soils, Res. Proj. 442, Technion, Israel Inst. of Technol., Haifa, Israel, 1976.

Mualem, Y., Hydraulic conductivity of unsaturated porous media: generalized macroscopic approach, *Water Resour. Res.*, 14(2), 325-334, 1978.

Mualem, Y., Hydraulic conductivity of unsaturated soils: prediction and formulas, in *Methods of Soil Analysis*, vol.1, *Physical and Mineralogical Methods*, edited by A. Klute, pp. 799-824, American Society of Agronomy, Madison, Wis., 1986.

Nimmo, J., Personal communication with Dr. Lynn Gelhar containing Hanford moisture retention and unsaturated conductivity data, 1997.

Parker, J. C., Multiphase flow and transport in porous media, *Reviews of Geophysics*, 27, 311-328, 1989.

Parker, J. C., R. J. Lenhard, and T. Kuppusamy, A parametric model for constitutive properties governing multiphase flow in porous media, *Water Resour. Res.*, 23(4), 618-624, 1987.

Purcell, W. R., Capillary pressures-their measurement using mercury and the calculation of permeability therefrom, *Pet. Trans. Am. Inst. Min., Metall. Pet. Eng.*, 186, 39-48, 1949.

Rijtema, P. E., An analysis of actual evapotranspiration, Agric. Res. Rep. 659, Center for Agricultural Publications and Documentation, Wageningen, The Netherlands, 1965.

Russo, D., Determining soil hydraulic properties by parameter estimation: on the selection of a model for the hydraulic properties, *Water Resour. Res.*, 24(3), 453-459, 1988.

Shakofsky, S., Changes in soil hydraulic properties caused by construction of a simulated waste trench at the Idaho National Engineering Laboratory, Idaho, U. S. Geological Survey Water-Resource Investigations Report 95-4058, 25 pp., 1995.

Stephens, D. B., and K. R. Rehfeldt, Evaluation of closed-form analytical models to calculate conductivity in a fine sand, *Soil Sci. Soc. Am. J.*, 49, 12-19, 1985.

Stephens, D. B., and R. K. Knowlton, Jr., Soil water movement and recharge through sand at a semiarid site in New Mexico, *Water Resour. Res.*, 22(6), 881-889, 1986.

Stephens, D. B., *Vadose Zone Hydrology*, 339 pp, CRC Press, Boca Raton, 1996.

TerraTek, DNAPL flow characterizations in aquifer sands, Hill Air Force Base, OU 2, Prepared for Radian Corporation, TR94-45, 1994.

van Genuchten, M. T., A closed form solution for predicting the hydraulic conductivity of unsaturated soils, *Soil Sci. Soc. Am. J.*, 44, 892-898, 1980.

van Genuchten, M. T., and D. R. Nielsen, On describing and predicting the hydraulic properties of unsaturated soils, *Ann. Geophys.*, 3(5), 615-628, 1985.

Wierenga, P., Personal communication with Dr. Lynn Gelhar containing Las Cruces moisture retention and unsaturated conductivity data, 1991.

Wierenga, P. J., R. G. Hills, and D. B. Hudson, The Las Cruces trench site: characterization, experimental results, and one-dimensional flow predictions, *Water Resour. Res.*, 27(10), 2695-2705, 1991.

Wind, G. P., Field experiment concerning capillary rise of moisture in heavy clay soil, *Neth. J. Agric. Sci.*, 3, 60-69, 1955.

Wyllie, M. R. J., and G. H. F. Gardner, The generalized Kozeny-Carman equation 11, *World Oil Prod. Sect.*, 146, 210-228, 1958.

Yates, S. R., M. T. van Genuchten, A. W. Warrick, and F. J. Leij, Analysis of measured, predicted, and estimated hydraulic conductivity using the RETC computer program, *Soil Sci. Soc. Am. J.*, 56, 347-354, 1992.

Yeh, T. C. J., L. W. Gelhar, and A. L. Gutjahr, Stochastic analysis of unsaturated flow in heterogeneous soils, 1, statistically isotropic media, *Water Resour. Res.*, 21(4), 447-456, 1985.

Yuster, S. T., Theoretical considerations of multiphase flow in idealized capillary systems, *Proc. World Pet. Congr., 3rd,*, 2, 437-445, 1951.

Appendix A: Table of Moisture Retention Parameters

	Data set	sample no	van Genuchten theta r	van Genuchten n	van Genuchten alpha	van Genuchten theta s
0	Hanford	0-072	0.045513	2.0967	0.0061531	0.32001
1		0-079	0.047929	2.4132	0.0058319	0.36001
2		0-080	0.025562	1.9640	0.0074827	0.37000
3		0-083	0.047300	1.8046	0.0042779	0.34002
4		0-099	0.032718	1.6567	0.011548	0.33000
5		0-107	0.013776	1.5492	0.20120	0.35028
6		0-113	0.016809	1.6849	0.067076	0.30003
7		1417	0.034391	1.8032	0.0047201	0.35500
8		1419	0.0067962	1.3821	0.56867	0.30153
9		1636	0.014573	1.4781	0.32462	0.31993
10		1637	0.010928	1.4607	0.26944	0.31404
11		1638	0.0061047	1.4112	0.061560	0.27150
12		1639	0.010065	1.4094	0.72627	0.32220
13		2225	0.019164	1.9237	0.036274	0.32300
14		2226	0.012350	1.3990	0.86617	0.28751
15		2227	0.014749	1.7259	0.11949	0.32706
16		2228	0.0095593	1.5019	0.51143	0.29107
17		2229	0.012465	1.5067	0.43734	0.30789
18		2230	0.033799	1.5170	0.017537	0.34016
19		2232	0.013081	1.5096	0.12186	0.24400
20		2233	0.0072686	1.3818	0.49604	0.29122
21		2234	0.0088423	1.5142	0.071112	0.27805
22	Cape Cod	12a	0.0100000	2.1163	0.25223	0.33000
23		13a	0.0100000	2.2586	0.24737	0.33700
24		14a	0.0100000	2.2200	0.24554	0.35300
25		15a	0.0100000	2.2107	0.19658	0.35100
26		16a	0.0100000	2.3956	0.16834	0.34800
27		17a	0.0100000	2.1054	0.26253	0.35600
28	INEL	u(a) 30	0.21804	1.2967	0.013416	0.40594
29		u(b) 30	0.21241	1.6957	0.022957	0.46150
30		d(a) 30	0.20605	2.0397	0.0096232	0.41295
31		d(b) 30	0.19438	1.7552	0.0093944	0.45980
32		u(a) 80	0.18255	1.4808	0.020355	0.43814
33		u(b) 80	0.18275	1.5455	0.057445	0.48210
34		d(a) 80	0.13970	1.4074	0.025617	0.46448

	Data set	sample no	van Genuchten theta r	van Genuchten n	van Genuchten alpha	van Genuchten theta s
35		d(b) 80	0.18362	1.5093	0.022140	0.44100
36		u(a) 145	0.21354	1.3182	0.014415	0.41237
37		u(b) 145	0.18930	1.3326	0.017178	0.40444
38		d(a) 145	0.13724	1.2651	0.16109	0.58272
39		d(b) 145	0.23377	1.5894	0.039510	0.57164
40		u(a) 225	0.22335	1.4823	0.015132	0.46436
41		u(b) 225	0.30040	1.7724	0.0068872	0.45122
42		d(a) 225	0.18619	1.6023	0.027161	0.45246
43		d(b) 225	0.18229	1.5140	0.048154	0.46015
44	Las Cruces	3-34	0.055267	1.4878	0.23637	0.33700
45		4-25	0.049440	1.3337	0.084432	0.31500
46		5-34	0.0084438	1.2776	0.11054	0.30500
47		7-21	0.077206	1.2922	0.055128	0.32200
48		8-49	0.061522	1.3896	0.18000	0.33200
49	Sevilleta	30.5	0.055984	3.8915	0.028241	0.34767
50		61.0	0.056102	3.4910	0.036458	0.35928
51		91.5	0.068606	4.5054	0.028012	0.32458
52	Maddock	1-1	0.19843	1.4556	0.041327	0.41800
53		1-2	0.13750	1.6024	0.044432	0.41800
54		1-3	0.14322	1.6645	0.047260	0.39900
55		1-4	0.11979	2.2131	0.051811	0.39000
56		1-5	0.069718	3.3949	0.039038	0.36700
57		1-6	0.12507	2.7622	0.045622	0.40600
58		1-7	0.10768	2.9120	0.068130	0.43600
59		2-1	0.20196	1.6439	0.040619	0.40800
60		2-2	0.15481	1.7328	0.036288	0.39100
61		2-3	0.14865	1.8019	0.032448	0.36700
62		2-4	0.099873	2.1251	0.049786	0.36300
63		2-5	0.083576	3.2581	0.037864	0.37100
64		2-6	0.088617	3.2814	0.046102	0.39400
65		2-7	0.12699	2.6059	0.075791	0.45600

	Data set	sample no	Brooks Corey theta r	Brooks Corey lambda	Brooks Corey psi b
0	Hanford	0-072	0.042312	0.78400	79.597
1		0-079	0.054027	1.0445	94.761
2		0-080	0.027662	0.91498	86.948
3		0-083	0.022778	0.46927	102.79
4		0-099	0.018926	0.45506	41.345
5		0-107	0.013680	0.54280	4.7178
6		0-113	0.016597	0.66471	13.355
7		1417	0.030052	0.65821	132.74
8		1419	0.0066998	0.38001	1.7186
9		1636	0.014483	0.47367	3.2179
10		1637	0.010847	0.45719	3.8878
11		1638	0.0051153	0.39605	14.312
12		1639	0.0099868	0.41674	1.3502
13		2225	0.018334	0.76590	15.187
14		2226	0.012324	0.39818	1.1562
15		2227	0.014706	0.71812	8.0089
16		2228	0.0095244	0.49983	1.8993
17		2229	0.012452	0.50517	2.2607
18		2230	0.034990	0.52467	59.552
19		2232	0.012761	0.49613	7.3941
20		2233	0.0071451	0.37914	1.9630
21		2234	0.0080274	0.48955	11.954
22	Cape Cod	12a	0.0100000	0.86425	2.8342
23		13a	0.0100000	1.0024	3.0247
24		14a	0.0100000	0.94350	2.9443
25		15a	0.0100000	0.92081	3.6077
26		16a	0.0100000	0.99606	4.1004
27		17a	0.0100000	0.93274	2.9482
28	Nimmo/Idaho	u(a) 30	0.21804	0.25230	39.053
29		u(b) 30	0.21241	0.57177	27.758
30		d(a) 30	0.20605	0.85273	70.821
31		d(b) 30	0.19438	0.58356	55.944
32		u(a) 80	0.18255	0.38372	26.484
33		u(b) 80	0.18275	0.56172	20.015
34		d(a) 80	0.13970	0.33613	22.524

	Data set	sample no	Brooks Corey theta r	Brooks Corey lambda	Brooks Corey psi b
35		d(b) 80	0.18362	0.40873	26.081
36		u(a) 145	0.26633	0.46938	29.354
37		u(b) 145	0.18930	0.27584	34.801
38		d(a) 145	0.13724	0.25311	5.1503
39		d(b) 145	0.23377	0.50226	16.140
40		u(a) 225	0.22335	0.39026	38.517
41		u(b) 225	0.30040	0.55632	76.218
42		d(a) 225	0.18619	0.49396	20.280
43		d(b) 225	0.18229	0.45317	13.595
44	Las Cruces	3-34	0.054744	0.46684	3.6048
45		4-25	0.040695	0.28030	7.8747
46		5-34	0.0000	0.23908	6.0231
47		7-21	0.044061	0.19510	9.5726
48		8-49	0.059871	0.36380	4.4293
49	Knowlton	30.5	0.042970	1.5349	23.522
50		61.0	0.050779	1.6976	21.086
51		91.5	0.061856	1.8389	22.467
52	Maddock	1-1	0.10464	0.20278	12.175
53		1-2	0.083099	0.33460	12.025
54		1-3	0.11662	0.43695	12.639
55		1-4	0.11771	1.0399	14.980
56		1-5	0.069535	2.0509	19.765
57		1-6	0.12449	1.4714	15.720
58		1-7	0.10760	1.7706	12.336
59		2-1	0.16921	0.37822	13.767
60		2-2	0.11447	0.40180	14.695
61		2-3	0.10937	0.42027	16.144
62		2-4	0.096538	0.93136	14.917
63		2-5	0.083227	1.8406	18.804
64		2-6	0.088395	1.9485	16.586
65		2-7	0.12680	1.4980	11.351

	Data set	sample no	Campbell psi e	Campbell b
0	Cape Cod	12a	2.7801	1.2391
1		15a	3.5445	1.1602
2		17a	2.8569	1.1611
3	INEL	u(a) 30	20.234	13.785
4		u(b) 30	5.2978	8.7186
5		d(a) 30	28.038	5.8580
6		d(b) 30	23.952	6.2032
7		u(a) 80	17.828	6.9436
8		u(b) 80	1.8582	8.4361
9		d(a) 80	13.668	6.0857
10		d(b) 80	13.240	7.1098
11		u(a) 145	7.0915	12.661
12		u(b) 145	19.144	10.519
13		d(a) 145	3.4767	6.6515
14		d(b) 145	10.137	5.8214
15		u(a) 225	20.912	8.4134
16		u(b) 225	37.440	11.510
17		d(a) 225	14.013	5.7495
18		d(b) 225	8.1387	6.1479
19	Las Cruces	3-34	0.95922	4.7307
20		4-25	5.6952	5.1302
21		5-34	6.0231	4.1826
22		7-21	8.1023	6.8135
23		8-49	1.8623	5.3017
24	Sevilleta	30.5	21.916	1.0442
25		61.0	18.669	1.1321
26		91.5	19.826	1.1759
27	Maddock	1-1	10.695	7.5128
28		1-2	9.8333	4.5437
29		1-3	8.1663	4.6785
30		1-4	5.5165	3.5225
31		1-5	9.6942	1.8798
32		1-6	8.2134	2.8173
33		1-7	5.8964	2.4743
34		2-1	9.4994	6.6670
35		2-2	11.176	4.7752
36		2-3	12.470	4.6204
37		2-4	6.7066	3.1787
38		2-5	10.570	2.0341
39		2-6	8.5554	2.1139
40		2-7	3.2078	3.2765

Appendix B: Cape Cod Curve Fits

core 12a

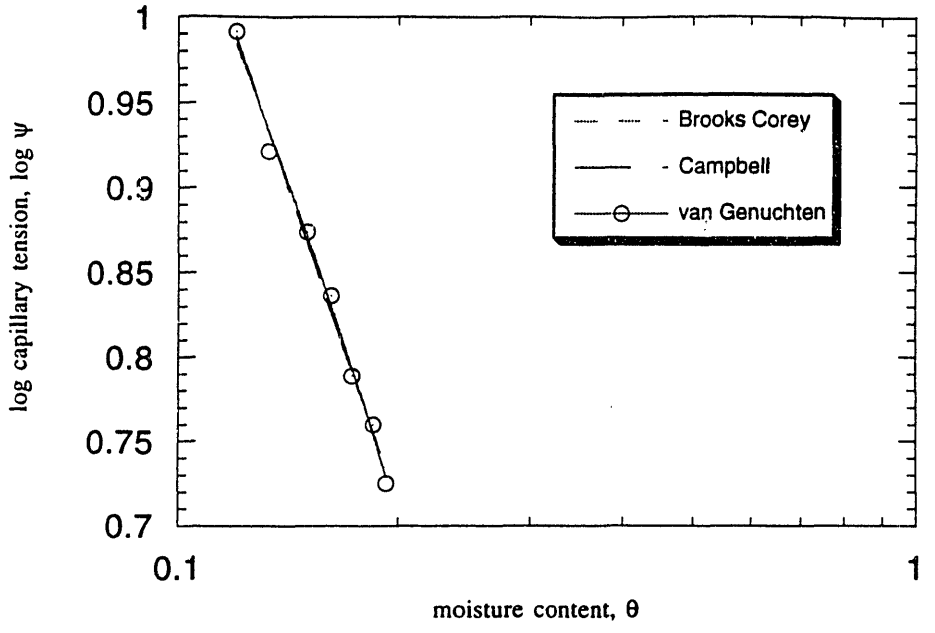

y = bc(.01,.1,1,.33)		
	Value	Error
λ	0.86425	0.032252
ψ_β	2.8342	0.097262
Chisq	0.00036602	NA
R	0.99654	NA

y = camp(1,.1,.33)		
	Value	Error
ψ_e	2.7801	0.095759
b	1.2391	0.045459
Chisq	0.00035418	NA
R	0.99665	NA

y = vg(0.01,1.5,.001,.33)		
	Value	Error
n	2.1163	0.047805
α	0.25223	0.0080068
Chisq	0.00030591	NA
R	0.99711	NA

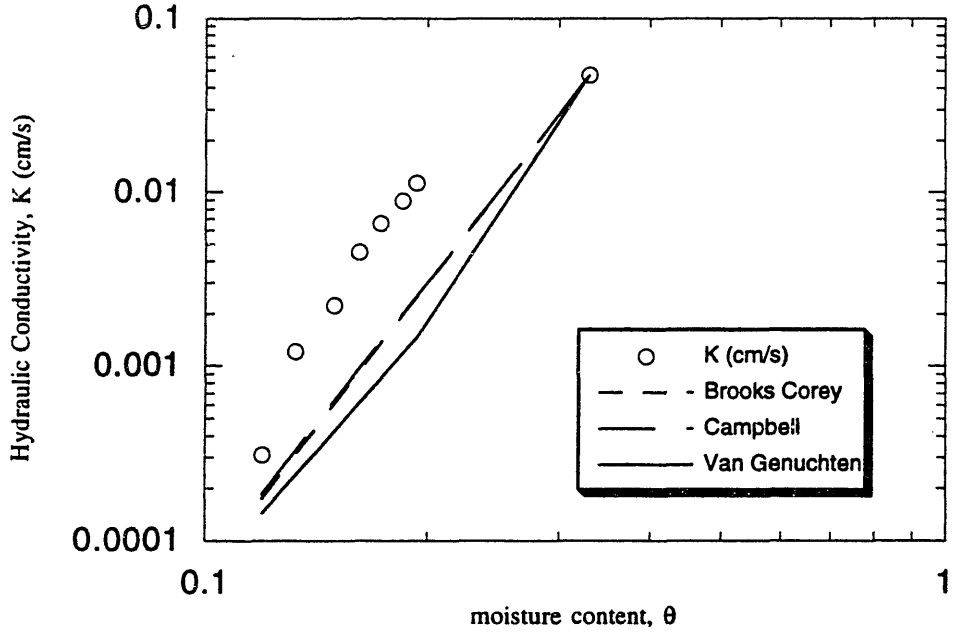

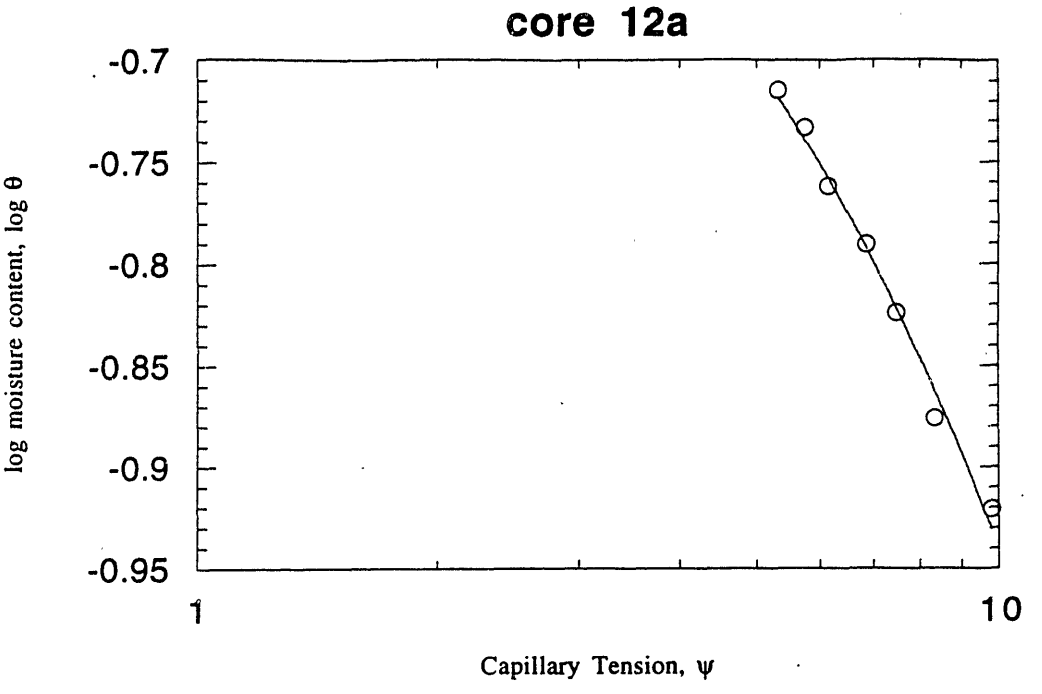

y = rus(.01,.1,.1,.33)		
	Value	Error
b	12.436	12.465
c	102	111.36
Chisq	0.00037838	NA
R	0.99447	NA

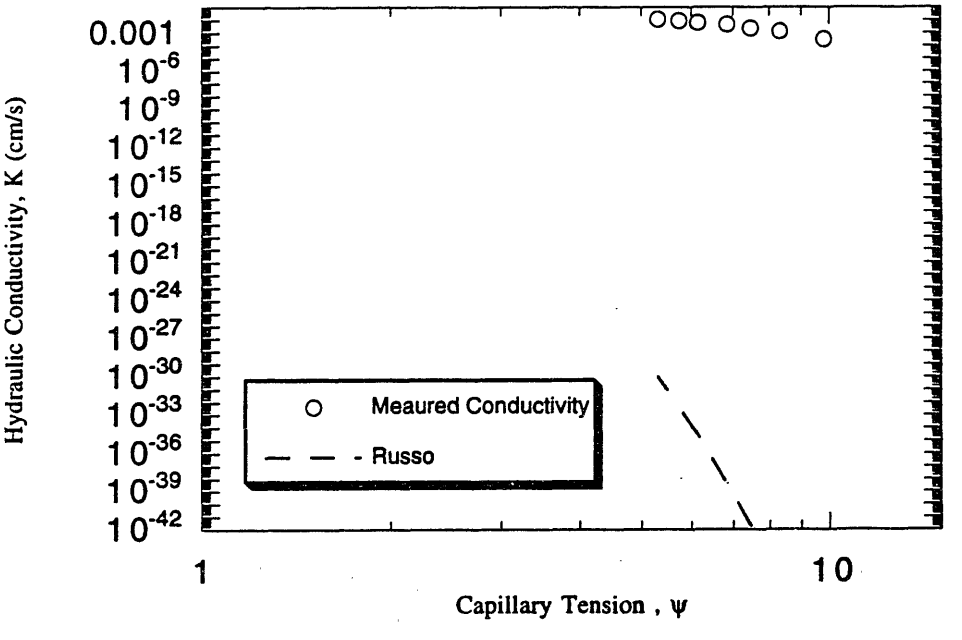

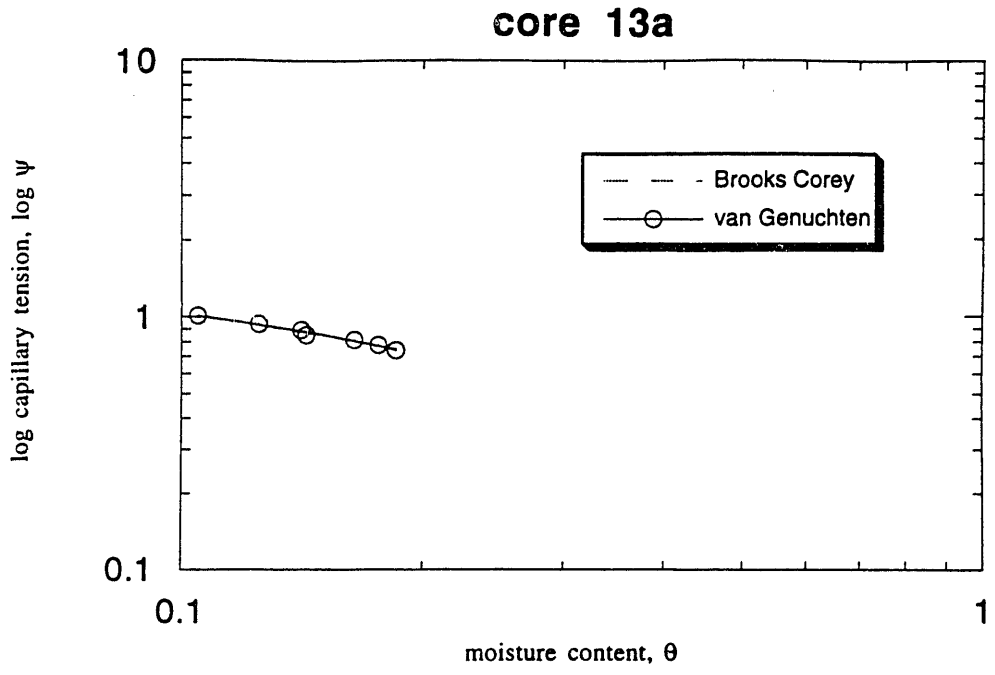

y = bc(.01,.1,1,.337)		
	Value	Error
λ	1.0024	0.053053
ψ_β	3.0247	0.14388
Chisq	0.00072892	NA
R	0.99308	NA

y = vg(0.01,1.5,.001,.337)		
	Value	Error
n	2.2586	0.082065
α	0.24737	0.011871
Chisq	0.00074697	NA
R	0.9929	NA

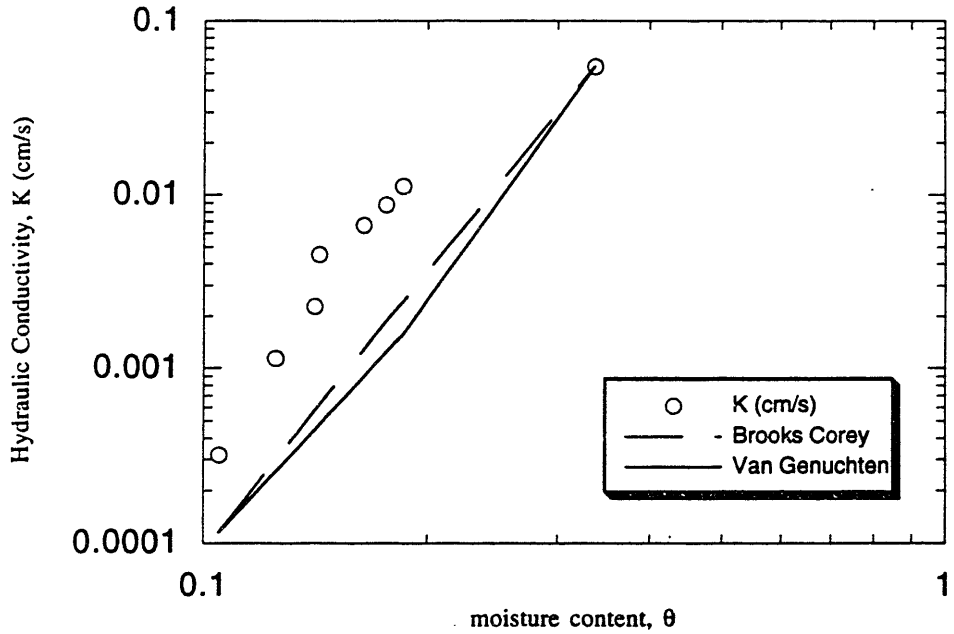

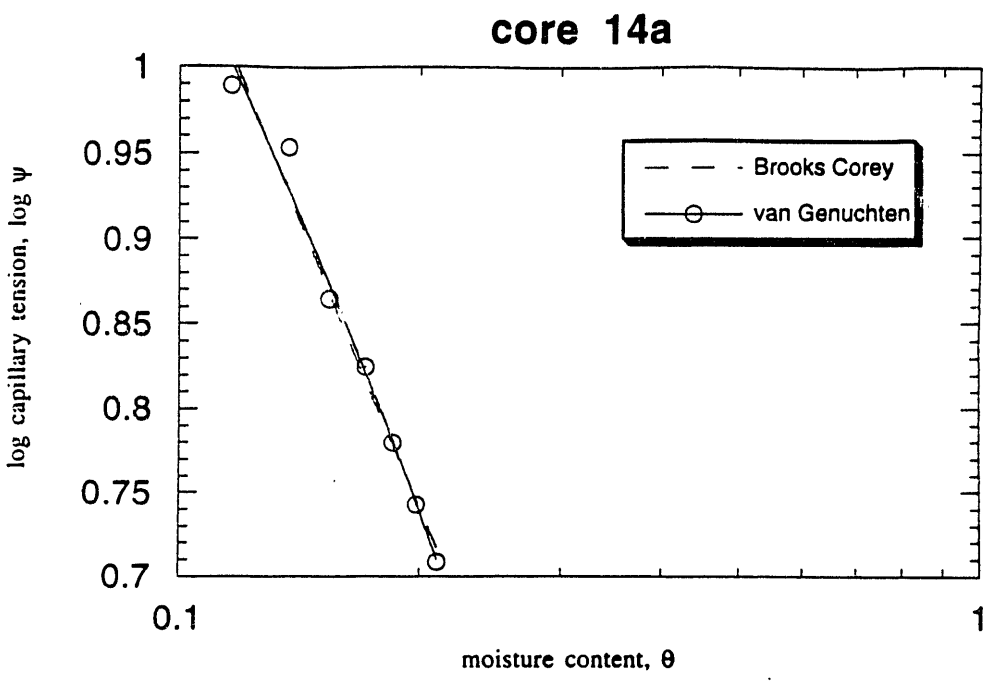

y = bc(.01,.1,1,.353)		
	Value	Error
λ	0.9435	0.060046
ψ_β	2.9443	0.16436
Chisq	0.0013185	NA
R	0.99004	NA

y = vg(0.01,1.5,.001,.353)		
	Value	Error
n	2.22	0.080748
α	0.24554	0.01135
Chisq	0.00092853	NA
R	0.99299	NA

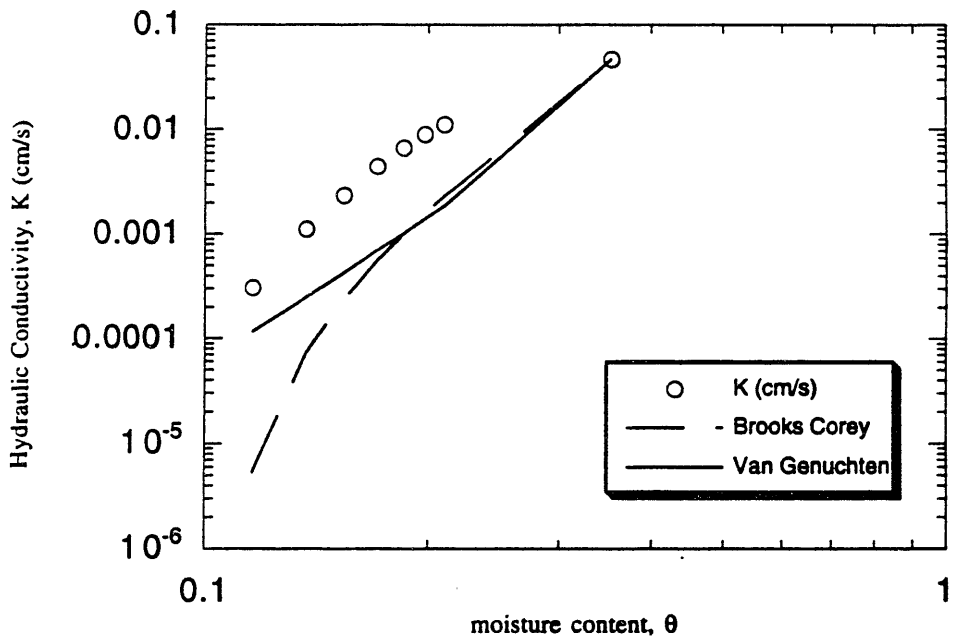

core 15a

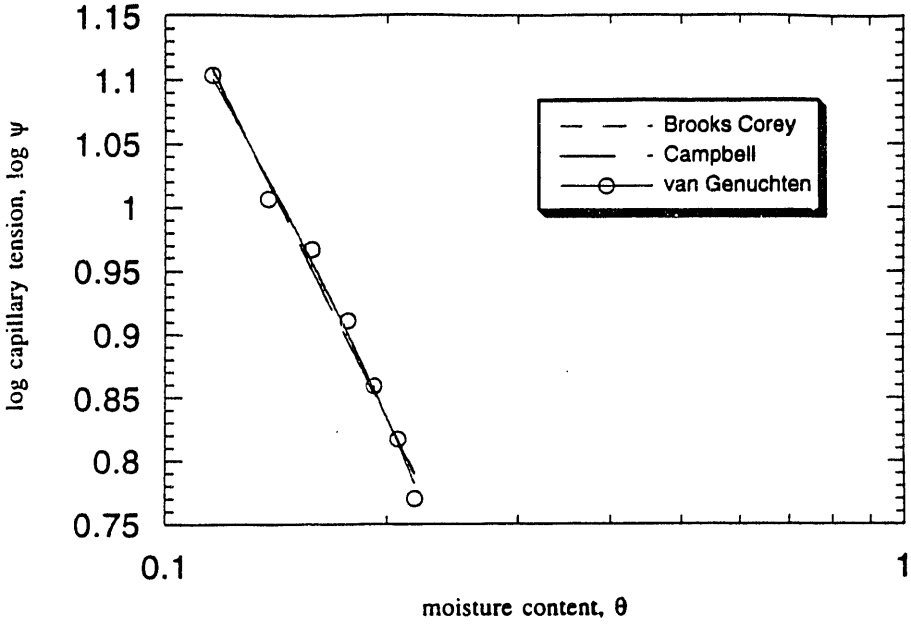

y = bc(.01,.1,1,.351)		
	Value	Error
λ	0.92081	0.050034
ψ_β	3.6077	0.17011
Chisq	0.0011654	NA
R	0.99271	NA

y = camp(1,.1,.351)		
	Value	Error
ψ_c	3.5445	0.16498
b	1.1602	0.061005
Chisq	0.0010934	NA
R	0.99316	NA

y = vg(0.01,1.5,.001,.351)		
	Value	Error
n	2.2107	0.058968
α	0.19658	0.006499
Chisq	0.00059922	NA
R	0.99626	NA

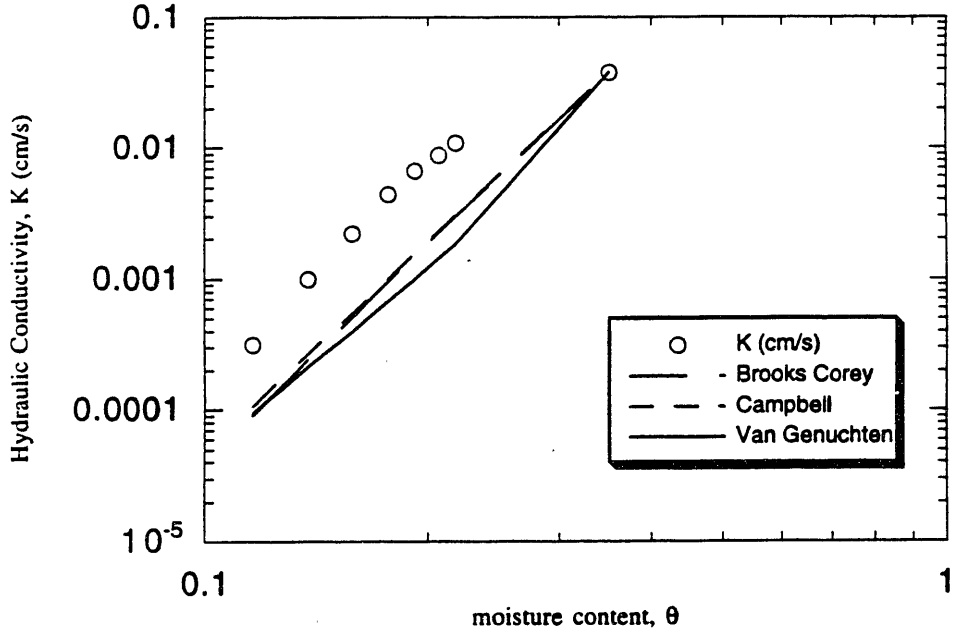

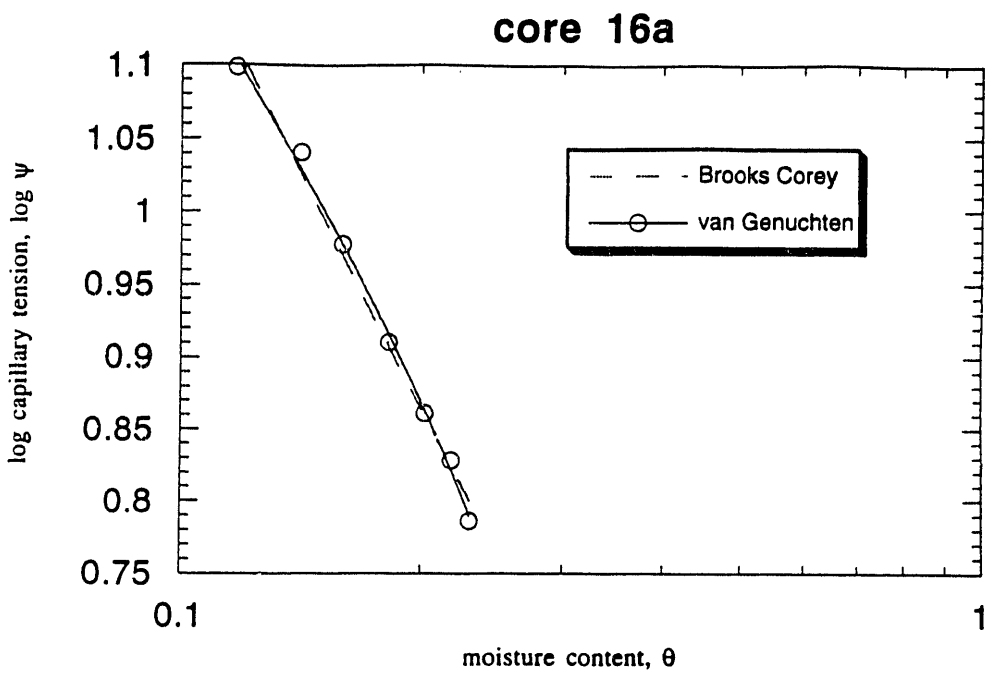

y = bc(.01,.1,1,.348)		
	Value	Error
λ	0.99606	0.043396
Ψ_β	4.1004	0.13704
Chisq	0.00074246	NA
R	0.99529	NA

y = vg(0.01,1.5,.001,.348)		
	Value	Error
n	2.3956	0.045262
α	0.16834	0.0029993
Chisq	0.00025964	NA
R	0.99836	NA

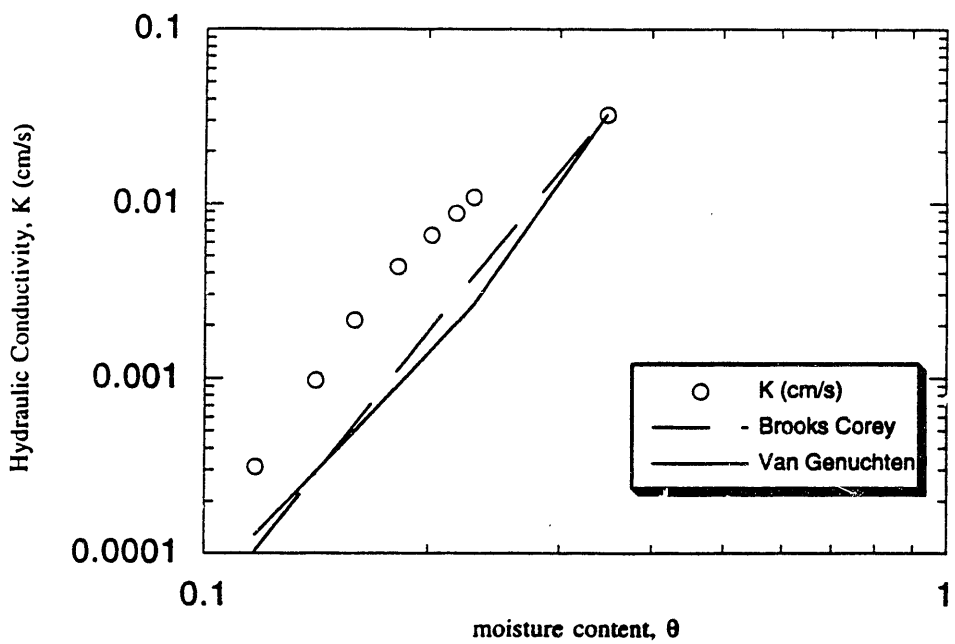

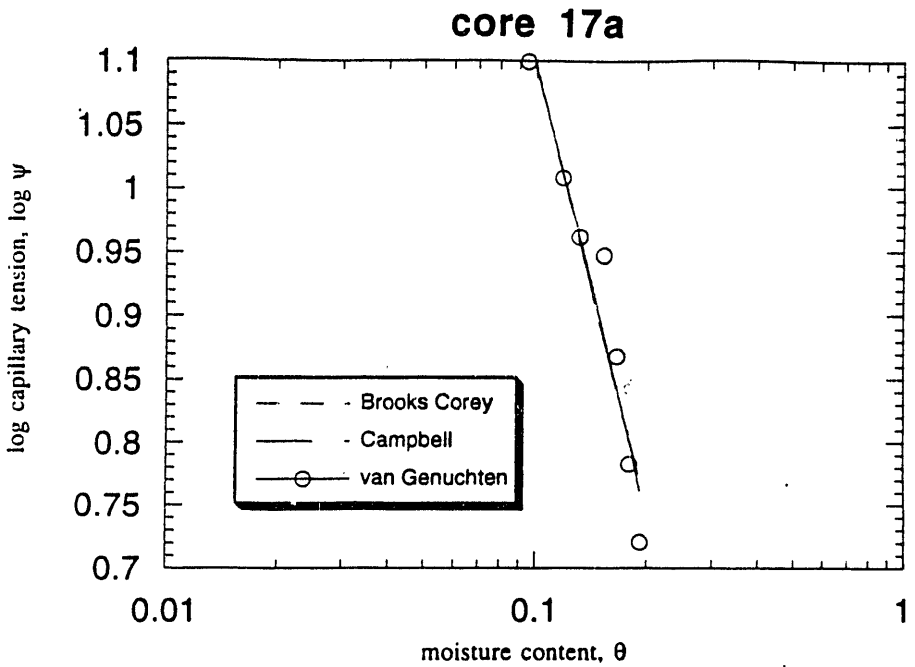

y = bc(.01,.1.1,.356)		
	Value	Error
c	0.93274	0.12449
d	2.9482	0.41483
Chisq	0.0084693	NA
R	0.95827	NA

y = camp(1,.1,.356)		
	Value	Error
a	2.8569	0.40507
b	1.1611	0.15168
Chisq	0.0081494	NA
R	0.95988	NA

y = vg(0.01,1.5,.001,.356)		
	Value	Error
b	2.1054	0.15769
c	0.26253	0.034451
Chisq	0.0068349	NA
R	0.96647	NA

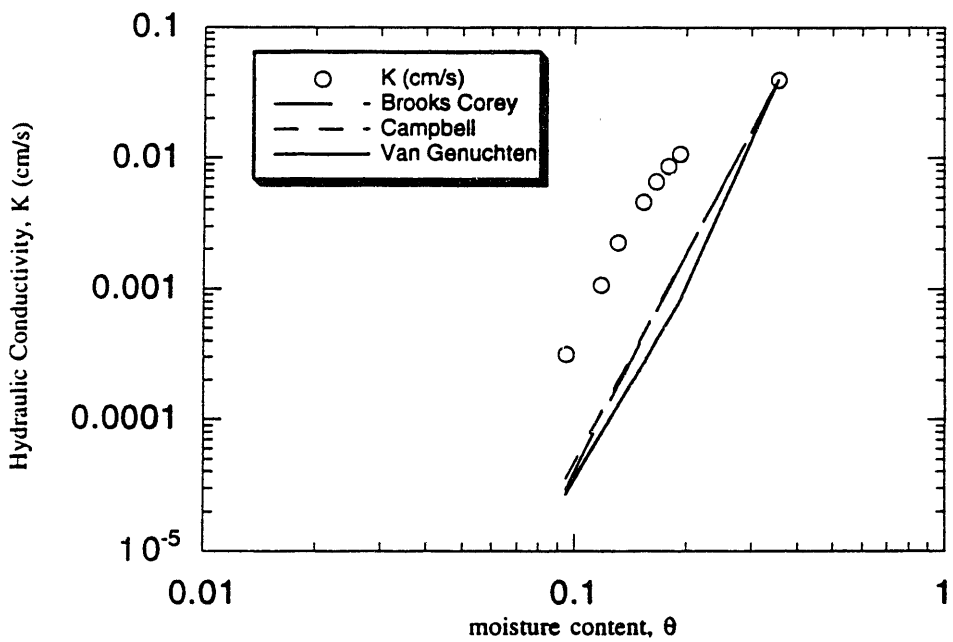

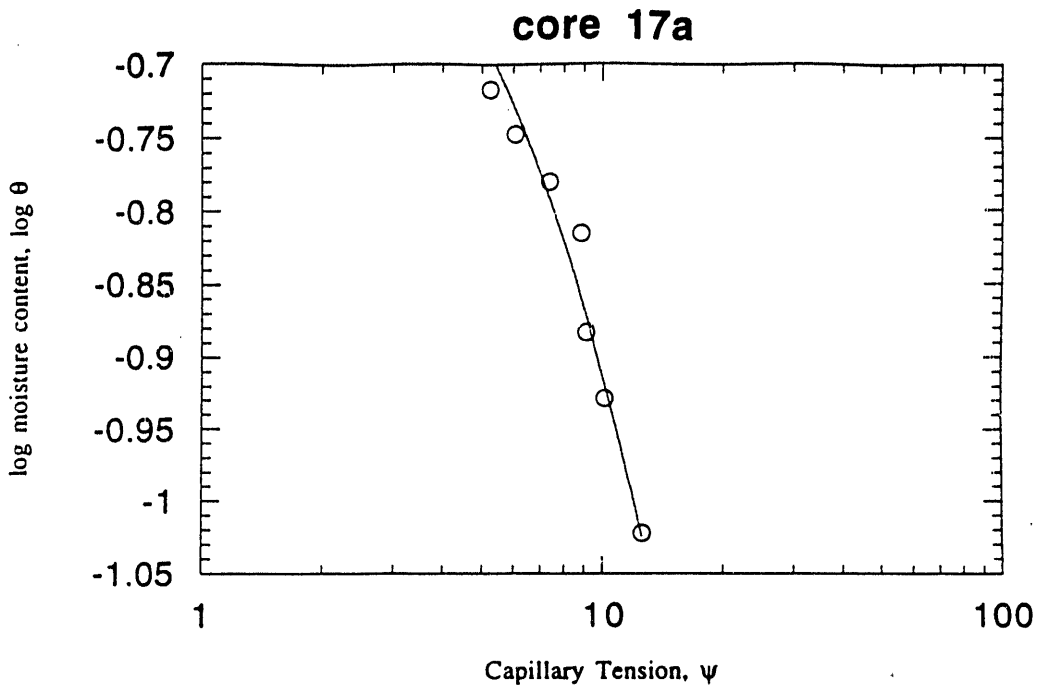

y = rus(.01,.1,.1,.356)		
	Value	Error
α	114.83	1208.2
m	1013	10793
Chisq	0.0030654	NA
R	0.97813	NA

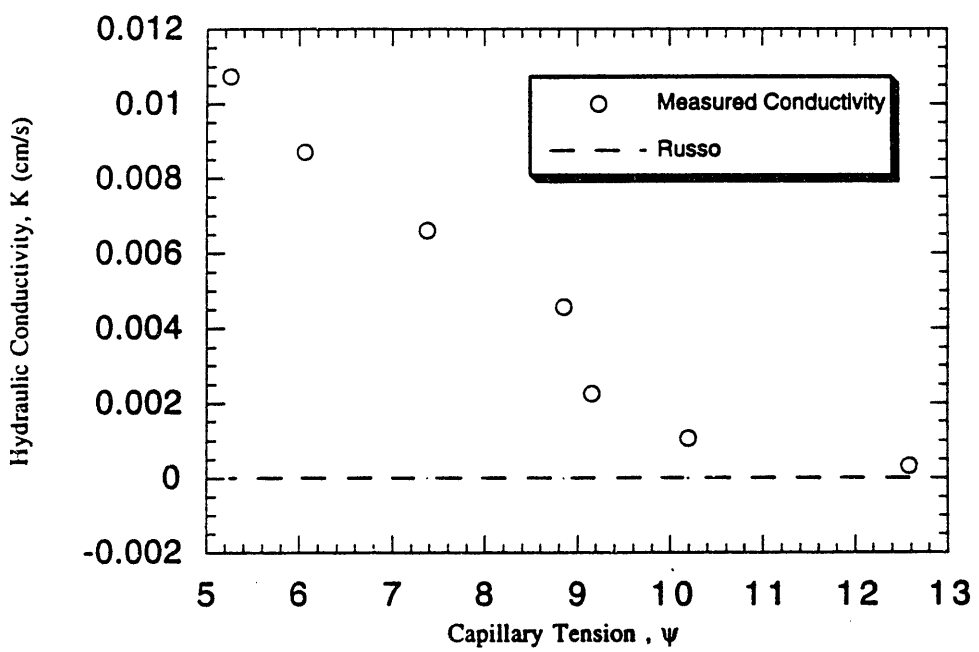

Appendix C: Hanford Curve Fits

0-072

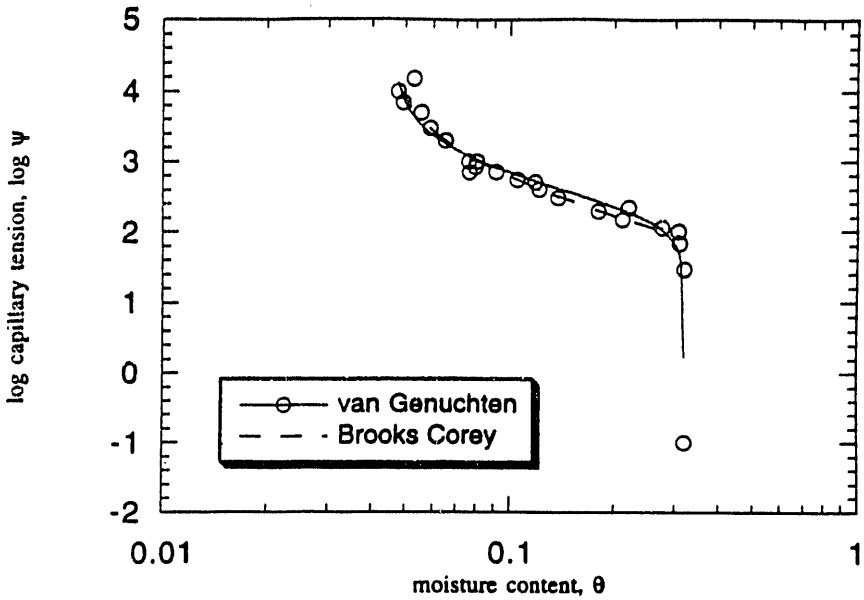

y = vg(0.01,1.5,.001,.3275)		
	Value	Error
θ_r	0.045513	0.0036503
n	2.0967	0.3058
α	0.0061531	0.0024439
θ_s	0.32001	0.00014252
Chisq	3.6257	NA
R^2	0.85409	NA

y = bc(.01,.1,1,.3275)		
	Value	Error
θ_r	0.042312	0.0023744
λ	0.784	0.07719
Ψ_b	79.597	12.269
Chisq	0.36548	NA
R^2	0.95975	NA

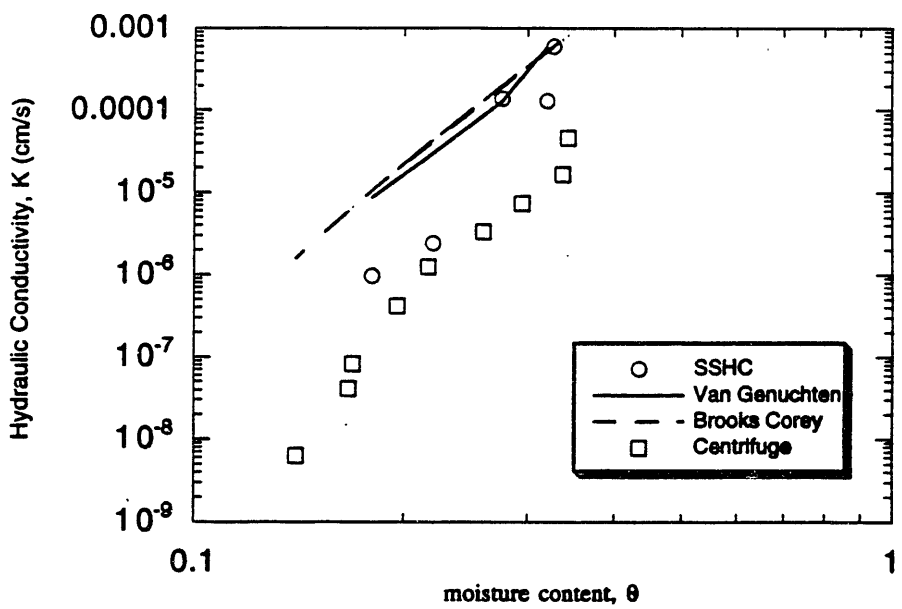

0-079

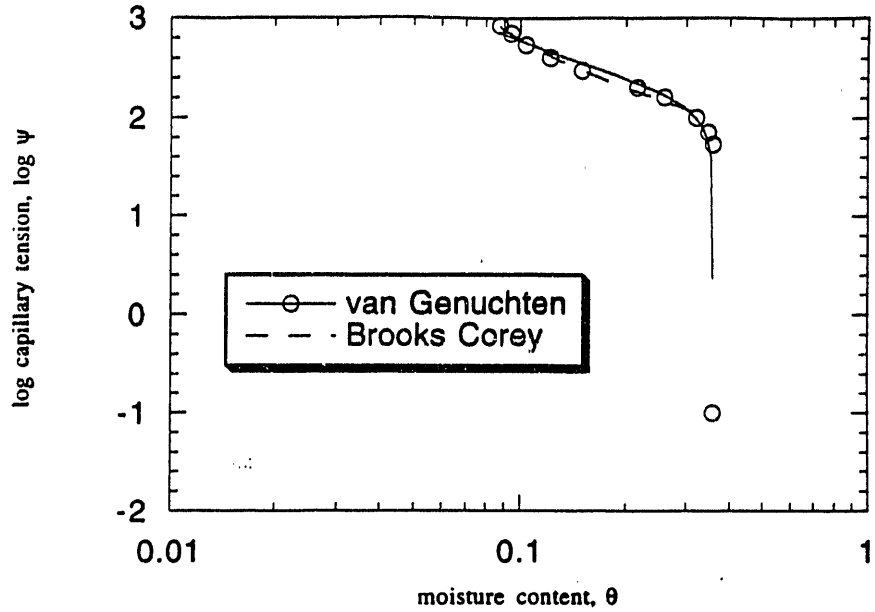

y = vg(0.01,1.5,.001,.3754)		
	Value	Error
θ_r	0.047929	0.28107
n	2.4132	3.1945
α	0.0058319	0.0057308
θ_s	0.36001	0.00069162
Chisq	3.7594	NA
R^2	0.68376	NA

y = bc(.01,.1,1,.3754)		
	Value	Error
θ_r	0.054027	0.014077
λ	1.0445	0.18384
Ψ_b	94.761	8.0822
Chisq	0.0071139	NA
R^2	0.99045	NA

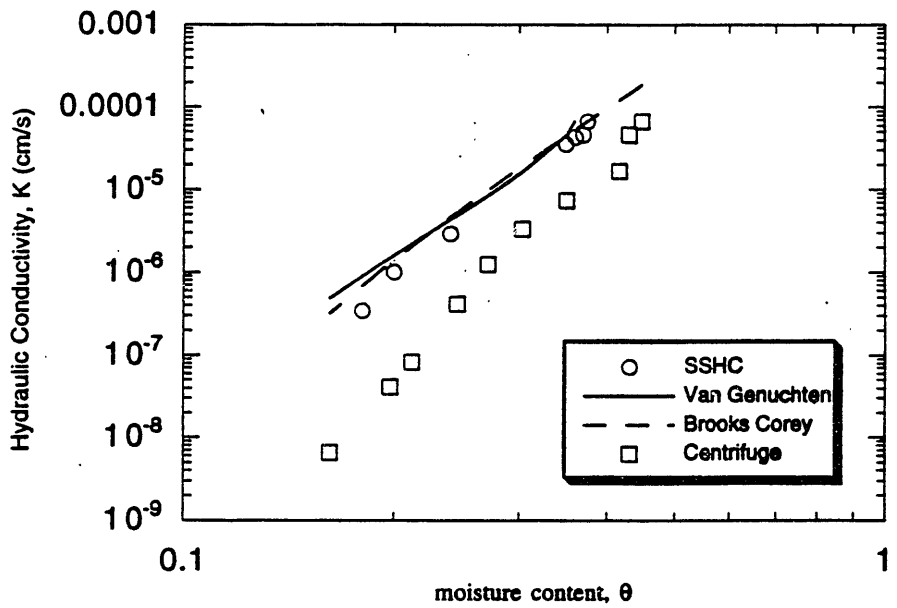

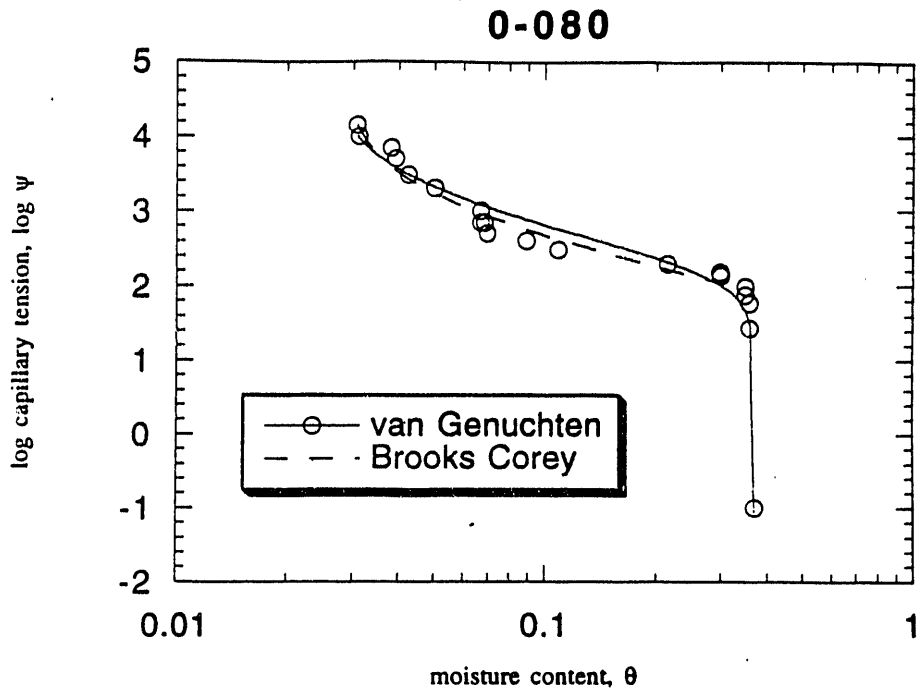

y = vg(0.01,1.5,.001,.375)		
	Value	Error
θ_r	0.025562	0.0035078
n	1.964	0.12308
α	0.0074827	0.0013148
θ_s	0.37	3.561e-05
Chisq	0.73307	NA
R^2	0.97081	NA

y = bc(.01,.1,1,.3669)		
	Value	Error
θ_r	0.027662	0.0015366
λ	0.91498	0.099997
Ψ_b	86.948	18.367
Chisq	0.25812	NA
R^2	0.95933	NA

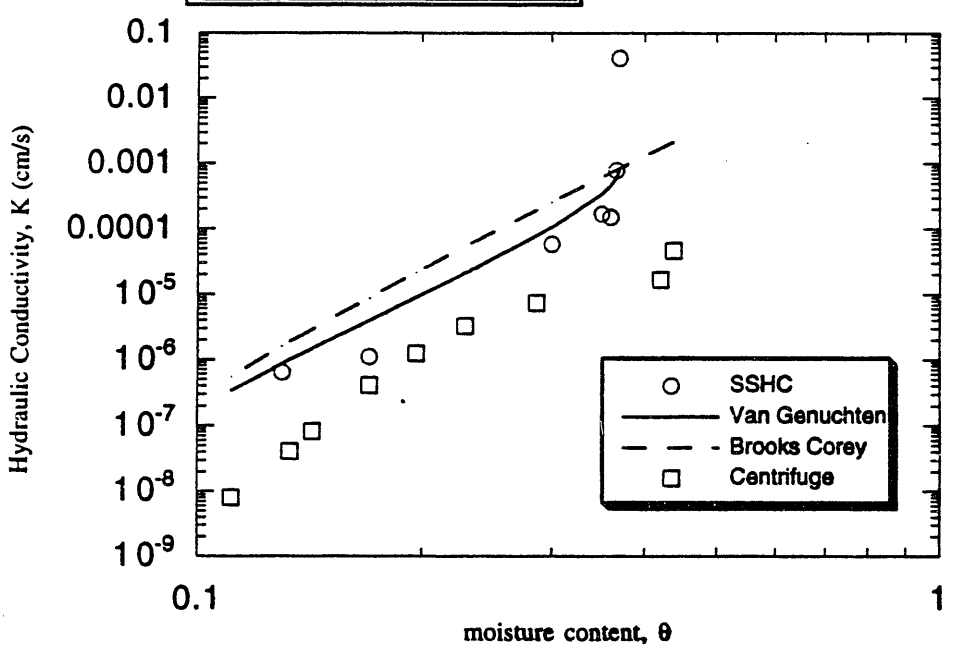

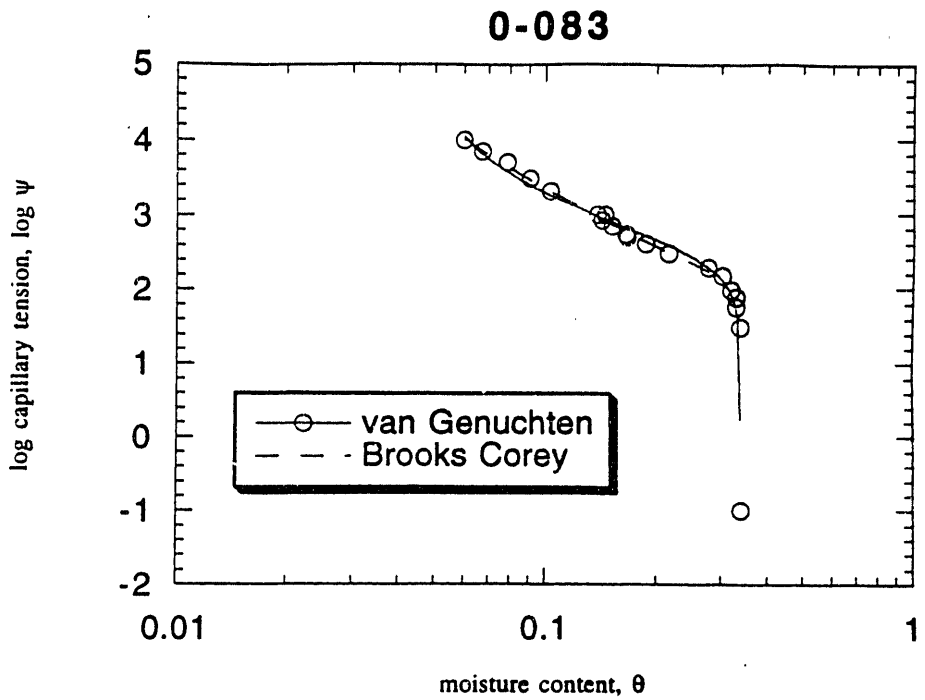

y = vg(0.01,1.5,.001,.3487)		
	Value	Error
θ_r	0.0473	0.021111
n	1.8046	0.34248
α	0.0042779	0.0016949
θ_s	0.34002	0.00017802
Chisq	3.2456	NA
R^2	0.85549	NA

y = bc(.01,.1.1,.3487)		
	Value	Error
θ_r	0.022778	0.0066166
λ	0.46927	0.036067
Ψ_b	102.79	8.4809
Chisq	0.023153	NA
R^2	0.99465	NA

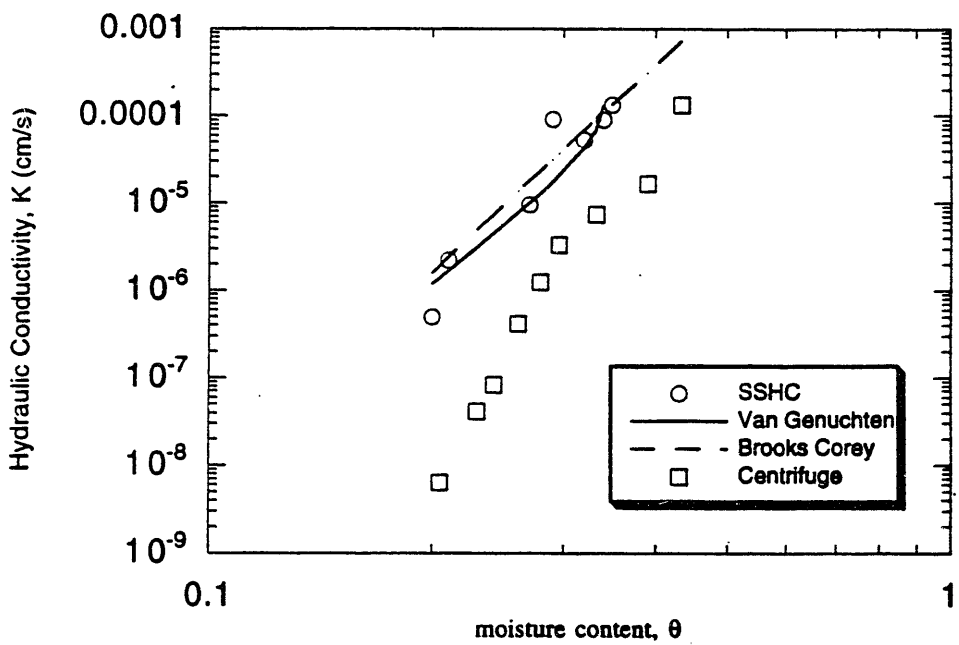

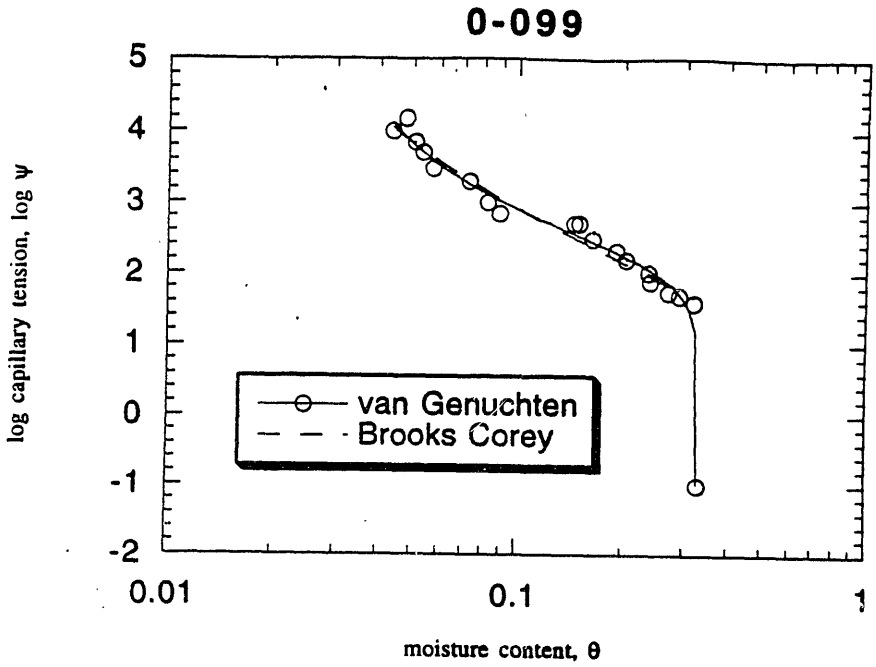

y = vg(0.01,1.5,.001,.3375)		
	Value	Error
θ_r	0.032718	0.0055012
n	1.6567	0.085824
α	0.011548	0.0018096
θ_s	0.33	3.3149e-05
Chisq	0.33276	NA
R^2	0.98689	NA

y = bc(.01,.1,1,.3375)		
	Value	Error
θ_r	0.018926	0.011292
λ	0.45506	0.073243
ψ_β	41.345	7.5924
Chisq	0.32981	NA
R^2	0.97256	NA

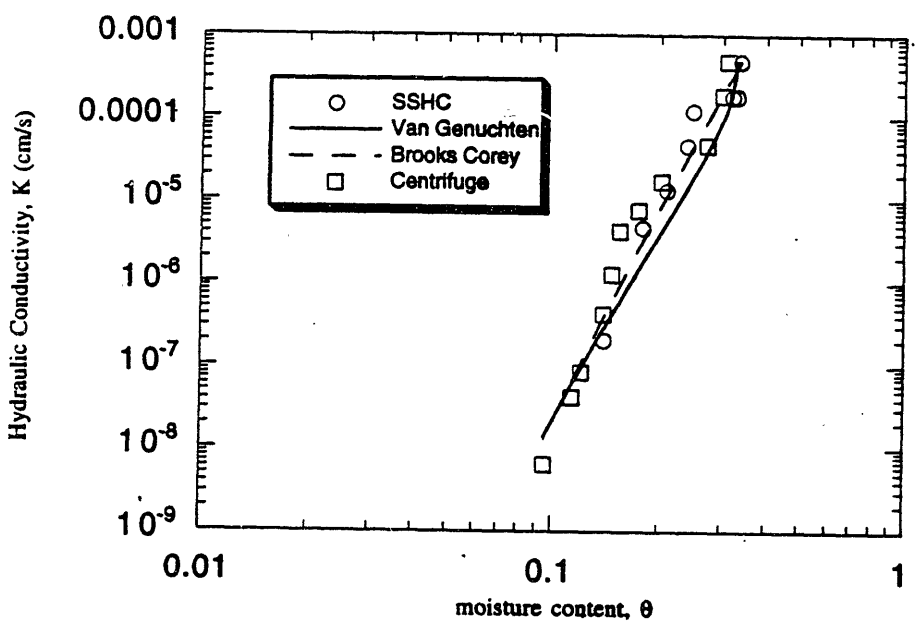

0-107

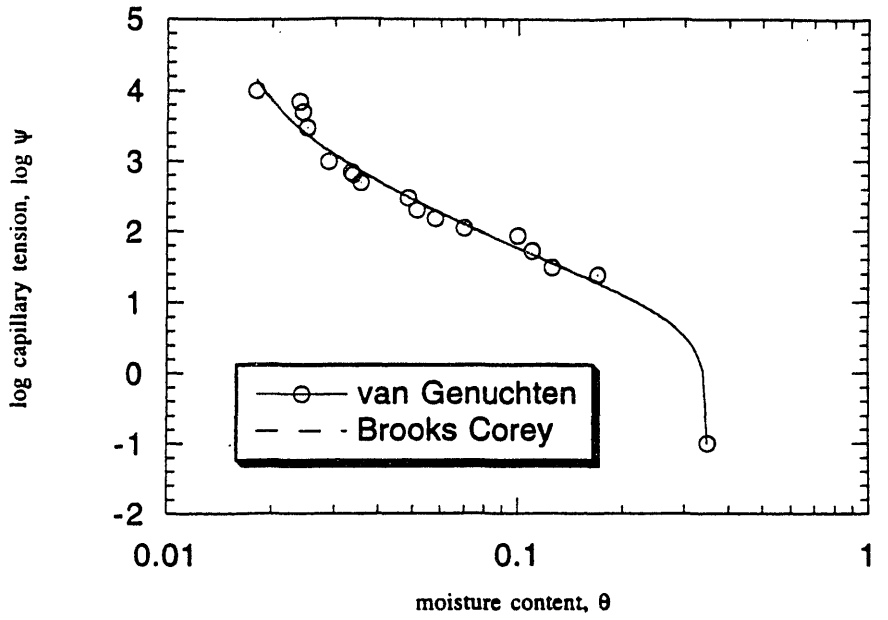

y = vg(0.01,1.5,.001,.3502)		
	Value	Error
θ_r	0.013776	0.0019766
n	1.5492	0.062442
α	0.2012	0.07503
θ_s	0.35028	0.00034999
Chisq	0.39262	NA
R^2	0.98262	NA

y = bc(.01,.1,1,.3502)		
	Value	Error
θ_r	0.01368	0.0019734
λ	0.5428	0.059962
Ψ_b	4.7178	1.7052
Chisq	0.385	NA
R^2	0.96244	NA

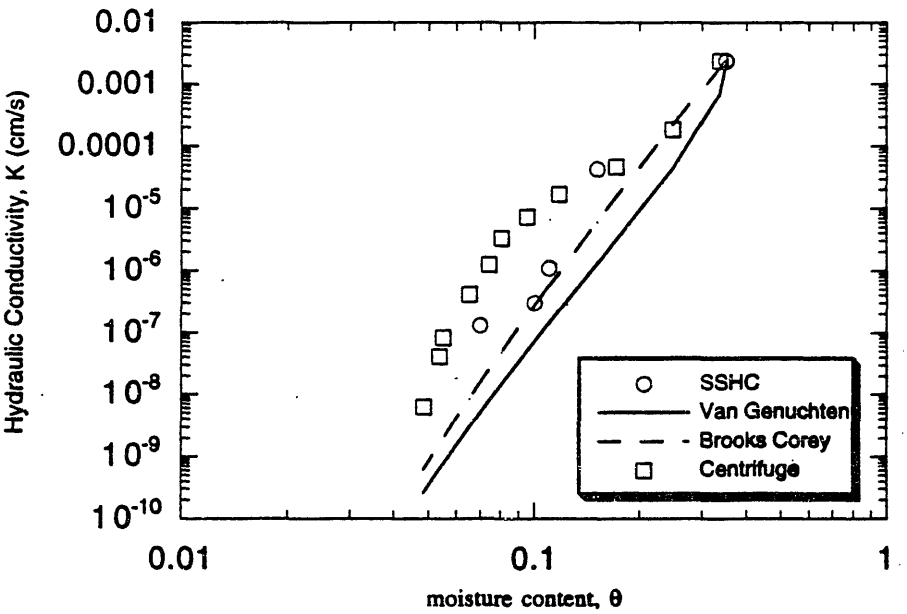

0-113

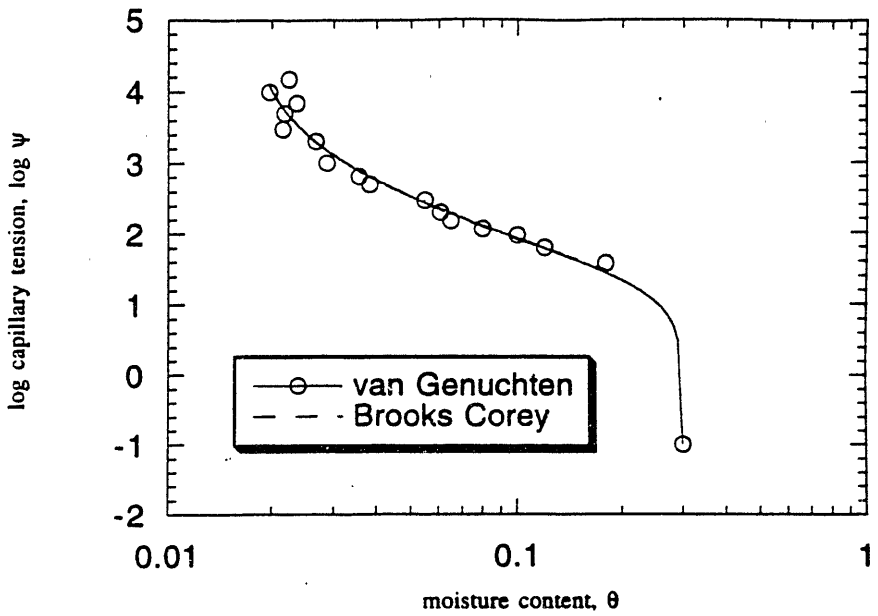

y = vg(0.01,1.5,.001,.3005)		
	Value	Error
θ_r	0.016809	0.0018438
n	1.6849	0.10275
α	0.067076	0.02642
θ_s	0.30003	0.0001039
Chisq	0.52793	NA
R^2	0.98906	NA

y = bc(.01,.1,1,.3005)		
	Value	Error
θ_r	0.016597	0.0018959
λ	0.66471	0.096583
Ψ_b	13.355	5.1152
Chisq	0.51021	NA
R	0.97514	NA

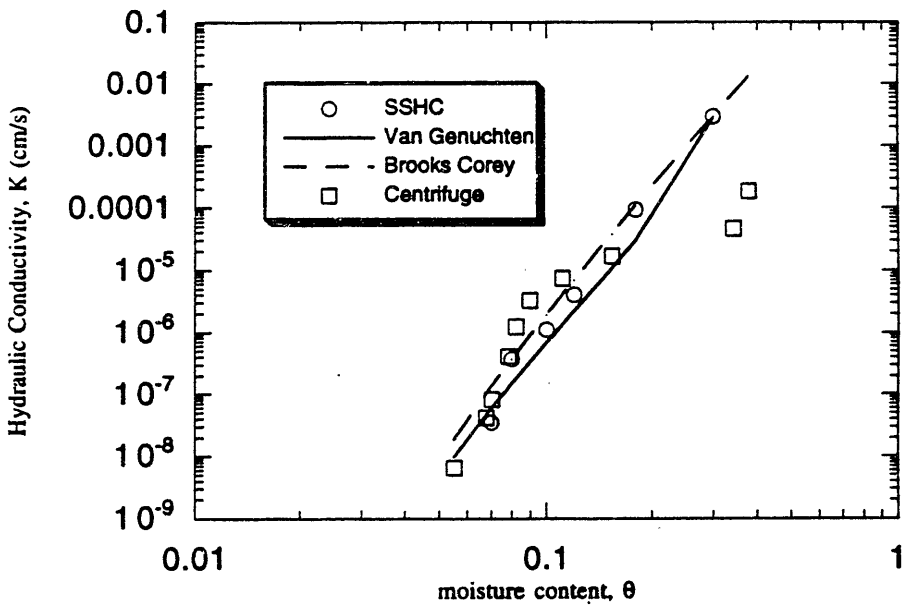

1-1417

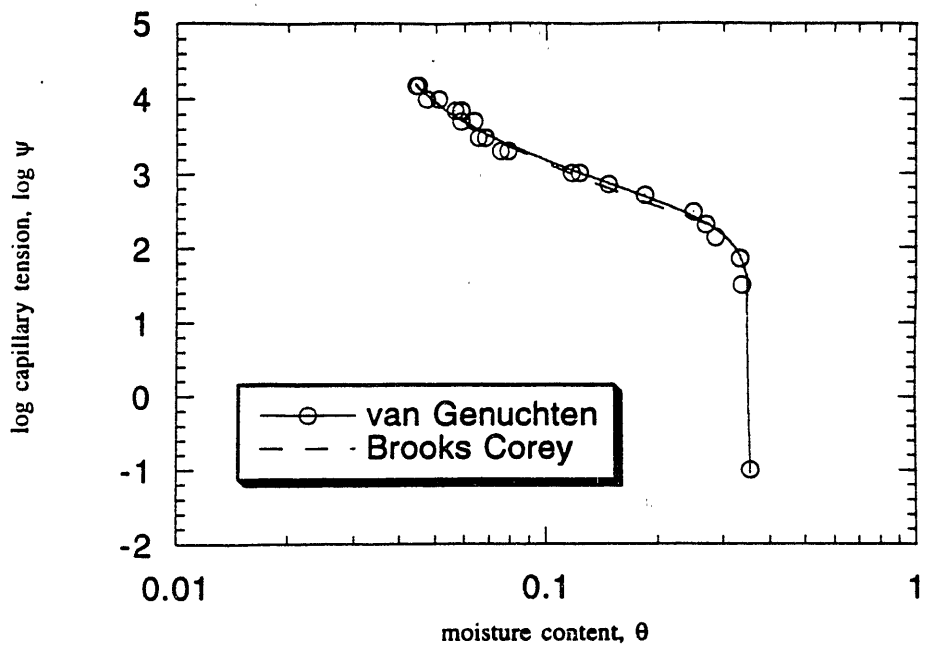

y = vg(.01,1.5,0.001,.355)		
	Value	Error
θ_r	0.034391	0.003354
n	1.8032	0.069208
α	0.0047201	0.00054206
θ_s	0.355	1.9699e-05
Chisq	0.22374	NA
R	0.99613	NA

y = bc(.01,.1,1, .3552)		
	Value	Error
θ_r	0.030052	0.0037713
λ	0.65821	0.055299
ψ_b	132.74	16.593
Chisq	0.1138	NA
R	0.99211	NA

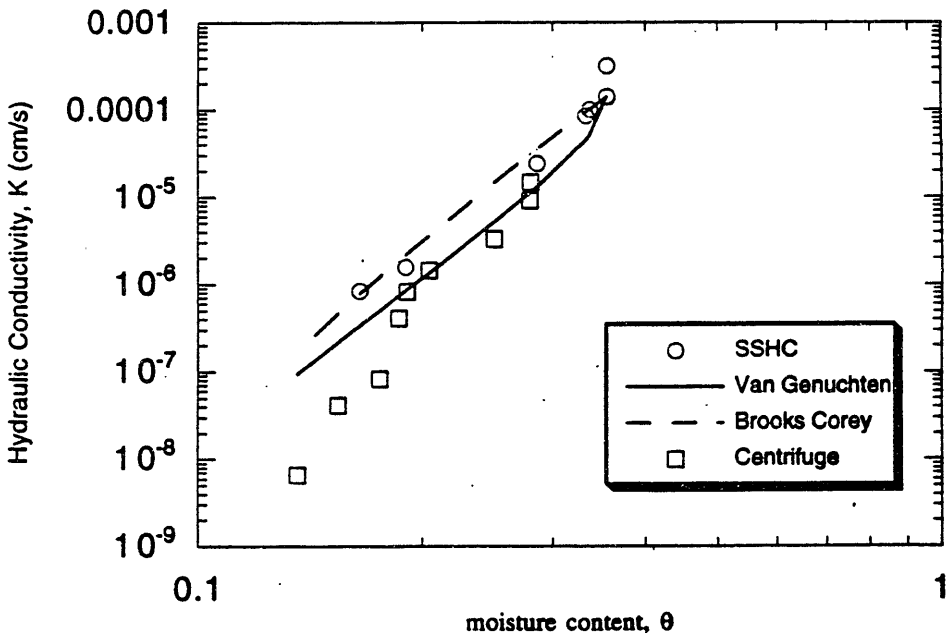

1-1419

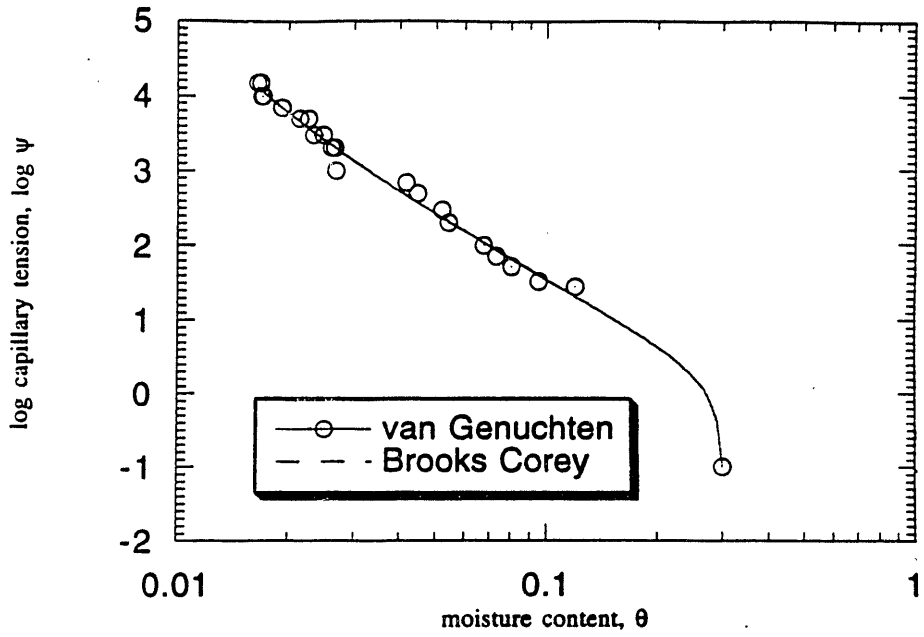

y = vg(0.01,1.5,.01,.301)		
	Value	Error
θ_r	0.0067962	0.0023296
n	1.3821	0.03664
α	0.56867	0.20404
θ_s	0.30153	0.001027
Chisq	0.22949	NA
R	0.9965	NA

y = bc(.01,.1,1,.3013)		
	Value	Error
θ_r	0.0066996	0.0023264
λ	0.38001	0.035958
ψ_b	1.7186	0.59544
Chisq	0.22839	NA
R	0.99335	NA

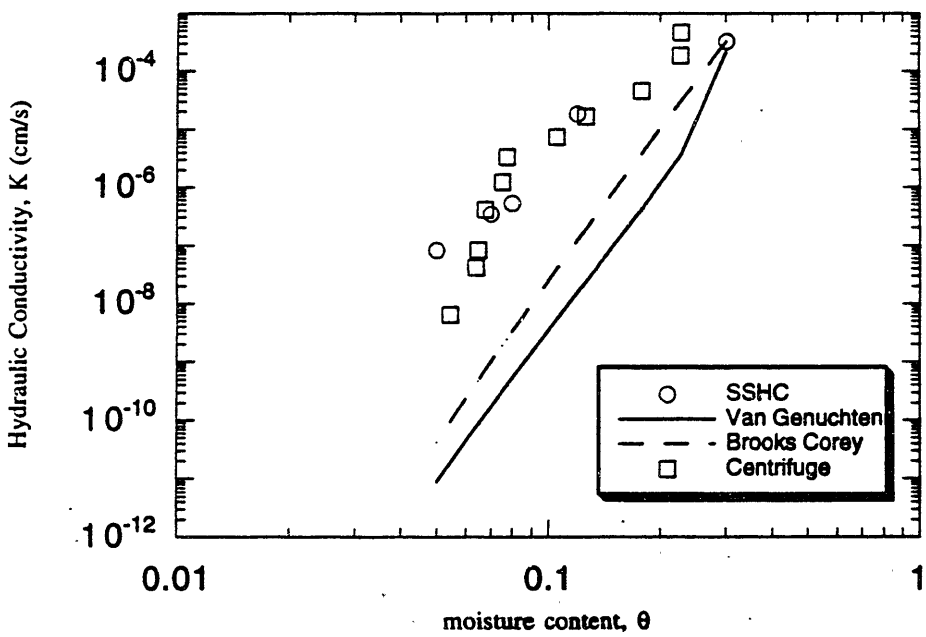

2-1636

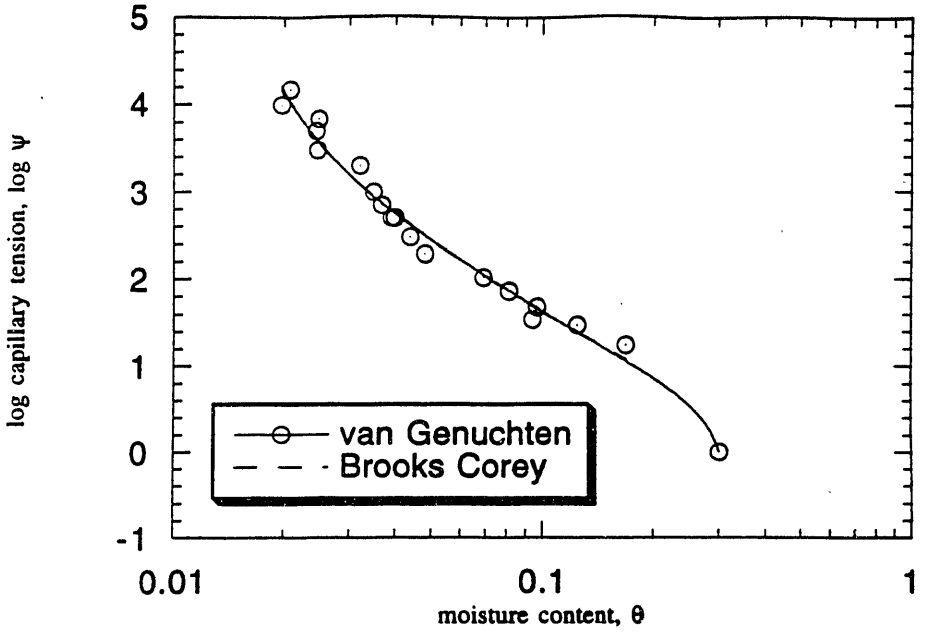

y = vg(0.01, 1.5,.01,.32)		
	Value	Error
θ_r	0.014573	0.0017608
n	1.4781	0.046843
α	0.32462	0.13338
θ_s	0.31993	0.013818
Chisq	0.35178	NA
R	0.99175	NA

y = bc(.01,.1,1,0.3073)		
	Value	Error
θ_r	0.014483	0.0017151
λ	0.47367	0.043906
ψ_b	3.2179	1.0071
Chisq	0.33842	NA
R	0.98832	NA

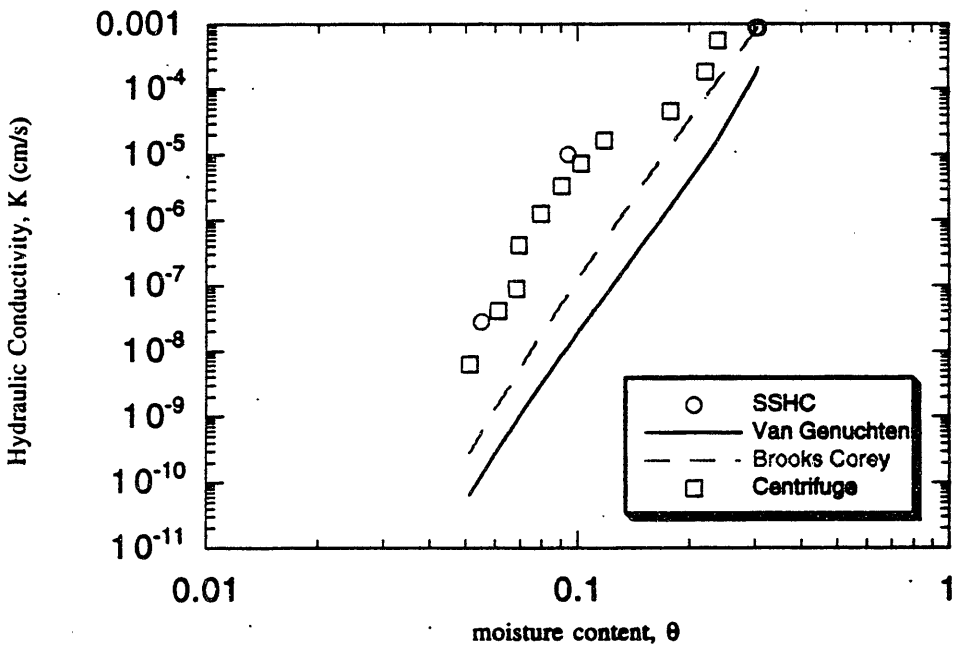

2-1637

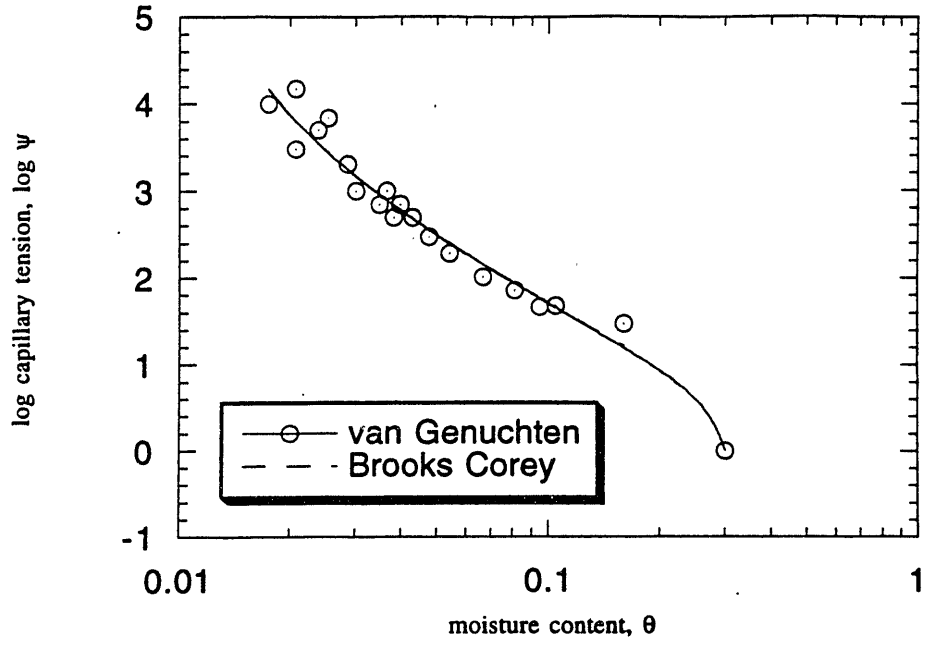

y = vg(0.01,1.5,.001,.3026)		
	Value	Error
θ_r	0.010928	0.0033498
n	1.4607	0.071127
α	0.26944	0.16396
θ_s	0.31404	0.01487
Chisq	0.6788	NA
R	0.9825	NA

y = bc(.01,.1,1,.3026)		
	Value	Error
θ_r	0.010847	0.0032728
λ	0.45719	0.067387
ψ_b	3.8878	1.9031
Chisq	0.66254	NA
R	0.97236	NA

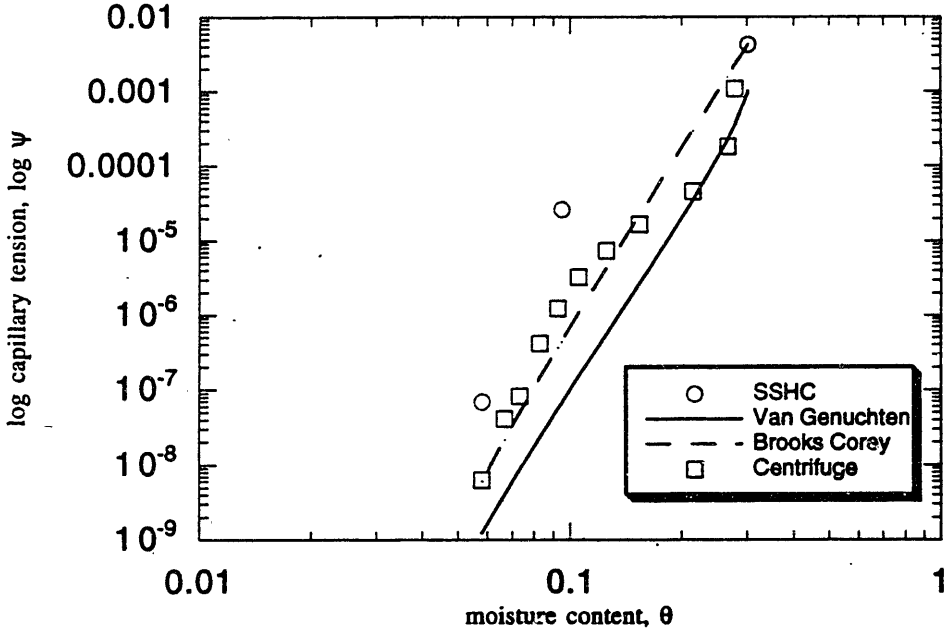

2-1638

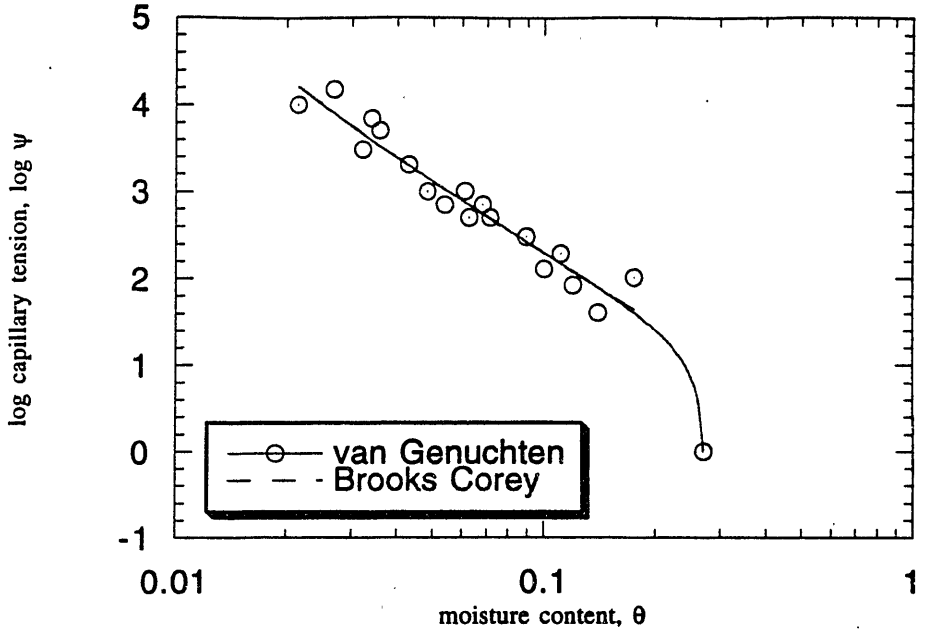

y = vg(0.01,1.5,.001,.272)		
	Value	Error
θ_r	0.0061047	0.0096753
n	1.4112	0.095528
α	0.06156	0.032267
θ_s	0.2715	0.0017373
Chisq	0.67359	NA
R	0.9805	NA

y = bc(.01,.1,1,.272)		
	Value	Error
θ_r	0.0051153	0.0096475
λ	0.39605	0.08651
Ψ_b	14.312	6.8591
Chisq	0.6396	NA
R	0.96586	NA

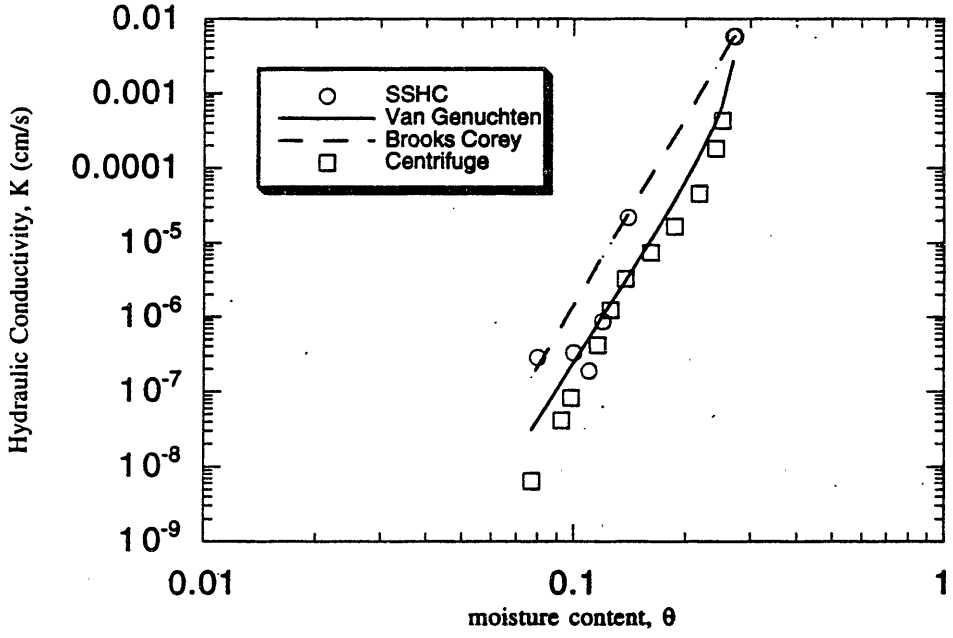

2-1639

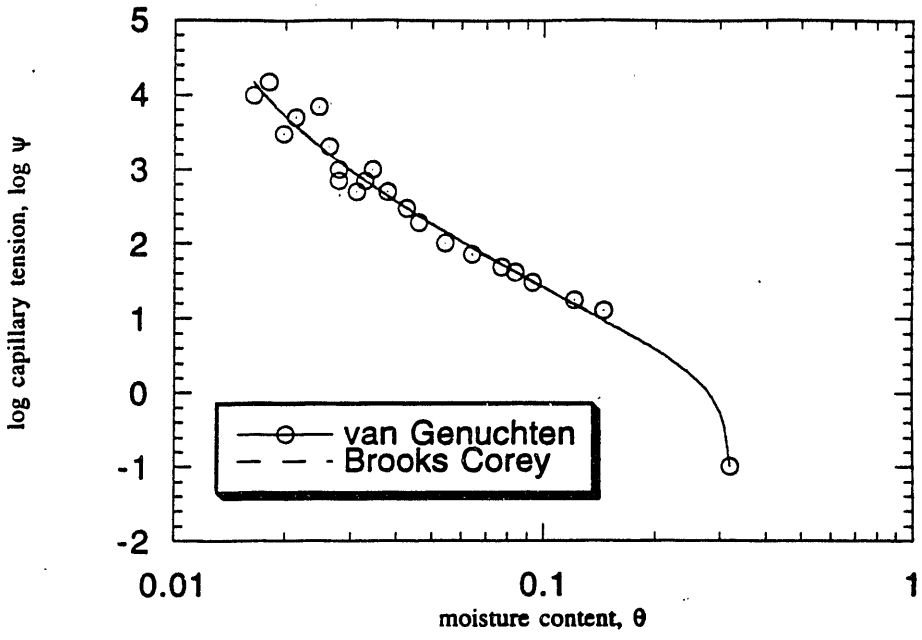

y = vg(0.01,1.5,.001,.3206)		
	Value	Error
θ_r	0.010065	0.0026125
n	1.4194	0.051567
α	0.72627	0.34925
θ_s	0.3222	0.0022284
Chisq	0.69688	NA
R	0.98815	NA

y = bC(.01,.1,1,.3206)		
	Value	Error
θ_r	0.0099868	0.0026034
λ	0.41674	0.050256
Ψ_b	1.3502	0.61831
Chisq	0.69159	NA
R	0.97939	NA

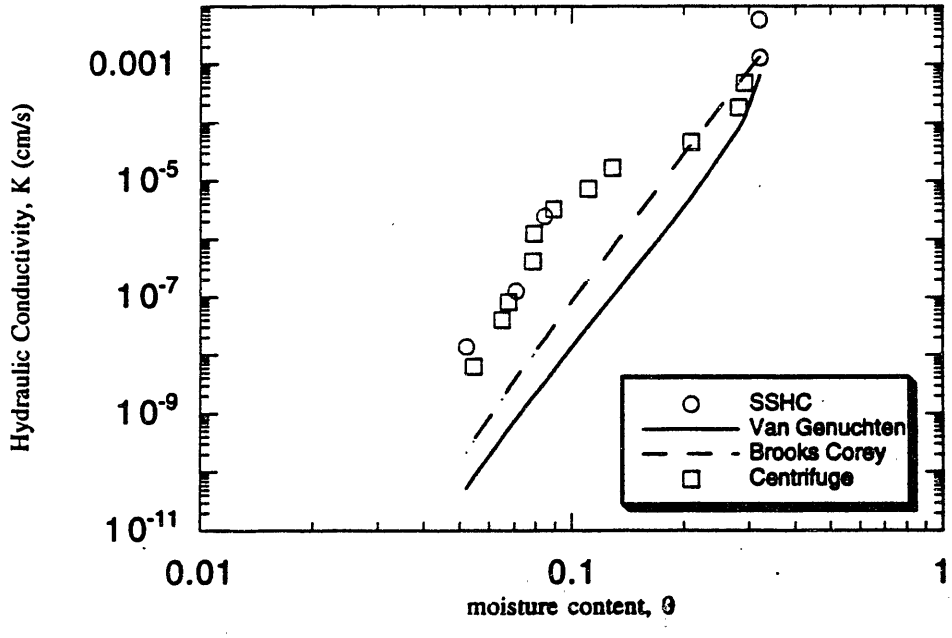

2-2225

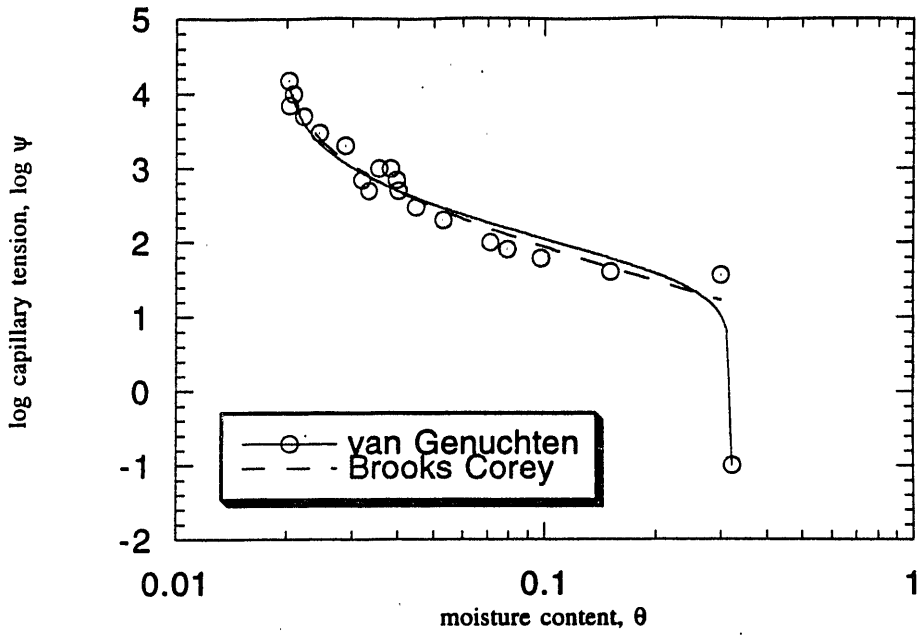

y = vg(0.01,1.5,.001,.3309)		
	Value	Error
θ_r	0.019164	0.00071768
n	1.9237	0.12651
α	0.036274	0.012727
θ_s	0.323	6.6737e-05
Chisq	0.89204	NA
R	0.98236	NA

y = bC(.01,.1,1,.3309)		
	Value	Error
θ_r	0.018334	0.00083396
λ	0.7659	0.07841
Ψ_b	15.187	4.4197
Chisq	0.51313	NA
R	0.97795	NA

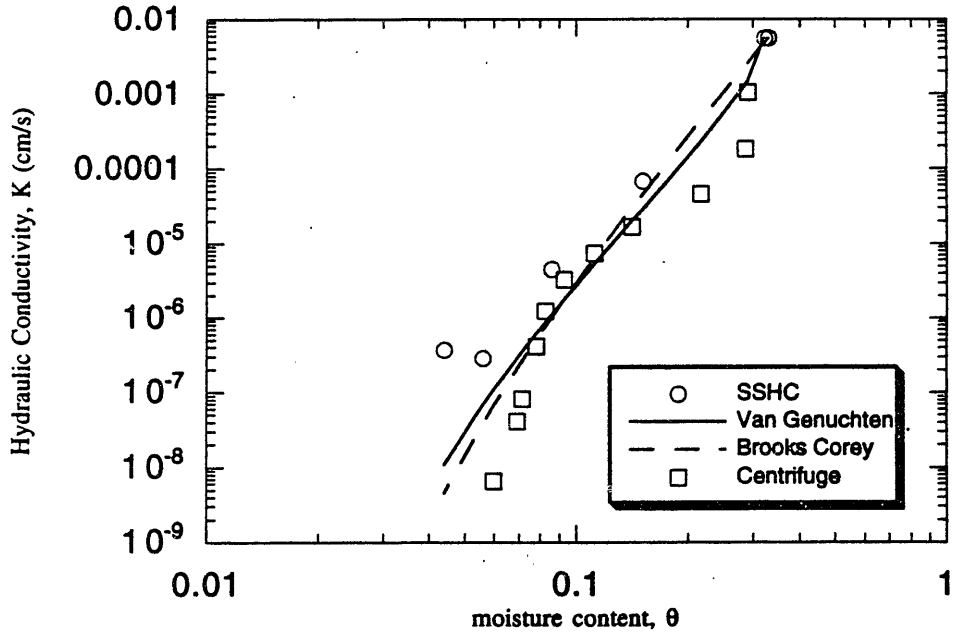

2-2226

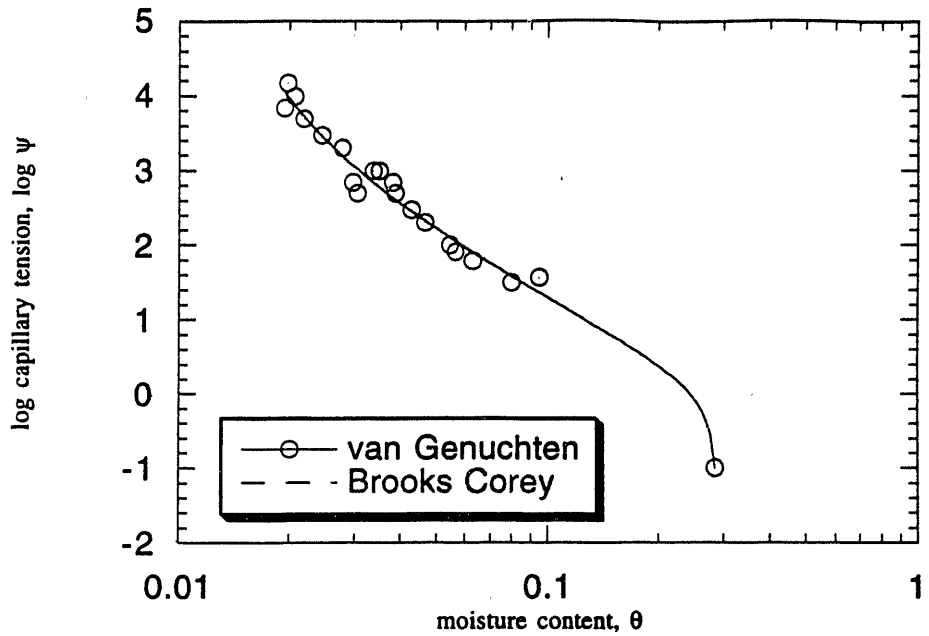

y = vg(0.01,1.5,.001,.2861)		
	Value	Error
θ_r	0.01235	0.0028043
n	1.399	0.06323
α	0.86617	0.58884
θ_s	0.28751	0.0029354
Chisq	0.47278	NA
R	0.99077	NA

y = bC(.01,.1,1,.2861)		
	Value	Error
θ_r	0.012324	0.0027928
λ	0.39818	0.062431
ψ_b	1.1562	0.74966
Chisq	0.47167	NA
R	0.9802	NA

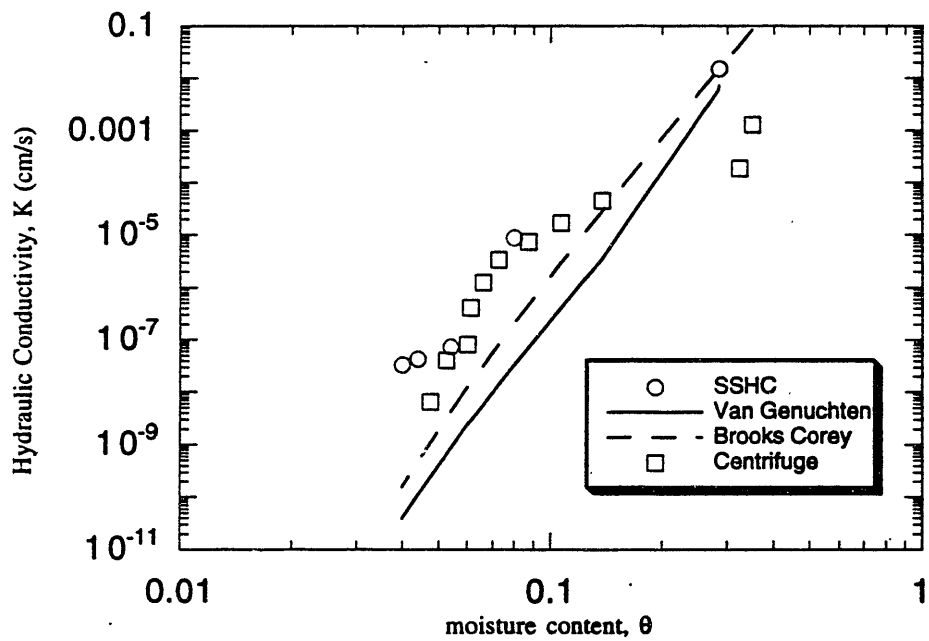

2-2227

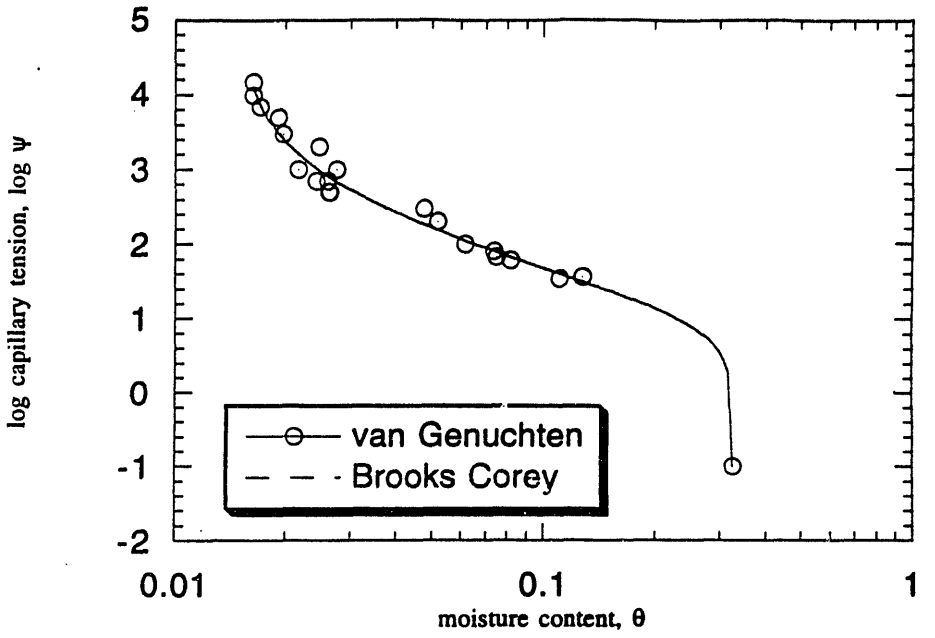

y = vg(0.01,1.5,.001,.3271)		
	Value	Error
θ_r	0.014749	0.00059032
n	1.7259	0.063859
α	0.11949	0.034382
θ_s	0.32706	0.00012236
Chisq	0.42217	NA
R	0.99192	NA

y = bC(.01,.1,1,.3271)		
	Value	Error
θ_r	0.014706	0.00059924
λ	0.71812	0.062307
ψ_b	8.0089	2.2773
Chisq	0.42232	NA
R	0.98339	NA

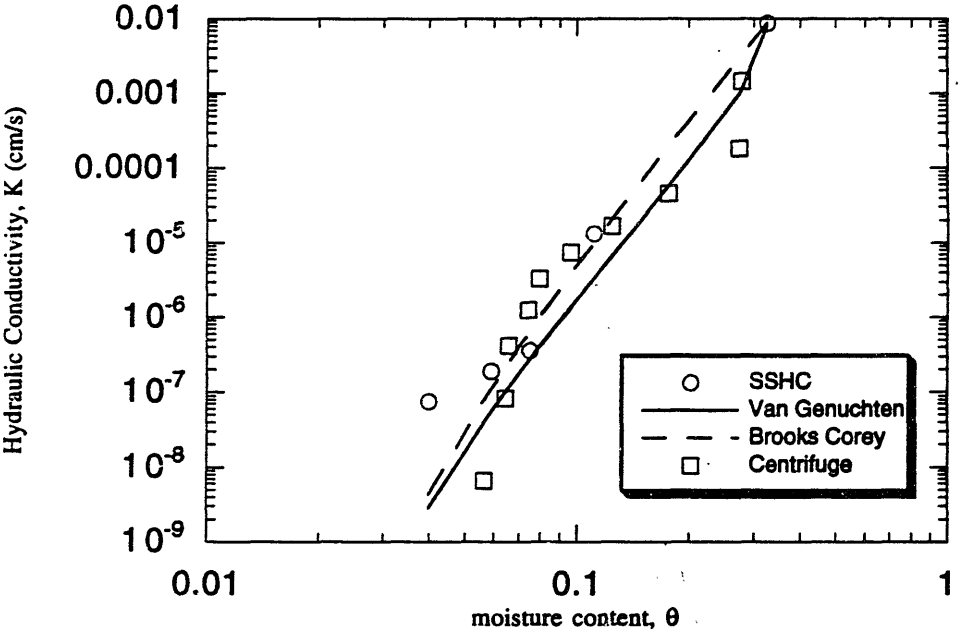

2-2228

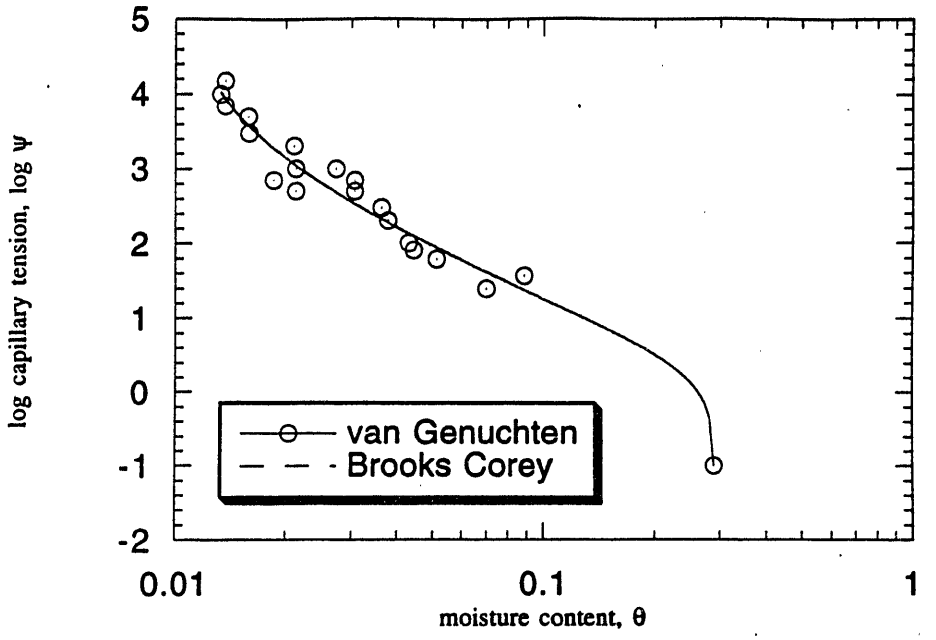

y = vg(0.01,1.5,.001,.2925)		
	Value	Error
θ_r	0.0095593	0.0021178
n	1.5019	0.095
α	0.51143	0.39345
θ_s	0.29107	0.0017596
Chisq	0.85624	NA
R	0.98338	NA

y = bC(.01,.1,1,.2925)		
	Value	Error
θ_r	0.0095244	0.002121
λ	0.49983	0.09377
Ψ_b	1.8993	1.4338
Chisq	0.85547	NA
R	0.96466	NA

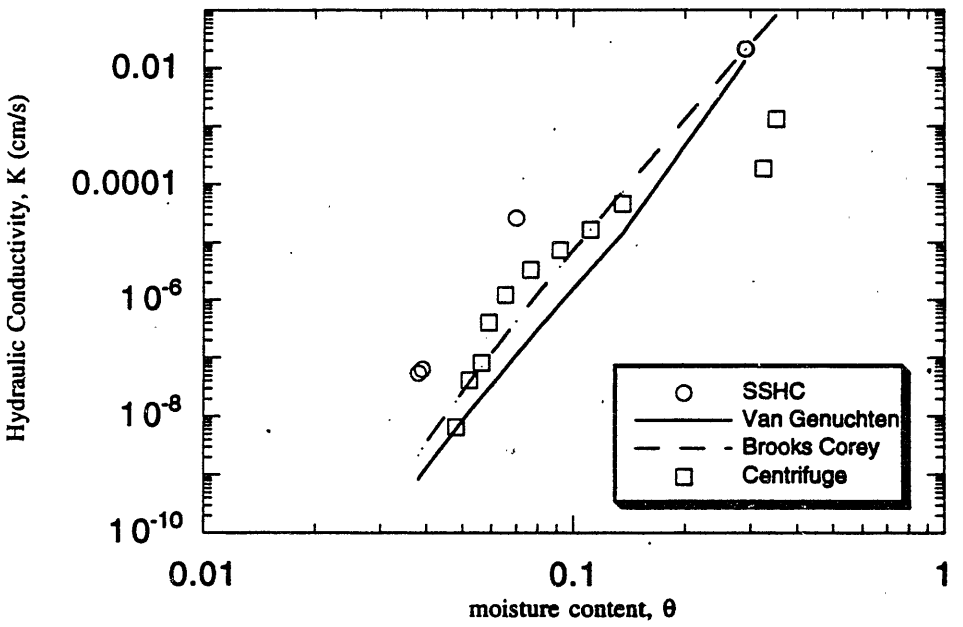

2-2229

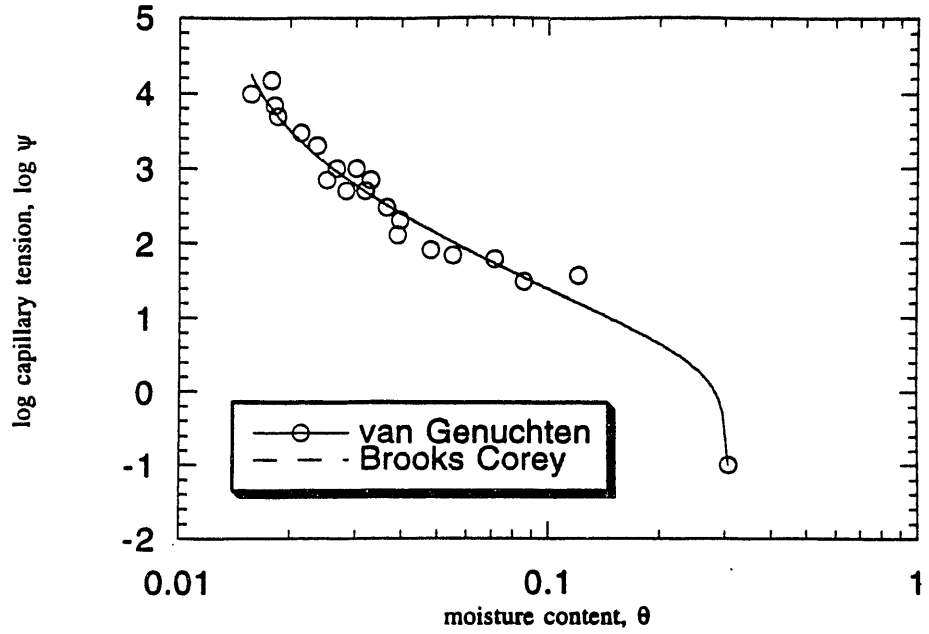

y = vg(0.01,1.5,.001,.31)		
	Value	Error
θ_r	0.012465	0.0015959
n	1.5067	0.068369
α	0.43734	0.24184
θ_s	0.30789	0.0011562
Chisq	0.75207	NA
R	0.98554	NA

y = bc(.01,.1,1,.307)		
	Value	Error
θ_r	0.012452	0.001578
λ	0.50517	0.066799
ψ_b	2.2607	1.2114
Chisq	0.74234	NA
R	0.97052	NA

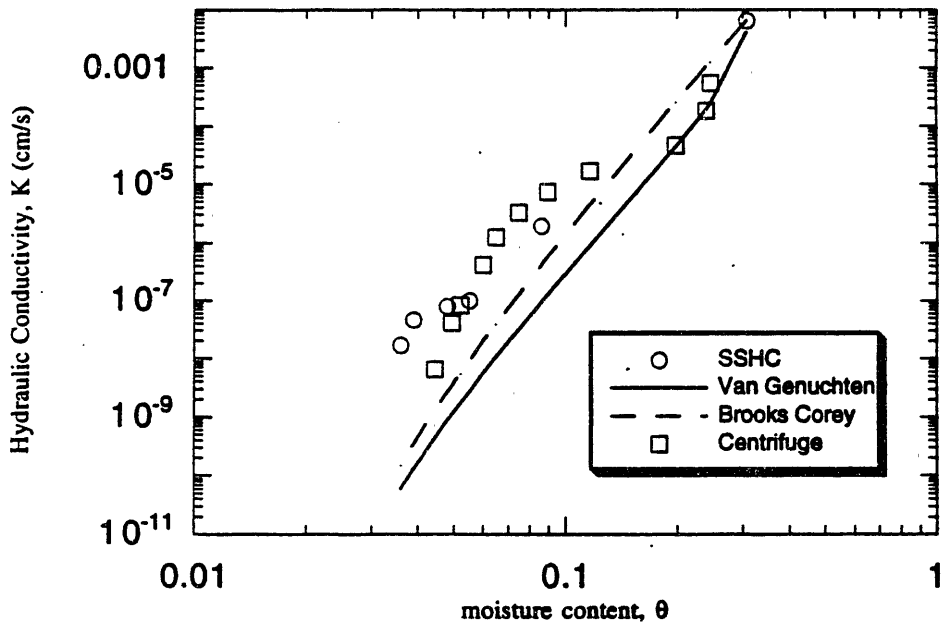

2-2230

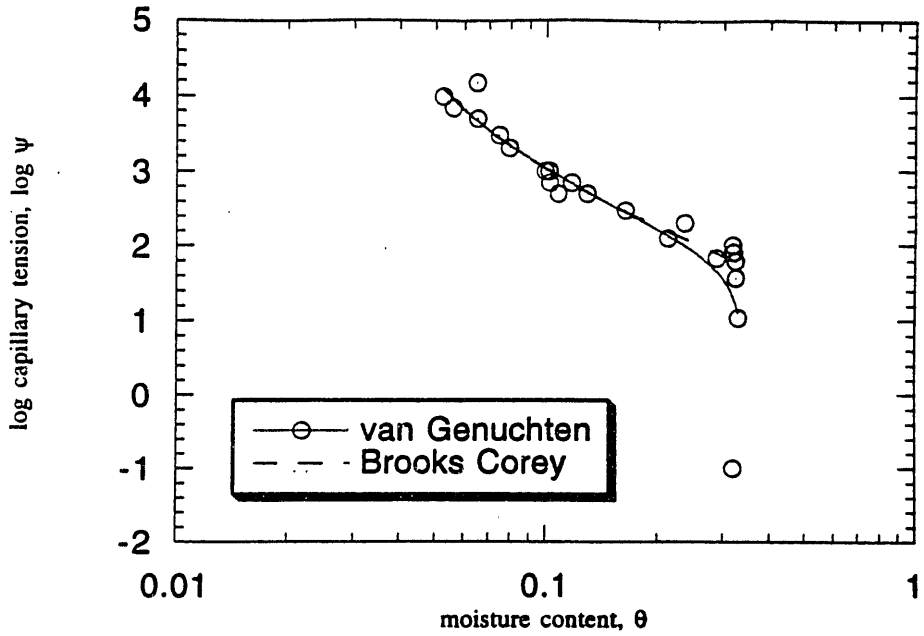

y = vg(0.01,1.5,.001,.3309)		
	Value	Error
θ_r	0.033799	0.037279
n	1.517	0.37127
α	0.017537	0.024204
θ_s	0.34016	0.034639
Chisq	7.0926	NA
R	0.86245	NA

y = bc(.01,.1,1,.3309)		
	Value	Error
θ_r	0.03499	0.0080853
λ	0.52467	0.07065
Ψ_b	59.552	10.137
Chisq	0.52205	NA
R	0.97758	NA

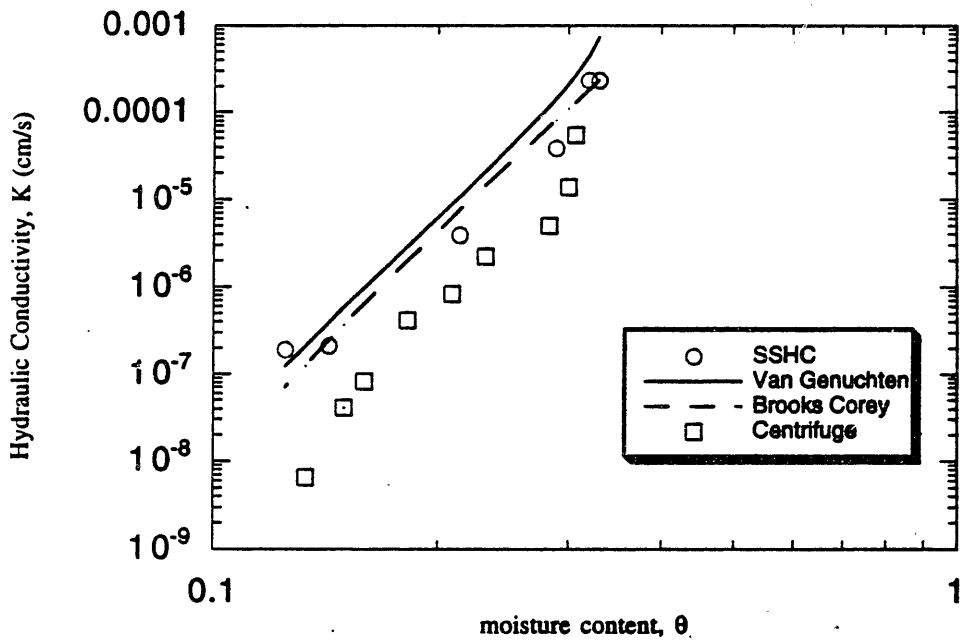

2-2232

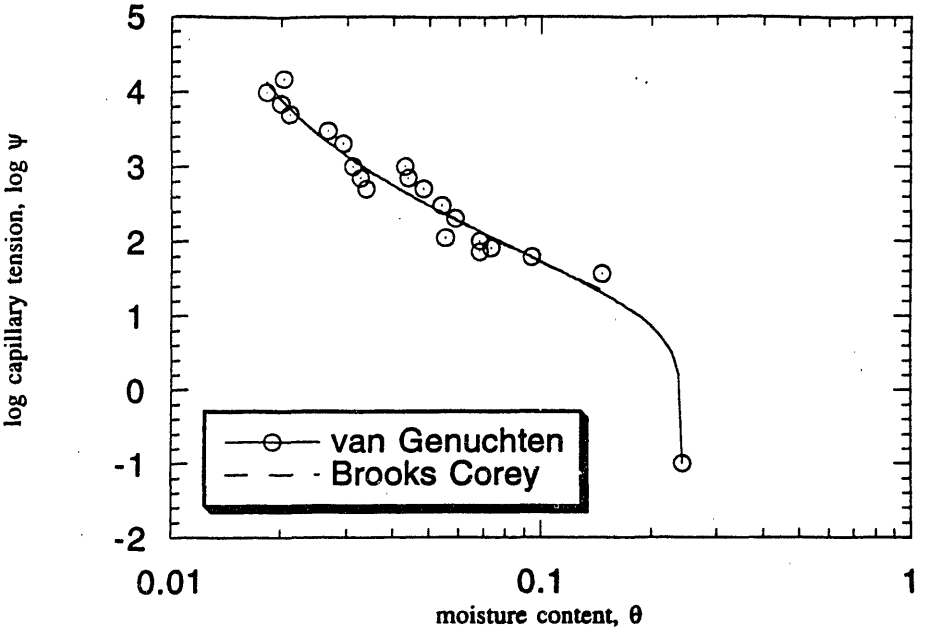

y = vg(0.01,1.5,.001,.25)		
	Value	Error
α_r	0.013081	0.0029082
n	1.5096	0.088386
α	0.12186	0.060686
θ_s	0.244	0.00019375
Chisq	0.7495	NA
R	0.98512	NA

y = bc(.01,.1,1,.245)		
	Value	Error
θ_r	0.012761	0.0029301
λ	0.49613	0.08243
ψ_b	7.3941	3.5479
Chisq	0.72414	NA
R	0.9688	NA

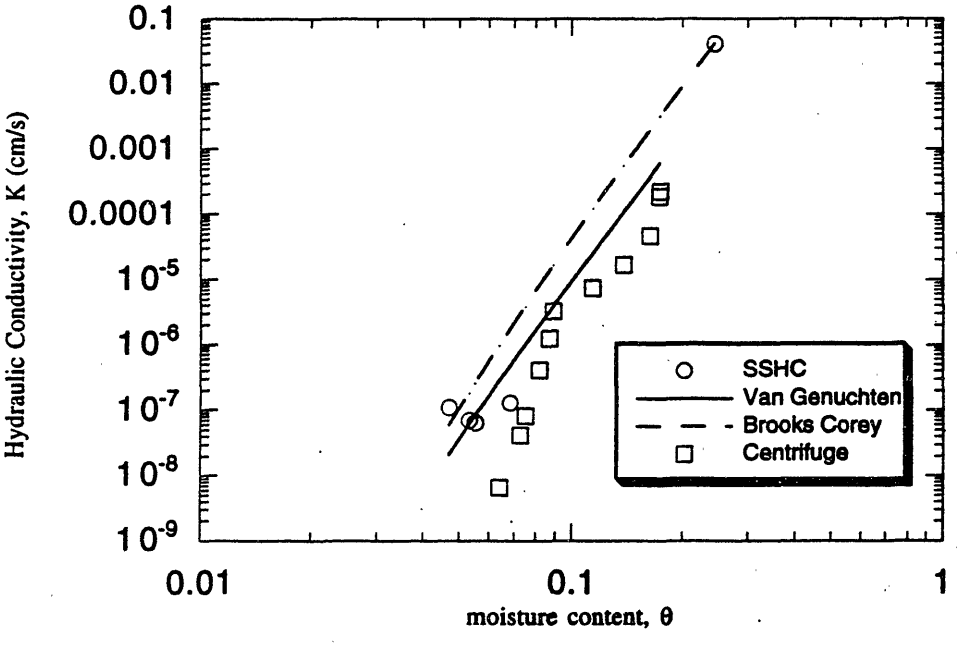

2-2233

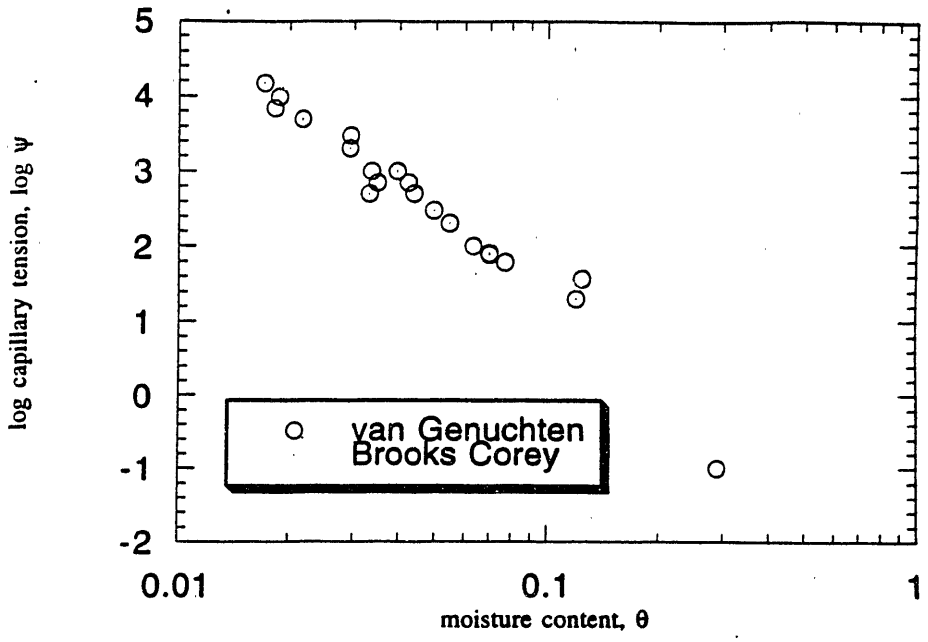

y = vg(0.01,1.5..001,.30)		
	Value	Error
θ_r	0.0072686	0.0034702
n	1.3818	0.051644
α	0.49604	0.24304
θ_s	0.29122	0.0011704
Chisq	0.44676	NA
R	0.9916	NA

y = bc(.01,.1,1,.2906)		
	Value	Error
θ_r	0.0071451	0.0034447
λ	0.37914	0.050094
ψ_b	1.963	0.92204
Chisq	0.44223	NA
R	0.98331	NA

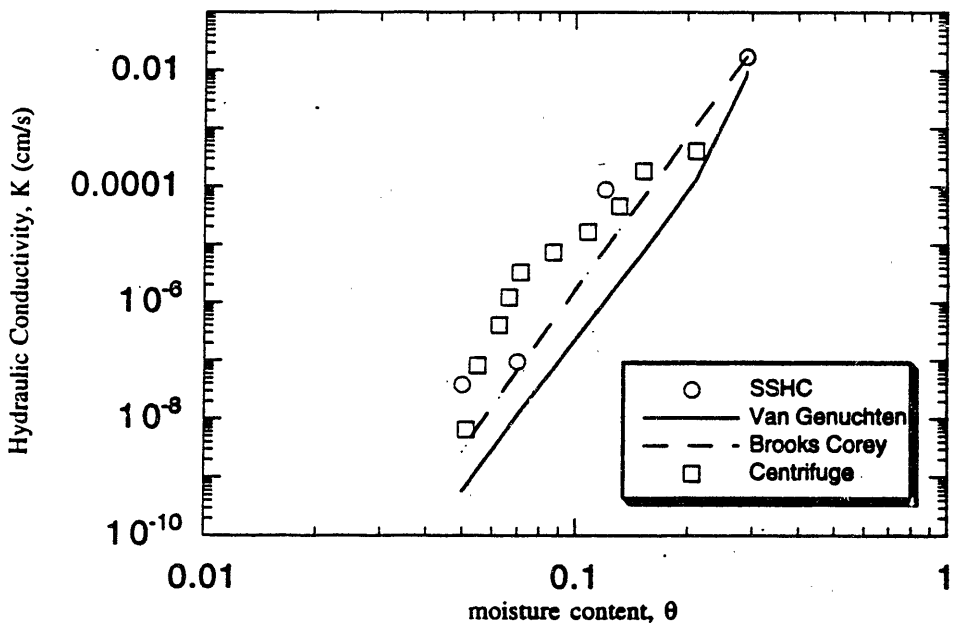

2-2234

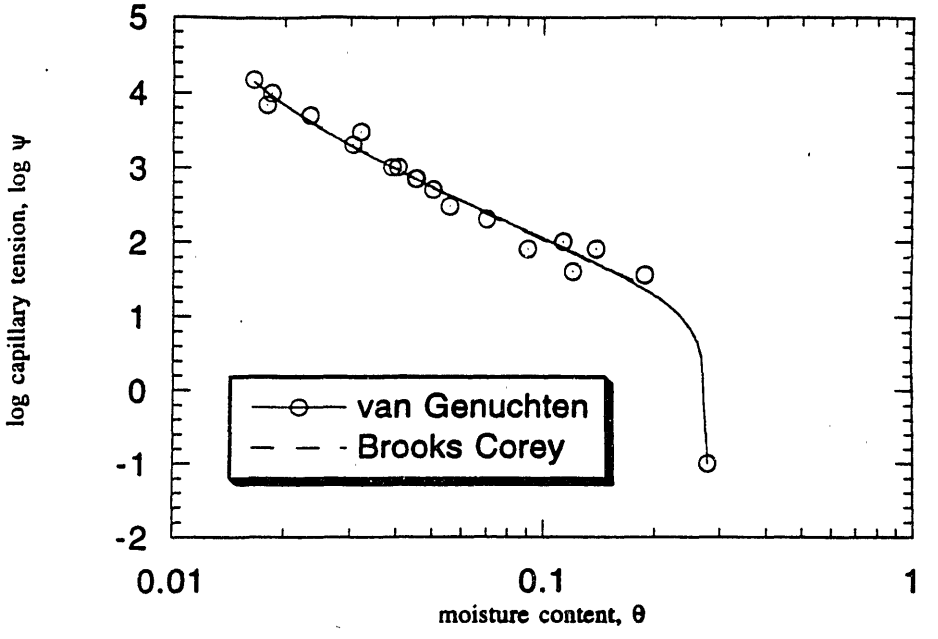

y = vg(0.01,1.5,.001,.28)		
	Value	Error
θ_r	0.0088423	0.0028522
n	1.5142	0.0603
α	0.071112	0.020706
θ_s	0.27805	8.9261e-05
Chisq	0.33355	NA
R	0.99339	NA

y = bc(.01,.1,1,.2782)		
	Value	Error
θ_r	0.0080274	0.0028406
λ	0.48955	0.052405
Ψ_b	11.954	3.1944
Chisq	0.29779	NA
R	0.987	NA

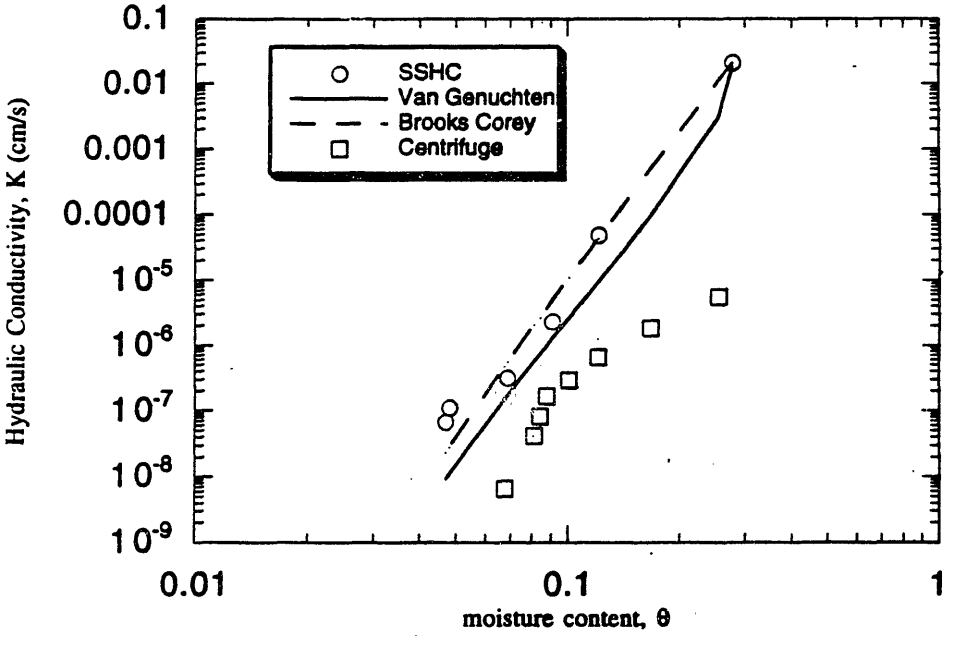

Appendix D: INEL Curve Fits

u(a) 30 cm

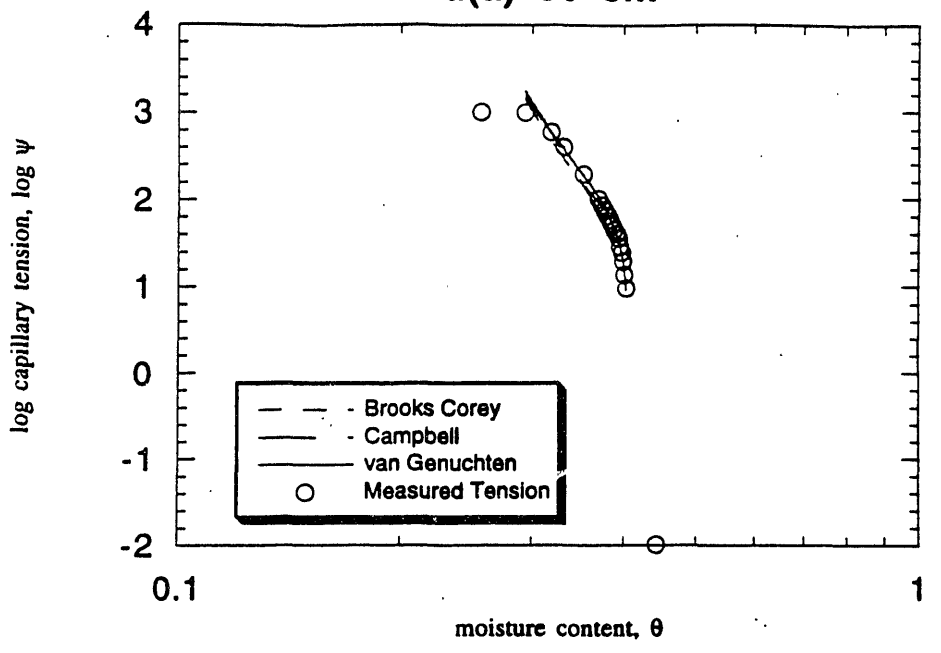

y = bc(.21804,.1,1..40594)		
	Value	Error
λ	0.2523	0.018848
ψ_b	39.053	4.8546
Chisq	0.083375	NA
R^2	0.95731	NA

y = camp(1,.1,.40594)		
	Value	Error
ψ_e	20.234	2.3919
b	13.785	0.97461
Chisq	0.37735	NA
R^2	0.92594	NA

y = vg(0.29,1.6,.02,.47)		
	Value	Error
θ_r	0.21804	0.042184
n	1.2967	0.10657
α	0.013416	0.0014499
θ_s	0.40594	0.0010649
Chisq	0.057853	NA
R^2	0.98865	NA

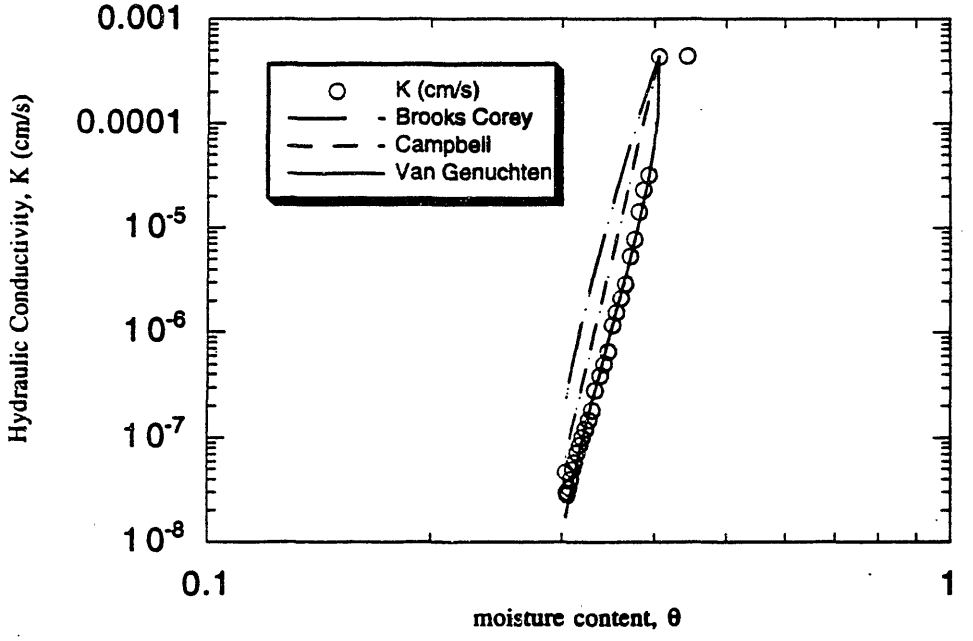

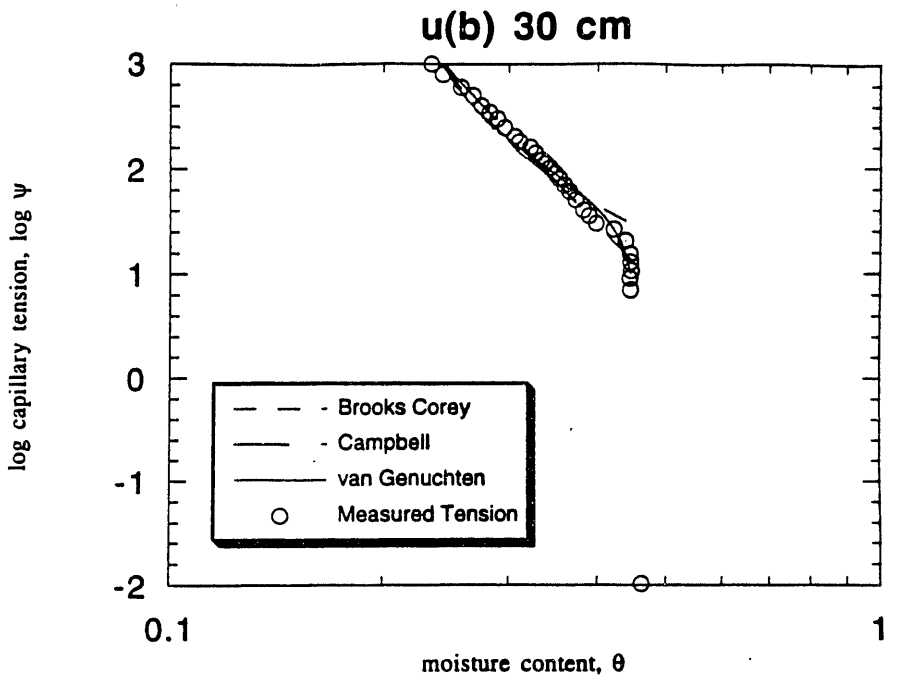

y = bc(.21,.1,1,.45422)		
	Value	Error
λ	0.54916	0.032477
ψ_b	28.417	3.1135
Chisq	0.40311	NA
R^2	0.92561	NA

y = camp(1,.1,.45422)		
	Value	Error
ψ_c	12.067	0.79685
b	7.0266	0.194
Chisq	0.21838	NA
R^2	0.9791	NA

y = vg(0.21,1.5,.01,.47)		
	Value	Error
n	1.6577	0.039722
α	0.022465	0.0025536
θ_r	0.45422	0.0024649
Chisq	0.26895	NA
R^2	0.97426	NA

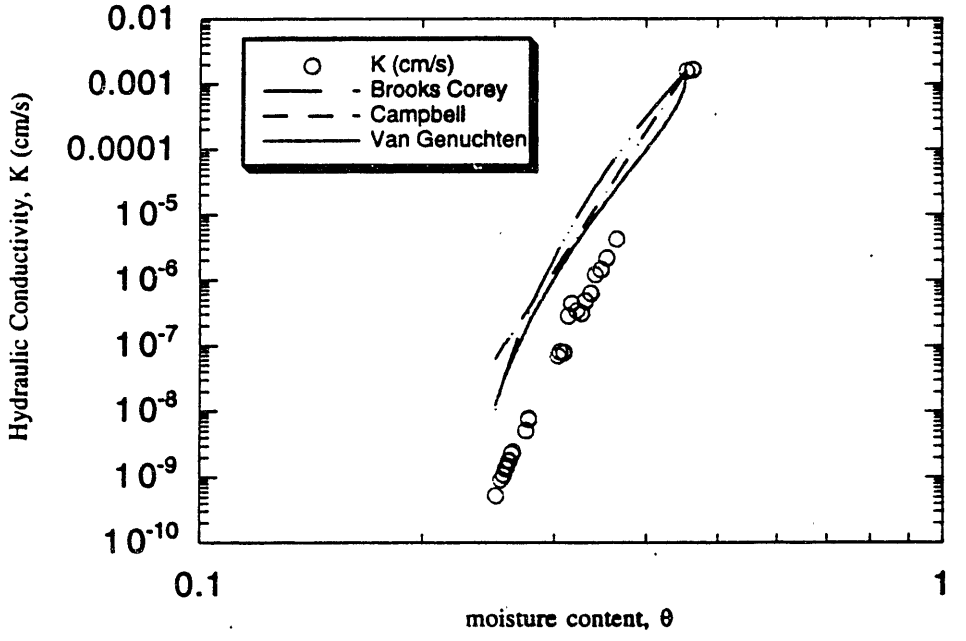

d(a) 30 cm

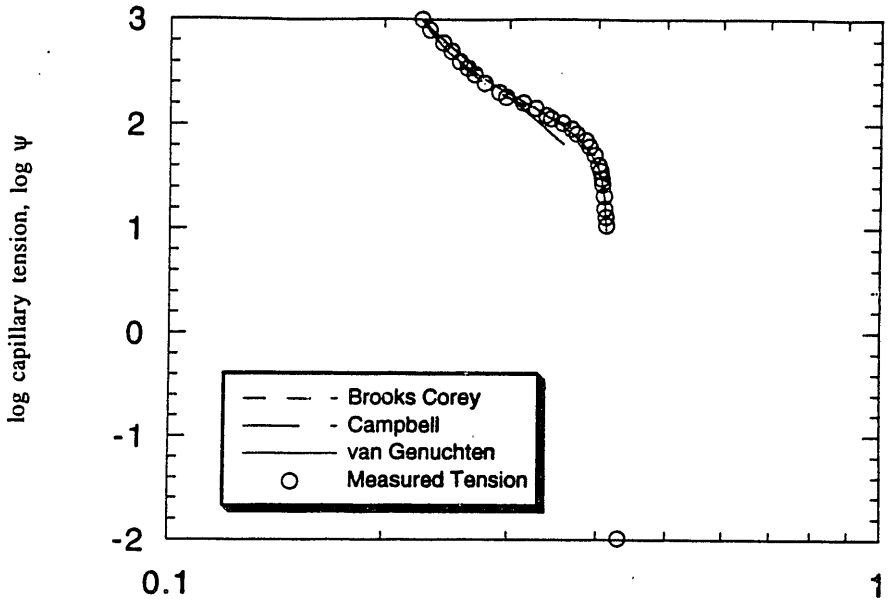

y = bc(.20605,.1,1,.41295)		
	Value	Error
λ	0.85273	0.018229
ψ_b	70.821	2.1508
Chisq	0.012539	NA
R^2	0.9932	NA

y = camp(1,.1,.41295)		
	Value	Error
ψ_e	28.038	3.0021
b	5.858	0.35561
Chisq	0.7124	NA
R^2	0.91257	NA

y = vg(0.22,1.5,.01,.4299)		
	Value	Error
θ_r	0.20605	0.0041554
n	2.0397	0.061143
α	0.0096232	0.00027747
θ_s	0.41295	0.00026464
Chisq	0.045589	NA
R^2	0.9944	NA

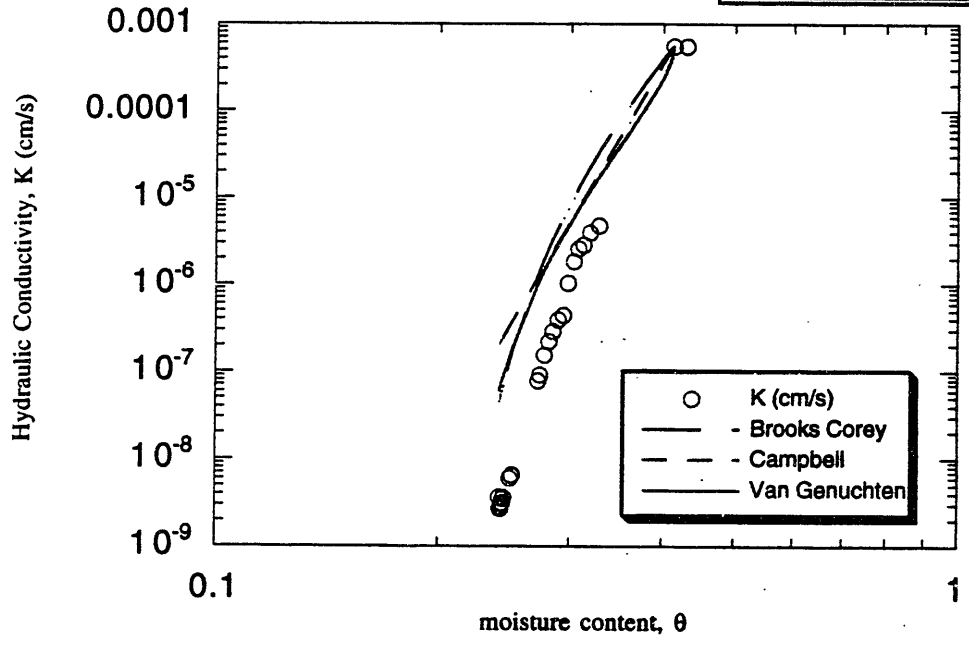

d(b) 30 cm

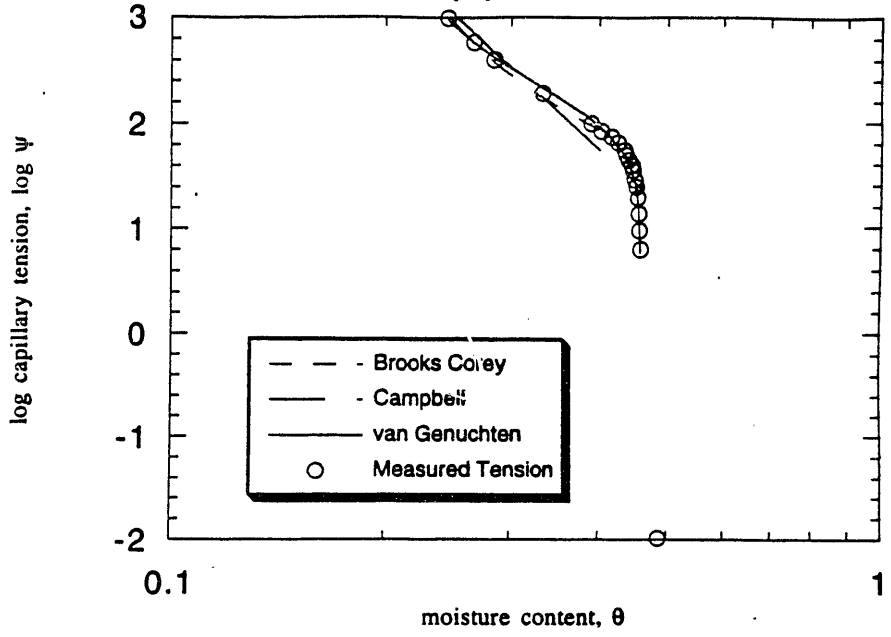

y = bc(.19438,.1,1,.4598)		
	Value	Error
λ	0.56356	0.013974
ψ_b	55.944	2.1822
Chisq	0.005293	NA
R^2	0.99633	NA

y = camp(1,.1,.4598)		
	Value	Error
ψ_e	23.952	3.6751
b	6.2032	0.63622
Chisq	0.9229	NA
R^2	0.8483	NA

y = vg(0.24,1.5,.2,.49)		
	Value	Error
θ_r	0.19438	0.015748
n	1.7552	0.085289
α	0.0093944	0.0004772
θ_s	0.4598	0.00025265
Chisq	0.037386	NA
R^2	0.99385	NA

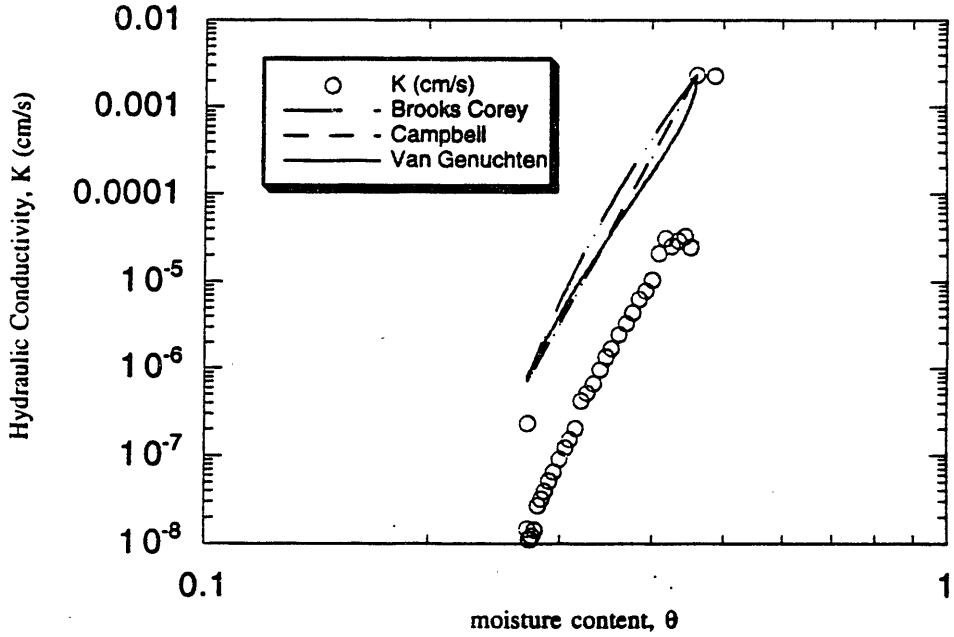

u(a) 80 cm

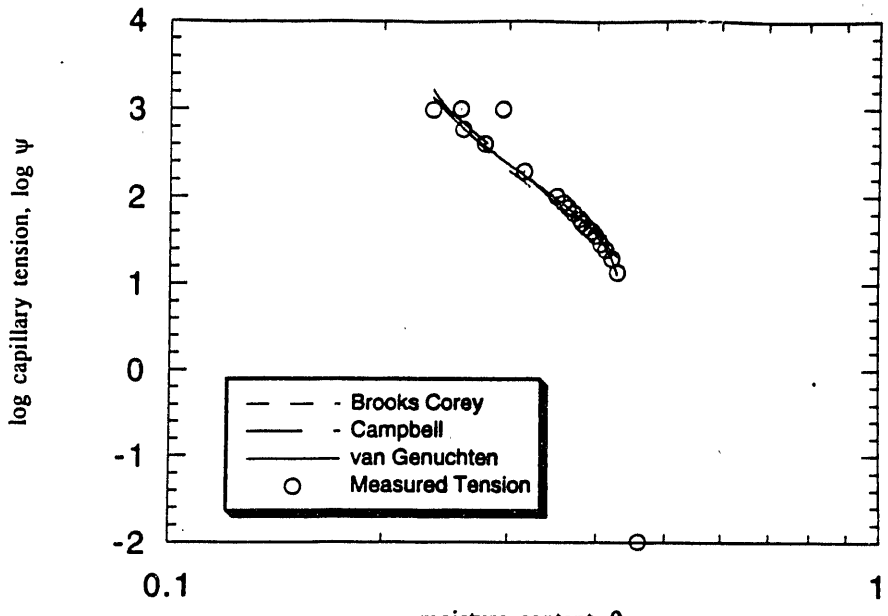

y = bc(.18225,.1,1,.43814)		
	Value	Error
λ	0.38372	0.020689
ψ_b	26.484	2.5945
Chisq	0.17119	NA
R^2	0.96093	NA

y = camp(1,.1,.43814)		
	Value	Error
ψ_e	17.828	1.3016
b	6.9436	0.25129
Chisq	0.11409	NA
R^2	0.97947	NA

y = vg(0.23,1.5,.01,.47)		
	Value	Error
θ_r	0.18255	0.026686
n	1.4808	0.12545
α	0.020355	0.0033093
θ_s	0.43814	0.0045193
Chisq	0.068051	NA
R^2	0.98776	NA

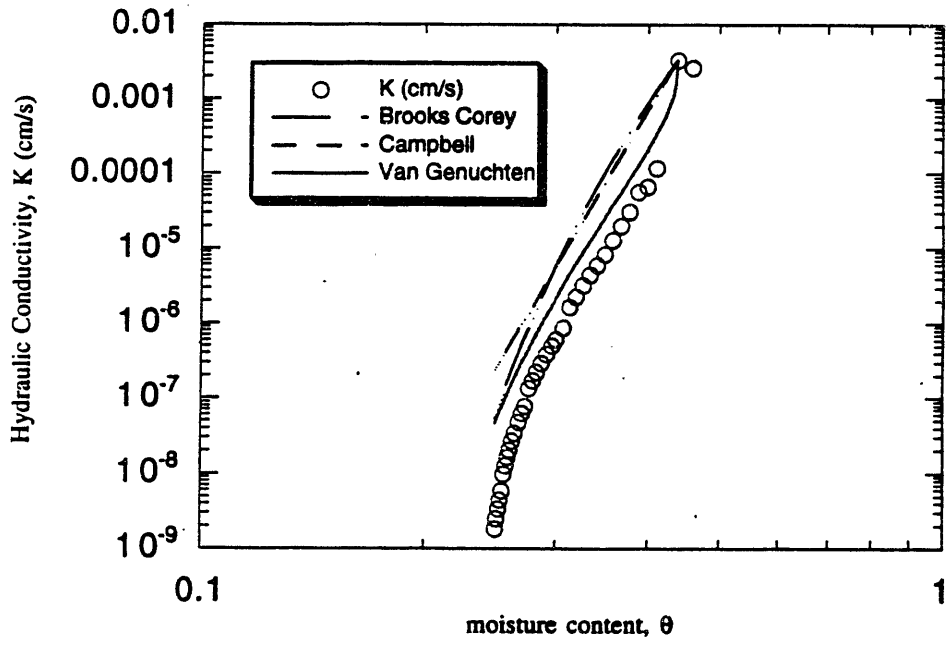

u(b) 80 cm

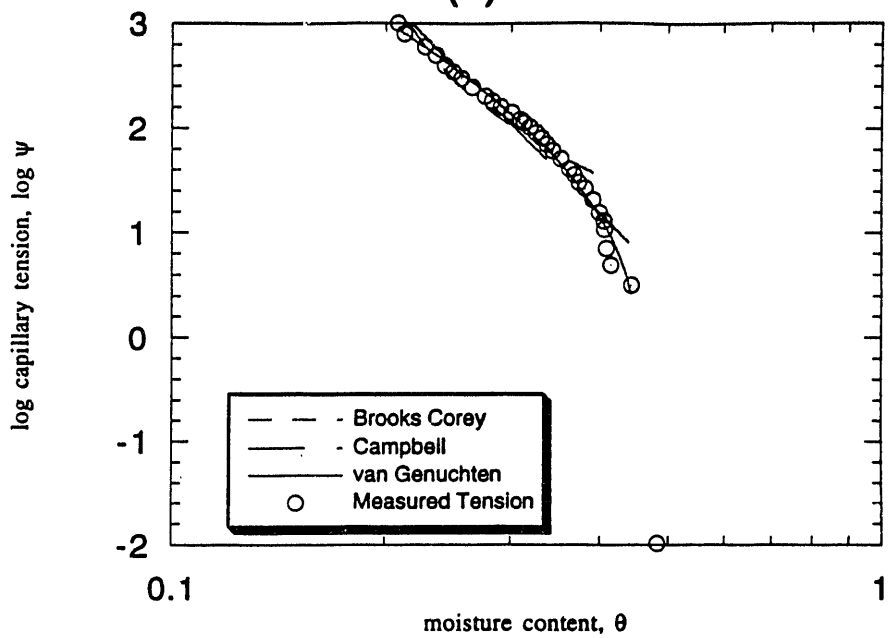

y = bc(.18,.1,1,.44631)		
	Value	Error
λ	0.53909	0.02929
Ψ_b	24.352	2.6274
Chisq	0.34421	NA
R^2	0.93648	NA

y = camp(1,.1,.44631)		
	Value	Error
Ψ_c	7.2523	0.88418
b	6.8579	0.30169
Chisq	0.69167	NA
R^2	0.94686	NA

y = vg(.18,1.5,.01,.49)		
	Value	Error
n	1.5199	0.033581
α	0.042876	0.0058183
θ_s	0.44631	0.0021862
Chisq	0.71343	NA
R^2	0.94519	NA

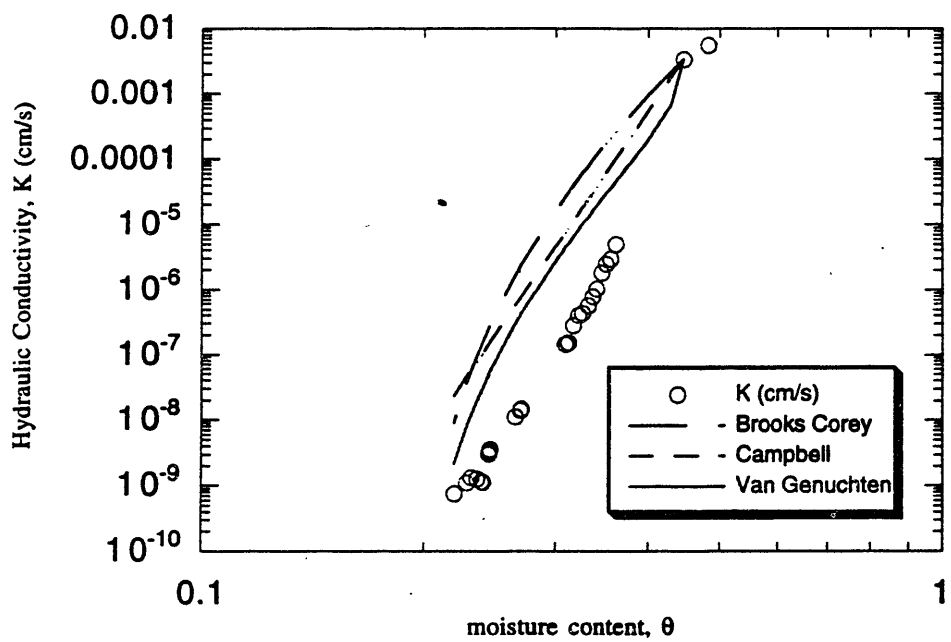

d(a) 80 cm

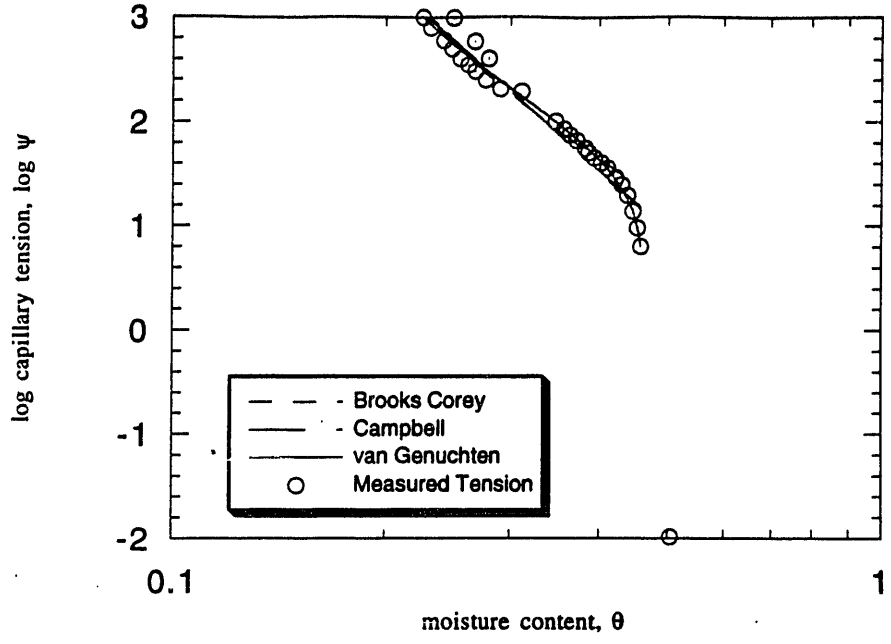

y = bc(.1397,.1,1,.46448)		
	Value	Error
λ	0.33613	0.013443
ψ_b	22.524	2.0674
Chisq	0.21622	NA
R^2	0.96604	NA

y = camp(1,.1,.46448)		
	Value	Error
ψ_e	13.668	1.4142
b	6.0857	0.24868
Chisq	0.46223	NA
R^2	0.95839	NA

y = vg(0.22,1.5,.01,.51)		
	Value	Error
θ_r	0.1397	0.041715
n	1.4074	0.10974
α	0.025617	0.0038071
θ_s	0.46448	0.0033816
Chisq	0.17314	NA
R^2	0.98441	NA

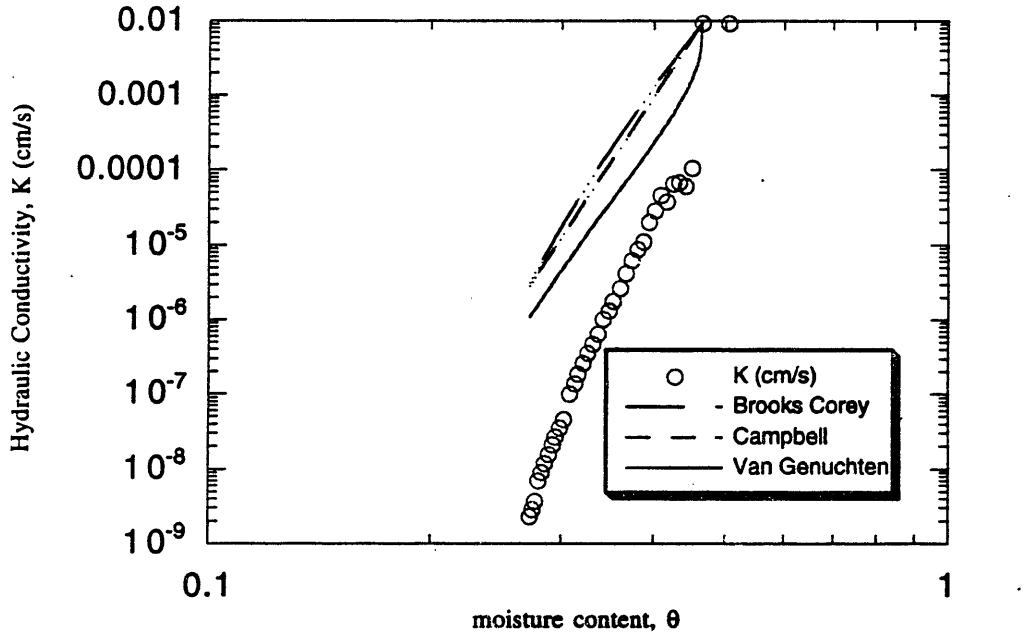

d(b) 80 cm

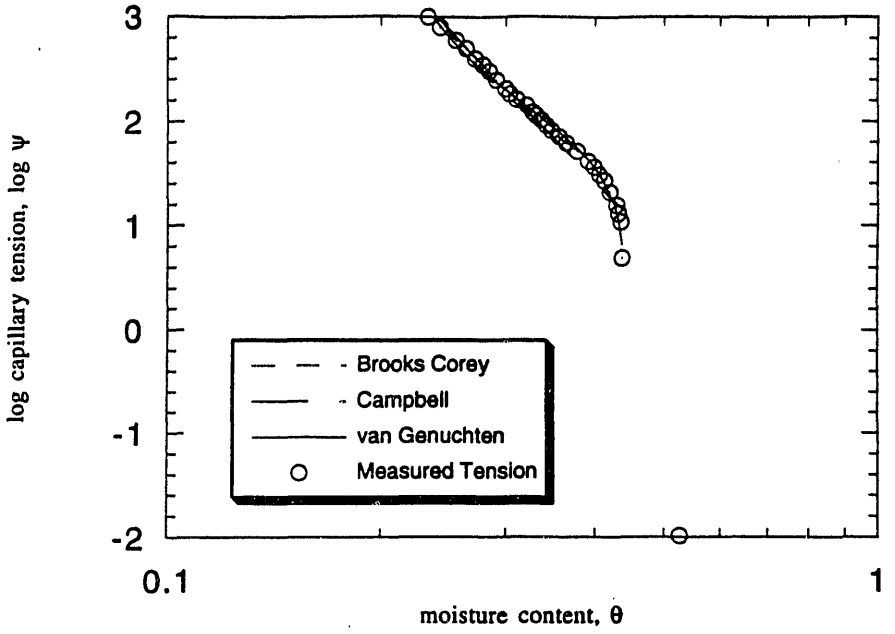

y = bc(.18362,.1,1,.441)		
	Value	Error
λ	0.40873	0.012607
ψ_b	26.081	1.5934
Chisq	0.096982	NA
R	0.98971	NA

y = camp(1,.1,.441)		
	Value	Error
ψ_e	13.24	1.1161
b	7.1098	0.25458
Chisq	0.32928	NA
R^2	0.96654	NA

y = vg(0.23,1.5,.01,.53)		
	Value	Error
θ_r	0.18362	0.012197
n	1.5093	0.059505
α	0.02214	0.0016475
θ_s	0.441	0.0012841
Chisq	0.066276	NA
R^2	0.99327	NA

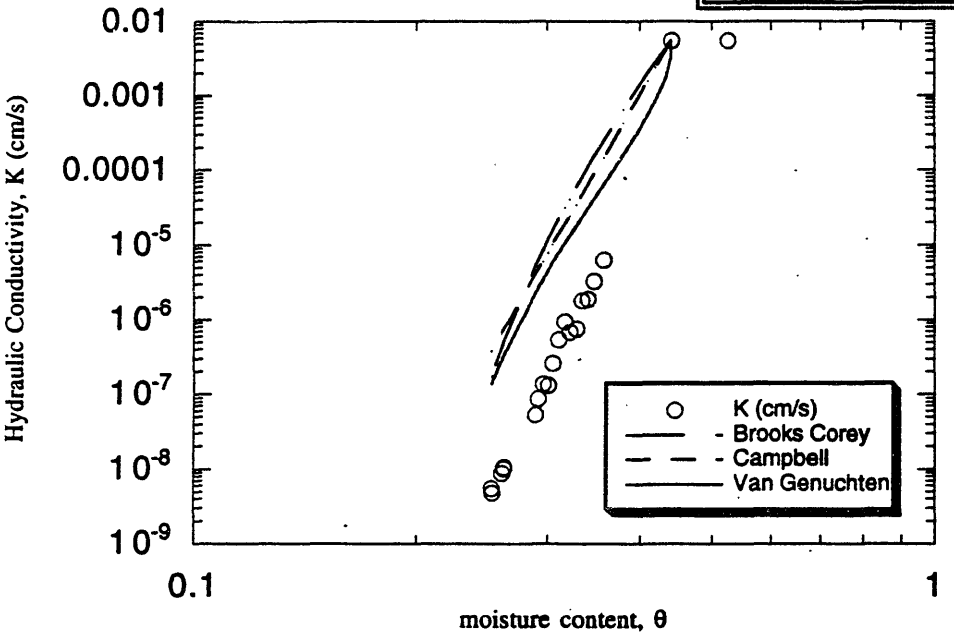

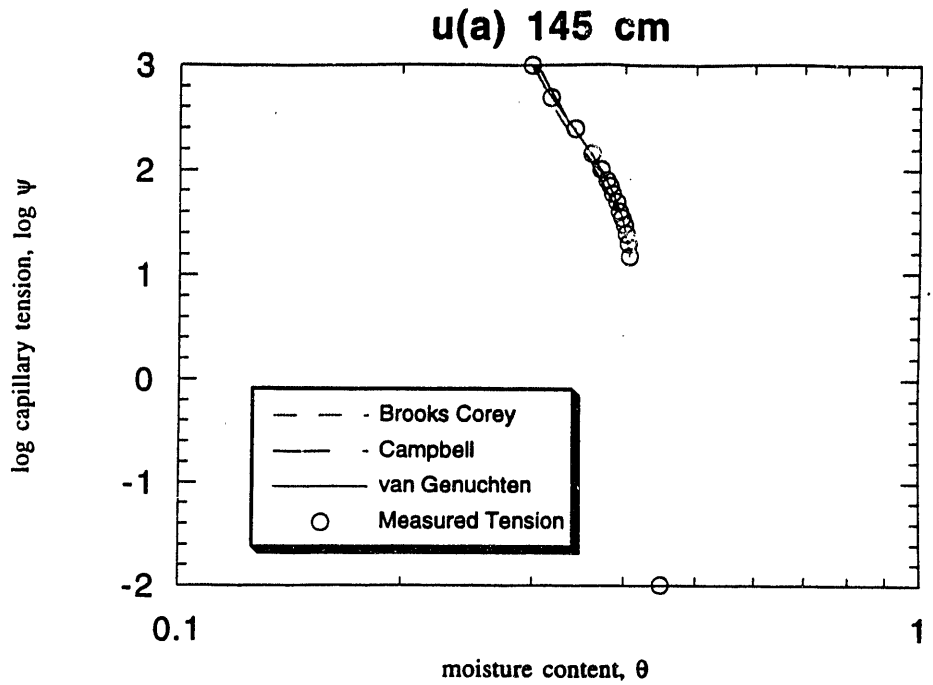

y = bc(.26633,.1,1,.449)		
	Value	Error
λ	0.46938	0.031922
ψ_b	29.354	3.9281
Chisq	0.036453	NA
R	0.98642	NA

y = camp(1,.1,.449)		
	Value	Error
ψ_e	7.0915	1.0114
b	12.661	0.698
Chisq	0.14292	NA
R	0.98081	NA

y = vg(0.28,1.5,.01,.51)		
	Value	Error
θ_r	0.26633	0.062924
n	1.6141	0.58766
α	0.024229	0.0094899
θ_s	0.449	0.00015173
Chisq	0.60748	NA
R	0.98266	NA

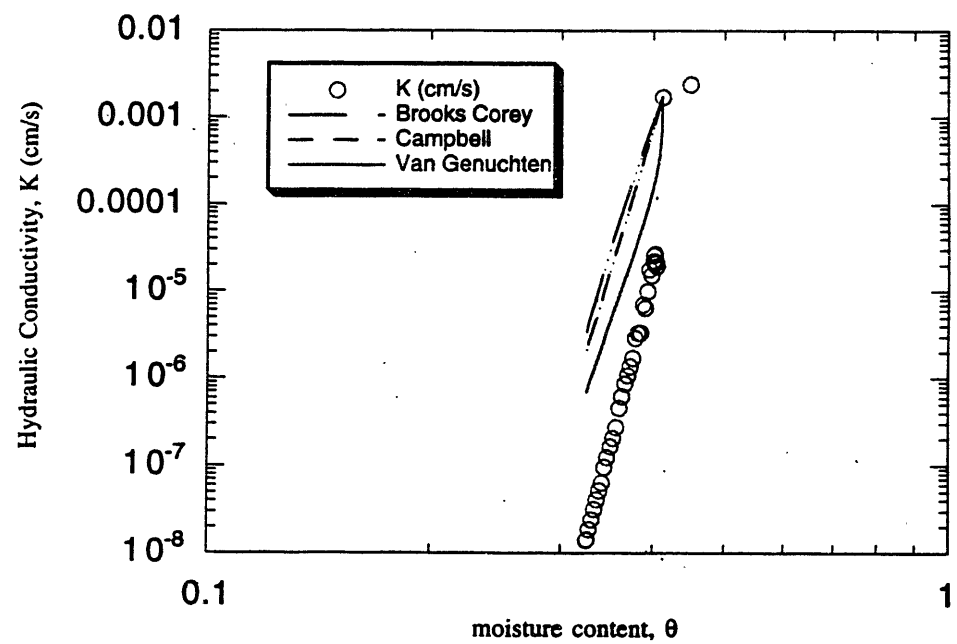

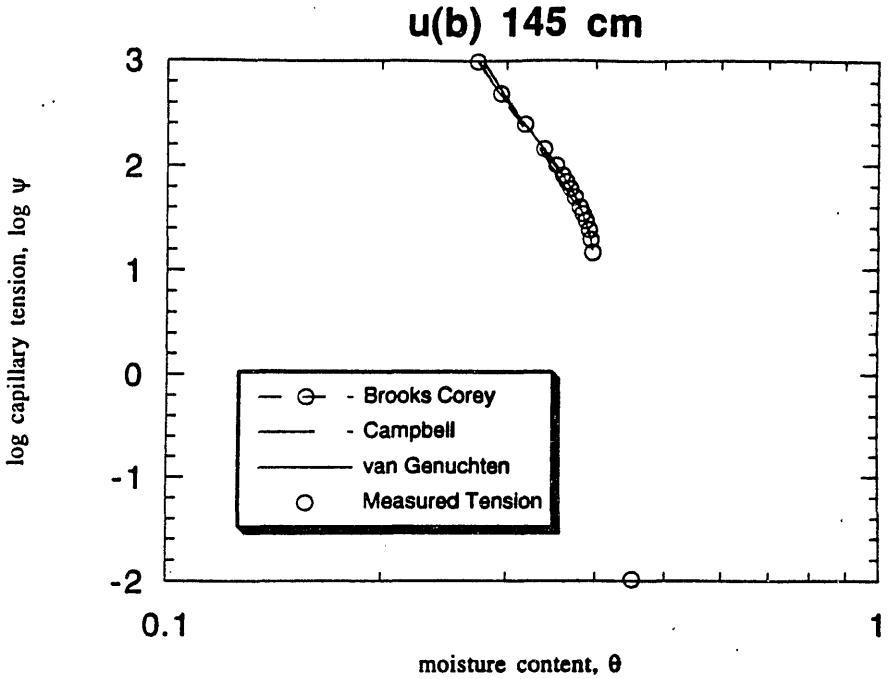

y = bc(.1893..1,1,.40444)		
	Value	Error
λ	0.27584	0.0099292
ψ_b	34.801	2.2849
Chisq	0.010426	NA
R^2	0.99229	NA

y = camp(1,.1,.40444)		
	Value	Error
ψ_e	19.144	1.5734
b	10.519	0.49357
Chisq	0.10492	NA
R^2	0.97217	NA

y = vg(0.27,1.5,.01,.57)		
	Value	Error
θ_r	0.1893	0.015227
n	1.3326	0.041672
α	0.017178	0.00094705
θ_s	0.40444	0.00097431
Chisq	0.0023125	NA
R^2	0.99939	NA

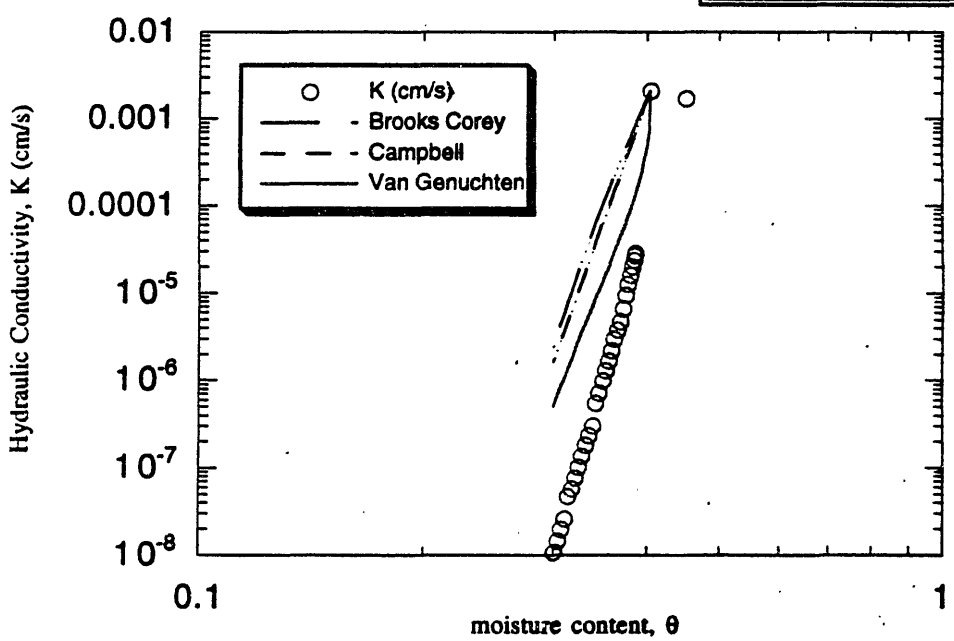

d(a) 145 cm

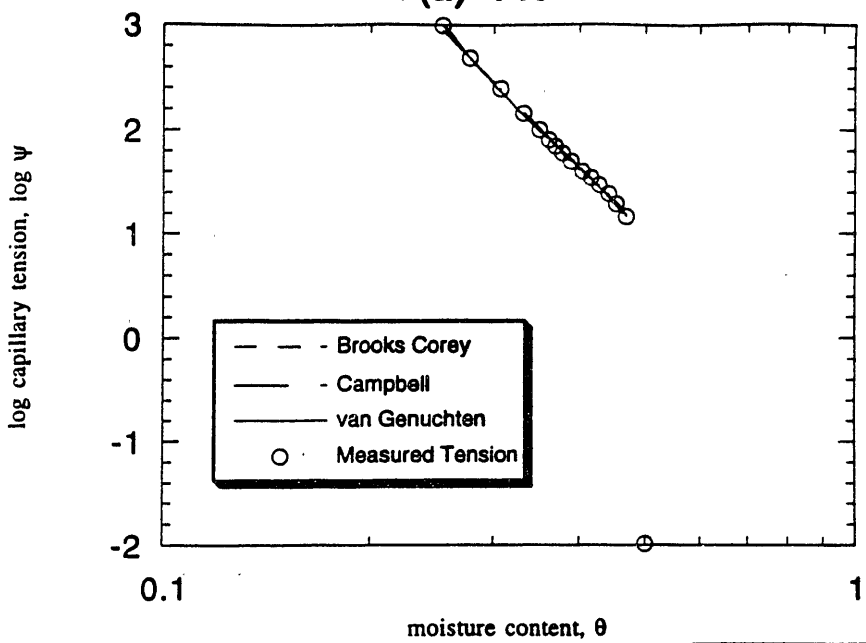

y = bc(.13724,.1,1,.58272)		
	Value	Error
λ	0.25311	0.0029118
ψ_b	5.1503	0.17068
Chisq	0.0065058	NA
R^2	0.99828	NA

y = camp(1,.1,.58272)		
	Value	Error
ψ_e	3.4767	0.14557
b	6.6515	0.085799
Chisq	0.0081838	NA
R^2	0.99784	NA

y = vg(0.25,1.5,.01,.51)		
	Value	Error
θ_r	0.13724	0.022232
n	1.2651	0.03659
α	0.16109	0.083206
θ_s	0.58272	0.039498
Chisq	0.0028162	NA
R	0.99963	NA

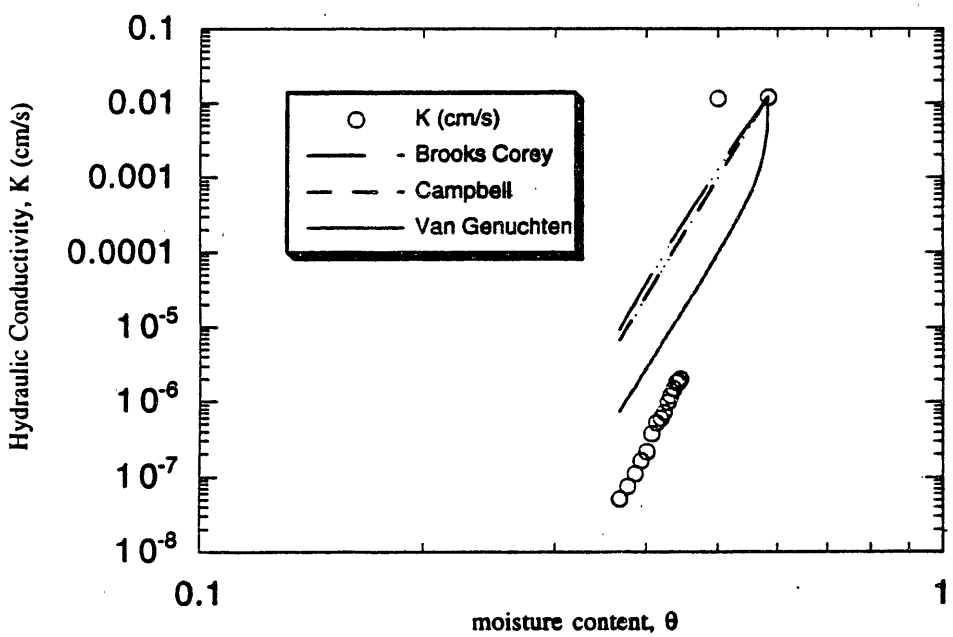

d(b) 145 cm

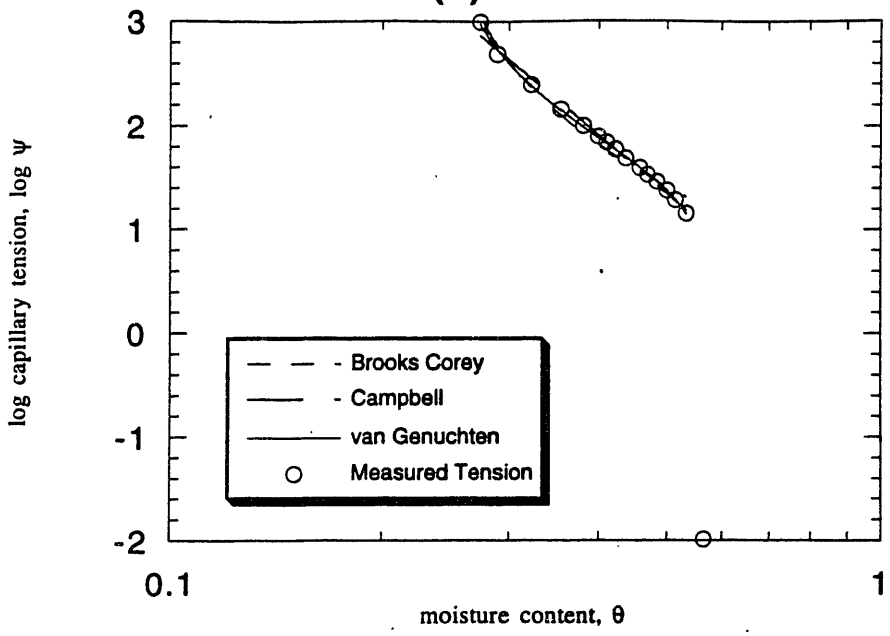

y = bc(.23377,.1,1,.57164)		
	Value	Error
λ	0.50226	0.018884
ψ_b	16.14	1.1431
Chisq	0.068738	NA
R^2	0.98197	NA

y = camp(1,.1,.57164)		
	Value	Error
ψ_e	10.137	0.58275
b	5.8214	0.14717
Chisq	0.03142	NA
R^2	0.99176	NA

y = vg(0.27,1.5,.01,.57)		
	Value	Error
θ_r	0.23377	0.005764
n	1.5894	0.041098
α	0.03951	0.0036966
θ_s	0.57164	0.0065464
Chisq	0.0036878	NA
R	0.99952	NA

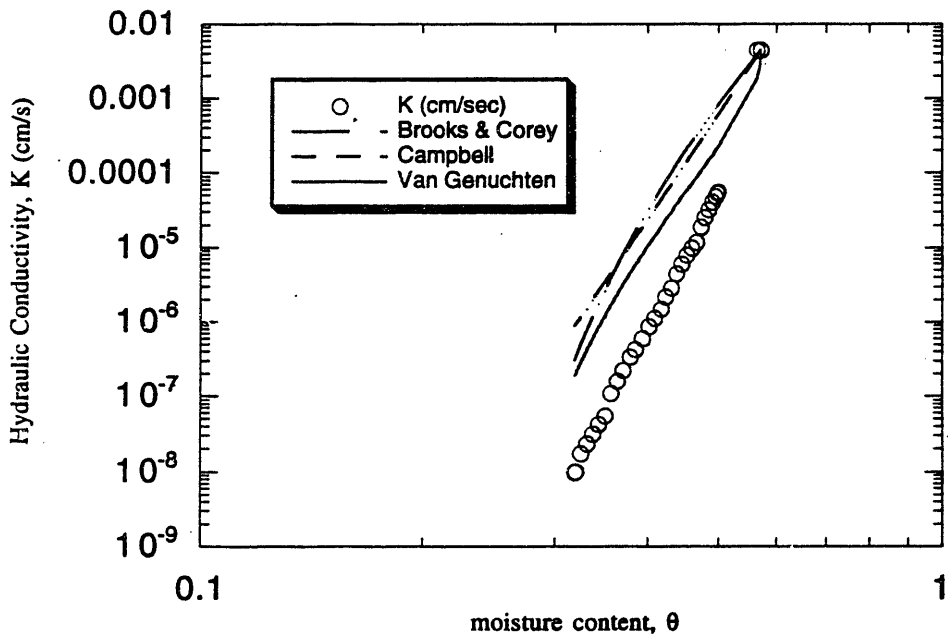

u(a) 225 cm

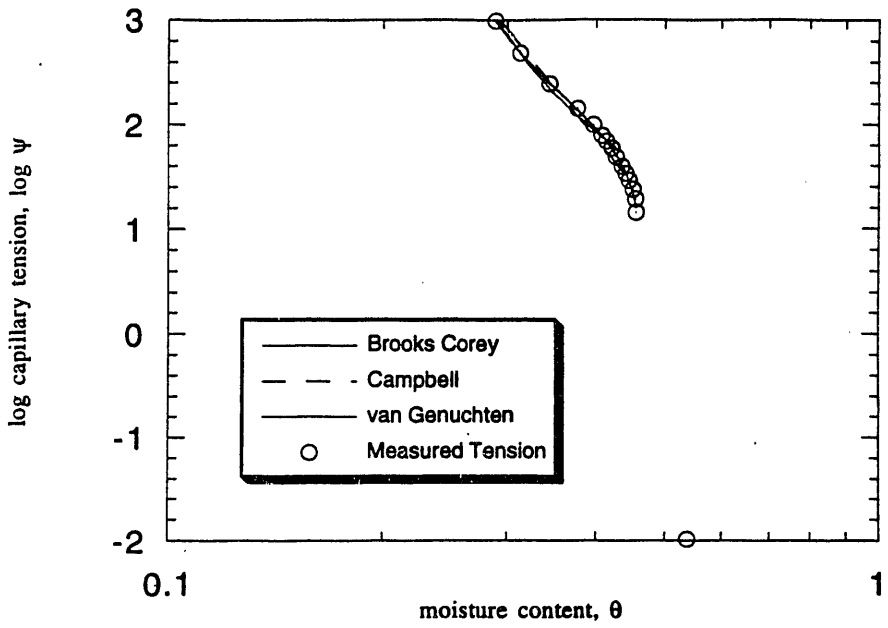

y = bc(.22335,.1,1,.46436)		
	Value	Error
λ	0.39026	0.016575
ψ_b	38.517	2.6782
Chisq	0.020016	NA
R	0.99375	NA

y = camp(1,.1,.46436)		
	Value	Error
ψ_c	20.912	1.8222
b	8.4134	0.4362
Chisq	0.12874	NA
R	0.98297	NA

y = vg(0.28,1.5,.01,.54)		
	Value	Error
θ_r	0.22335	0.014222
n	1.4823	0.060319
α	0.015132	0.00082392
θ_s	0.46436	0.0013885
Chisq	0.0052136	NA
R^2	0.99863	NA

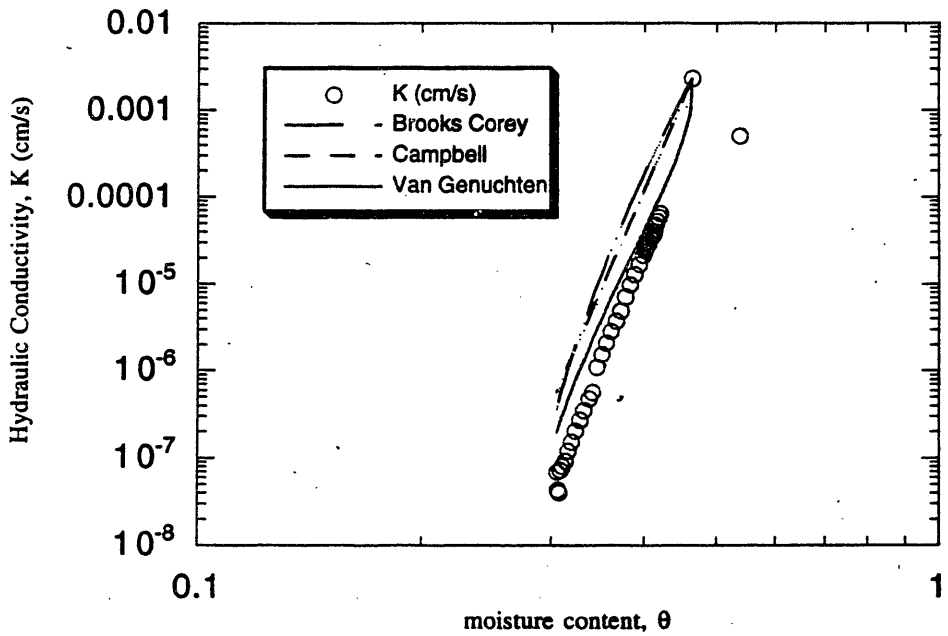

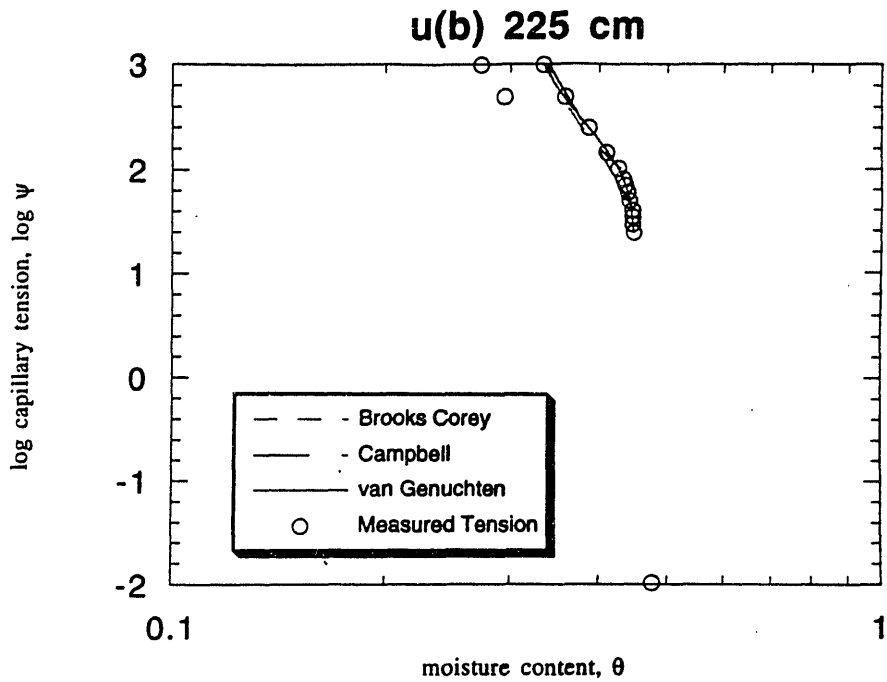

y = bc(.30044,.1,1,.45122)		
	Value	Error
λ	0.55632	0.045027
ψ_b	76.218	8.6571
Chisq	0.022848	NA
R^2	0.97449	NA

y = camp(1,.1,.45122)		
	Value	Error
ψ_e	37.44	3.6554
b	11.51	0.81923
Chisq	0.15002	NA
R^2	0.94722	NA

y = vg(0.27,1.5,.01,.48)		
	Value	Error
θ_r	0.30044	0.0088312
n	1.7724	0.096068
α	0.0068872	0.00025951
θ_s	0.45122	0.0006644
Chisq	0.0058463	NA
R^2	0.99794	NA

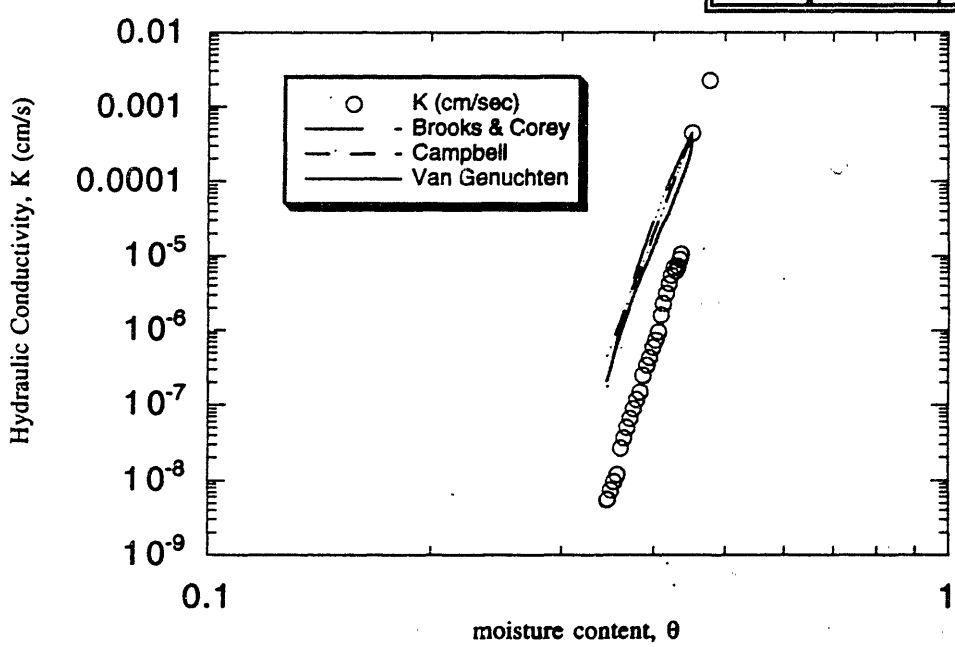

d(a) 225 cm

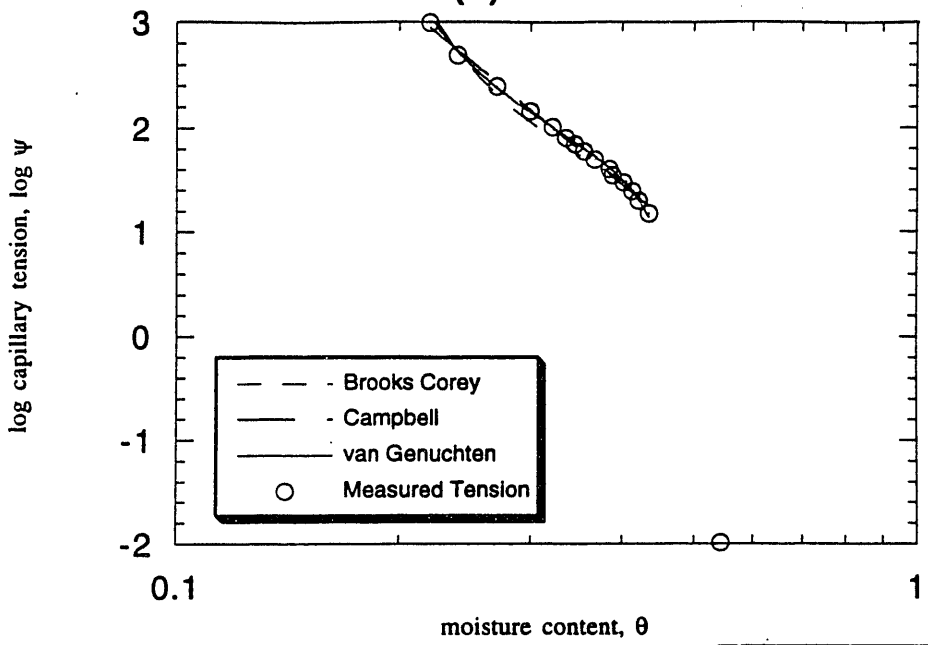

y = bc(.18619,.1,1,.45246)		
	Value	Error
λ	0.49396	0.025228
ψ_b	20.28	1.7676
Chisq	0.12286	NA
R^2	0.96723	NA

y = camp(1,.1,.45246)		
	Value	Error
ψ_e	14.013	0.52298
b	5.7495	0.10683
Chisq	0.016754	NA
R^2	0.99553	NA

y = vg(0.21,1.5,.01,.55)		
	Value	Error
θ_r	0.18619	0.008491
n	1.6023	0.070581
α	0.027161	0.0030562
θ_s	0.45246	0.0048208
Chisq	0.013428	NA
R^2	0.99642	NA

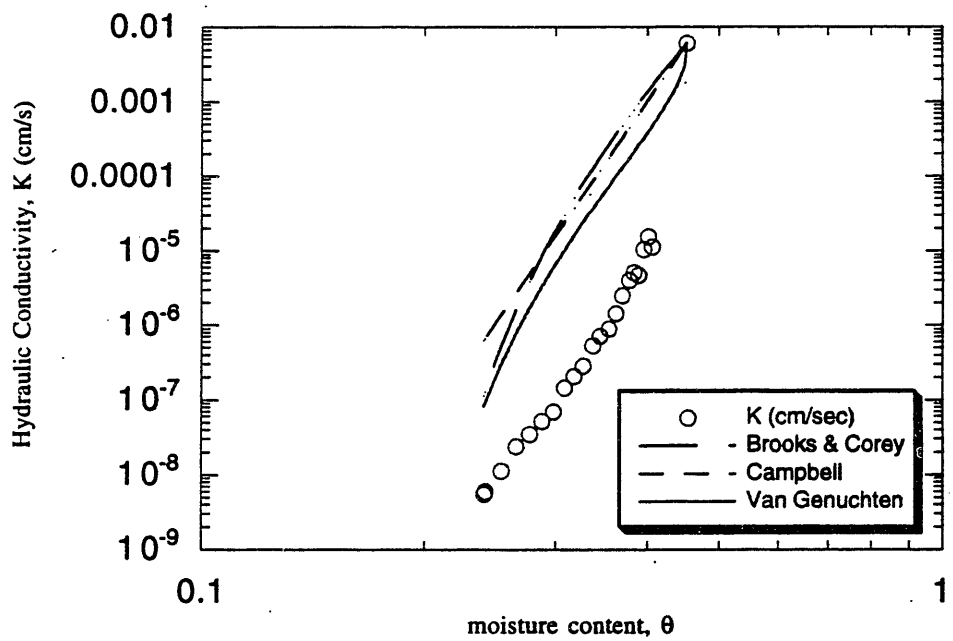

d(b) 225 cm

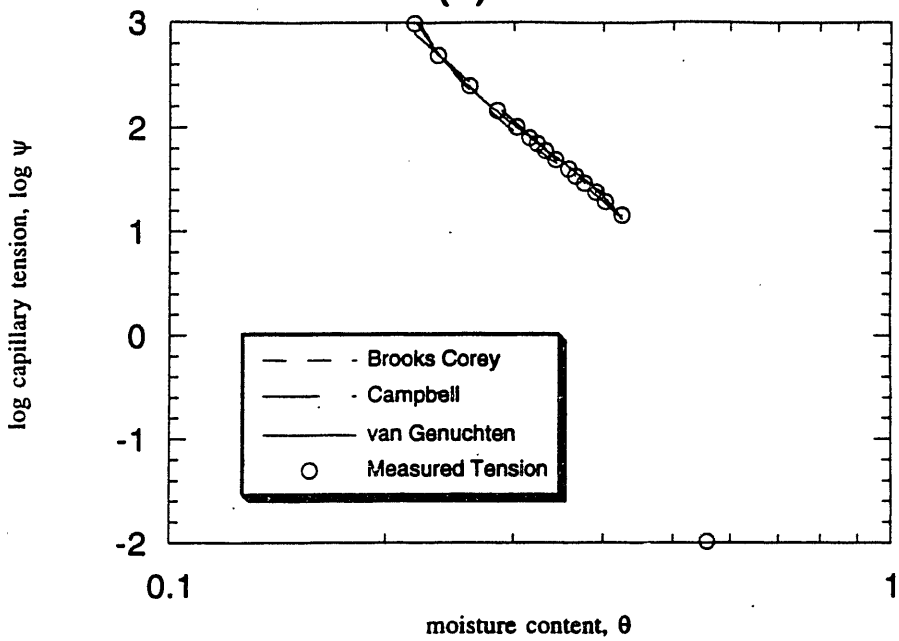

y = bc(.18229,.1,1,.46015)		
	Value	Error
λ	0.45317	0.014177
Ψ_b	13.595	0.86093
Chisq	0.047858	NA
R^2	0.98745	NA

y = camp(1,.1,.46015)		
	Value	Error
Ψ_e	8.1387	0.36293
b	6.1479	0.11115
Chisq	0.016133	NA
R^2	0.99577	NA

y = vg(0.21,1.5,.01,.56)		
	Value	Error
θ_r	0.18229	0.0087279
n	1.514	0.062945
α	0.048154	0.009288
θ_s	0.46015	0.010718
Chisq	0.012085	NA
R^2	0.99683	NA

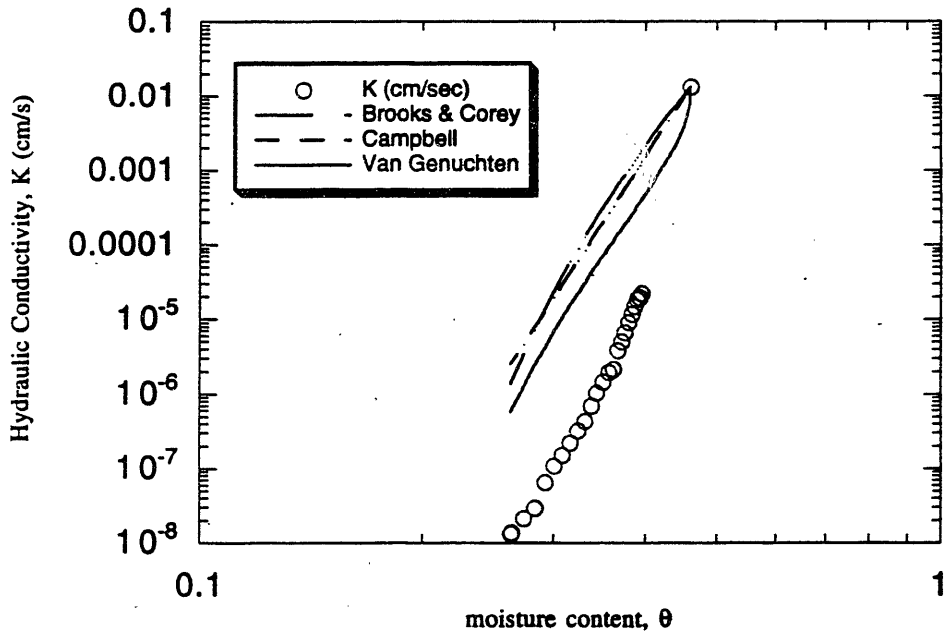

Appendix E: Las Cruces Curve Fits

Core 3-34

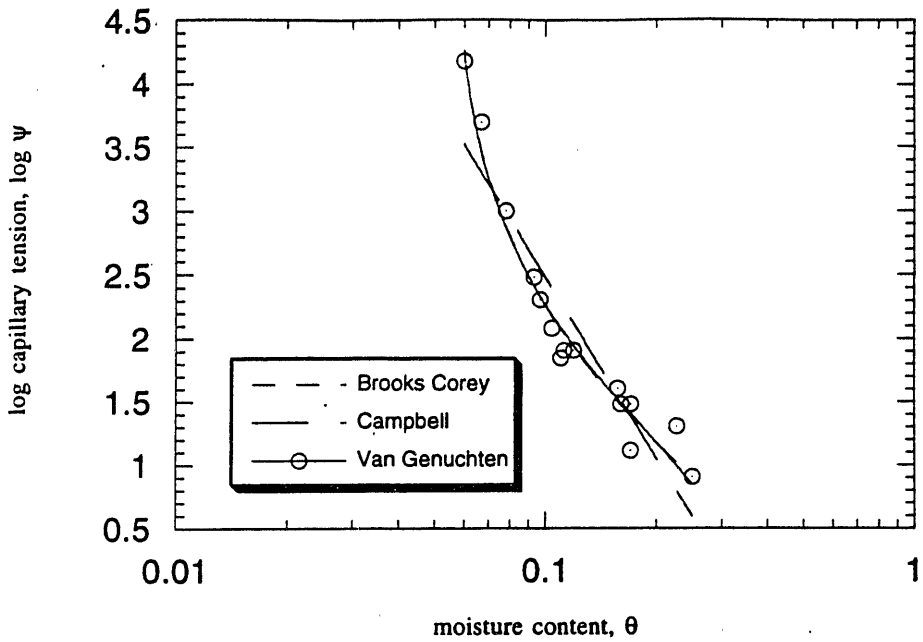

y = bc(.01,.1,1,.337)		
	Value	Error
θ_r	0.054744	0.0021027
λ	0.46684	0.04787
ψ_β	3.6048	0.98334
Chisq	0.33426	NA
R^2	0.9723	NA

y = camp(1,.1,.337)		
	Value	Error
ψ_c	0.95922	0.53316
b	4.7307	0.5046
Chisq	1.5547	NA
R^2	0.87115	NA

y = vg(0.01,1.5,.001,.337)		
	Value	Error
θ_r	0.055267	0.0021032
n	1.4878	0.055218
α	0.23637	0.070537
Chisq	0.37649	NA
R^2	0.9688	NA

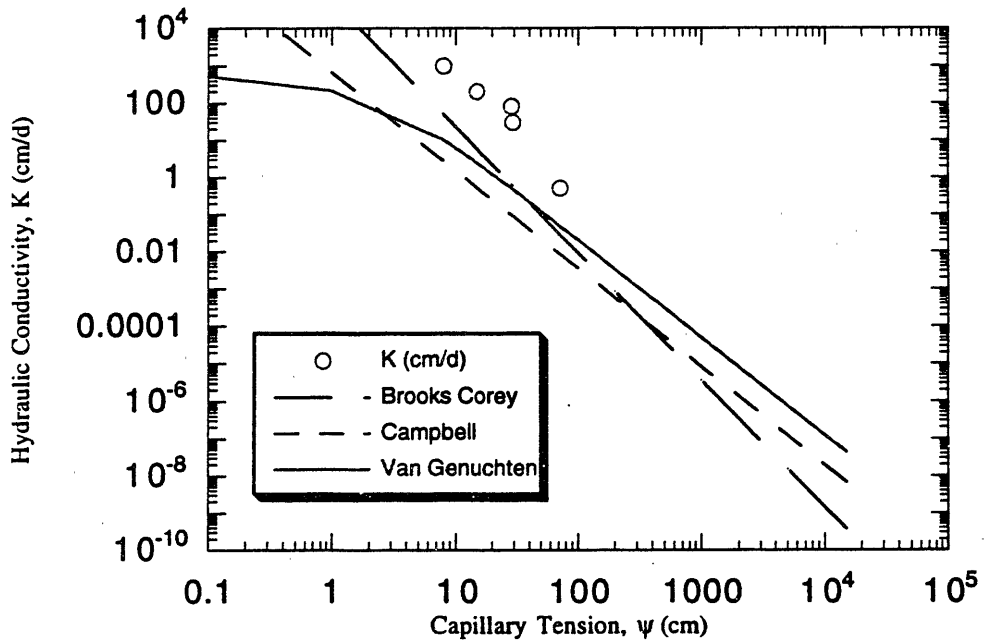

Core 4-25

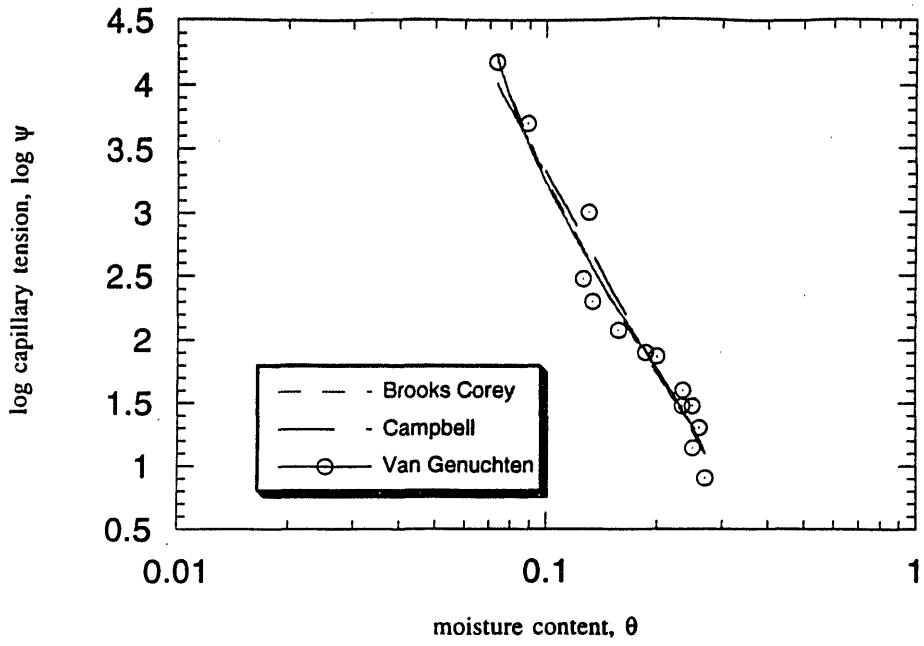

y = bc(.01,.1,1,.315)		
	Value	Error
θ_r	0.040695	0.016432
λ	0.2803	0.057792
ψ_β	7.8747	2.2195
Chisq	0.47777	NA
R^2	0.96015	NA

y = camp(1,.1,.315)		
	Value	Error
ψ_c	5.6952	1.2934
b	5.1302	0.31759
Chisq	0.56901	NA
R^2	0.95255	NA

y = vg(0.01,1.5,.001,.315)		
	Value	Error
θ_r	0.04944	0.012441
n	1.3337	0.066577
α	0.084432	0.024302
Chisq	0.44408	NA
R^2	0.96296	NA

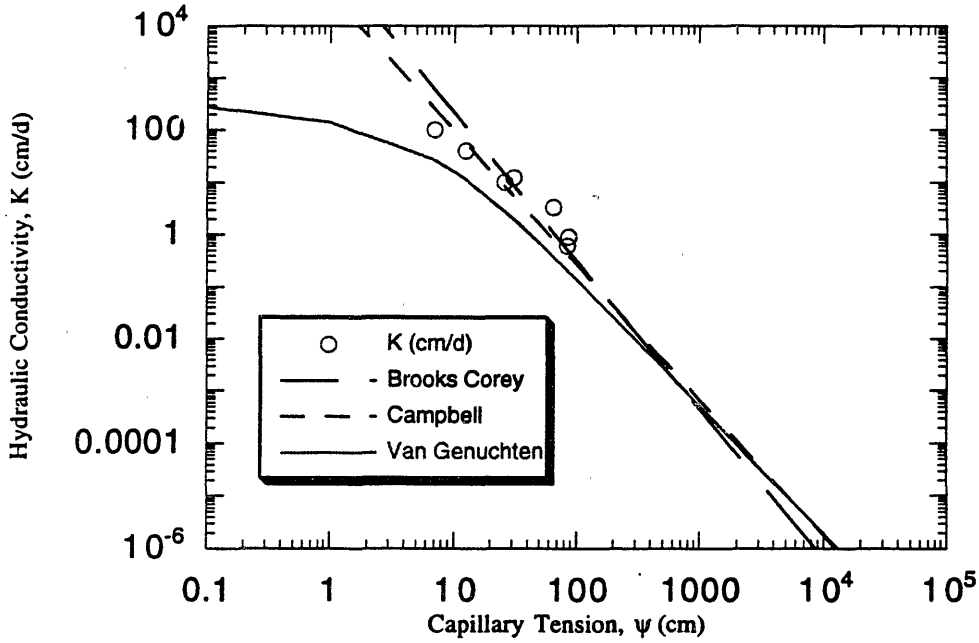

Core 5-34

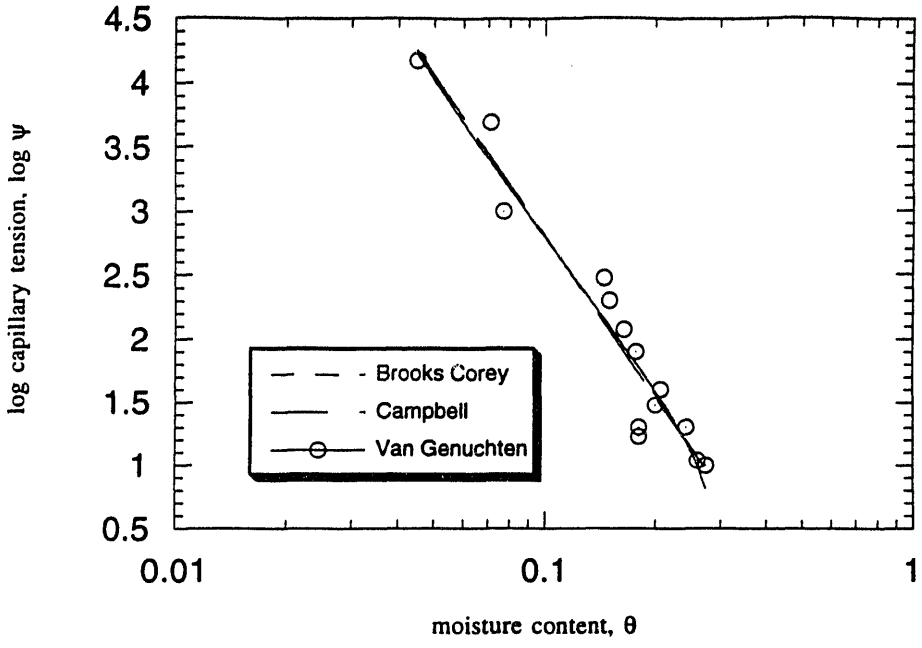

y = bc(0,.1,1,.305)		
	Value	Error
λ	0.23908	0.01848
ψ_β	6.0231	1.6774
Chisq	0.85891	NA
R^2	0.93316	NA

y = camp(1,.1,.305)		
	Value	Error
ψ_c	6.0231	1.6774
b	4.1826	0.32313
Chisq	0.85891	NA
R^2	0.93316	NA

y = vg(0.01,1.5,.001,.305)		
	Value	Error
θ_r	0.0084438	0.031398
n	1.2776	0.10189
α	0.11054	0.05459
Chisq	0.93089	NA
R^2	0.92756	NA

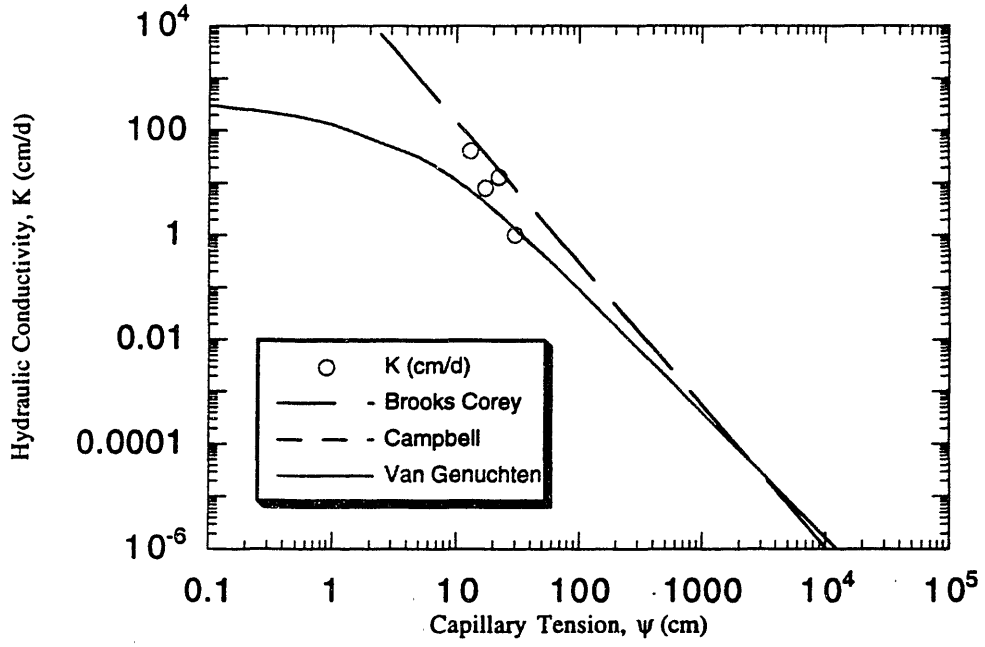

Core 7-21

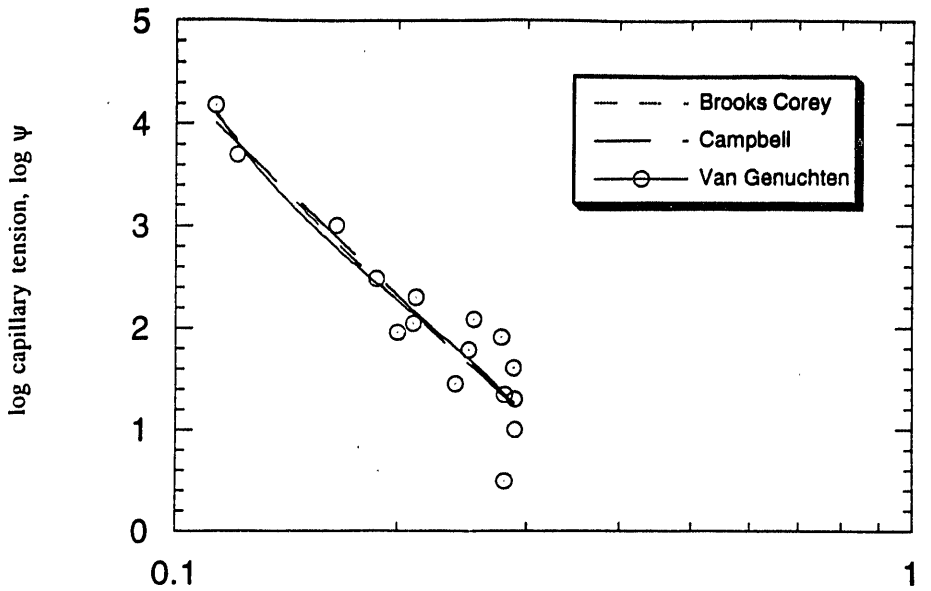

y = bc(.01,.1,1,.322)		
	Value	Error
θ_r	0.044061	0.074636
λ	0.1951	0.11501
ψ_β	9.5726	4.7785
Chisq	1.7294	NA
R^2	0.87329	NA

y = camp(1,.1,.322)		
	Value	Error
ψ_e	8.1023	2.7193
b	6.8135	0.69913
Chisq	1.7533	NA
R^2	0.87153	NA

y = vg(0.01,1.5,.001,.322)		
	Value	Error
θ_r	0.077206	0.041637
n	1.2922	0.15504
α	0.055128	0.028947
Chisq	1.7154	NA
R^2	0.87431	NA

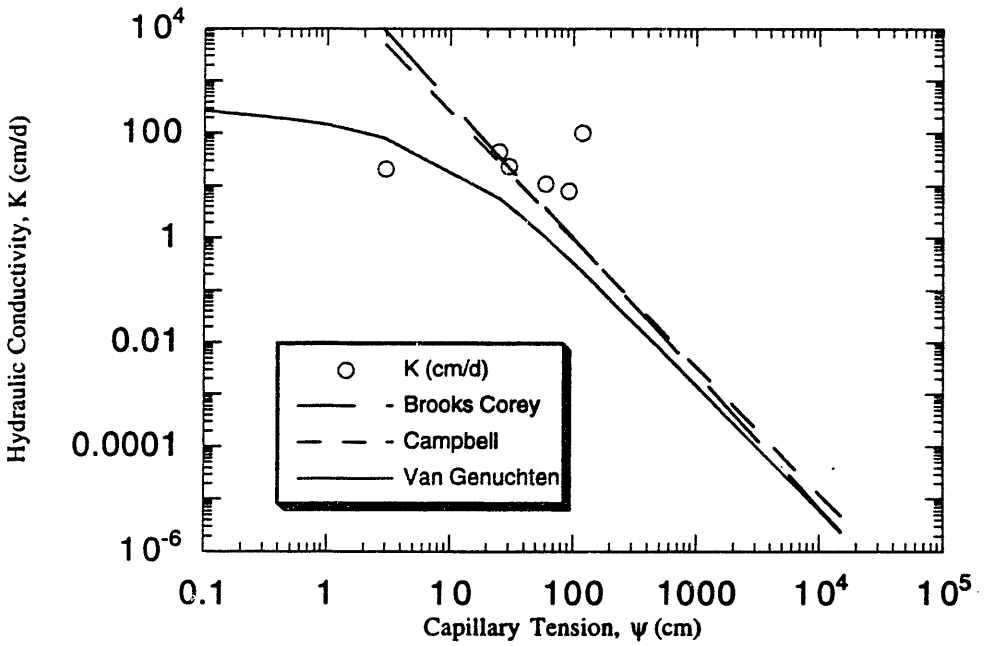

Core 8-49

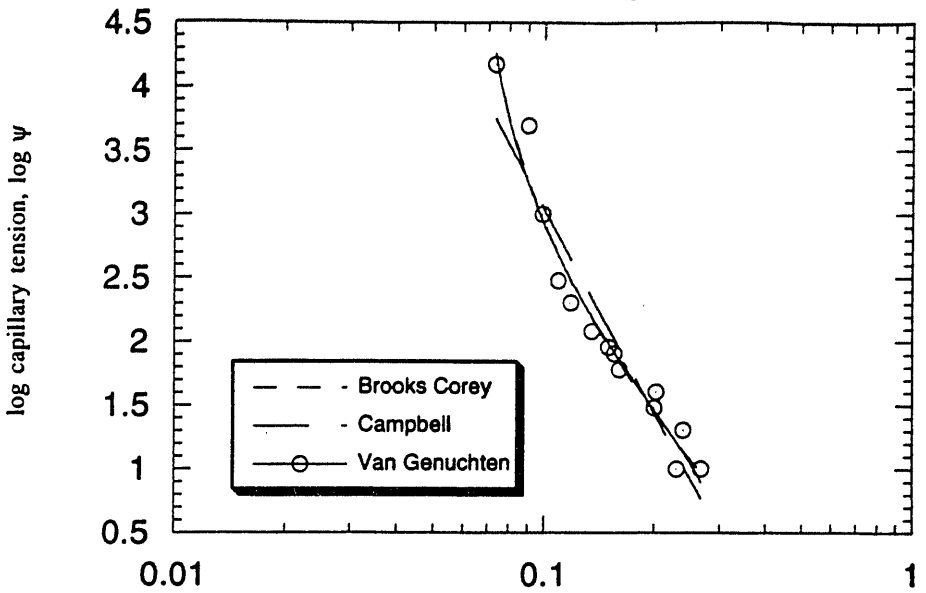

y = bc(.01,.1,1,.332)		
	Value	Error
θ_r	0.059871	0.0056796
λ	0.3638	0.049691
ψ_β	4.4293	1.3401
Chisq	0.38786	NA
R^2	0.96688	NA

y = camp(1,.1,.332)		
	Value	Error
ψ_e	1.8623	0.74387
b	5.3017	0.44809
Chisq	0.92445	NA
R^2	0.92105	NA

y = vg(0.01,1.5,.001..332)		
	Value	Error
θ_r	0.061522	0.0054165
n	1.3896	0.057438
α	0.18	0.059009
Chisq	0.41614	NA
R^2	0.96446	NA

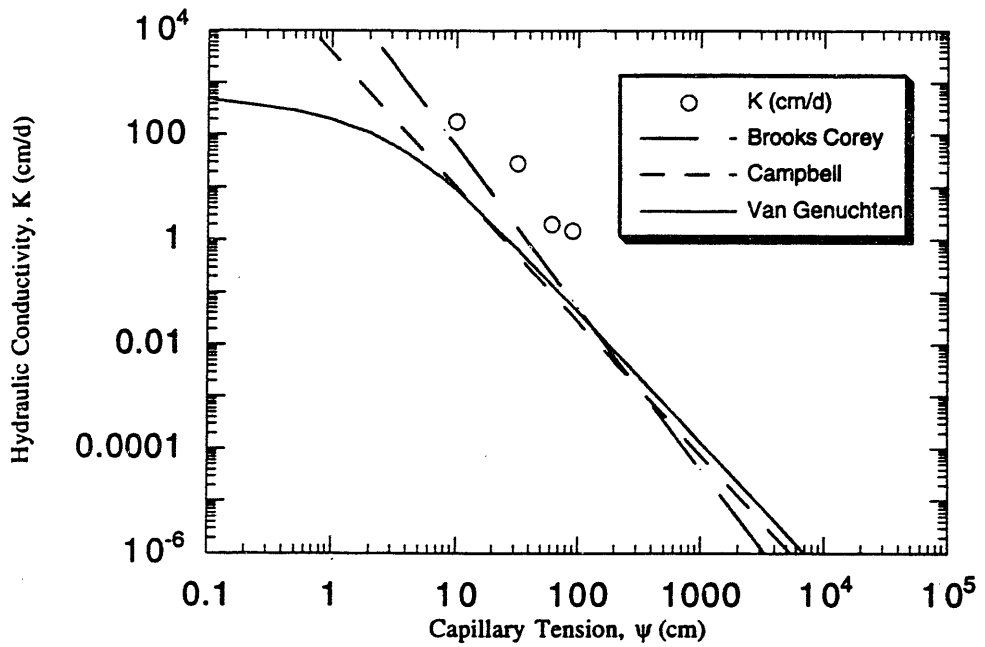

Appendix F: Maddock Curve Fits

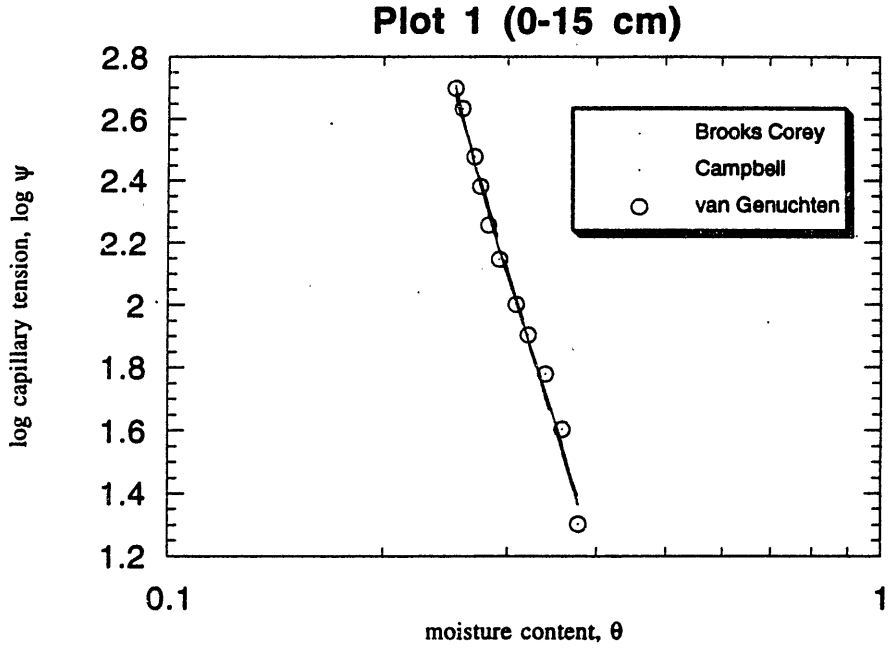

y = bc(.01,.1,1,.418)		
	Value	Error
θ_r	0.10464	0.091661
λ	0.20278	0.09427
ψ_b	12.175	2.3245
Chisq	0.022509	NA
R	0.99415	NA

y = camp(1,.1,.418)		
	Value	Error
ψ_c	10.695	1.0584
b	7.5128	0.27944
Chisq	0.023716	NA
R	0.99383	NA

y = vg(0.1,1.5,.01,.418)		
	Value	Error
θ_r	0.19843	0.018302
n	1.4556	0.088717
α	0.041327	0.0043972
Chisq	0.012644	NA
R	0.99672	NA

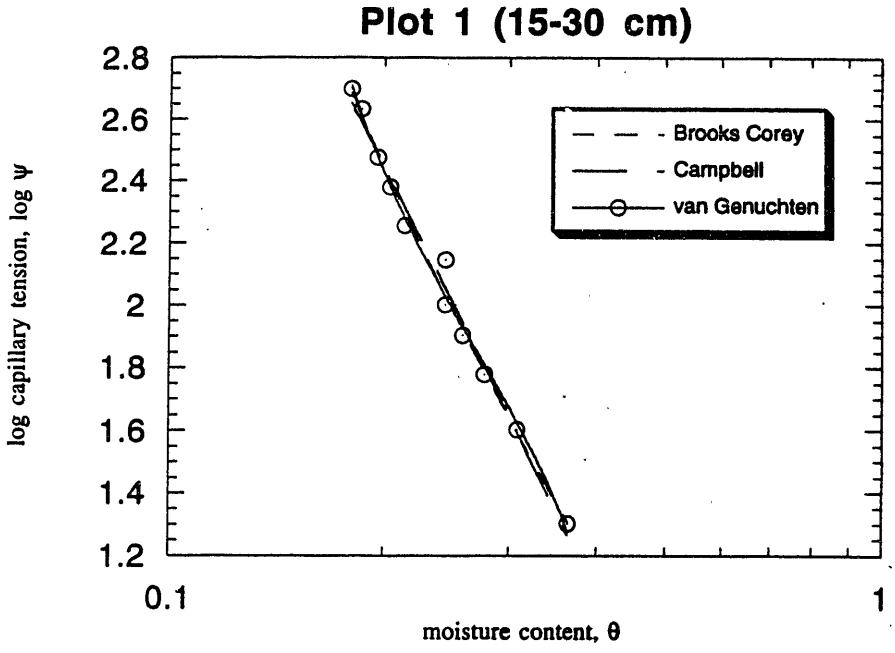

y = bc(.1,.1,1,.418)		
	Value	Error
θ_r	0.083099	0.034478
λ	0.3346	0.075458
Ψ_b	12.025	1.7981
Chisq	0.01794	NA
R	0.99534	NA

y = camp(1,.1,.418)		
	Value	Error
Ψ_e	9.8333	0.98965
b	4.5437	0.16694
Chisq	0.023147	NA
R	0.99398	NA

y = vg(0.1,1.5,.01,.418)		
	Value	Error
θ_r	0.1375	0.014178
n	1.6024	0.099843
α	0.044432	0.0054616
Chisq	0.01856	NA
R	0.99518	NA

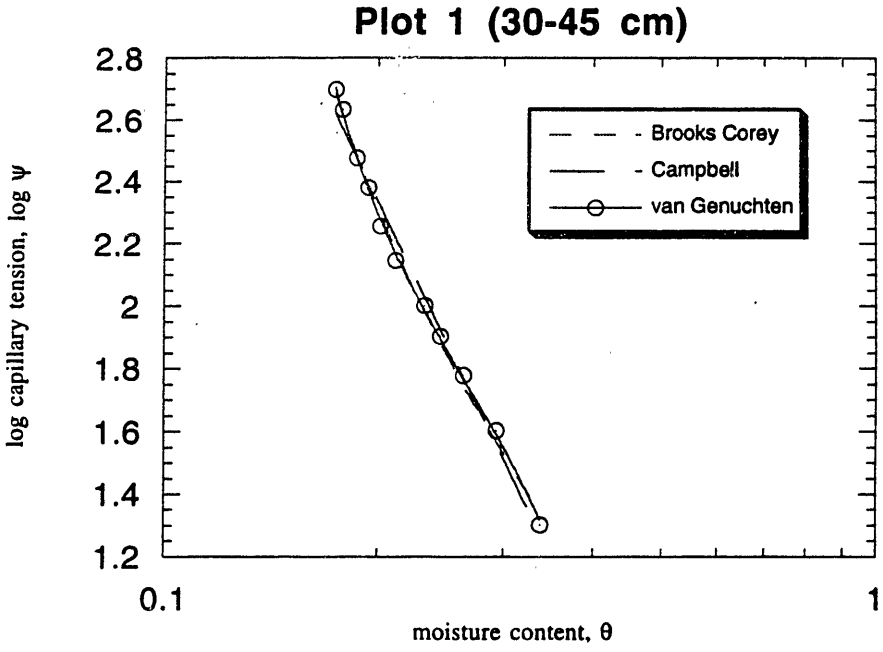

y = bc(.15,.1,1,.399)		
	Value	Error
θ_r	0.11662	0.012098
λ	0.43695	0.051821
Ψ_b	12.639	1.17
Chisq	0.0073288	NA
R	0.9981	NA

y = camp(1,.1,.399)		
	Value	Error
Ψ_e	8.6163	0.90292
b	4.6785	0.17122
Chisq	0.022968	NA
R	0.99403	NA

y = vg(0.1,1.5,.01,.399)		
	Value	Error
θ_r	0.14322	0.0031597
n	1.6645	0.031729
α	0.047726	0.001869
Chisq	0.0018336	NA
R	0.99952	NA

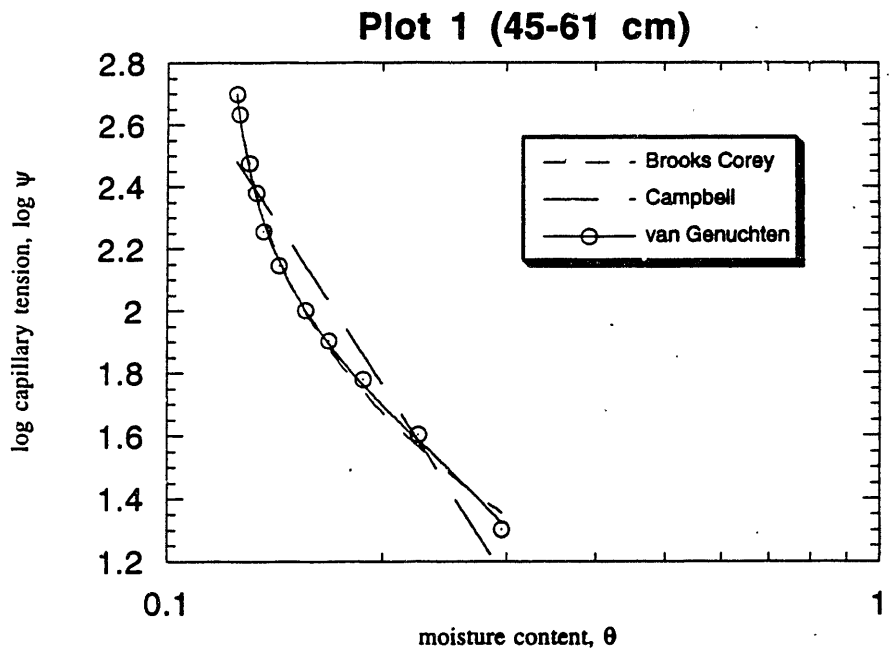

y = bc(.1,.1,1,.39)		
	Value	Error
θ_r	0.11771	0.0014528
λ	1.0399	0.06513
ψ_b	14.98	1.1982
Chisq	0.0091718	NA
R	0.99762	NA

y = camp(1,.1,.39)		
	Value	Error
ψ_e	5.5165	1.8382
b	3.5225	0.3582
Chisq	0.16419	NA
R	0.95648	NA

y = vg(0.1,1.5,.01,.39)		
	Value	Error
θ_r	0.11979	0.00065566
n	2.2131	0.043674
α	0.051811	0.0023082
Chisq	0.0032783	NA
R	0.99915	NA

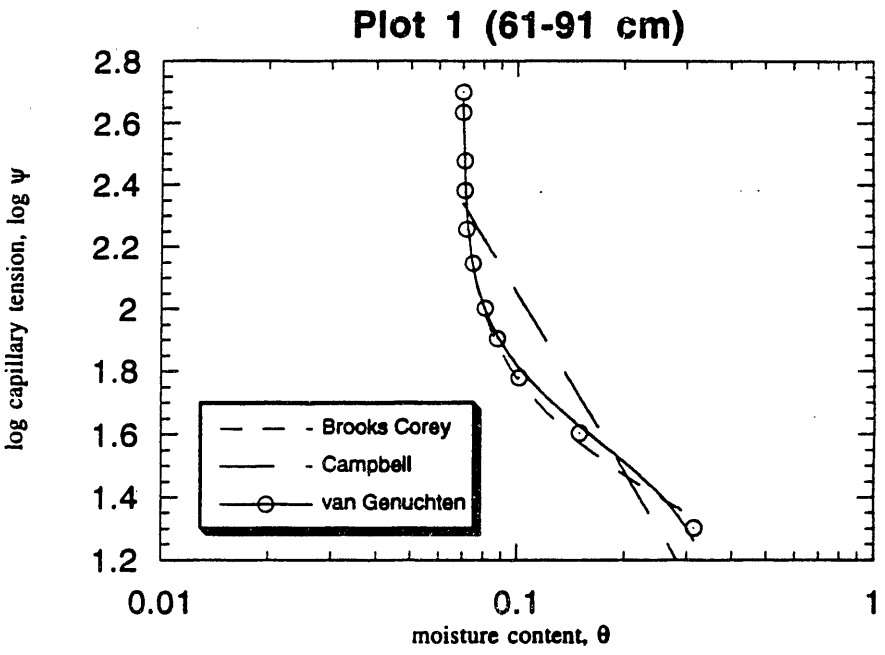

y = bc(.05,.1,1,.367)		
	Value	Error
θ_r	0.069535	0.00011857
λ	2.0509	0.099665
ψ_b	19.765	1.4192
Chisq	0.012861	NA
R	0.99666	NA

y = camp(1,.1,.67)		
	Value	Error
ψ_e	3.1269	2.317
b	1.8798	0.36614
Chisq	0.49086	NA
R	0.8634	NA

y = vg(0.05,2,.01,.367)		
	Value	Error
θ_r	0.069718	7.6679e-05
n	3.3949	0.11551
α	0.039038	0.0025756
Chisq	0.013475	NA
R	0.9965	NA

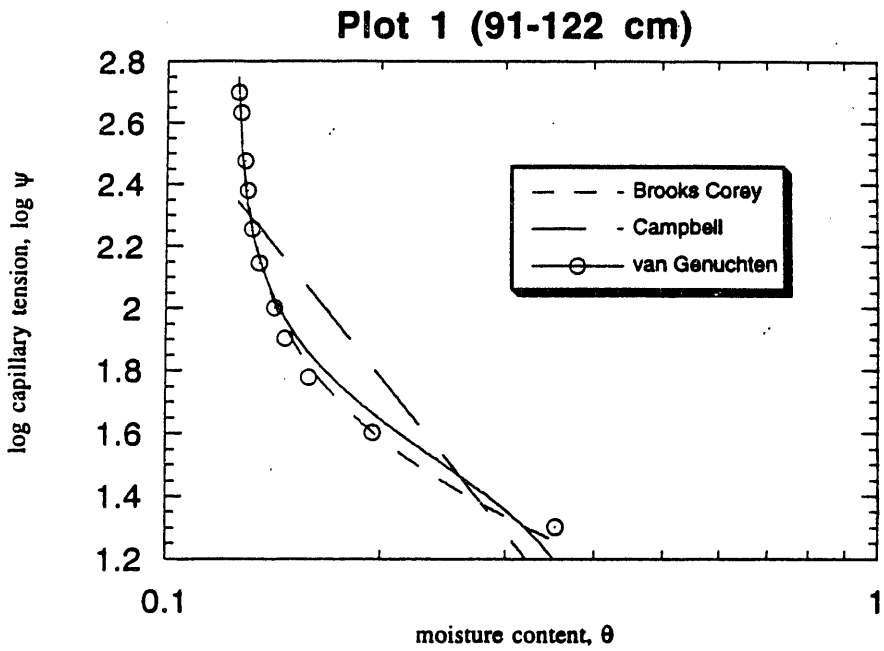

y = bc(.1,.1,1,.406)		
	Value	Error
θ_r	0.12449	0.00036918
λ	1.4714	0.075401
ψ_b	15.72	1.2926
Chisq	0.013373	NA
R	0.99653	NA

y = camp(1,.1,.406)		
	Value	Error
ψ_e	8.2134	4.8514
b	2.8173	0.58064
Chisq	0.53333	NA
R	0.85056	NA

y = vg(0.1,1.5,.1,.406)		
	Value	Error
θ_r	0.12507	0.00044204
n	2.7622	0.15592
α	0.045622	0.0059946
Chisq	0.042843	NA
R	0.98883	NA

Plot 1 (122-152 cm)

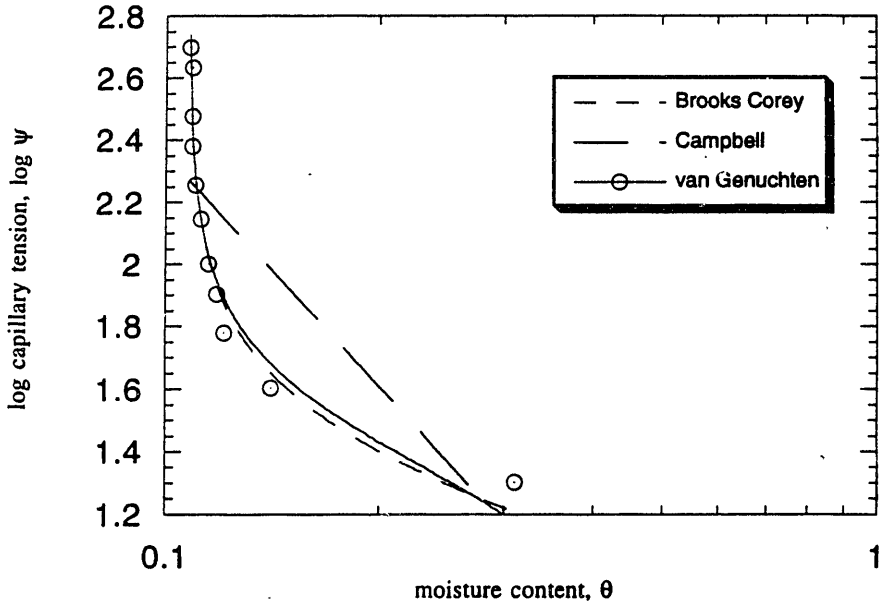

y = bc(.1,.1,1,.436)		
	Value	Error
θ_r	0.1076	0.00022898
λ	1.7706	0.18029
Ψ_b	12.336	2.5197
Chisq	0.071614	NA
R	0.98126	NA

y = camp(1,.1,.436)		
	Value	Error
Ψ_c	5.8964	5.3325
b	2.4743	0.70733
Chisq	0.81728	NA
R	0.75908	NA

y = vg(0.1,1.5,.01,.436)		
	Value	Error
θ_r	0.10768	0.0002155
n	2.912	0.22106
α	0.06813	0.015129
Chisq	0.091922	NA
R	0.97588	NA

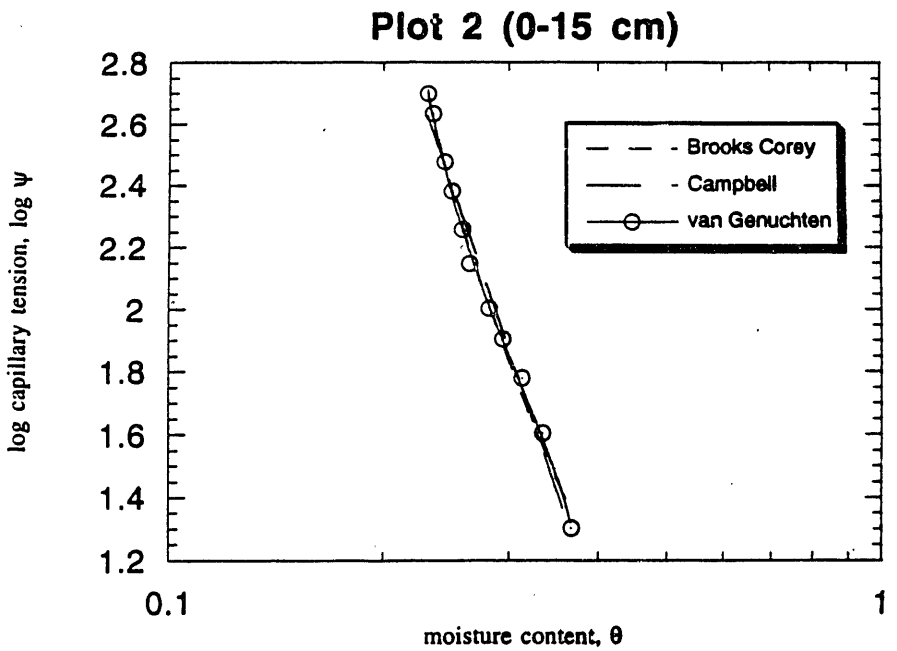

y = bc(.2,.1,1,.408)		
	Value	Error
θ_r	0.16921	0.017608
λ	0.37822	0.064739
ψ_b	13.767	1.5288
Chisq	0.01159	NA
R	0.99699	NA

y = camp(1,.1,.408)		
	Value	Error
ψ_c	9.4994	1.0539
b	6.667	0.26691
Chisq	0.027421	NA
R	0.99286	NA

y = vg(0.1,1.5,.01,.408)		
	Value	Error
θ_r	0.20196	0.0046003
n	1.6439	0.048446
α	0.040619	0.0021844
Chisq	0.0042302	NA
R	0.9989	NA

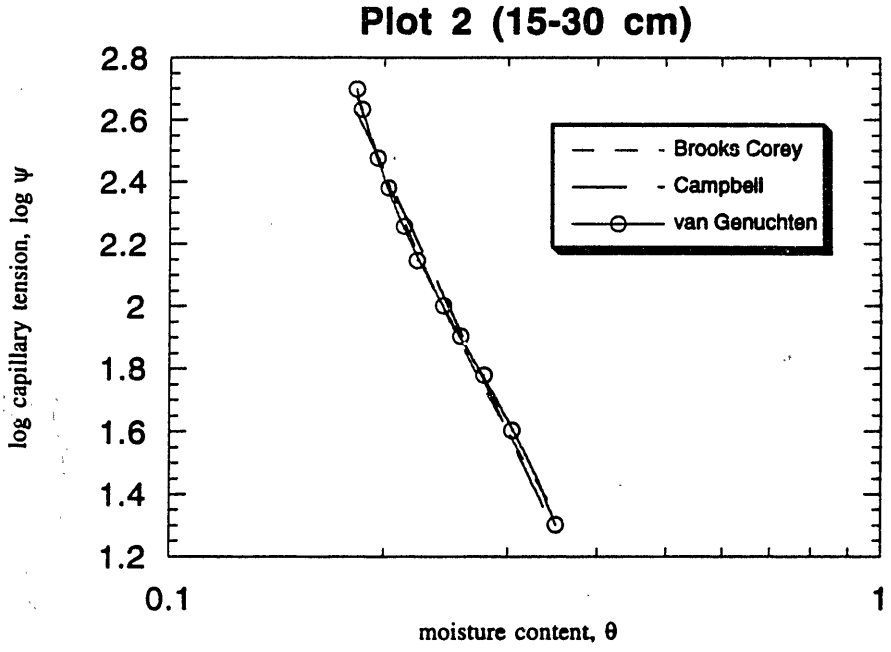

y = bc(.15,.1,1,.391)		
	Value	Error
θ_r	0.11447	0.013829
λ	0.4018	0.047972
ψ_b	14.695	1.1312
Chisq	0.0063296	NA
R	0.99836	NA

y = camp(1,.1,.391)		
	Value	Error
ψ_e	11.176	0.94873
b	4.7752	0.15471
Chisq	0.018048	NA
R	0.99531	NA

y = vg(0.1,1.5,.01,.391)		
	Value	Error
θ_r	0.15481	0.001456
n	1.7328	0.016889
α	0.036288	0.00059407
Chisq	0.00048591	NA
R	0.99987	NA

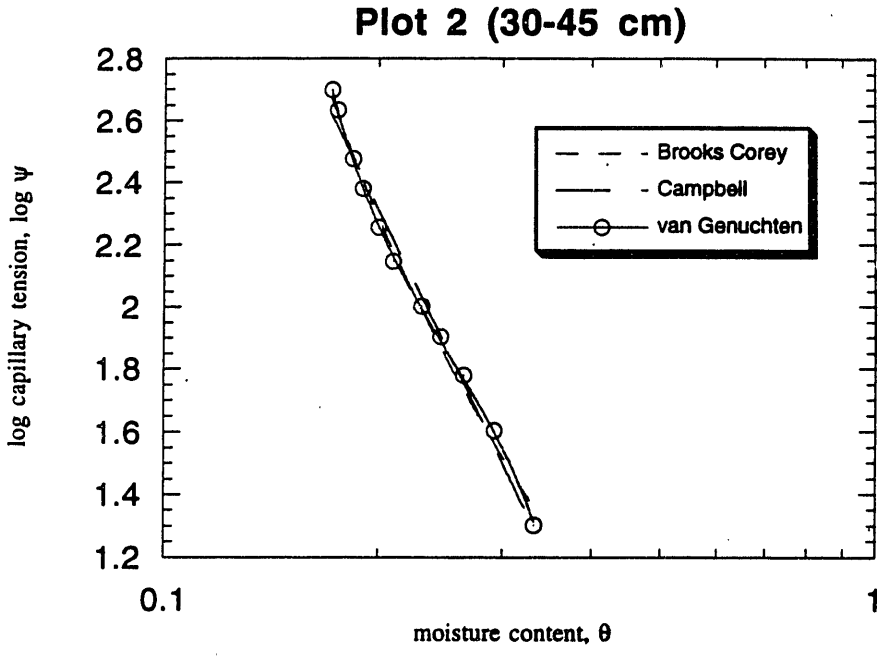

y = bc(.15,.1,1,.367)		
	Value	Error
θ_r	0.10937	0.017563
λ	0.42027	0.06856
ψ_b	16.144	1.604
Chisq	0.011838	NA
R	0.99693	NA

y = camp(1,.1,.367)		
	Value	Error
ψ_e	12.47	1.1499
b	4.6204	0.16921
Chisq	0.023	NA
R	0.99402	NA

y = vg(0.10,1.5,.01,.367)		
	Value	Error
θ_r	0.14865	0.0015509
n	1.8019	0.022325
α	0.032448	0.00061347
Chisq	0.00079003	NA
R	0.9998	NA

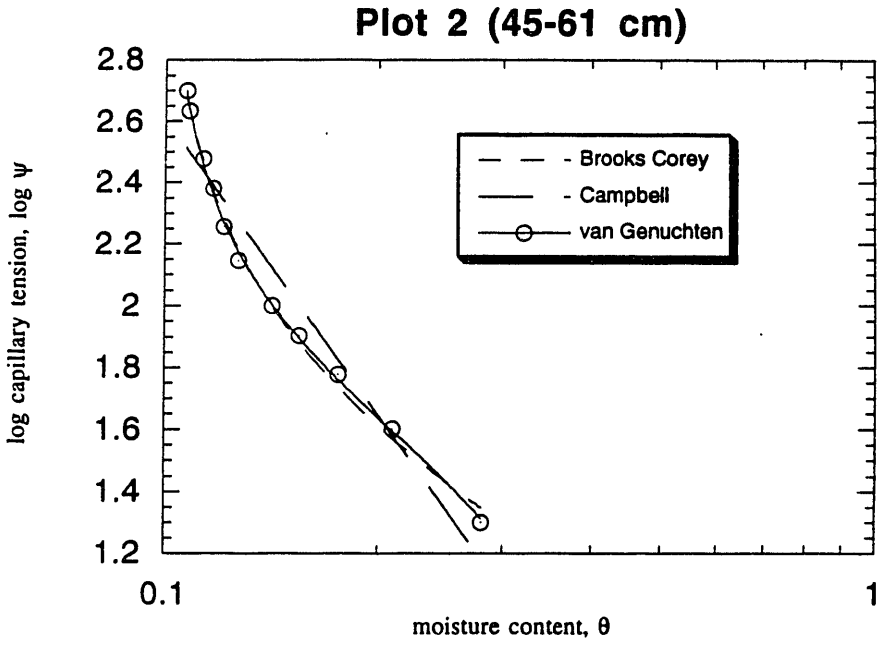

y = bc(.1,.1,1,.363)		
	Value	Error
θ_r	0.096538	0.0019274
λ	0.93136	0.059487
Ψ_b	14.917	1.1451
Chisq	0.0081593	NA
R	0.99788	NA

y = camp(1,.1,.363)		
	Value	Error
Ψ_c	6.7066	1.7773
b	3.1787	0.27232
Chisq	0.11949	NA
R	0.96852	NA

y = vg(0.1,1.5,.01,.363)		
	Value	Error
θ_r	0.099873	0.00082777
n	2.1251	0.040586
α	0.049786	0.0020914
Chisq	0.0029016	NA
R	0.99925	NA

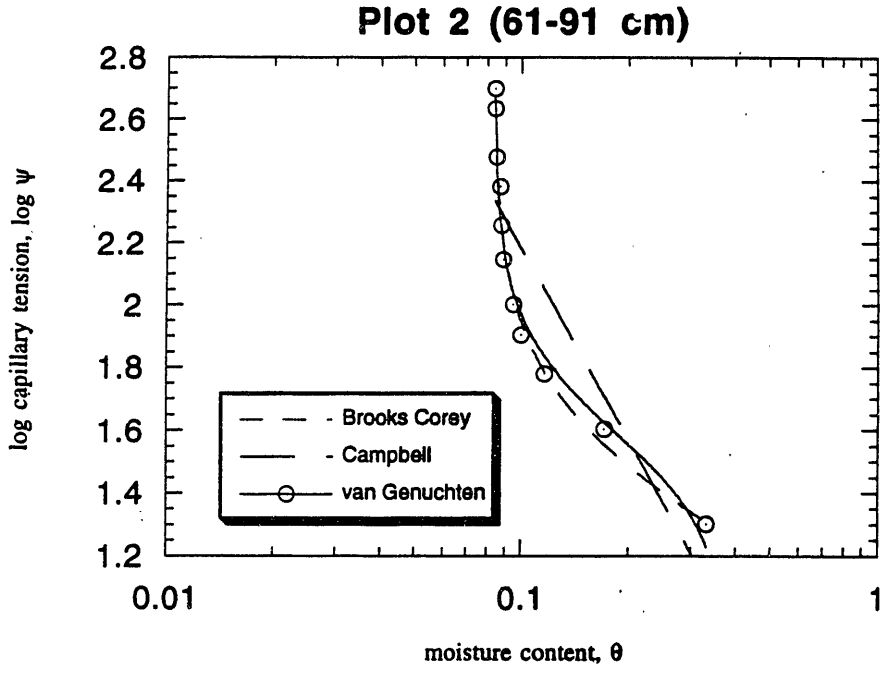

y = bc(.05,.1,1,.371)		
	Value	Error
θ_r	0.083227	0.00020785
λ	1.8406	0.10354
Ψ_b	18.804	1.5893
Chisq	0.016827	NA
R	0.99563	NA

y = camp(1,.1,.371)		
	Value	Error
Ψ_e	10.57	5.5998
b	2.0341	0.41027
Chisq	0.51682	NA
R	0.85557	NA

y = vg(0.01,1.5,.01,.371)		
	Value	Error
θ_r	0.083576	0.00017294
n	3.2581	0.17336
α	0.037864	0.0038957
Chisq	0.032599	NA
R	0.99151	NA

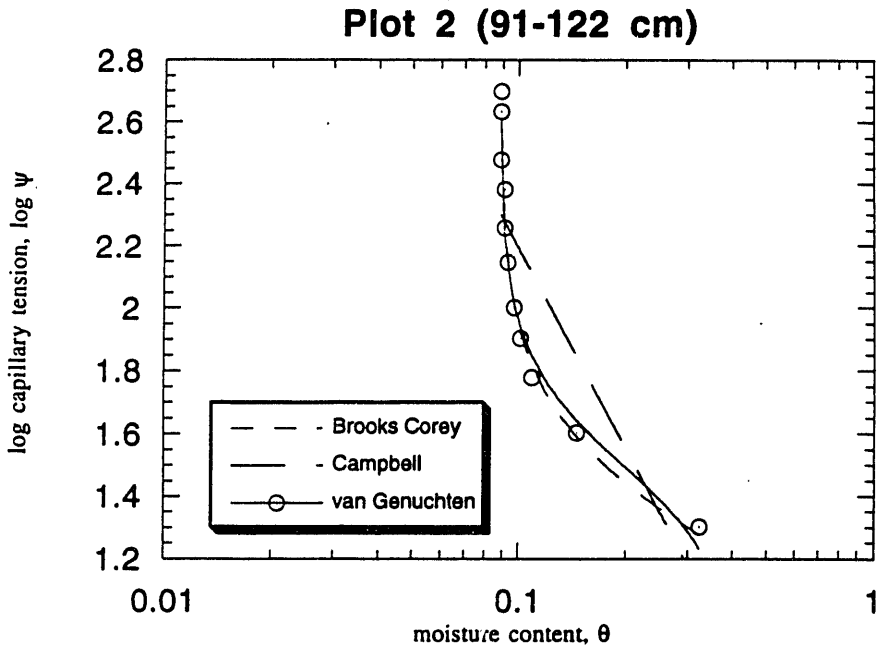

y = bc(.05,.1,1,.394)		
	Value	Error
θ_r	0.088395	0.00024335
λ	1.9485	0.18001
Ψ_b	16.586	2.3783
Chisq	0.039952	NA
R	0.98959	NA

y = camp(1,.1,.394)		
	Value	Error
Ψ_c	8.5554	5.7935
b	2.1139	0.50832
Chisq	0.66008	NA
R	0.811	NA

y = vg(0.01,1.5,.01,.394)		
	Value	Error
θ_r	0.088617	0.00019362
n	3.2814	0.24742
α	0.046102	0.006995
Chisq	0.054075	NA
R	0.98588	NA

Plot 2 (122-152 cm)

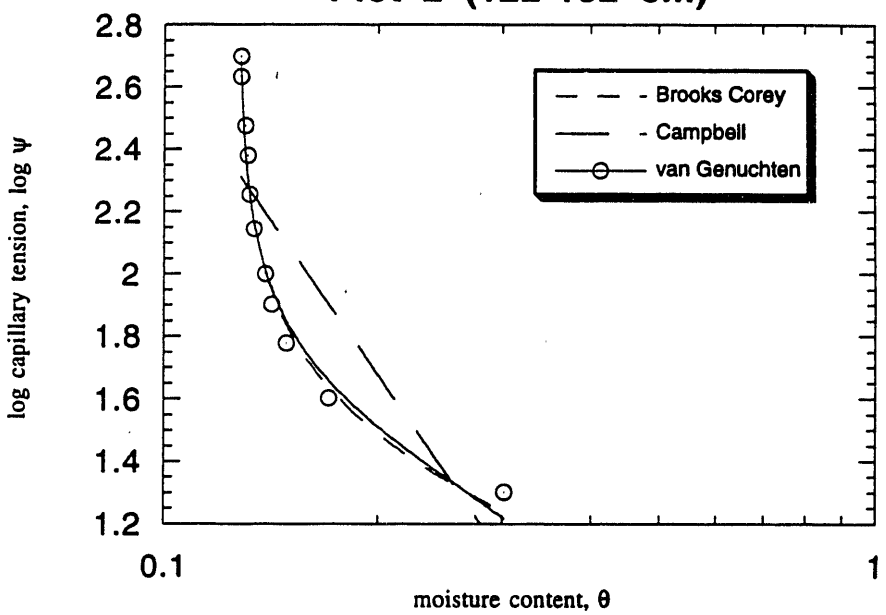

y = bc(.1,.1,1,.456)		
	Value	Error
θ_r	0.1268	0.00033508
λ	1.498	0.10417
ψ_b	11.351	1.4892
Chisq	0.023536	NA
R	0.99388	NA

y = camp(1,.1,.456)		
	Value	Error
ψ_c	3.2078	2.8694
b	3.2765	0.77755
Chisq	0.64867	NA
R	0.81464	NA

y = vg(0.1,1.5,.01,.456)		
	Value	Error
θ_r	0.12699	0.00035128
n	2.6059	0.13536
α	0.075791	0.011579
Chisq	0.033496	NA
R	0.99128	NA

Appendix G: Sevilleta Curve Fits

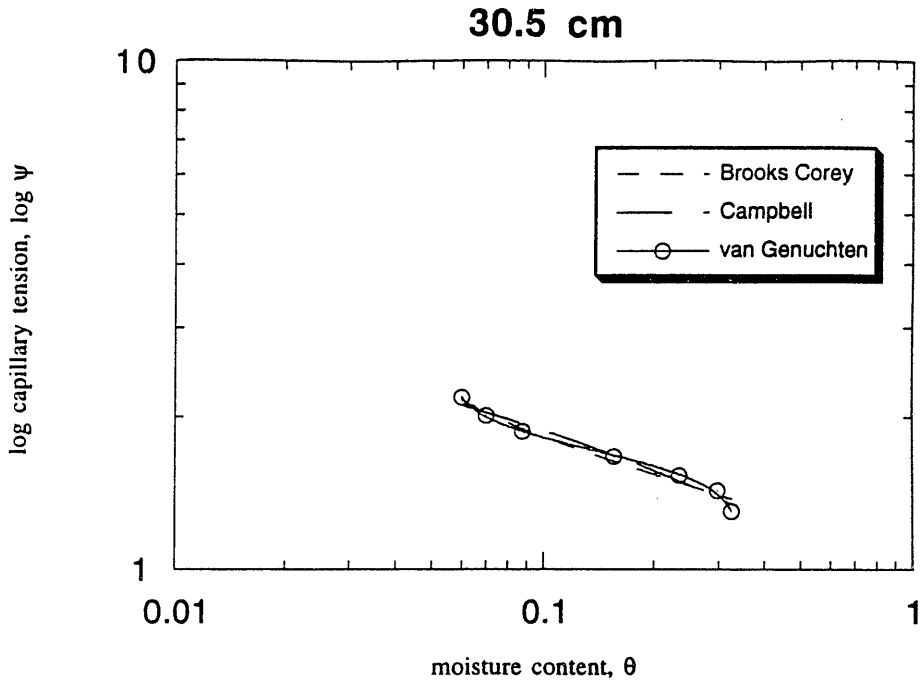

y = bc(.01,.1,1,.33)		
	Value	Error
θ_r	0.04297	0.011471
λ	1.5349	0.32794
ψ_β	23.522	1.892
Chisq	0.011367	NA
R	0.9909	NA

y = camp(1,.1,.33)		
	Value	Error
ψ_e	21.916	1.7972
b	1.0442	0.077813
Chisq	0.016955	NA
R	0.9864	NA

y = vg(0.01,1.5,.001,.33)		
	Value	Error
θ_r	0.055984	0.0010686
n	3.8915	0.19589
α	0.028241	0.0012086
θ_s	0.34767	0.0072733
Chisq	0.00076006	NA
R	0.99939	NA

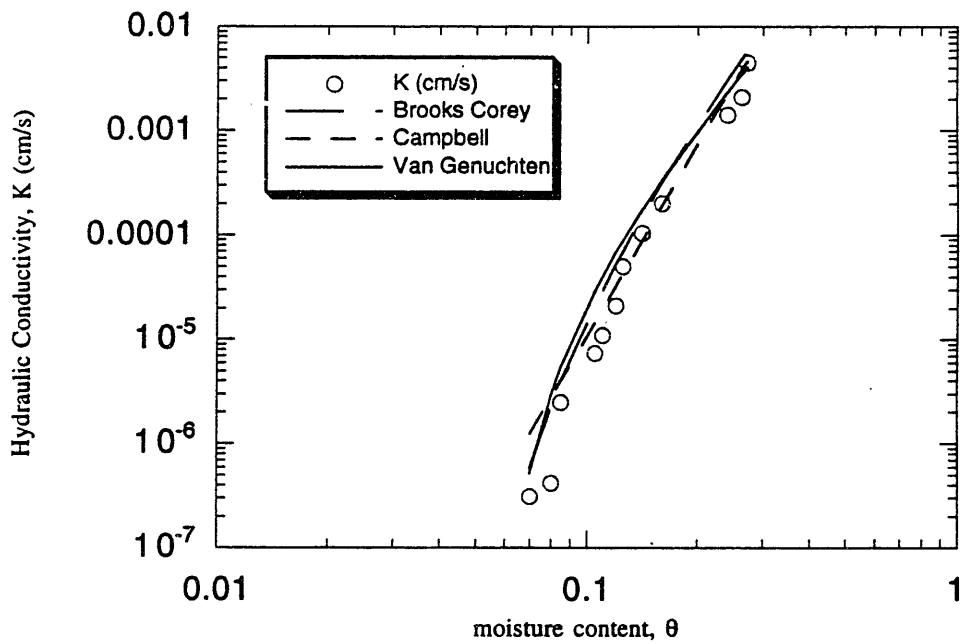

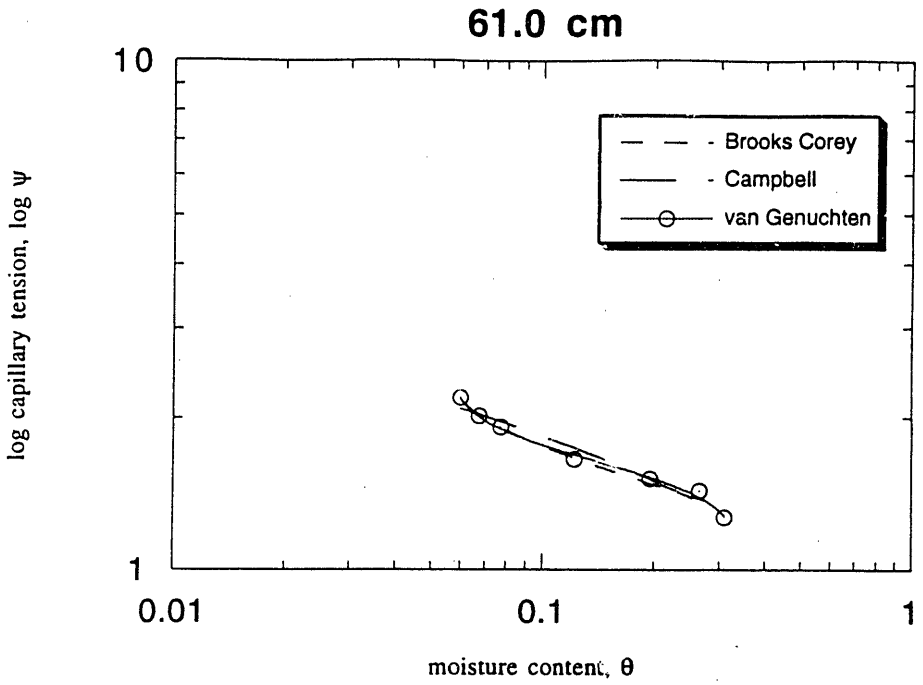

y = bc(.01,.1,1,.318)		
	Value	Error
θ_r	0.050779	0.0047932
λ	1.6976	0.24198
ψ_β	21.086	1.4945
Chisq	0.0080611	NA
R	0.9941	NA

y = camp(1,.1,.318)		
	Value	Error
ψ_e	18.669	2.0724
b	1.1321	0.10151
Chisq	0.026485	NA
R	0.98049	NA

y = vg(0.01,1.5,.001,.318)		
	Value	Error
θ_r	0.056102	0.0020807
n	3.4911	0.37464
α	0.036458	0.0054763
θ_s	0.35928	0.036312
Chisq	0.0035467	NA
R	0.99741	NA

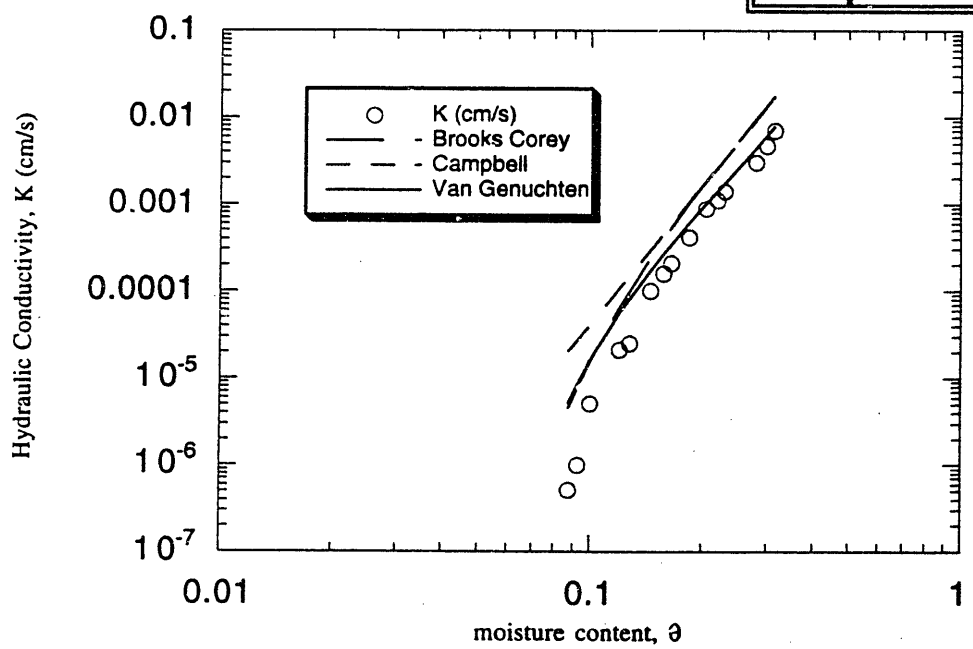

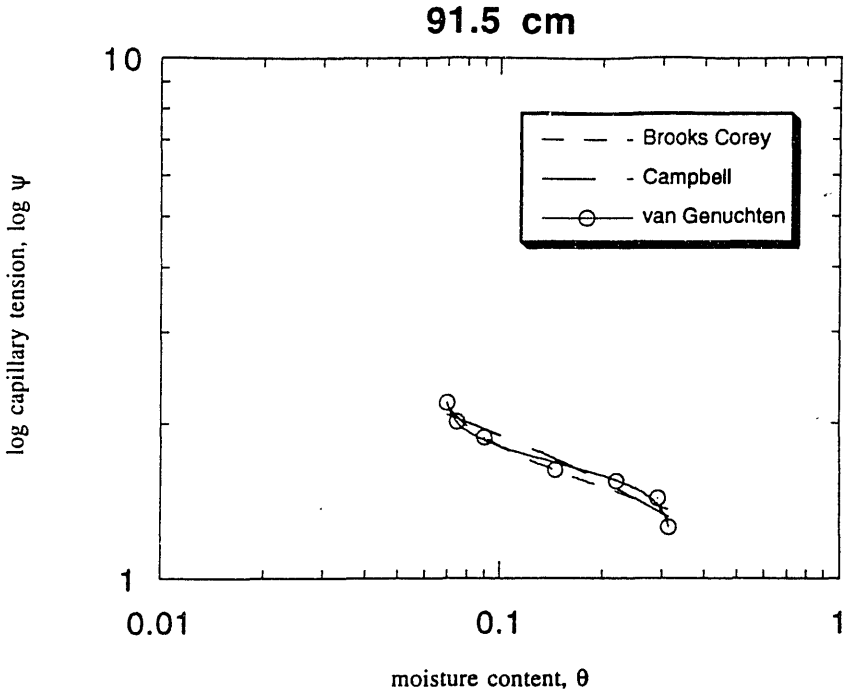

y = bc(.01,.1,1,.325)		
	Value	Error
θ_r	0.061856	0.0074636
λ	1.8389	0.44996
ψ_β	22.467	2.445
Chisq	0.021005	NA
R	0.98441	NA

y = camp(1,.1,.325)		
	Value	Error
ψ_c	19.826	2.53
b	1.1759	0.12794
Chisq	0.03794	NA
R	0.97166	NA

y = vg(0.01,1.5,.001,.325)		
	Value	Error
θ_r	0.068606	0.00098292
n	4.5054	0.48832
α	0.028012	0.0022145
θ_s	0.32458	0.0078751
Chisq	0.0051939	NA
R	0.99617	NA

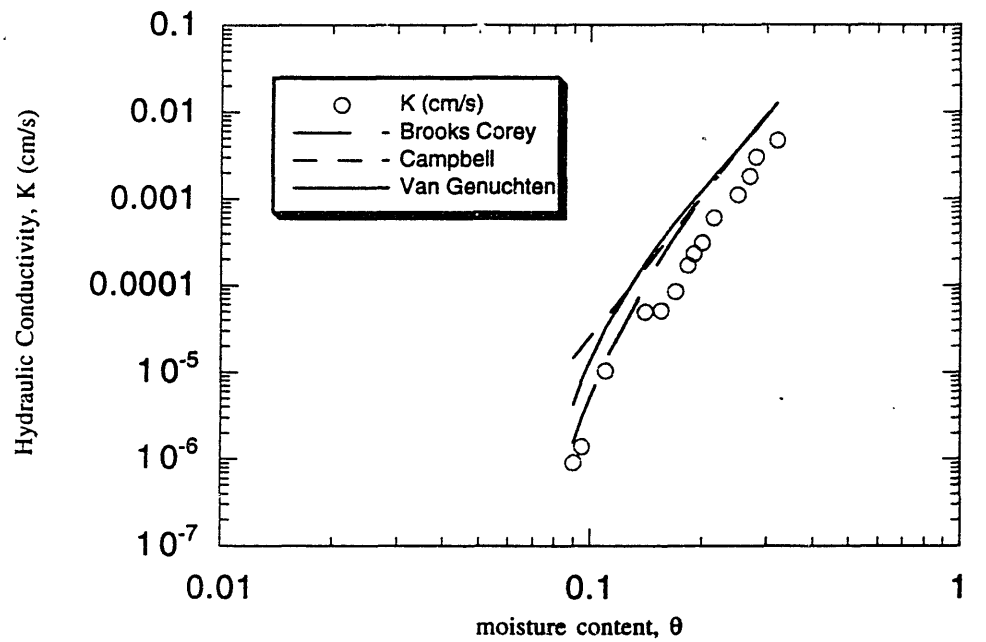

THESIS PROCESSING SLIP

FIXED FIELD: ill. _____ name _____

index _____ biblio _____. _____

▶COPIES: (Archives) Aero Dewey (Eng) Hum

Lindgren Music Rotch Science

TITLE VARIES: ▶☐ _____

_____

_____

NAME VARIES: ▶☐ _____

_____

IMPRINT: (COPYRIGHT) _____

▶COLLATION: 198 l; 1 disk

_____

▶ADD. DEGREE: _____ ▶DEPT.: _____

SUPERVISORS: _____

_____

_____ __ _____

_____ __ _____

_____ __ _____

_____ __ _____

_____ __ _____

_____ __ _____

_____ __ _____

NOTES:

cat'r: date:

page: 1/29

▶DEPT: C.E.

▶YEAR: 1997 ▶DEGREE: M.S.

▶NAME: TSE, Rosanna

_____